



HAL
open science

Slurry coatings from aluminium microparticles on Ni-based superalloys for high temperature oxidation protection

Benoît Rannou

► **To cite this version:**

Benoît Rannou. Slurry coatings from aluminium microparticles on Ni-based superalloys for high temperature oxidation protection. Other. Université de La Rochelle, 2012. English. NNT : 2012LAROS377 . tel-00839790

HAL Id: tel-00839790

<https://theses.hal.science/tel-00839790>

Submitted on 30 Jun 2013

HAL is a multi-disciplinary open access archive for the deposit and dissemination of scientific research documents, whether they are published or not. The documents may come from teaching and research institutions in France or abroad, or from public or private research centers.

L'archive ouverte pluridisciplinaire **HAL**, est destinée au dépôt et à la diffusion de documents scientifiques de niveau recherche, publiés ou non, émanant des établissements d'enseignement et de recherche français ou étrangers, des laboratoires publics ou privés.



ÉCOLE DOCTORALE

Sciences et Ingénierie en Matériaux, Mécanique, Énergétique et Aéronautique (SIMMEA)

Université de La Rochelle

Laboratoire des Sciences de l'Ingénieur pour l'Environnement (LaSIE)

FRE-CNRS 3474

THÈSE

présentée par :

Benoit RANNOU

soutenance prévue le 20 Novembre 2012

pour l'obtention du grade de Docteur de l'Université de La Rochelle

Discipline : Sciences des matériaux

Slurry coatings from aluminium microparticles on Ni-based superalloys for high temperature oxidation protection

Composition du jury:

Rapporteurs :

Pr. Dr.-Ing. Michael SCHÜTZE

Professeur à l'Université d'Aix la Chapelle, Directeur de l'institut
DECHEMA Forschungsintitut, Allemagne

Pr. Francisco Javier PEREZ TRUJILLO

Professeur à l'Universidad Complutense de Madrid, Espagne

Examineurs :

Pr. Henri BUSCAIL

Professeur à l'Université de Clermont Ferrand I

Pr. Michel VILASI

Professeur à l'Université de Lorraine

Pr. Francisco Javier VELASCO LOPEZ

Professeur à l'Universidad Carlos III de Madrid, Espagne

Directeurs de thèse :

Pr. Fernando PEDRAZA-DIAZ

Professeur à l'Université de La Rochelle

Dr. Vladislav KOLARIK

Directeur de recherche à l'Institut Fraunhofer ICT, Allemagne

Encadrant scientifique :

Dr. Baptiste BOUCHAUD

Ingénieur de recherche, Université de La Rochelle

Invité :

Pascal BILHE

Ingénieur R&D, Direction Technique Groupe SAFRAN

*Chi va piano va sano
e chi va sano va lontano.*

Remerciements

Ces travaux de thèse ont été réalisés au sein du laboratoire LaSIE (FRE-CNRS 3474) dans la thématique de recherche B2 portant sur la « Protection des matériaux et revêtements », ainsi qu'au sein du laboratoire Fraunhofer ICT dans l'équipe de recherche « Matériaux à Haute Température », grâce au support financier de l'Europe dans le cadre du projet de recherche PARTICOAT (FP7 / 2007-2013 NMP3-LA-2008-211329-2).

Je souhaite tout d'abord remercier Messieurs X. Feaugas et K. Aït-Mokhtar, professeurs à l'Université de La Rochelle, et directeurs successifs des laboratoires LEMMA (EA 3167) et du laboratoire LaSIE (FRE-CNRS 3474), pour m'avoir accueilli.

Je remercie au même titre Monsieur P. Elsner, Professeur Docteur et Directeur du Fraunhofer ICT, pour m'avoir permis de réaliser plusieurs échanges, d'une durée totale de sept mois au sein du Fraunhofer ICT, notamment dans le cadre de la validation du label européen.

Je remercie Monsieur M. Vilasi, Professeur à l'Université de Lorraine, pour m'avoir fait l'honneur d'accepter de présider ce jury qui a évalué les travaux présentés dans ce manuscrit.

Je souhaite exprimer ma profonde reconnaissance à Monsieur M. Schütze, Professeur (Pr.Dr.-Ing.) à l'Université d'Aix-la-Chapelle et Directeur de l'Institut DECHEMA Forschungsinstitut de Francfort sur le Main (Allemagne) pour avoir accepté d'être rapporteur de ces travaux.

J'exprime aussi mes sincères remerciements à Monsieur F.J. Perez Trujillo, Professeur à l'Universidad Complutense de Madrid (Espagne), pour avoir été rapporteur, et avoir pris part à la critique des travaux présentés lors de cette thèse européenne.

Je suis très reconnaissant envers Monsieur H. Buscail, Professeur à l'Université de Clermont Ferrand I, pour avoir consacré une partie de son temps à l'évaluation de ces travaux, ainsi que pour avoir siégé dans ce jury.

J'adresse mes sincères remerciements à Monsieur F.J. Velasco Lopez, Professeur à l'Universidad Carlos III de Madrid (Espagne), pour les discussions scientifiques que nous avons pu avoir, ainsi que pour les différents conseils qu'il a pu me prodiguer.

Je remercie également Monsieur P. Bilhé, Ingénieur R&D au sein de la Direction Technique du groupe SAFRAN, pour avoir pris de son temps pour évaluer les travaux présentés, ainsi que pour avoir assisté à ce jury.

J'exprime ma sincère gratitude à Monsieur B. Bouchaud, Ingénieur de recherche au laboratoire LaSIE de La Rochelle, pour avoir partagé son expérience de la haute température, pour sa disponibilité ainsi que pour avoir siégé au sein de ce jury.

Je tiens à exprimer ma vive reconnaissance à mon directeur de thèse, Monsieur F. Pedraza Diaz, Professeur à l'Université de La Rochelle, pour m'avoir permis de réaliser ces travaux de thèse dans cet environnement de travail à forte connotation européenne. Je le remercie aussi pour sa disponibilité et pour m'avoir transmis sa passion pour le domaine de la haute température.

Je souhaite exprimer ma profonde reconnaissance à mon second directeur de thèse, Monsieur V. Kolarik, Directeur du groupe de recherche pour les matériaux à haute température à l'Institut Fraunhofer ICT de Pfinztal (Allemagne), pour m'avoir permis d'intégrer le projet de recherche PARTICOAT ainsi que pour tous les échanges que nous avons eus pendant toute l'étude.

Je tiens à remercier Madame Z. Maache - Rezzoug, Maitre de Conférence à l'Université de La Rochelle, pour sa collaboration à la mise en place des essais de rhéologie au sein du LaSIE ainsi que pour ses conseils avisés.

J'exprime mes sincères remerciements à Madame J. Balmain et Monsieur G. Bonnet, respectivement Maitre de Conférences à l'Université de La Rochelle et Professeur à l'Université de La Rochelle, pour leurs conseils avisés, leurs pédagogies et leurs relativismes.

Je souhaite exprimer mes remerciements au personnel technique de La Rochelle avec qui j'ai pu évoluer lors de ces trois années, merci Danielle, Isabelle, Martine, Christelle, Stéphane, Cyril et Bruno, ainsi que Monique et Egle du CCA. Je remercie aussi les personnes de l'ICT que j'ai pu côtoyer lors de cette thèse, Mar, Carmen, Martina, Harald & Harald. For sure I forgot many people but they know that I really appreciated all my periods with them.

Je remercie les « jeunes » du LEMMA / LaSIE pour les bons moments passés à La Rochelle, merci Nadège, Geoffroy, Simon, Maël, Loïc, Abdelali, Mathieu, Dan, Hervé, et les plus jeunes: Daniella, Niusha, Maxime, Alexandre, Alaric, Bachir, Yves, Geoffrey. Thank also to the foreigners: Belén, Raquel, Teresa, Veronica, Martin, Nicolas, Alberto, Spirros, Leo, Viktor with whom I had some good time when I was in Germany but also when I was in Spain.

Finalement, je tiens à remercier mes amis qui m'ont soutenu, ainsi que ma famille pour leur patience et compréhension qu'ils ont su me témoigner. Je ne donnerai pas de noms car ils se reconnaîtront d'eux même si ils lisent ces quelques lignes.

Table of contents

Remerciements

Table of contents

Preface & introduction

Chapter I – State of the art and background of the study

I – The degradation of metallic materials: a matter of dimensioning and of lifetime issues.	17
II – Materials for gas turbine components.	18
A. The turbofan engine.	19
a. The element of thrust.	19
b. Impacts on the choice of the material.	20
B. Superalloys.	21
a. Nickel-based superalloys.	21
b. Compositional and microstructural evolutions.	21
C. Degradation mechanisms in service conditions.	23
a. Generalities.	23
b. High temperature oxidation.	25
III – Industrial protective coatings.	25
A. The overlay coatings.	26
B. Aluminide coatings.	27
a. The simple aluminide coatings.	27
b. The modified aluminide coatings.	29
C. Additional protective systems.	30
a. Thermal barrier coating.	30
b. Diffusion barriers.	31
IV – The slurry coating technology.	31
A. Definition of a slurry.	32
B. Commercial slurries and recent orientations.	32
C. Processing properties.	33
V – Motivations and concerns of the present study: explanation of the PARTICOAT concept.	33
References.	36

Chapter II – Experimental methods

I – The substrates.	45
A. The raw materials.....	45
B. The conventional aluminized substrate.	46
II – The PARTICOAT slurries	47
A. The aluminium microspheres.....	47
B. The composition and preparation of the slurries.	48
III – The special design structure.	48
IV – Formation and oxidation tests of the PARTICOAT systems.	49
A. The thermal treatment.	49
B. The isothermal oxidation tests.....	49
V – Physico-chemical characterization of the systems.	50
A. Rheological properties.	50
a. Stability measurements using the Turbiscan® technology.	50
b. Rheometer.....	50
B. Spectroscopic measurements.	50
a. Fourier Transform Infrared (FTIR).	50
b. Raman micro-spectroscopy.....	50
C. Calorimetric measurements.....	51
a. Differential Scanning Calorimetry (DSC).....	51
b. Differential Thermal Analysis (DTA).	51
D. Microscopy analysis.	51
a. Optical observations.....	51
b. Scanning Electron Microscopy (SEM) coupled Energy-Dispersive Spectroscopy (EDS).	51
E. X-Ray Diffraction (XRD).....	52
VI – Thermodynamic modelling.	52
A. Thermocalc® software.....	52
B. DICTRA® software.	53
References.....	54

Chapter III – Elaboration and characterization of a water-based slurry containing PVA and Al microspheres for aluminizing purposes

I. Rheological behaviour.....	59
A. Composition of the slurries and ageing phenomena.....	59
B. Rheological behaviour of the slurry.....	59
a. Sedimentation characterization of the slurries.....	59
b. Viscosity measurements.....	63
II. Physico-chemical properties of the slurry.....	65
A. Room temperature properties.....	66
B. Thermal annealing till the melting point of Al.....	67
C. Thermal annealing over the melting point of Al.....	72
III. Drying of the slurry.....	74
Summary and outlook.....	76
References.....	78

Chapter IV – Formation of a Thermal Barrier Coating (TBC) system onto nickel-based substrates from a slurry containing aluminium microparticles

I. Mechanisms of coating formation onto model substrates.....	83
A. Considerations about the thermal treatment for the application of PARTICOAT.....	83
B. The formation of the topcoat.....	85
C. The formation of the diffusion zone.....	88
a. Polycrystalline nickel.....	88
i. Formation of intermetallics at the intermediate step.....	88
ii. Intermetallic formations after the complete thermal treatment.....	93
b. Polycrystalline Ni20Cr.....	95
II. Formation of the coatings on industrial Ni-based superalloys.....	98
A. First stage thermal treatment.....	98
B. Complete thermal treatment.....	101
Summary and outlook.....	106
References.....	107

Chapter V – High temperature isothermal oxidation behaviour of PARTICOATED Ni-based superalloys: the effect of the chemical composition of the substrate

I. Considerations about the behaviour of materials at high temperatures.	113
A. On the thermodynamics of the oxide scale formation.	113
B. Growth kinetics of the oxide scale: the case of the alumina scales.....	114
II. Investigation of the oxidation resistance of the PARTICOATED superalloys.....	115
A. The limitation of the materials with respect of the service conditions.	115
B. The isopleth as a tool to understand and predict the behaviour of the coating and the substrate.	118
C. Characterization of the PARTICOAT system during isothermal oxidation tests.....	121
a. Oxidation kinetics.	121
b. Evolution of the top coat as a function of the chemistry of the systems.	125
c. Evolution of the thermally grown oxide (TGO).	126
d. Microstructural evolution of the bond coat.....	127
e. Comparison between the PARTICOATED samples and the SVPA ones.	140
Summary and outlook	142
References.....	143

Chapter VI – Investigation of a special design: Influence of a rare-earth oxide-based diffusion barrier in combination with the PARTICOAT concept

I. Characterization of the special design using a proprietary interlayer and the PARTICOAT concept.	149
A. Deposition process of the “diffusion barrier”.	151
B. Evolution with temperature of the microstructure of the special design onto pure Ni.....	154
II. Extrapolation to Ni-based superalloy: example of CM 247 LC.....	156
A. Reactivity towards the PARTICOAT and high temperature oxidation behaviour.	156
1. Formation mechanisms influenced by the temperature and the chemical composition.	156
2. High temperature behaviour.....	159
B. Considerations for the formation of the special design.....	161
Summary and outlook	164
References.....	166

Conclusions & Outlook

Annexes

Résumé français

Preface

Metallic structural materials exposed to high temperature environments have to face extreme service conditions, i.e. mechanical strains and stresses coupled to the presence of corrosive and/or oxidizing agents contained in the surrounding atmosphere (molten and gas phases mainly). The combined mechanical-chemical action tends to degrade the integrity of the structure through very complex phenomena coined “high temperature corrosion”. The full comprehension of such complex degradation mechanisms often requires the study of the phenomena in an independent manner before studying the synergistic effect between them. Overall, such multidisciplinary approach of these problems allows to get more familiar with the domain of the extreme environments before any consideration on the development of innovative protective systems to fight against “high temperature corrosion”.

The following work, realized within the framework of the 7th European Framework Programme “PARTICOAT”, implemented a multidisciplinary approach to provide answers for enhanced durability of materials at high temperature ($900^{\circ}\text{C} \leq T \leq 1100^{\circ}\text{C}$) and oxidizing (air) conditions through the study and development of a new protective coating system (PARTICOAT – www.particoat.eu) onto four types of Ni-based superalloys, with potential applications in the gas turbine industry (aero and land-based).

The new protective coating system proposed shall respond to several criteria. Therefore, the manuscript will first deal with the elaboration of the coating system, before investigating their high temperature oxidation behaviour under isothermal conditions. A special design of diffusion barrier aiming at limiting the interdiffusion processes between the thermal oxide and between the coating and the substrate, hence degradation phenomena will be also investigated as a preliminary work.

This study will be articulated in independent chapters to facilitate the reading. Each chapter contains specific bibliographic review to support the scientific background and help in the comprehension and interpretation of the results.

Introduction

Metallic structural materials are used in a wide field of applications and are submitted to the inevitable degradation phenomena. Therefore, the industry aims at limiting the costs associated with the manufacturing steps to produce, maintain or replace some defective parts. The service conditions imposed, for example, in gas and steam turbine in electric power generation and aeroengines, lead to the enhancement of the degradation kinetics by the influence of both the aggressive atmospheres (O_2 , SO_2 , H_2O ...) and the high temperatures (up to about $1500^\circ C$ in specific aero engines).

When considering oxidizing conditions at high temperatures, the chemical resistance of a material is usually provided by the formation and the growth of a protective oxide layer at the gas phase / substrate interface. It will further act as a diffusion barrier between the flux of aggressive agents and the structural material. Nonetheless, this protection has to be thermodynamically stable regarding the service conditions, but also adherent, homogeneous and finally, it has to display slow growth kinetics.

Depending on the chemistry of the base materials, which can be iron-, cobalt- or nickel-based superalloys, alloying elements like chromium (Cr) and aluminium (Al) may lead to the growth of such protective scales. Considering these requirements, the oxides (Cr_2O_3 , Al_2O_3) formed from these elements (Cr, Al) fulfill the appropriate characteristics and kinetics of growth of their respective layer, up to $950^\circ C$ and $1300^\circ C$, respectively. Their initial amounts in the base material has to be high enough to take advantage of the selective oxidation process occurring at high temperature, in order to form a chromia (Cr_2O_3) or an alumina ($\alpha-Al_2O_3$) scale, respectively. One has to note that alumina has a higher stability compared to chromia and is therefore the preferred oxide at temperatures over $950^\circ C$ till about $1300^\circ C$.

In the particular case of aero and land-based gas turbines, the hottest sections are composed of Ni-based superalloys due to their excellent mechanical properties at high temperature. Indeed, their chemistries have been optimized since decades to withstand the mechanical loads (thermomechanical fatigue, creep) impaired with the service conditions at the expense of the oxidation resistance. Because of this compromise between the mechanical resistance and the chemical resistance, their respective aluminium content is not high enough to build up a protective oxide layer, which can remain for long service conditions.

To overcome this limitation, different technical solutions have been designed, such as the diffusion coatings applied by CVD- related techniques. They allow to enrich the sub-surface of the substrates in Al to increase the high temperature oxidation resistance by forming nickel aluminide compounds. Several other technical solutions exist to enhance this required resistance at high temperature, which can be also modified by the use of the overlay coatings, i.e. the deposition of MCrAlY (M=Fe, Co, Ni), often elaborated by spray techniques. Both type of coatings can, in principle, be employed for high and low pressure turbines since they promote the formation of the $\alpha-Al_2O_3$ oxide, which is the most thermodynamically stable polymorphic phase of the sesquioxide aluminas for temperature over $1000^\circ C$. However, the MCrAlY coatings are mostly used for land based turbine application.

In addition to these first technical solutions designed to improve the mechanical and oxidation resistances at high temperatures, advanced manufacturing steps have been elaborated to contribute to decrease the effect of the temperature at the surface of the metallic substrate. In this view, a patented coating system comprising a Pt-modified NiAl bond-coat and a top thermal barrier coating (TBC) of yttria partially stabilised zirconia (YSZ) has been tailored. However, it is important to remark

that (a) the use of Pt is extremely costly, about 40€.g⁻¹ depending on the shares, but also due to the patented electrolytic process and the payment of royalties; (b) the cheap CVD processes employed to elaborate the Al diffusion coating is quite harmful (current use of NH₄F as activator) and (c) the highly directional, very costly and low yield electron beam physical vapour deposition (EB-PVD) process to deposit the thermal barrier of YSZ (often less than 15-20% of the raw material is deposited).

Despite the good performances of the (Ni,Pt)Al + YSZ thermal barrier systems, the degradation mechanisms are provided by oxidation phenomenon coupled with the interdiffusion of the chemical elements present in the alloys and their protective systems. As a result, the formation and the growth of the secondary reaction zone (SRZ) lead to the embrittlement of the mechanical properties during the service conditions, while cyclic oxidation service conditions may lead to the spallation and / or delamination of the thermal barrier coating (partially or fully).

In order to delay these degradation phenomena, new technical solutions have been designed. The doping by reactive elements (RE) allows to enhance the adhesion properties as well as lowering the oxidation kinetics of the active surfaces. The behaviour of such solutions is greatly influenced by the introduction method of these RE. Recently, the γ / γ' coatings have been developed by depositing likely similar chemical compositions than the bare Ni-based superalloy, thus modifying the interdiffusion mechanisms of the element to delay the degradation of the system.

In spite of this complex system, the degradation mechanisms still occur with the thermo-activated Al consumption by interdiffusion and oxidation to maintain the protective α -Al₂O₃ layer. Therefore, the development of diffusion barrier coatings has been proposed in the literature (Cr, Re, SiAlON...) to refrain such phenomena.

Considering these technical solutions developed over the last decades, several ameliorations still have to be done for answering the new considerations and legislations. Efficiencies of the aeroengines are meant to be enhanced by increasing the service temperatures, which implies either the modification of the substrate material or of the coating, or both. From these requirements, the coating technology has also to be improved by reducing the impact on the environment imposed by the REACH directives, for example. One of the concepts, which tends to satisfy these problems is the European project "PARTICOAT". The overall idea in this project is to take advantage of the use of Al microspheres as a raw material, and to integrate them in a slurry preparation to perform the aluminizing of the substrate and to investigate the possible formation of a ceramic topcoat structure expected to act as a thermal insulating barrier in a cost-efficient and environmentally friendly manner.

The following manuscript aims at introducing a part of the investigation realized within the framework of this PARTICOAT concept. In addition, a special design of diffusion barrier is also investigated, through the electrolytic application of a proprietary reactive element oxide diffusion barrier previously patented in the LaSIE laboratory. Several aspects have been considered and gathered in separated chapters, to facilitate the reading.

Chapter I presents the specific State of the Art necessary to understand the issues related to the high temperature features introduced in this work, for aeroengine applications. From the basis of the degradation mechanisms to the development of the protective system, which allow to protect and increase the lifetime of the structural Ni-based materials, a general overview of the technological breakthrough is summarized.

Chapter II aims at introducing the materials used in this study, while parameters of the surface treatment techniques and the techniques of characterizations are also presented.

The elaboration of the water-based slurry containing Al microspheres is investigated in Chapter III to provide knowledge on its stability with time. Furthermore, its rheological properties and its reactivity to the temperature are also discussed.

Chapter IV focuses on the mechanisms of formation of the coatings, first on model alloys such as pure Ni and Ni₂₀Cr(1.5Si). Once the different physical and chemical processes have been determined as a function of the temperature parameter, the PARTICOAT concept has been extrapolated to four types of Ni-based superalloys: René N5, CM 247 LC, PWA 1483 and INCO 738. This allowed to study the effect of more complex chemistries (alloying elements) and crystal structures (single crystal, directionally solidified and equiaxed).

Due to its primary aim, the reference PARTICOAT design had to be characterized to consider its high temperature oxidation behaviour. In this view, Chapter V discusses the high temperature oxidation resistance provided by this new type of coating, as a function of the chemistry of the alloy considered but also regarding the service temperature condition ($900^{\circ}\text{C} \leq T \leq 1100^{\circ}\text{C}$). A special attention to the influence of the topcoat has been emphasized regarding the respective chemistries of the different alloys, and their interactions with the ceramic quasi-foam topcoat structure.

Finally, Chapter VI presents the combined effect of a rare-earth oxide-based film with the PARTICOAT slurry deposited on top of it. The use of the thermal treatment defined in Chapter IV is investigated to monitor the effect of an overlay coating on the diffusion mechanisms, whether during the formation of the intermetallics or during high temperature oxidation experiments.

A general conclusion of the PARTICOAT concept investigated in this study will be presented whether if considering the slurry aspects, the “simple” design or the special one. Then, outlooks to the features relative to this aluminizing by the slurry technique as well as the behaviour at high temperatures will be introduced.

Chapter I

State of the art and background of the study

This chapter explains the context and the motivations of the present study. In this view, a bibliographic summary of the aero-domain of interest is realized, focused on the materials and the protective systems in use for the high temperature turbine components. In addition their degradation mechanisms are explained to explicit the aim of the present study.

A focus on the slurry technology formulated for the high-temperature applications is included to emphasize the evolution of this technique since the PARTICOAT project aims at using this coating method. They have been of interest for enhancing the high temperature resistance properties of the materials by means of the deposition of several types of elements. Nevertheless, this bibliographic review attempts to summarize information regarding the aluminizing purposes to compete the conventional processes, which are widely used nowadays.

Table of contents

I – The degradation of metallic materials: a matter of dimensioning and of lifetime issues.	17
II – Materials for gas turbine components.	18
A. The turbofan engine.	19
a. The element of thrust.	19
b. Impacts on the choice of the material.	20
B. Superalloys.	21
a. Nickel-based superalloys.	21
b. Compositional and microstructural evolutions.	21
C. Degradation mechanisms in service conditions.	23
a. Generalities.	23
b. High temperature oxidation.	25
III – Industrial protective coatings.	25
A. The overlay coatings.	26
B. Aluminide coatings.	27
a. The simple aluminide coatings.	27
b. The modified aluminide coatings.	29
C. Additional protective systems.	30
a. Thermal barrier coating.	30
b. Diffusion barriers.	31
IV – The slurry coating technology.	31
A. Definition of a slurry.	32
B. Commercial slurries and recent orientations.	32
C. Processing properties.	33
V – Motivations and concerns of the present study: explanation of the PARTICOAT concept.	33
References.	36

I – The degradation of metallic materials: a matter of dimensioning and of lifetime issues.

For each structural application, the dimensioning of materials is a crucial matter. One key parameter is to satisfy the mechanical properties respecting the size requirements, and another one is to tolerate as long as possible the service conditions to obtain a **durable structure**. As shown in *Figure I-1*, the latter will induce evolution of the raw material, to regain the state it has in the nature in the oxidized form. This evolution is promoted by several parameters among which the time, the corrosive environment and the temperature will contribute to affect the **degradation mechanisms** of the metals. Such mechanisms are complex and are ascribed to the **working conditions** whether if they are running in wet atmospheres or if they are employed in dry ones for temperatures above 300°C.

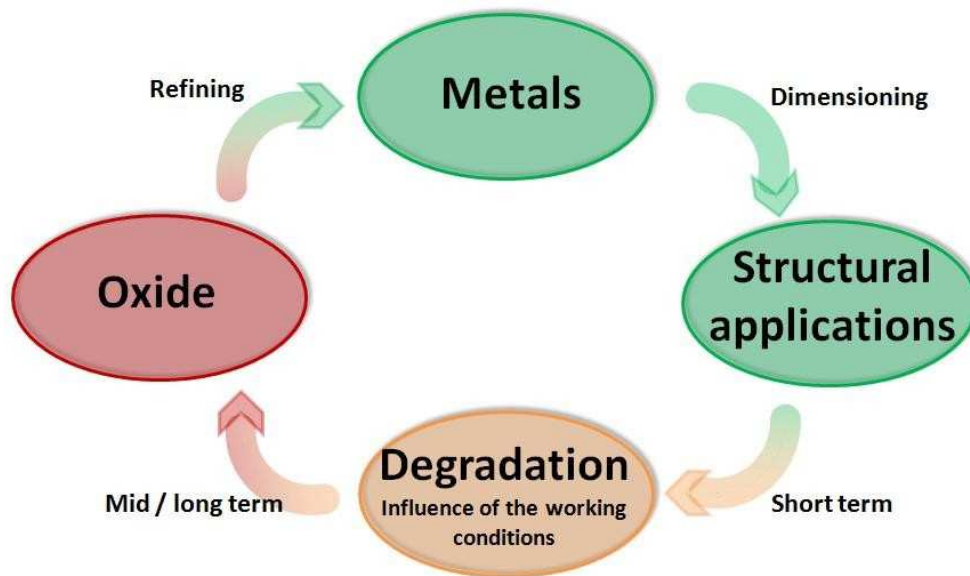


Figure I-1 – Simplified life cycle sketch of the metallic materials.

From a **thermodynamic** point of view, the metallic materials will **corrode** or **oxidize** in wet or in dry atmospheres, following the main mechanisms depicted in *Figure I-2*. The degradation mechanisms are dependent on **electrochemical reactions for the wet corrosion** processes, while **ionic oxidation mechanisms** degrade the materials **for the dry corrosion** processes. After the adsorption and dissociation of the gas species at the gas / solid interface followed by a dissolution process, the first germs of the oxide will develop from the interaction between an anion and a cation. Then this oxide skin will grow homogeneously or not, depending on its nature, which is a direct function of the mechanisms involved.

These reactions depend of the industrial process and technological application with the influence of the **temperature**, which acts as a **catalyst for the solid diffusion mechanisms**. The higher the temperature, the faster the solid diffusion.

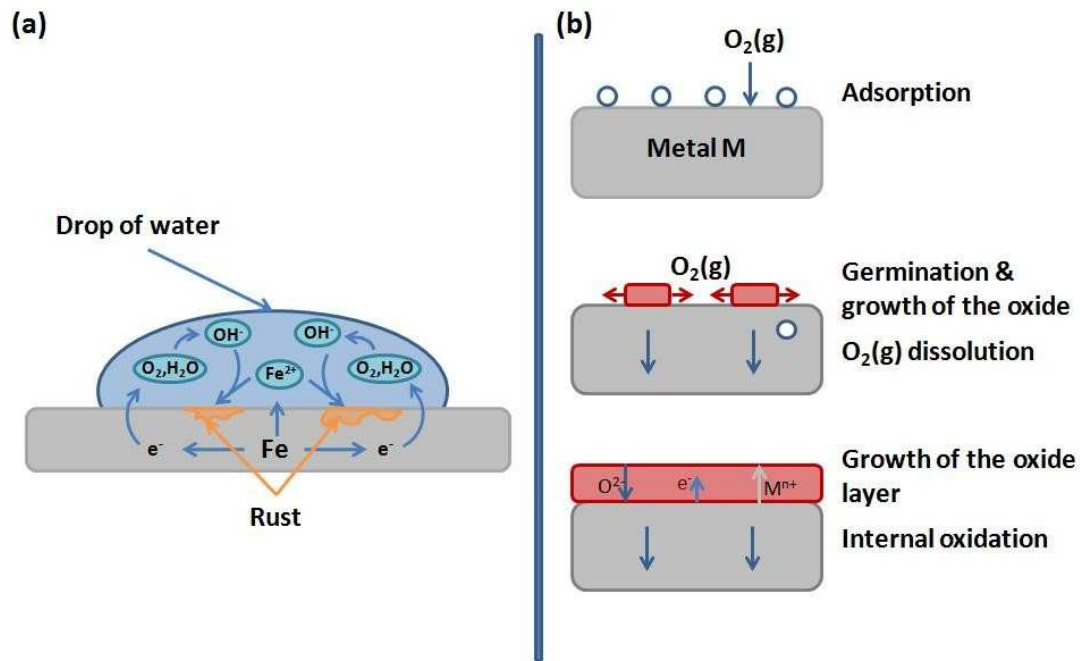


Figure I-2 - Representation of the main (a) corrosion and (b) oxidation mechanisms [1-2].

Those mechanisms rely on the industrial processes themselves, governed by temperature, pressure and environmental influences. Furthermore, from an industrial point of view, they are problematic due to the **modifications of the physico-chemical properties** compared to the initial material. Usually, the cations generated will be dissolved into the liquid phases for the “wet” corrosion processes to form an hydroxide (in most cases). For the “dry” corrosion conditions, a solid oxide layer will form.

In addition to this, **three harmful agents** promote these complex mechanisms **at high temperature**. The influence of the **nature of the gas**, the **molten-salts** and the **molten-metals** contribute to reduce the durability of the materials.

In the case of **turbines**, the **yield** is a function of the gas temperature, which govern the overall performance of the engine. Furthermore, the working **conditions evolve**, i.e. due to variations of the atmosphere, of the cycle of the regime (time and temperature), leading to the **combination of several complex degradation processes**. In order to extend the durability of the materials at high temperatures, those mechanisms have to be understood to **provide solutions to increase lifetime**. Such technical response is usually given by the use of coatings.

II – Materials for gas turbine components.

The application field related to the present work is focused on gas turbines for the aeronautic domain, which include the turbofan, the turbojet and the turboprop. As a representative example of the commercial aircraft, a special attention will be given to the first one, the turbofan engine.

A. The turbofan engine.

a. The element of thrust.

Since many decades **scientific and technological breakthrough** allowed to **improve the efficiency of the engine**, and after many evolutions [3-4], designs of the aero-engines in use are close to the one depicted in *Figure I-3*. **Drawing air in the jet engine** is used to create the aircraft's propulsion. This aspiration is then **separated in two sections**: a cold one in blue colours and a hot one in red colours. From this separation, a direct gas flux exists, which goes directly through the inner elements of the turbine and represent 20% of the air breathed, while an indirect one also exists.

The direct flux is composed of the environmental air, which is compressed by the low and high pressure combustors. Then a mixture of compressed air and kerosene burns in the combustion chamber and the flux expands in the direction of the high and low pressure turbines, respectively HPT and LPT, to be exhausted through the nozzle for providing the thrust.

The indirect flux allows to improve the efficiency of the turbofan by means of a reduction of the temperature imposed to the materials, using turbine blade cooling, to grant higher mechanical resistances. In the meantime, this design allows a noise reduction compared to turbojet engine.

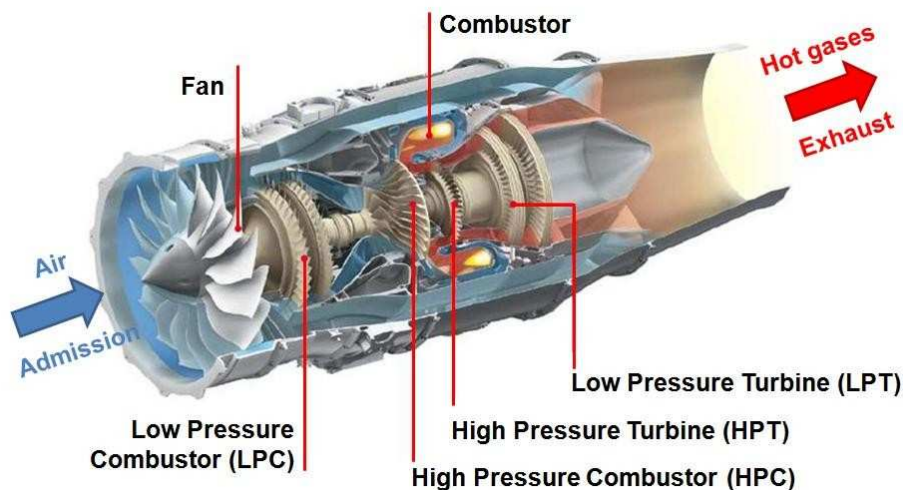


Figure I-3 - Representation of a high-bypass turbofan engine [5].

Because of thermodynamic considerations [3] the **hotter the turbine inlet temperature (TIT)**, the **greater the efficiency** of the overall engine. Therefore the major components of the turbine (nozzle guide vanes –NGVs- and blades) are exposed to a flux of gas coming out from the combustion chamber at very high temperatures ($T \gg 1000^{\circ}\text{C}$) and pressures ($P > 10$ bars). In addition, the blades rotate at high speed to produce the rotation of the compressor through a shaft. The combined effect of **T, P and velocity** results in **highly stressed components**, in particular those placed in the hottest section (HPT) rather than in the LPT one.

The **structure** of the engine has been **optimized** to tailor the different stages using appropriate materials **to answer the limitations implied by the service conditions** as well as the economic ones. In the meantime, this dimensioning is also linked to the progress of the development of the material, which is in constant evolution.

b. Impacts on the choice of the material.

Materials integrity in service conditions is of major interest for **the global performance** of the engine. Since a weight reduction is also sought, **over-dimensioning is unthinkable to realize**, also due to **economic reasons** [6-7]. *Figure I-4* gives an example of the different materials in use for one kind of recent civil engine. One can also note the use of materials with low melting points in the coldest section (engine entrance) with the low-cost composite and Al-based alloys and on the contrary, the ones with high melting points in the hottest parts of the turbine (combustion chamber) with the Ti and Ni-based alloys. This **dimensioning** allows the turbine to support a **full charging in power** using the intrinsic mechanical properties of materials, hence to create the higher efficient energy conversion ratio.

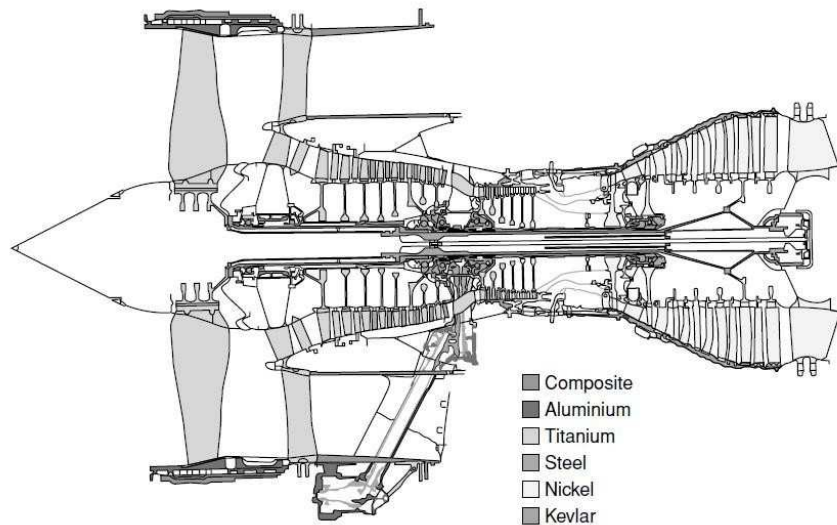


Figure I-4 - Materials in use in the Rolls Royce Trent 800 engine [8].

The global aim is to improve the yield of the turbine and to reduce the consumption of the fuel. Both considerations rely on a **higher TIT**, however this **impacts directly the HPT and LPT sections**. The HPT is subjected to the effect of hot corrosive gases, while the LPT has to face an evolution of the degradation mechanisms imposed by the evolution of the working conditions due to the increase of the temperature, i.e. from hot corrosion processes to oxidation degradation mechanisms. Due to these conditions of stresses (temperature, degradation mechanisms and mechanical solicitations), the **materials themselves constitute the limitation** of the industrial processes.

Progress has been made so far concerning the materials whether from an **elaboration** point of view or from **composition**, to optimize both the microstructure and the mechanical resistance. Typically, the metals in use for the hot sections of the turbines are the superalloys. In the aim of using higher TIT to increase the yield of the turbines, such **structures** have been **extensively studied and upgraded** in order to provide a **better response** to increase their tolerance in regard of **the extreme conditions** imposed by such **high temperature process**.

This evolution has been impaired to an optimization of the chemical composition but also a modification of the metallurgical state of the alloys using solidification processing and air cooling technology of the parts. All these modifications allow the superalloys to tolerate higher solicitations at high temperatures.

B. Superalloys.

Iron (Fe), cobalt (Co) and nickel (Ni) based alloys are well known and each of them have specific properties fitting to several industrial applications. The **iron-based** do not withstand high temperature stresses [3] while the **cobalt-based** are mostly used for the landbased energy plant due to the high density of the cobalt [3]. In comparison, even if the **nickel** is as heavier than the Co, it possesses higher specific modulus [3] as well as higher resistance for extreme conditions compared to the cobalt. This explains why the nickel is mostly used for the hot section parts for turbine components.

a. Nickel-based superalloys.

In essence, their complex chemistry allows the substrate to possess high mechanical properties, which **relies on the γ -Ni / γ' -Ni₃X phases coherence (X=Al, Ta, Ti).**

The nickel-based materials possess a face-centred cubic crystallographic structure (FCC A₁ type), which confers it twelve sliding systems. For sustaining high temperature stresses, structural strengthening has been done by adding elements in solid solution to increase the mechanical resistance of the **γ -Ni matrix**. To this purpose, chromium (Cr), cobalt (Co), molybdenum (Mo), tungsten (W) and sometimes niobium (Nb), vanadium (V) and hafnium (Hf) [9] are used in appropriate proportions but also with respect of their own solubility limitations into the Ni matrix. To increase the mechanical resistance of this phase, an additional strengthening has been done by **precipitating coherently the γ' -Ni₃X phase** (FCC L₁₂ type). By optimizing the elemental contents, further increase of the strengthening is done by the control of the volume ratio of the γ/γ' phases, the size of the precipitates and the interstice of the γ' cuboidal precipitates into the γ matrix for reducing the parametric mismatches [9-11]. This refinement of the structure of the superalloys allows to delay the initiation of cracking during service conditions.

In the meantime, it has to be noted that **detrimental phases** appear **during the service conditions**, like the “Topologically Close-Packed” (TCP) phases. They segregate inside the substrate leading to the formation of brittle phases. Usually, they form by consuming strengthening elements (Cr, W, Ta, Mo), which contributes to **reduce the mechanical properties** of the system in service [12-13]. Impaired with the microstructure of the alloys, low content elements can be present in polycrystalline structure such as carbon (C), boron (B) and zirconium (Zr). They will segregate at the grain boundaries interfaces, i.e. M₂₃C₆ and M₆C carbides, to block the sliding plans at high temperature for avoiding the initiation of failure. Nevertheless, such kind of precipitates has to remain well dispersed enough to maintain the structural stability.

From this elemental basis, which constitutes the **first generation** of Ni-based superalloys, optimization of the chemistry and of the manufacturing (single crystal, directionally solidified, equiaxed) has been done to increase the mechanical resistance required for the turbine application. In addition, all these contributions have been done through several generations of Ni-based superalloys.

b. Compositional and microstructural evolutions.

It has been found that a maximum addition 3 wt.% of rhenium (Re) improved the creep resistance at high temperature [14], giving birth to the **second generation** of Ni-based superalloys. Like the Cr, Mo and W, Re acts as a γ strengtheners but due to the overall strengthening element amount, Cr, Mo and W contents had to be decreased to restrict the formation of the TCP phase.

At the expense of the hot corrosion / oxidation resistance, a **third generation** has been elaborated by increasing the Re content to 6 wt.% with small additions of ruthenium (Ru) in peculiar cases. In the meantime, the Cr content has been decreased again close to 4 wt.%, lowering the hot-corrosion resistance properties. Recently, it has been shown that the use of Ru modified the partition of the

alloying elements between the γ and γ' phases and improved the stability of the global microstructure [14-16].

As a result, a **fourth and fifth generation** of superalloys emerged with higher content of Re and Ru while a **sixth generation** is in development [17]. The additions of these two last elements make the last Ni based superalloys more costly compared to previous generations. They also have higher mechanical resistance properties but the microstructural stability is slightly reduced as well as the oxidation resistance. Basically, **ameliorations are a matter of compromise** between each properties, i.e. a high content of Al decreases the mechanical resistance but highly increases the oxidation resistance also.

The modifications of the chemical compositions, in order to improve the global microstructure integrity and its strengthening, were not the only technical solution to provide ameliorations. **Different manufacturing technologies** have also been developed to slow down the degradation processes of materials, all by **improving the mechanical properties**.

Figure 1-5 represents the microstructural evolutions between the polycrystalline equiaxed structures, to the higher performance single-crystal ones. The **conventional casting equiaxed grain (EQ)** structure possesses multiple grain boundaries, which act as preferential site for crack initiation. In the meantime, this position allows also the carbides to segregate to form brittle phases during the high temperature stresses, even if the use of Hf tends to reduce this diffusion at the grain boundaries considerations [3]. To increase the mechanical limitations due to the grain boundaries, the **directional solidification (DS)** has been used to orientate the crystal in the direction of the stress axis. This allows to increase the creep strength at high temperature by eliminating the grain boundaries normal to the stress direction [3]. Finally, the **single crystal (SX)** morphology has been developed suppressing all the grain boundaries to improve again the high temperature behaviour of the materials [3].

Those two evolutions (chemical and structural) have contributed to increase the performance of the Ni based superalloys as depicted in *Figure 1-6*, which gathers several types of generation of alloys. Nevertheless, one can also note the temperature improvement through the technical solutions provided for the same creep stress applied. In spite of these evolutions, **a trend of stabilization** of the materials performances can be revealed with the **temperatures close to 1100°C** [18]. One of the reasons of such a limitation is the materials themselves while a second reason is the degradation processes. For the first reason, new alloy compositions are developed, i.e. niobium-silicide alloys to enhance high temperature behaviour [19-21].

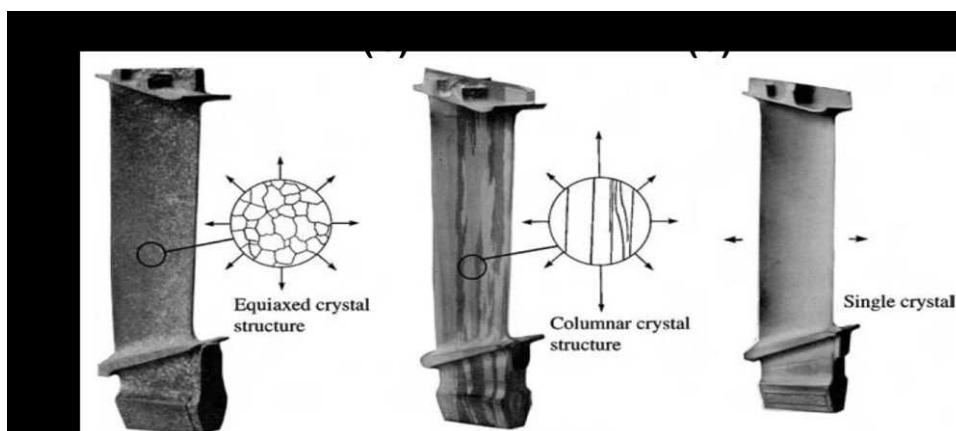


Figure 1-5 - Illustration of the materials evolution for the blade component with (a) the conventional casting equiaxed microstructure and the two directional solidified structures as (b) the columnar grain and (c) the single-crystal structures taken from [8].

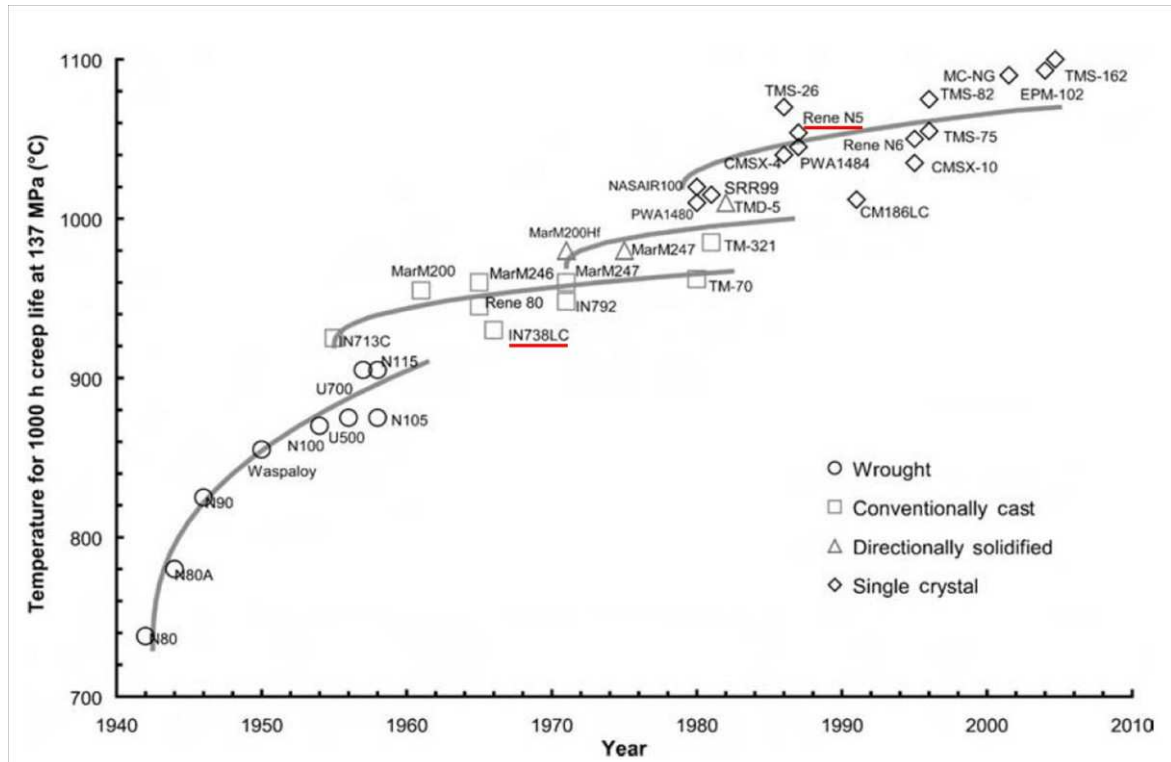


Figure I-6 - Evolution of the high-temperature capability of several superalloys through the evolution of the microstructure [8].

In this study, four superalloys will be investigated. The **INCO 738 LC** (1st generation, LC: Low Carbon content), is investigated as a polycrystalline material, while the **CM 247** (2nd generation) is investigated as directionally solidified one. Finally, two single crystals are also used with the **PWA 1483** and the **René N5** alloys, which have relatively similar compositions except by the absence of titanium (Ti) and presence of reactive elements for the last one.

In the case of the use of the turbomachine where the efficiency of the component is strongly correlated to the service conditions (temperature, pressure and atmosphere), the designs of the turbine as well as the material in use, the **degradation** is a **crossover** between the **corrosion and the oxidation processes** [2]. Considering the industrial processes (T, P, environment, cycling..), a **full understanding** of these mechanisms of the degradation is **essential** to provide technical solutions suitable to improve the **durability** of the engine.

C. Degradation mechanisms in service conditions.

a. Generalities.

During an aircraft flight, the engine has to support **thermal cycling** and transitions between intermediate ($500^{\circ}\text{C} < T < 600^{\circ}\text{C}$) and high temperatures ($T > 900^{\circ}\text{C}$), as illustrated in *Figure I-7 (a)*. These **changes** of conditions imply the modification of the **mechanisms of degradation**, which are function of the temperature, as depicted in *Figure I-7 (b)* [22]. The **low temperature hot corrosion (LTHC - type II)** corresponds to sulphidation processes usually observed for temperatures from 600°C up to 800°C with a maximum corrosion rate located at 700°C , concerns mainly the LPT parts. On the temperature range of 800°C to 950°C , the **high temperature hot corrosion (HTHC - type I)** appears

provided by acidic / base dissolutions of the oxides by the corrosion products with a maximum corrosion rate at 850°C. These thermally activated corrosion phenomena induce severe degradation processes [23], which are detrimental for the overall integrity of the material. For higher temperatures, the **oxidation** processes rule the degradation mechanisms.

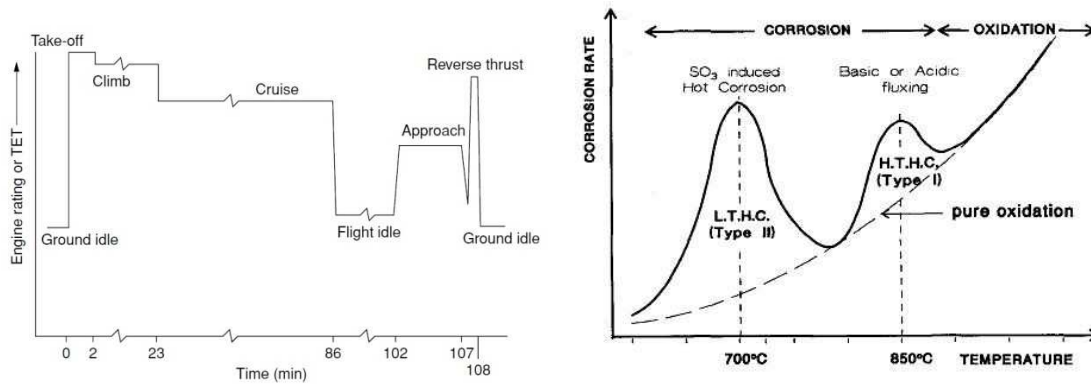


Figure I-7 - Influence of the temperature on the chemical degradation processes with a) a flight cycle representing the temperature variation [8] and b) the chemical degradation processes regarding the applied temperature [24].

Even if the corrosion mechanisms (type II and I) exist at lower temperatures, the dissolution and the formation of the corrosion products will not be studied in this manuscript. This study enrolls at the influence of the **TIT increase** and its influence on the HPT / LPT blades, i.e. the **LPT blades** will be aimed to work at temperature over 900°C. As a consequence, the **main degradation mode** will be **switched** from LTHC and HTHC to oxidation degradation mode.

In spite of the complex degradation mechanisms impaired with the corrosion processes, it is known that, depending of its nature and amount, the alloying elements improve the global mechanical properties but reduces the high temperature oxidation resistance behaviour. The use of coatings allows to enhance this property, but destabilizes the structure by enhancing phase transformation. In the meantime, they promote the appearance of a secondary reaction zone (SRZ), which creates fragile interfaces inside the material, lowering the mechanical properties during service conditions. As an answer to this concern, thermodynamically stable coatings have been recently investigated such as the “EQ coating” [25] and the “ γ / γ' based coating” [26], which disable the SRZ formation by reducing the interdiffusion mechanisms.

Among these phenomena, **other mechanisms of degradation** occur such as the Foreign Object Damage (**FOD**) [27], which can destroy thermal barrier coatings system by impacts, whereas if the TIT increases new degradation modes may appear by the influence of the calcium, magnesium, aluminium silicate (**CMAS**), or of volcanic ashes [28-29]. FOD and CMAS will not be developed in this study, neither the influence of **H₂O** [30], but they have to be mentioned since efficient protective system may encounter all kind of damage during their lifetime. **The present work will therefore focus on the high temperature oxidation** as a main degradation mode for HPT and LPT materials if the TIT increases.

As an introduction to this study, further details are given below about the high-temperature oxides, which shall protect the alloys at different temperature ranges.

b. High temperature oxidation.

Usually, metals or alloys at high temperatures get oxidized under oxygen-containing atmospheres, leading to one or several oxide compounds at the substrate / gas interface. The growth of such chemical species can protect the substrate material as long as this compound provides **an adherent, homogeneous, dense and stable oxide layer** to the surface while it reduces the transport of oxidizing element to the scale. **Only few oxides display such characteristics at high-temperature**, where all the diffusion processes are more activated. As a matter of fact, chromium oxide (chromia: Cr_2O_3), α -aluminium oxide (α -alumina: $\alpha\text{-Al}_2\text{O}_3$) and silicon oxide (silica: SiO_2) exhibit those properties but also possess specificities regarding the temperature range. The growth of such oxides has raised huge interest because of their complexities. In essence, several diffusion processes are involved, i.e. diffusion in volume and / or at the grain boundaries, cationic and / or anionic diffusion processes, which can be revealed, e.g. by SIMS measurements [31 -32]. The effect of alloying elements into the substrate can promote (Ti) or slow down (Y, Zr, La, Hf) [33-34] the oxide formation. The initial surface preparation has also a critical role on the oxide scale formation, i.e. for the development of the α -alumina layer [35-36].

The **chromia** scale constitutes a good hot-corrosion resistant barrier till temperatures of 950°C-1000°C [37]. Nevertheless, depending on the partial pressure of O_2 at high temperature, Cr vapour may form and volatilize while CrO_3 develops for the high O_2 partial pressure ($p\text{O}_2$) thus leading to thinning down of the protective Cr_2O_3 layer [37 -38].

The **silica** is very stable at high temperature but it forms a glassy structure, which does not have good thermal shock resistance [37;39-40].

Finally, the **α -alumina** forms also at high temperature [37;41] as it is the most stable aluminium oxide. Several phase transformation sequences have been reported in the literature impaired with the starting raw material chemical composition [42]. This polymorphic transformation is also impaired with a contraction of the volume in the oxide scale, which can be critical during the establishment of the protective oxide layer [43].

Due to the service conditions in the HPT aero-engine components ($T > 1000^\circ\text{C}$), an α -alumina oxide grows at the surface of the substrate, which implies that the global content of aluminium is slightly lowered from the initial γ' phase. Thus, the thermo-mechanical properties remain unchanged, while the oxidation resistance of the scale decreases, being dependent of the lifetime of the $\alpha\text{-Al}_2\text{O}_3$ layer. Because of the optimization of their chemical composition, the superalloys have to be coated to improve their sustainability [23;44], with respect to limitation of the formation of brittle phases, i.e. Al addition increases the oxidation resistance but decreases the mechanical resistance [45].

III - Industrial protective coatings.

In order to **improve the lifetime** cycle of components subjected to oxidation at high-temperature, several industrial surface systems have been developed by the use of the coating technology. They can be **divided in two classes**, the diffusion coatings provided by chemical vapour deposition (CVD) related techniques and the overlay ones relying on spray related techniques, both aiming at the same purpose: **to provide oxidation resistant layers**. When subjected to high-temperature, an α -alumina layer forms and acts as a physical barrier, therefore to reduce the oxidation kinetics. After the deposition, they are stabilized at high temperature through specific thermal treatments. Such protective coatings are realized by several techniques.

A. The overlay coatings.

This section will only present briefly the MCrAlX coatings, which is a widely used type of coatings. In the MCrAlX, “M” stands for Ni and / or Co while “X” stands for reactive elements, usually yttrium (Y). *Figure I-8* represents the comparison between the different coatings nowadays in use. **MCrAlX** exhibits **improved protective properties** compared to both simple and modified aluminides, whose specificity can be due to the diversity and the flexibility of the process. **Graded structures** are also possible to manufacture as studied in the SMARTCOAT project [46]. For resisting to the high temperature oxidation processes, the chemical composition of such an overlay will be designed between NiCrAlX and NiCoCrAlX structure as represented in *Figure I-8*.

The main difference **between CVD related techniques and MCrAlX** is the nature of the process themselves. **CVD** is a **diffusion process**, which means there is no physical interface between the substrate and the modified layer (β -NiAl).

On the contrary, MCrAlX deposits form an **overlay coating**, which means the existence of a **physical interface** between the substrate and the protective coating. Indeed, the top-coat **chemical composition** has to be tailored to **match the coefficients of thermal expansion (CTE)** as well as insuring good adhesion properties. One has to take in account that the MCrAlX overlay coatings are metallic compounds of similar compositions to the substrate; basically, their CTE mismatch is compatible with the Ni-based superalloys.

The choice of using diffusion coatings instead of the overlay ones depends on the final application for the component as long as the chosen technique allows to withstand the service conditions. Such **lifetime cycle** for the final structure (substrate + oxidation protective layer) is **ruled by interdiffusion processes, its integrity of the oxide scale and its thermo-mechanical behaviour** [47]. These three mechanisms are all strongly temperature dependent. As a matter of fact, the couple time / temperature is the worst degradation parameter since the industrial requirements are to improve the efficiency by increasing the engine temperature in the case of thermomachine application. Of course, a second requirement is to minimize the reparation cost because the adage “time is money” exists at it paroxysm for industrial applications.

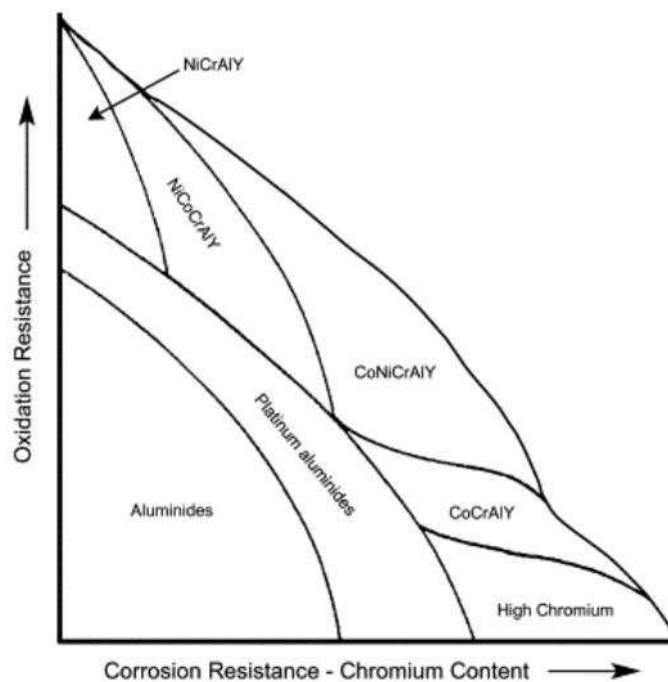


Figure I-8 - Relative oxidation and corrosion resistance of high temperature coating system [46].

In regard of this evolution of the coatings, other solutions have been investigated by the deposition of several metallic elements, already present in the initial superalloy chemical composition. Such process in one step provides an overlay coating on top of the substrate [48], relying on optimum mechanical adhesion properties. From a manufacturing point of view, overlay coatings can be preferred for the energy production landbased turbines compared with the conventional CVD related technique, which relies on chemical diffusion bonding.

B. Aluminide coatings.

The nickel aluminide compounds formed by an **Al enrichment of the substrate** will modify the mechanical and oxidation resistance properties of the outer part of the substrate to protect and provide an aluminium **reservoir** to develop an **exclusive α -Al₂O₃ layer**.

a. The simple aluminide coatings.

This aluminium enrichment is provided by **CVD related techniques**, i.e. CVD, pack cementation or above the pack processes [38]. Both techniques rely on the use of metallic halide activators, which react depending on the temperature range [49] to form **gaseous compounds** of the metal to deposit at the surface of the substrate to coat [38]. In addition to this chemical reaction, diffusion mechanisms are ruled by the aluminium activity, which is a function of the temperature. Two processes are often applied: the **high Al-activity / low temperature** and the **low Al-activity / high temperature** processes. Depending on these coating conditions, the microstructures of the aluminized systems are different in terms of number of zones, which may include alloying and / or refractory element precipitates [49-52]. In fact, aluminium diffusion coatings are based on the Al-Ni binary phase diagram represented in *Figure I-9*. The phase of prime interest is the β -NiAl, mainly due to its greater Al content, hence its oxidation resistance properties. As represented, this intermetallic compound has a high melting point temperature as well as a wide domain of stability.

The **CVD related techniques** are widespread since they allow to obtain an homogeneous layer whether if it is from a thickness point of view or from a compositional one. Such control is possible by the use of gas phases, which permit to treat complex shapes. Patented extensions of this technique have been done, i.e. by Snecma, who developed their own Snecma Vapour Phase Aluminising (SVPA®), using a 70Cr-30Al cement mixed with a NH₄F activator [53]. One of the main drawbacks of those methods is the use such harmful chemicals and the need of a chemical treatment for neutralizing the non-reacted halide activator gases, which will condense at room temperature. Due to their toxic and harmful behaviours, such compounds are problematic for the workers as well as for the environment.

In comparison with the CVD techniques, the **pack-cementation technique** implies the use of powders into which the parts are embedded [38]. These powders may stick to the surface of the parts after treatment and the use of powders require special safety issues.

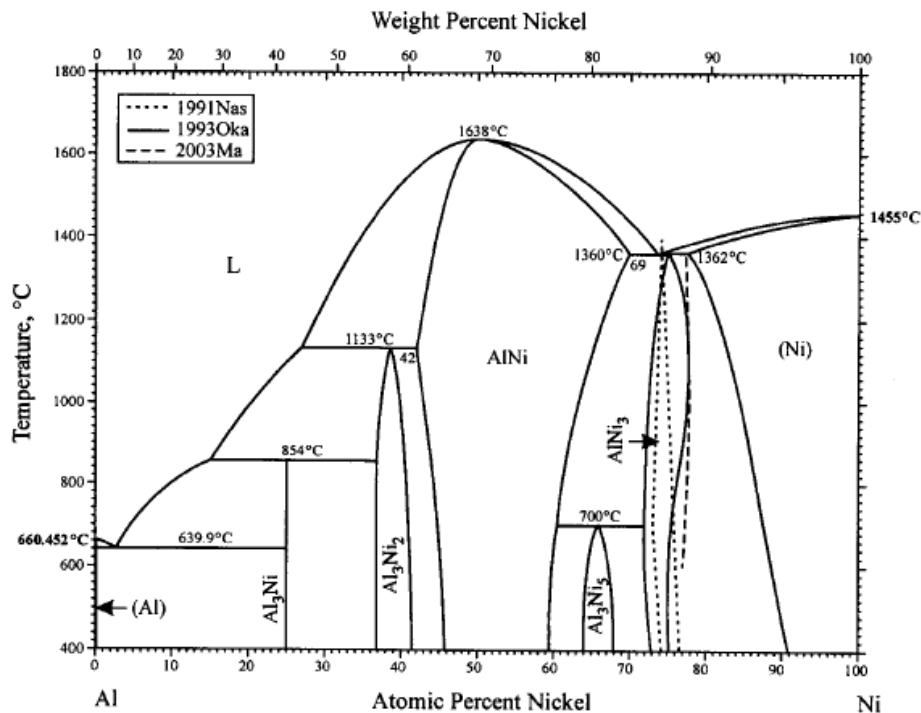


Figure I-9 - Al-Ni binary phase diagram [54].

Two main processes of formation exist for the Ni-based alloys enrichment in Al, as a **function** of the **aluminium chemical activity** of the gaseous phase transporting the Al.

The low activity, high temperature process: The aluminium activity is low enough to obtain a β -NiAl layer with a low Al content (< 50 at.%) in a single step treatment. Such low activity is also promoted by the thermal process temperatures comprised between 1000°C and 1200°C, which allow a preferential outward diffusion of the Ni even if other elements could diffuse in a smaller proportion. The microstructure of the final system is composed of an interdiffusion zone with many TCP phases (refractory elements rich phases) appearing over which an additional layer is formed by the β -NiAl compound [50;55].

The high activity, low temperature process: The aluminium activity is maintained very high at low to moderate temperatures (750°C < T < 800°C). During this aluminizing process, the Al inward diffusion is promoted and a δ -Ni₂Al₃ brittle phase is formed. As a matter of fact, carbides (M_xC_y) precipitation but also alloying element precipitations can occur due to elemental solubility limitation into Al-rich nickel aluminide phases. A second thermal homogenization treatment at higher temperature is required to diffuse the “excess” of Al. This temperature is higher than 1000°C and implies the Ni outward diffusion to allow the formation of the β -NiAl (> 50 at.% Al) phase. The final microstructure is composed of the later β -NiAl phase and precipitates [50;55].

Even if the chemical composition of the substrate is modified, **several mechanisms promote its degradation**. Its integrity is impaired with the **thermo-mechanical service conditions**. The formation of a coherent protective oxide layer will insure the substrate insulation against complex degradation mechanisms of high temperature corrosion at the surface. In another proportion, the thermal cycling will stress the system leading to the oxide scale spall off because of the thermal expansion mismatch between metals and oxide components [56]. From this oxide scale failure, a new part of the substrate will be protected as long as the Al content will be high enough to form a new α -alumina layer, assuming that the growth of the TCP and the SRZ will not be detrimental enough to provoke the failure of the system.

In the same way, the **thermo activated interdiffusion mechanisms** will blend the distribution of the elements between the Al enriched zone and its the initial concentration in the raw material (Ni-based superalloy). Transformation of phases enhanced by diffusion processes lead to additional destabilization of the microstructure, i.e. the Al content will diffuse into the matrix from the β -NiAl to the γ'/γ matrix, which will expel the coarse refractory elements because of a 2.2% volume contraction [57-59], leading to TCP formations [13].

In a smaller proportion, the **formation of a dense, homogeneous and oxidation resistant oxide scale** consumes also the elements of the Al enriched zone, which provides enhanced oxidation resistance properties. The adhesion of a protective scale is of a major interest for the system since transformation of phases and / or polymorphic transformations, i.e. from the transient aluminas to the stable α -alumina [42], induce additional stress at the surface of the system to protect.

For the aero-engine domain, materials are subjected to cyclic oxidation due to the different flight sequences (*Figure I-7 (a)*). In order to provide a successful protection of the substrates, an improvement of these adhesion properties is of a prime interest. Progresses have been done so far by the use of modified aluminide coatings, i.e. by the addition of platinum (Pt) as well as the use of several rare earth elements, which showed an improved oxidation resistance of the systems.

b. The modified aluminide coatings.

i. Pt modified aluminide.

Nowadays, this system is the **most commonly used** system of modified aluminides. Since its first use in 1963 [60], it has been shown [61-62] that Pt modified aluminide provided a **beneficial effect** by increasing by three times the **high temperature lifetime** as well as the **hot corrosion resistance** compared to the simple aluminides. Later on, several studies were carried out to improve the efficiency of the Pt modified aluminide (β -NiAl) whether to provide high temperature oxidation resistance or to be used as bond coats for TBC [63]. Nevertheless, the **Pt phases have to be tailored** to maintain the **mechanical properties** of the global system even if they allow a better adhesion of the alumina oxide scale [64]. Appropriate thermal treatment impaired with a controlled thickness of the coating allows to avoid the formation of detrimental phases, , i.e. the brittle PtAl_2 [55].

Many studies tried to explain the Pt effects on the Al diffusion mechanisms [62;65-66] as well as its influence on the outward diffusion of the refractory elements [67-68]. Pt also reduces the sulphur segregation at the oxide / metal interface by modifying the mechanisms of diffusion at grain boundaries interfaces [69-70].

Overall, Pt modified aluminide coatings allow the substrate to behave better at high temperatures than the simple aluminide components under both isothermal oxidation [71], and cyclic oxidation conditions [72]. Nevertheless, it has to be noted that Pt addition enhances the **rumpling** during cyclic solicitations [73-75].

In spite of all its improvements on the high temperature behaviour, **the use of Pt** will no longer be compatible with the economic situation neither the environmental restrictions. First of all, the formation of (Ni,Pt)Al compound is **patented**, which induce the payment of royalties to use this technology, and in the meantime, platinum is **expensive** [6]. **In addition** to those economic concerns, the Pt is usually **electrodeposited** using amino and / or phosphate compounds, which are **harmful** and incompatible with future norms [76]. Therefore, several attempts to replace Pt have been studied, the most common being the addition of reactive elements (RE).

ii. RE modified aluminide.

The use of the reactive elements (RE) has already shown ameliorations of the high temperature resistance properties for several types of materials (stainless steel, Ni-based superalloys) but their **global effect** is still a subject of **controversy**. Furthermore, their beneficial effects **depend of the**

addition technique [77-79] as well as of their **amount** into the substrate rules the behaviour of the oxidation resistance whether considering isothermal tests [80] or cyclic ones [81]. Despite their controversy effect, they are known to form pegs for keying the protective oxide scale to the underlying metal, prevent the coalescence of vacancies at the oxide scale / metal interface, eliminating the impurity dissociation at the scale / metal interface [82-83]. All these effects induce the **enhancement of the adhesion properties, i.e. of the alumina oxide scales** submitted to the high temperatures oxidation conditions [79-80;84-85]. In the meantime, they **improve creep resistance** by a **controlled dispersion** in volume as alloying elements or as oxide dispersions strengtheners (ODS). Since the studies of Bianco *et al.* [86] and Pint *et al.* [33] who respectively investigated the doping effect of Y_2O_3 and ZrO_2 for the first and Y_2O_3 , La_2O_3 , HfO_2 , TiO_2 , ZrO_2 and Al_2O_3 for the second. In addition to this, they can be used to **stabilize the oxide scale** by mean of their intermediate thermo-mechanical properties compared to the metallic substrates or conventional protective scales (SiO_2 , Cr_2O_3 and Al_2O_3) (Table I-1).

The behaviour of reactive element oxide (REO) - modified aluminide has been more recently studied using Y_2O_3 [87], La_2O_3 [88] and CeO_2 [82;89] compound additions, but the mechanisms involved for the system behaviour are still a matter of controversy regarding the substrate chemical compositions. Nevertheless, on the basis of the surface applied REO technique, the protective effect of a REO electrodeposited film has been recently investigated by Bouchaud *et al.* [90-94], leading to the enhancement of the oxidation resistance behaviour of René N5 aero-engine substrate whether if isothermal oxidation conditions were tested or cyclic ones.

Table I-1 - Density (ρ), coefficient of thermal expansion (α) and thermal conductivity (λ) of several compounds taken from [95]

Compounds	IN-738	SiO_2	Cr_2O_3	Al_2O_3	CeO_2	MgO	Y_2O_3	ZrO_2	HfO ₂	La_2O_3
ρ (g.cm ⁻³)	-	2.2-2.6	5.22	3.86	7.20	3.58	5.03	5.80 - 6.04	9.68	6.51
α (10 ⁻⁶ .K ⁻¹)	17.6	a: 0.5 c: 9.6	9.6	8.9	13.0	13.9	9.3	m: 7.0 t: 12.0	5.86	11.9
λ (W.m ⁻¹ .K ⁻¹)	-	- a: 1.38	-	35.6-39	-	50-72	-	-	1.14	-

a: amorphous, c: crystallized, m: monoclinic, t: tetragonal.

C. Additional protective systems.

In order to limit the effect of the three described degradation mechanisms, additional protective systems may be used **depending on the stages** into the turbine components. Two of them shall be highlighted in the present work; the first allows a temperature insulation of the metallic substrate while the second one is a concept for maintaining the mechanical properties by controlling the interdiffusion mechanisms.

a. Thermal barrier coating.

The gas existing in the combustion chamber, which flows in the direction of the HPT and LPT blades, possesses a temperature close to the melting point of the base materials. Such a condition is critical for maintaining good mechanical properties of the Ni based superalloys. As shown in Figure I-6, a temperature limitation of the material in service conditions exists, even with a processing and manufacturing optimization.

A **thermal barrier coating**, mostly using the EB-PVD process, is deposited on top of the α -alumina oxide scale grown from the aluminized bond-coat β -(Ni,Pt)Al. This layer, usually realized in yttria partially stabilized zirconia (YSZ) [96-97], **reduces the temperature** applied on the metallic parts from the hot gas temperature of about 100-150°C, depending of its thickness. It has to be noted that the EB-PVD deposited layer can also be applied on MCrAlX. Due to the expensive process, this thermal insulation layer is only applied to the first stage of the HPT blades.

The final **TBC system** has different physical properties regarding the thermal expansion coefficients mismatch (*Table I-1*), but the use of a **graded structure** gives rise to an enhancement of the thermal stress resistivity in the meantime than thermo-mechanical stress accommodation. As summarized by Cao *et al.* [56], dilatation compatibility from the metallic substrate including the aluminized bond-coat, the α -alumina thermally grown oxide and the YSZ layer, are necessary to withstand volume expansion and contraction due to thermal cycling. The material of the thermal insulating layer is **permeable to O₂** component, which authorize the **growth of an α -alumina oxide scale** at the metallic substrate outer interface. Due to the growing interest of increasing the TIT, several materials have been studied in order to surpass the yttria stabilized zirconia properties. In spite of many researches, this material is still the most efficient one. Because of its **ceramic nature**, this oxide layer does not degrade by interdiffusion processes but is more sensitive to the CMAS effect as well as the FOD [27-29].

b. Diffusion barriers.

The second option to control the degradation mechanism by maintaining the chemical composition is to **reduce the Al consumption by interdiffusion processes**, but also to prevent the refractory elements to segregate at the substrate / oxide scale interface as well as the TCP formations in the SRZ.

Several groups already investigated such topic [98-102] using the RE element properties. A special attention has to be taken into account since the reactive element introduction method can also destabilize a bit further the substrate equilibrium leading to more precipitations in the SRZ. A recent study in the LaSIE laboratory proposed to use the electrodeposition to apply a rare-earth oxide on top of the Ni-based superalloy to reduce such interdiffusion phenomena [91-92] and will be further investigated in this work.

The use of all those technical solutions allows to improve the Ni based superalloys high temperature oxidation and thermo-mechanical resistances. Besides, the development of additional protective systems, the final design is tailored for both LPT (β -NiAl) and HPT blades (β -(Ni,Pt)Al + YSZ). **In view of a TIT increase, the design of protective system of the LPT blades might change** as it will be discussed in the section V of this chapter.

Furthermore, the industrial normalization orientation changed so far as a cost reduction and less hazardous compounds [76;103] are aimed concerning both workers and the environment itself. In essence, the investment related to the equipment and the efficiency of the processes are the more important drawbacks of these conventional techniques.

The research of new efficient alternatives is of a growing interest for such industrial applications. As a result of those decisions, the use of the slurry technology has been developed, as repairing solution at first and later on as an aluminizing technique for the metallic substrate.

IV – The slurry coating technology.

The evolution of the chemical composition of the slurries follows also the industrial normalization. Paints, slurries are **easily applicable** nevertheless they were not widespread for the aero domain, except for repairing. Nowadays, due to the **flexibility** of the process, a **tailoring** of the elements has been carried out **to provide a better** response regarding several domains of applications, i.e. aeronautics.

A. Definition of a slurry.

As a large definition, a slurry is composed of a suspension of insoluble particles mixed in a liquid phase. It can include a wide range of application domains such as sunscreens [104], concretes [105], photocatalytic materials [106], gel explosives [107], tape casting for ceramic shapes applications [108], plasma spray technology [109], paints [110]... In fact, considering the tailoring of particle sizes dispersed into an appropriate liquid phase, it can have a colloidal behaviour (stable) or possess an unstable character as described by Lerche *et al.* [111]. Instead of reviewing all the different types of slurry, the next sections will focus on the ones designed for the high-temperature protection applications.

B. Commercial slurries and recent orientations.

The slurry technology is known since the 70s since Goward *et al.* [50], Tamarin *et al.* [45] have successfully applied such a paint-like protection to aluminize Ni-based superalloys, while Young *et al.* [112] and Fuhui *et al.* [113] used this deposition technique to realise a silicon enrichment and an yttrium deposition, respectively. Nevertheless, it has to be noted that the group of Goward *et al.* [50] were the first to report, in 1971, the achievement of similar intermetallic microstructures on Ni-based superalloys compared to the aluminizing by gas phase techniques. Even if the slurries were used to provide the high-temperature corrosion protection and / or oxidation protection, these authors did not describe completely the phenomena occurring during the manufacturing processes.

Nowadays, commercial slurry applied coatings offer oxidation protection of the gas turbine hot section part at temperatures up to 1000°C by companies such as Indestructible Paints (UK) [114], Morant GmbH (D) [115], Coating for Industry (USA) [116] and Sermatech (USA) [117]. However, most of the slurries are based either on organic binders, hence releasing volatile organic compounds (VOCs) upon heat treatment or contain phosphates and Cr(VI) species [118] making them hazardous for the workers and polluting for the environment.

Slurries can be fully composed of organic compounds, for instance, based either on poly-ethylene-glycol (PEG) [119] or using polyvinyl acetate resin and methanol as realized by Kirvani *et al.* [120]. Furthermore, the use of water-based binders, i.e. latexes, PEG, polyvinyl alcohol (PVA) has already been documented [121], e.g. in the aim of satisfying the requirements for applications such as tape-casting [122]. Among the organic components, the PVA (*Figure I-10*) is well known for its ability to be used as a binder [123-124], for its water-solubility [122 ;125-126] but also to protect aluminium surfaces by adsorbing on it [127-128], which provides a protection of the Al surfaces (the later are usually passivated before being supplied).

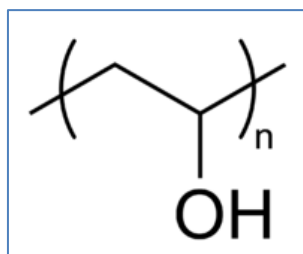


Figure I-10 - Simplified chemical representation of a PVA molecule.

By means of reducing the use of harmful and toxicological compounds, the **PVA** reveals good physico-chemical properties in order to be used as a water-based binder to allow the reduction of the VOCs release and will be therefore employed in this study. However, it has to have appropriate processing behaviour regarding the **aluminizing process**.

C. Processing properties.

From an industrial point of view, the knowledge of the slurry behaviour is required as a key parameter in regard of its performance for the final application as well as for the reproducibility of an efficient process. A control of such lifetime is possible by means of rheological measurements to control the degradation mechanisms. The variation of the viscosity [129-131], by tailoring the water / organic ratio [129;132], is of prime interest for possessing appropriate wettability properties. Such covering of the surface has to be correlated to the existence of a necessary green strength responsible of the homogeneity of the coatings. Furthermore, it has to be noted that the amount of load will also play a role on the viscosity value. From another perspective, the stability of the slurry through time ageing is also important for the industrials. Physico-chemical interactions of the chemical compounds can modify the chemistry of the component inducing also physical modification by modification of the viscosity.

Recently, the group of Murakami *et al.* realized Al-enrichments by powder liquid coatings on high purity iron and on stainless steel [133-134], while the group of Visuttipitukul *et al.* performed it on Ni-based superalloy [135]. More complex shapes are also aluminizable as Omar *et al.* showed by aluminizing nickel foam [136]. The versatility of such a technique, as reported by Armstrong *et al.* [137], allows the user to adapt the slurry properties for various applications, while the number of processing steps has to be reduced as much as possible. In contrast to the slurry method employed by Rasmussen *et al.* [118], who removed the debris crust over the aluminized layer, the PARTICOAT project [138] employs microspherical Al particles to produce hollow alumina spheres at the top coat after diffusion of Al into the substrate. This structured coating shall therefore provide both thermal insulating effect (top coat) and oxidation resistance (diffusion coating).

V – Motivations and concerns of the present study: explanation of the PARTICOAT concept.

Nowadays, due to economic and environmental considerations [76], the turbines service temperatures need to be increased for reducing the fuel consumption and to improve efficiency [139]. Such decision will have an impact on the materials in use for both HPT and LPT components in aero-engine turbine. As a consequence, the metallic parts to protect against high temperature oxidation will be extrapolated to the LPT sections, which will obviously have an impact on the costs. In essence, two options are possible:

- The protective systems will have to be more robust against even more critical time / temperature degradation couple. Basically, the lifetime cycle between each repairing step will have to be improved.
- The numbers of production steps will have to be decreased. As a matter of fact, each manufacturing step for assembling a protective system increase the global cost to provide the protection system.

Another option exists by means of changing the materials due to the limitation of performances of the Ni-based superalloys. The industries want to react as soon as possible to such imposed decision and new material development takes time. This option is not compatible for both short and intermediate terms. The most reasonable option seems to improve or find alternative techniques to develop the high-temperature protection systems by taking inspiration of what is currently in use by the industrials.

In this view, the group of Kolarik *et al.* [140] used successfully the slurry technology on austenitic steel using aluminium microparticles to provide the Al supply as depicted in *Figure I-11*. After an appropriate heat treatment, they observed two major effects. The first one was the formation of an additive layer enriched in Al, which is well known to provide the oxidation resistant property once the substrate will be used at high temperature. The second effect was that the skeleton of the Al microspheres remained on top of the substrate as hollow spheres since the major part of the aluminium content had diffused into the metallic substrate. Furthermore, due to the thermal treatment, the formation of an α -alumina hollow sphere topcoat was realized.

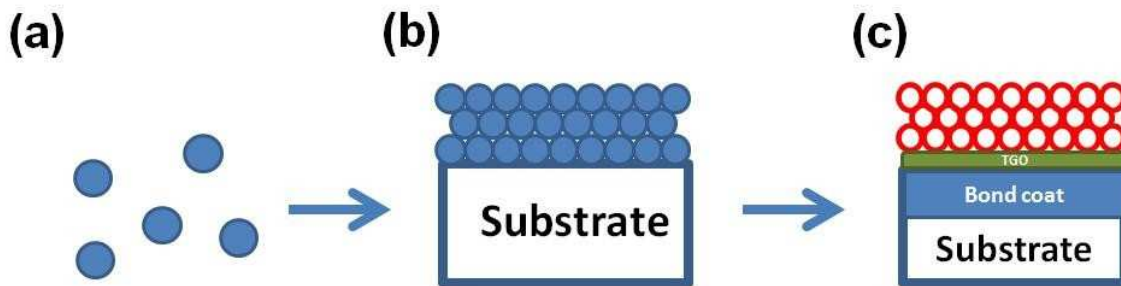


Figure I-11 - Manufacturing step of the PARTICOAT concept with (a) the Al microsphere embedded in a binder before (b) being deposited onto substrate. Afterwards an appropriate thermal treatment, the resulting structure (c) is composed of a bondcoat over which one a thermally grown oxide scale make the connection with a ceramic topcoat foam.

From these two results, one comparison was done. The global system microstructure may resemble the design already in use for the actual HPT blades of the first stage (*Figure I-12(a)*). By comparing the structure obtained by Kolarik *et al.* [140] on austenitic steel and by Montero *et al.* [141] and Pedraza *et al.* [142] on Ni-based substrates (*Figure I-12(b)*) have similarities by means of the Al enriched layer on top of which one ceramic topcoat developed, the later one is expected to provide a thermal insulation resistance due to gas phase insulation.

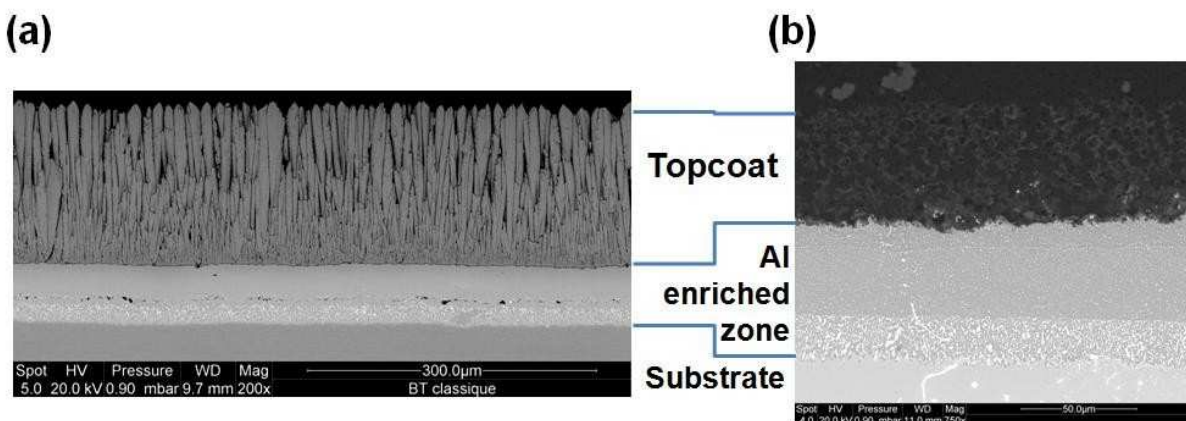


Figure I-12 – Comparison of (a) a conventional TBC system and (b) the system achieved using the slurry coating process.

In view of this quite simple process, several scientific questions as well as industrial ones have emerged regarding the overall capability of the final structure and application on scale. This is the aim of the PARTICOAT project.

This manuscript will explain several characteristics of this process such as the elaboration of the slurry, the formation mechanisms of the intermetallics and finally, the mechanisms of degradation of these coatings at high temperatures both as single coatings and in the presence of a diffusion barrier.

References

- [1] www.gordonengland.co.uk/corrosion.htm
- [2] P. Kofstad, High Temperature Corrosion, Elsevier Applied Science, 1988
- [3] C.T. Sims, N.S. Stoloff, W.C. Hagel, Superalloys II, Wiley, 1987
- [4] M.J. Donachie, S.J. Donachie, Superalloys: A Technical Guide 2nd edition, ASM International 2002
- [5] <http://world.honda.com>
- [6] S. Chevalier, Coût de la corrosion: une approche macro-économique et métallurgique, Corrosion et protection des matériaux à haute températures, Presse des Mines ParisTech 2011
- [7] http://bourse.lesechos.fr/bourse/matieres/matieres_premieres.jsp
- [8] R.C. Reed, The Superalloys: fundamentals and applications, Cambridge University Press (2006)
- [9] P. Caron, T. Khan, Aerospace Science and Technology. 3 (1999) 513
- [10] J.J. Jackson, M.J. Donachie, R.J. Henricks, M. Gell, Metallurgical Transactions A 8(1977) 1615
- [11] A.M. Ges, O. Fornaro, H.A. Palacio, Material Science And Engineering A 458 (2007) 96;
- [12] B. Seiser, R. Drautz, D.G. Pettifor, Acta Materialia 59 (2011) 749
- [13] C.M.F. Rae, M.S. Hook, R.C. Reed, Material Science And Engineering A 396 (2005) 231
- [14] A.C. Yeh, A. Sato, T. Kobayashi, H. Harada, Material Science And Engineering A 490 (2005) 445
- [15] A. Heckl, S. Neumeier, S. Cenanovic, M. Göken, R.F. Singer, Acta Materialia 59 (2011) 6563
- [16] A.C. Yeh, S. Tin, Metallurgical and Materials Transactions A 37A (2006) 2621
- [17] M. Gebura, Materialovy inzinier 2007-2009 ISSN 1337-8953
- [18] D.J. Young, High Temperature Oxidation and Corrosion of Metals, Elsevier Corrosion Series 2008
- [19] S. Drawin, J.F. Justin, High Temperature Materials, Advanced lightweight silicide and nitride based materials for turbo-engine applications, Onera report
- [20] F. Zamoum, T. Benlaharche, N. David, R. Podor, M. Vilasi, Intermetallics 16 (2008) 498
- [21] S. Mathieu, S. Knittel, P. Berthod, S. Mathieu, M. Vilasi, Corrosion Science 60 (2012) 181
- [22] L. Antoni, A. Galerie, Tech. de l'Ingénieur, Corrosion sèche des métaux, cas industriels: dépôts, milieux fondus, M 4 227
- [23] G.W. Goward, Surface and Coatings Technology 108-109 (1998) 73
- [24] R. Streiff, Journal De Physique IV 3 (1993) 17
- [25] K. Kawagishi, A. Sato, H. Harad, High-Temperature Alloys (2008)
- [26] T. Izumi, N. Mu, L. Zhang, B. Gleeson, Surface and Coatings Technology 202 (2007) 628
- [27] D. Nowell, P. Duo, I.F. Stewart, International Journal of Fatigue 25 (2003) 963

- [28] L. Li, N. Hitchman, J. Knapp, J. Thermal Spray Technology 19 (2010) 148;
- [29] J. Wu, H. Guo, Y. Gao, S. Gong, Journal of the European Ceramic Society 31 (2011) 1881
- [30] B. Bouchaud, J. Balmain, F. Pedraza, On the high temperature oxidation resistance of rare-earth oxide coated nickel superalloy exposed to water environments 18th International Corrosion Congress, Perth (2011) 233
- [31] S. Chevalier, F. Desserrey, J.P. Larpin, Oxidation of Metals 64 (2005) 219
- [32] J. Balmain, M.K. Loudjani, A.M. Huntz, Materials Science and Engineering A224 (1997) 97
- [33] B.A. Pint, M. Treska, L.W. Hobbs, Oxidation of Metals 47 (1997) 1
- [34] A.H. Heuer, D.B. Hovie, J.L. Smialek, B. Gleeson, Journal of American Ceramic Society 94 (2011) 146
- [35] M. Mellali, P. Fauchais, A. Griamud, Surface and Coatings Technology 81 (1996) 275
- [36] M. Mellali, A. Grimaud, A.C. Leger, P. Fauchais, J. Lu, Journal of Thermal Spray Technology 6 (1997) 217
- [37] S. Bose, High Temperature Coatings, Elsevier (2007)
- [38] N. Birks, G.H. Meier, F.S. Pettit, Introduction to the high-temperature oxidation of metals second edition, University of Pittsburg 2006
- [39] J. Sehgal, S. Ito, Journal of the American Ceramic Society 81 (1998) 2485
- [40] T. Rouxel, J.C. Sangleboeuf, Journal of Non-Crystalline Solids 271 (2000) 224;
- [41] N. Eisenreich, H. Fietzek, M. Juez-Lorenzo, V. Kolarik, A. Koleczko, V. Weiser, Propellants Explosives Pyrotechnics 29 (2004) 137
- [42] I. Levin, D. Brandon, Journal of the American Ceramic Society 81 (1998) 1995
- [43] J. Favergeon, D. Brancherie, Corrosion et protection des matériaux à haute temperature, Ed. Presses des Mines ParisTech (2011) 205
- [44] M. Schütze, M. Malessa, V. Rohr, T. Weber, Surface and Coatings Technology 201 (2006) 3872
- [45] Y.A. Tamarin, Protective Coatings for Turbine Blades (2002) ASM International
- [46] J.R. Nicholls, N.J. Simms, W.Y. Chan, H.E. Evans, Surface and Coatings Technology 149 (2002) 236
- [47] M.P. Bacos, P. Josso, N. Vialas, D. Poquillon, B. Pieraggi, D. Monceau, J.R. Nicholls, N. Simms, A. Encinas-Oropesa, T. Ericsson, S. Stekovic, Applied Thermal Engineering 24 (2004) 1745
- [48] O. Lavigne, Corrosion et protection des matériaux à haute temperature, Ed. Presses des Mines ParisTech (2011) 317
- [49] F. Pedraza, C. Tuohy, L. Whelan, A.D. Kennedy, Materials Science Forum 461-464 (2004) 305
- [50] G.W. Goward, D.H. Boone, Oxidation of Metals 3 (1971) 475
- [51] D.K. Das, V. Singh, S.V. Joshi, Metallurgical and Materials Transactions A 29 (1998) 2173
- [52] J. Angenete, K. Stiller, E. Bakchinova, Surface and Coatings Technology 176 (2004) 272

- [53] C. Cleach, Elaboration et caractérisation des revêtements en aluminium modifié platine des superalliages base nickel, PhD Thesis, University of Poitiers, France (2000)
- [54] H. Okamoto, Al-Ni (aluminium-nickel), *J. Phase Equilibria and Diffusion* 25 (2004) 394
- [55] D.K. Das, V. Singh, S.V. Joshi, *Metallurgical and Materials Transactions A* 31 (2000) 2037
- [56] X.Q. Cao, R. Vassen, D. Stoeber, *Journal of European Ceramic Society* 24 (2004) 1
- [57] R.C. Pennefather, D.H. Boone, *Surface and Coatings Technology* 76-77 (1995) 47
- [58] V.K. Tolpygo, D.R. Clarke, *Acta Materialia* 52 (2004) 5115
- [59] P.Y. Hou, A.P. Paulikas, B.W. Veal, *Materials at High Temperatures* 22 (2005) 535
- [60] A.T. Cape, US Patent 3, 107175 (1963)
- [61] K. Bungardt, G. Lehnert, H.W. Meinhardt, US Patent 3, 677789 (1972)
- [62] G. Lehnert, H.W. Meinhardt, *Electrodeposition and Surface Treatment* 1 (1973) 189
- [63] E.C. Duderstadt, A.N. Bangalore, US Patent 5238752 (1993)
- [64] Y. Zhang, W.Y. Lee, J.A. Haynes, I.G. Wright, B.A. Pint, K.M. Cooley, P.K. Liaw, *Metallurgical and Materials Transactions A* 30 (1999) 2679
- [65] B. Gleeson, W. Wang, S. Hayashi, D. Sordelet, *Material Science Forum* 461-464 (2004) 213
- [66] E.J. Felten, *Oxidation of Metals* 10 (1976) 23
- [67] M.R. Jackson, J.R. Rairden, *Metallurgical Transaction A* 8 (1977) 1697
- [68] R. Streiff, O. Cerclier, D.H. Boone, *Surface and Coatings Technology* 32 (1987) 111
- [69] B.M. Warnes, D.C. Punola, *Surface and Coatings Technology* 94-95 (1997) 1
- [70] J.A. Haynes, Y. Zhang, W.Y. Lee, B.A. Pint, I. G. Wright, K.M. Cooley, *Elevated temperature coatings: science and technology III* (TMS, USA 1999)
- [71] H.M. Tawancy, N. Sridhar, N.M. Abbas, D. Rickey, *Journal of Materials Science* 35 (2000) 3615
- [72] A. Littner, M. Schütze, *Journal of Corrosion Science and Engineering* 6 (2003) 20
- [73] B. Sudhangshu, *High Temperature Coating*, Elsevier Science & Technology Books 2007
- [74] V.K. Tolpygo, D.R. Clarke, *Acta Materialia* 48 (2000) 3283
- [75] B.A. Pint, S.A. Speakman, C.J. Rawn, Y. Zhang, *Research Summary High-Temperature Applications* (2006) 47
- [76] ACARE report, *European Aeronautics: a vision for 2020* (2001)
- [77] S. Chevalier, *Traitements de surface et nouveaux matériaux: quelles solutions pour lutter contre la dégradation des matériaux à hautes températures?* Ed Universitaire de Dijon (2007)
- [78] C. Choux, *Elaboration et réactivité à hautes température de revêtements d'intermétalliques: applications aux atmosphères complexes*, PhD Thesis, University of Bourgogne, France (2008)

- [79] P.Y. Hou, J. Stringer, *Materials Science and Engineering A202* (1995) 1
- [80] A. Paul, S. Elmrbabet, J.A. Odriozola, *Journal of Alloys and Compounds* 323-324 (2001) 70
- [81] P. Becker, M. Panasko, D.J. Young, *Oxidation of Metals* 64 (2005) 281
- [82] Y. Zhou, X. Peng, F. Wang, *Scripta Materialia* 55 (2006) 1039
- [83] A. Rahmel, M. Schütze, *Oxidation of Metals* 38 (1992) 255
- [84] J.K. Tien, F.S. Pettit, *Metallurgical Transactions* 3 (1972) 1587
- [85] B.A. Pint, *Surface and Coatings Technology* 188-189 (2004) 71
- [86] R. Bianco, R.A. Rapp, *Journal of Electrochemical Society* 140 (1993) 1181
- [87] W. Zhou, Y.G. Zhao, W. Li, B. Tian, S.W. Hu, Q.D. Qin, *Materials Science and Engineering A458* (2007) 34
- [88] X. Peng, T. Li, W.P. Pan, *Scripta Materialia* 44 (2001) 1033
- [89] H. Lui, W. Chen, *Corrosion Science* 49 (2007) 3453
- [90] B. Bouchaud, *Electrosynthèse de nouveaux revêtements à base d'élément de terres rares destinés à accroître la durabilité à hautes températures des matériaux des turbines*, PhD Thesis, University of La Rochelle, France (2009)
- [91] F. Pedraza, B. Bouchaud, J. Balmain, G. Bonnet, J. Menuey, Patent WO 2011/012818 A1
- [92] F. Pedraza, B. Bouchaud, J. Balmain, G. Bonnet, J. Menuey, Patent WO 2011/012819 A1
- [93] F. Pedraza, B. Bouchaud, J. Balmain, G. Bonnet, V. Kolarik, J. Menuey, *Material Science Forum* 696 (2011) 284
- [94] F. Pedraza, B. Bouchaud, J. Balmain, G. Bonnet, J. Menuey, *Material Science Forum* 696 (2011) 278
- [95] W. Martienssen, H. Warlimont, *Handbook of Condensed Matter and Materials Data* (2005) Springer
- [96] R.A. Miller, *Journal of Thermal Spray Technology* 6 (1997) 35
- [97] W. Beele, G. Marijnissen, A. Van Lieshout, *Surface and Coatings Technology* 120-121 (1999) 61
- [98] J. Müller, M. Shierling, E. Zimmermann, D. Neuschütz, *Surface and Coatings Technology* 120-121 (1999) 16
- [99] J.A. Haynes, Y. Zhang, K.M. Cooley, L. Walker, K.S. Reeves, B.A. Pint, *Surface and Coatings Technology* 188-189 (2004) 153
- [100] T. Narita, F. Lang, K.Z. Thosin, T. Yoshioka, T. Izumi, H. Yakuwa, S. Hayashi, *Oxidation of Metals* 68 (2007) 343
- [101] E. Cavaletti, S. Naveos, S. Mercier, P. Josso, M.P. Bacos, D. Monceau, *Surface and Coatings Technology* 204 (2009) 761
- [102] Y. Wang, H. Guo, H. Peng, L. Peng, S. Gong, *Intermetallics* 19 (2011) 191

- [103] REACH report, Official Journal of the European Union (2006) EC. No 1907/2006
- [104] C. Botta, J. Labille, M. Auffan, D. Borschneck, H. Miche, M. Cabié, A. Masion, J. Rose, J.Y. Bottero, *Environmental Pollution* 159 (2011) 1543
- [105] H. Paiva, A. Velosa, P. Cachim, V.M. Ferreira, *Cement and concrete Research* 42 (2012) 607
- [106] Y. Yu, J. Wang, J.F. Pan, *Procedia Engineering* 27 (2012) 448
- [107] L. Guo, W. Song, M. Hu, C. Xie, X. Chen, *Applied Surface Science* 254 (2008) 2413
- [108] O. Burgos-Montes, R. Moreno, *Journal of European Ceramic Society* 29 (2009) 603
- [109] A. Schrijnemakers, S. André, G. Lumay, N. Vandewalle, F. Boschini, R. Cloots, B. Vertruyen, *Journal of the European Ceramic Society* 29 (2009) 2169
- [110] C. Deya, G. Blustein, B. del Amo, R. Romagnoli, *Progress in Organic Coatings* 69 (2010) 1
- [111] D. Lerche, T. Sobisch, *Journal of Dispersion Science and Technology* 32 (2011) 1799
- [112] S.G. Young, D.L. Deadmore, *NASA Technical Memorandum* 79178
- [113] W. Fuhui, L. Hanyi, B. Linxiang, W. Weitao, *Material Science and Engineering A* 121 (1989) 387
- [114] www.indestructible.co.uk
- [115] www.morant-industriereiniger.de
- [116] www.coating4ind.com
- [117] www.sermatech.com
- [118] A.J. Rasmussen, A. Agüero, M. Gutierrez, M.L.J. Östergaard, *Surface and Coatings Technology* 202 (2008) 1479
- [119] V. Kolarik, M. Juez-Lorenzo, H. Fietzek, *Material Science Forum* 696 (2011) 290
- [120] K. Shirvani, M. Saremi, A. Nishikata, T. Tsuru, *Materials Transactions* 43 (2002) 2622
- [121] J.M. LeBeau, Y. Boonyongmaneerat, *Materials Science and Engineering A* 458 (2007) 17
- [122] A. Kristoffersson, E. Roncari, C. Galassi, *Journal of the European Ceramic Society* 18-14 (1998) 2123
- [123] W.P. Yang, S.S. Shyu, E.S. Lee, A.C. Chao, *Materials Chemistry and Physics* 45 (1996) 108
- [124] G. Bertrand, P. Roy, C. Filiatre, C. Coddet, *Chemical Engineering Science* 60 (2005) 95
- [125] J.C.J.F. Tacx, H.M. Schoffeleers, A.G.M. Brands, L. Teuwen, *Polymer* 41 (2000) 947
- [126] J.H. Feng, F. Dogan, *Materials Science and Engineering A* 283 (2000) 56
- [127] S.A. Umoren, O. Ogbobe, P.C. Okafor, E.E. Ebenso, *J. Applied Polymer Sci.* 105 (2007) 3363
- [128] P. Stoyanov, S. Akhter, J.M. White, *Surface and Interface Analysis* 15 (1990) 509
- [129] S. Ananthakumar, A.R.R Menon, K. Prabhakaran, K.G.K. Warriar, *Ceramics International* 27 (2001) 231

- [130] T. Mitsumata, T. Hachiya, K. Nitta, *European Polymer Journal*. 44 (2008) 2574
- [131] U. Teipel, U. Förther-Barth, *Propellants Explosives Pyrotechnics* 26 (2001) 268
- [132] Z. Lei, Z.Ke-Chao, L. Zhi-you, Z. Xiao-yong, *Metal Powder Report* 61-11 (2206) 28
- [133] K. Murakami, N. Nishida, K. Osamura, Y. Tomota, *Acta Materialia* 52 (2004) 1271
- [134] K. Murakami, N. Nishida, K. Osamura, Y. Tomota, T. Suzuki, *Acta Materialia* 52 (2004) 2173
- [135] P. Visuttipitukul, N. Limvanutpong, P. Wangyao, *Materials Transactions* 51 (2010) 982
- [136] H. Omar, D.P. Papadopoulos, S.A. Tsipas, H. Lefakis, *Materials Letters* 63 (2009) 1387
- [137] L.B. Armstrong, K.M. Cooley, L.R. Walker, B.A. Pint, 22nd Annual Conference on Fossil Energy Materials, Pittsburg, PA (2008)
- [138] www.particoat.eu
- [139] T. Korakianitis, D.G. Wilson, *J. of Eng. For gas turbines and power* 116 (1994) 381
- [140] V. Kolarik, M.M. Juez-Lorenzo, M. Anchustegui, H. Fietzek, *Materials Science Forum* 595-598 (2008) 769
- [141] X. Montero, M. Galetz, M. Schütze, *Surface and Coatings Technology* 206 (2011) 1586
- [142] F. Pedraza, M. Mollard, B. Rannou, J. Balmain, B. Bouchaud, G. Bonnet, *Materials Chemistry and Physics* 134 (2012) 700

Chapter II

Experimental methods

This section focuses on giving information and parameters on the materials and the equipments used during this study to investigate the efficiency of the PARTICOAT slurry. The overall techniques allowed a full characterization of the elaboration of the water-based containing Al microparticles slurry as well as the performance of the coating through long term oxidation tests up to 1000h.

Table of contents

I – The substrates.	45
A. The raw materials.....	45
B. The conventional aluminized substrate.	46
II – The PARTICOAT slurries	47
A. The aluminium microspheres.....	47
B. The composition and preparation of the slurries.	48
III – The special design structure.	48
IV – Formation and oxidation tests of the PARTICOAT systems.	49
A. The thermal treatment.	49
B. The isothermal oxidation tests.....	49
V – Physico-chemical characterization of the systems.	50
A. Rheological properties.	50
a. Stability measurements using the Turbiscan® technology.	50
b. Rheometer.....	50
B. Spectroscopic measurements.	50
a. Fourier Transform Infrared (FTIR).	50
b. Raman micro-spectroscopy.....	50
C. Calorimetric measurements.....	51
a. Differential Scanning Calorimetry (DSC).....	51
b. Differential Thermal Analysis (DTA).	51
D. Microscopy analysis.	51
a. Optical observations.....	51
b. Scanning Electron Microscopy (SEM) coupled Energy-Dispersive Spectroscopy (EDS).	51
E. X-Ray Diffraction (XRD).....	52
VI – Thermodynamic modelling.	52
A. Thermocalc® software.....	52
B. DICTRA® software.	53
References.....	54

I – The substrates.

A. The raw materials.

The use of the PARTICOAT slurries was investigated on different types of Ni-based substrates (compositions and microstructures) summarized in *Table II-1*. Three crystal structures will be studied (SX: single crystal, DS: directionally solidified and Equiaxed (polycrystalline)). The two model substrates (pure Ni and the Ni20Cr both in the equiaxed condition) were supplied by Goodfellow. The René N5 superalloy was provided by Snecma, while the PWA 1483, CM 247 and INCO 738 LC were supplied by Siemens. Therefore, using the substrates both the effect of the crystal structure and of compositions can be investigated. Note that the Cr content increases from the model Ni through the superalloys till the Ni20Cr model alloy. As a matter of fact, this alloying element will provide information regarding the PARTICOAT concept feasibility because of its solubility limitation into nickel aluminide phases.

Table II-1 - Data of the chemical compositions (at.%) of the substrate investigated for this study.

Substrate	Ni	Cr	Co	Mo	W	Ta	Nb	Al	Ti	Fe	Mn	Si	Others
Ni	≈100	traces											
Ni20Cr	Bal	20										1.5	
René N5 (SX)	Bal	8.1	8.2	1.3	1.6	2.3	-	14	-	-	-	-	0.07 Hf 1 Re
CM 247 (DS)	Bal	9.3	9.3	0.3	3.1	1.1	-	12	0.9	-	-	-	0.5 Hf
PWA 1483 (DS)	Bal	13.8	9	0.6	1.2	1.6	-	7.8	5	-	-	-	-
INCO 738 (EQ)	Bal	17.6	8.3	1	0.8	0.5	0.5	7.2	4	traces	traces	traces	0.45 Hf

The pure Ni, Ni20Cr and René N5 materials were used as cylindrical coupons of (12.3 ± 0.1) , (12.0 ± 0.1) and (12.0 ± 0.1) mm of diameter, respectively. The PWA 1483, the CM 247 and the INCO 738 LC were cut from plates with a (10 ± 0.1) mm x (15 ± 0.1) mm shape. All the thicknesses of the samples were measured at (2.0 ± 0.1) mm. Before applying the PARTICOAT slurries, the samples were polished to the SiC #180 grade and ultrasonically rinsed in ethanol.

These superalloys were investigated because of their uses for components of turbine (aero or landbased) running at high-temperatures. As a matter of fact, each of them are employed at different temperature regime, i.e. whereas René N5 and PWA 1483 are employed at the first stage of aero-turbine and landbased turbine, respectively CM 247 and INCO 738LC at lower temperature and lower pressure stages [1-4]. This requires the need of high mechanical properties coupled with the use of an appropriate oxidation resistant system, sometimes completed by the deposition of a TBC system (René N5 SX).

The pure nickel and Ni20Cr possess a γ -Ni matrix while the others substrates rely on the existence of the γ / γ' strengthened microstructure. The XRD patterns, depicted on *Figure II-1*, gather the signals of the raw materials analyzed using the Bragg-Brentano configuration. It has to be noted that the SX and DS microstructures should have provided only one signal due to the crystallographic orientation of their respective atomic plans. Indeed, this deviation might be explained by the manufacturing process (cutting and polishing), which can induce strain into the metal, while a second possibility can be the remaining of a past thermal history with the accumulation of stress [5]. Both factors can shift the peaks or reveal other crystallographic plans regarding the XRD technique.

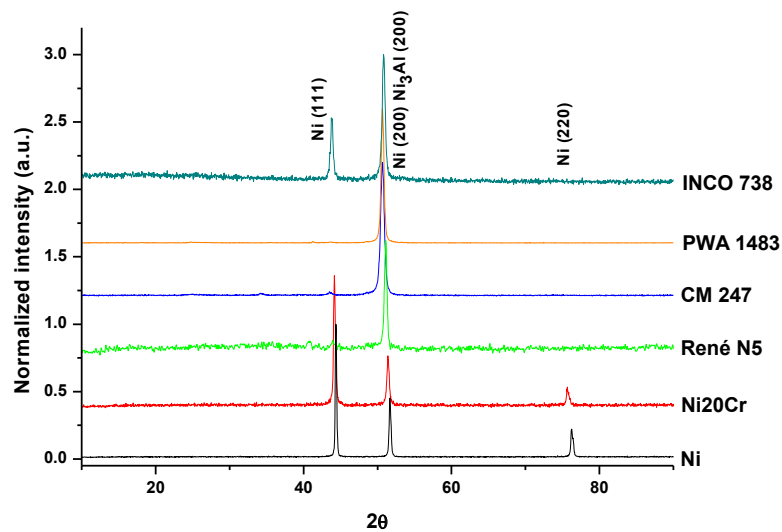


Figure II-1 - XRD patterns of the substrates of interest.

B. The conventional aluminized substrate.

In order to compare the efficiency of the PARTICOAT slurries with the conventional industrial techniques, SVPA[®] aluminization has been manufactured on René N5 (SX) realized at SR Technics (Ireland). The microstructure of the aluminide has been investigated during this study (*Figures II-2*) and compared with the PARTICOAT slurry. The system is composed by an external additive layer grown on top of the initial surface (low activity process = mainly Ni outward diffusion). This zone has an Al enriched content compared to the initial concentration in aluminium of the superalloy, which is 6.2 wt.% in case of René N5. On top of the SVPA[®] deposit, a brighter contrast can be observed, probably resulting of an undiffused Al content during the use of the CVD related technique. The chemical composition of this zone, nearby the surface of the sample, is due to the formation of an aluminium rich β -NiAl while the additive layer is composed of a β -NiAl matrix. *Figure II-3* gathers the phases identified by room temperature XRD measurements, using the θ - 2θ mode, for the samples analyzed after the aluminizing processes. As a result of the Al enrichment process, the formation of a β -NiAl layer is confirmed by the XRD measurement, which allows the enhancement of the oxidation resistance properties at the surface and subsurface of the samples. Underneath this additive layer, an interdiffusion zone (IDZ) containing high amounts of alloying elements forms as a result of the solubility limitation of the refractory element into the NiAl phases [6-7]. In addition to this, a secondary reaction zone (SRZ) forms at the interface of the IDZ / substrate due to the Al inward diffusion into the γ / γ' microstructure. Both zones (IDZ and SRZ) are detrimental for the alloy integrity during long term sollicitation at high temperatures, due to the modification of the mechanical properties (SRZ). In the meantime, the IDZ is known for promoting the initiation of cracks by the accumulation of precipitates, which leads to accelerated degradation mechanisms [7].

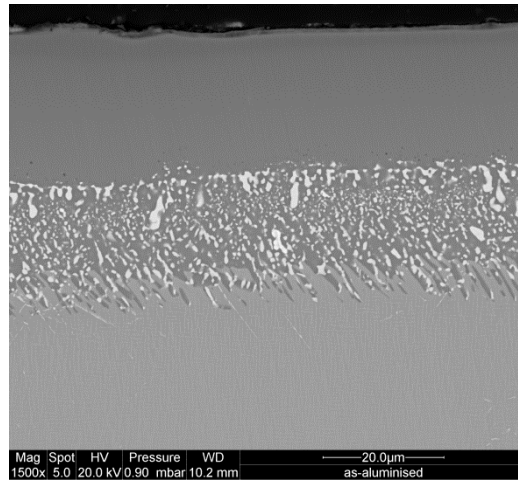


Figure II-2 - Microstructure of the coatings realized on René N5 single crystal (SX) by SVPA® method.

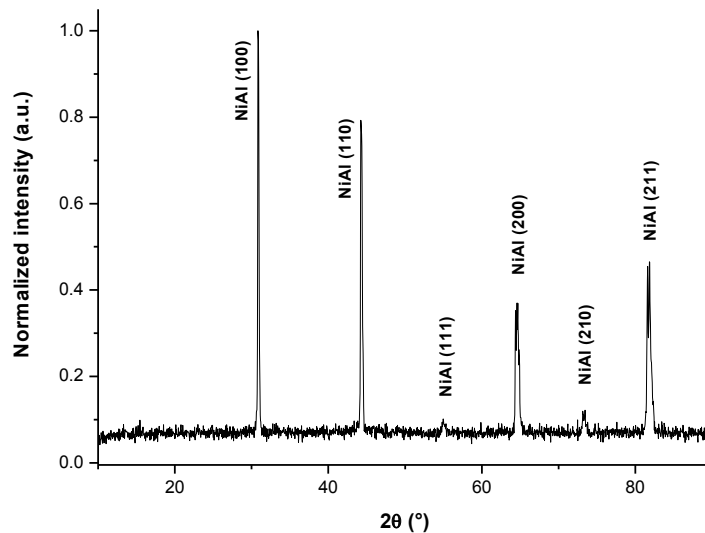


Figure II-3 – XRD measurement of René N5 aluminized by the SVPA® method.

II – The PARTICOAT slurries

Because the PARTICOAT purpose is to find an alternative process to form a full TBC system, this section gives information on the raw material involved in the chemical compositions of the slurries.

A. The aluminium microspheres.

To aluminize the substrates, aluminium microspheres (CAS n°: 7429-90-5) were used as load material for the slurries. Sibthermochim, a Russian project partner, manufactured the powders using the “wire electrical explosion” (WEE) technique [8-10]. Because of the great reactivity of the Al with water [11] and also with air [12], the microspheres were passivated before being supplied to the partners [13-14].

Two Al particle size distributions were used during the experimentations: one centred at 5-6 µm, a second centred at 20 µm. The size of the particles was controlled by granulometric measurements

[13]. The size of the particle may slightly shift the melting temperature of the raw material as demonstrated by Sun *et al.* [15].

B. The composition and preparation of the slurries.

To realize the aluminizing process, the particles were mixed with a binder before being air-sprayed on top of the substrates.

The water-based binder is composed of 90 wt.% of ultra-pure water ($R=18.2 \text{ M}\Omega\cdot\text{cm}^{-1}$) and the remaining 10 wt.% of polyvinyl alcohol (PVA) produced by MERCK (CAS n°: 9002-89-5). The water soluble PVA powder [16] was added to hot water (85°C, close to its glass-transition temperature) under magnetic stirring to allowing the polymer to dissolve faster. Thereafter, the Al particles (load agent) was added to the binder, in a pill box with the proportions gathered in *Table II-2*, and finally shaken mechanically for obtaining the homogeneity. Thereafter, the solutions were stored in the same pill boxes closed with a cap and placed in a hood at room temperature where the natural UV light could induce the degradation of the polymer. The storage conditions are important to highlight in view of investigations on the ageing measurements, which will be detailed in Chapter III, in which a full characterization of the slurries will be presented.

Table II-2 - Mass and mass ratios of the PARTICOAT slurries.

Slurry	Mass (g)			Mass ratio		
	Al	H ₂ O	PVA	H ₂ O/PVA	PVA/Al	H ₂ O/Al
A	1	2.12	0.21	≈10	0.21	2.12
B	1	1.37	0.14	≈10	0.14	1.37
C	1	0.91	0.09	≈10	0.09	0.91

III – The special design structure.

Two designs have been investigated during this research project. The PARTICOAT slurries have been first used (*Figure II-4(a)*) while a special design has also been tested. An electrodeposited cerium oxide based film, placed between the substrate and the slurry (*Figure II-4(b)*), allowed to tailor the coating for strengthening and controlling the interdiffusion mechanisms, respectively.

This technique has been set up during the PhD of B. Bouchaud [17-19]. This study resulted in the formation of a dry mud like layer composed of an oxide of a reactive element deposited on top of aero substrates, i.e. René N5 (SX).

The deposition process has been performed as described by the patents [18-19], using a Potentiostat / Galvanostat PARSTAT 2273 controlled with the software PowerCORR.

The combination of this film followed by the deposition of the PARTICOAT slurry, as represented by *Figure II-4(b)*, should offer the possibility to form a TBC system on top of the rare earth oxide film to increase the durability of the materials at high-temperatures by the creation of a new type of TBC system ($\alpha\text{-Al}_2\text{O}_3$ hollow spheres structure combined with a CeO_2 interlayer).

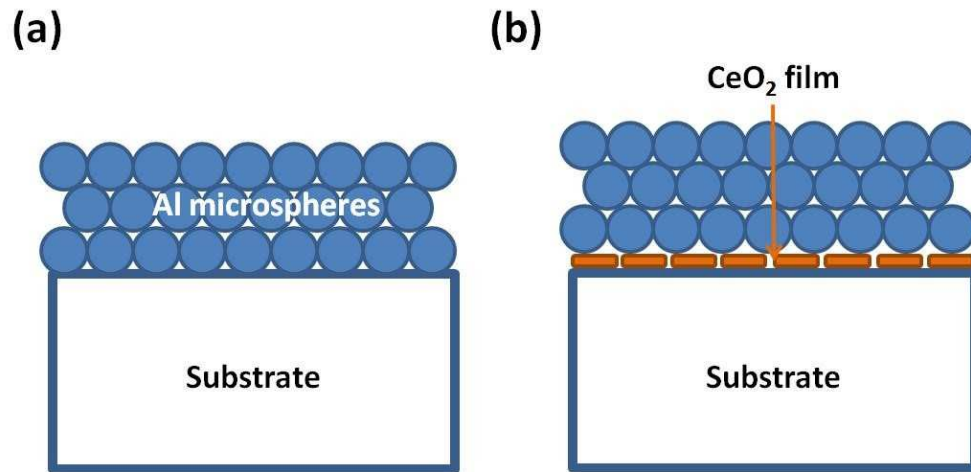


Figure II-4 - Representation of the PARTICOAT structure investigated with (a) the main design with the deposition of the water based containing PVA and Al microspheres and (b) the special design using an electrodeposited film based of cerium oxide.

IV – Formation and oxidation tests of the PARTICOAT systems.

Once the single and graded structures realized, a thermal treatment is applied in view of both short and long term isothermal oxidation measurements.

A. The thermal treatment.

This treatment is composed of three temperature steps, which allow the removal of the binder (400°C – 1h), the Al inward diffusion (700°C – 2h) and finally, the topcoat consolidation and the homogenization of the intermetallic phases of the substrate enriched in Al (1100°C – 2h). The complete heat treatment is carried out in a thermo-gravimetric device (Setaram TGA 92, 10⁻⁶ g of precision) under flowing Ar(g) atmosphere (16 ml.min⁻¹), which contains enough oxidizing species (2 ppm H₂O) to oxidize the aluminium material [20]. In addition, evaporation of the binder shall lead to H₂O vapour and CO₂ that may also oxidize the Al particles. Before treating the samples, a pump allows to realize a partial vacuum (2.10⁻¹ mbar) before filling the chamber with Ar(g).

B. The isothermal oxidation tests.

Thereafter, the heat-treated samples were oxidized for short and long term measurements using a synthetic air atmosphere (80 v.% of N₂ and 20 v.% of O₂) introduced after purging the system with inert Ar(g).

In this view, a Setaram Setsys Evolution 1750 [21], with a precision of 10⁻⁶g, has been used. The chamber of treatment was purged by pumping (10⁻¹ mbar) and filled with Ar(g) till the desired temperature was reached, using a 50°C.min⁻¹ heating rate. Then, the gas was switched to synthetic air (16 ml.min⁻¹) to perform the oxidation tests for 100h.

Isothermal long term measurements have been additionally realized up to 500h and 1000h, using similar conditions (gas flow rate, procedure) using a Pyrox furnace. To extrapolate the short term measurements, the mass evolution was acquired after both oxidation durations using a 10⁻⁵g balance (Precisa XR-205 SM-DR).

V – Physico-chemical characterization of the systems.

A full characterization of the systems of interest has been realized by the use of several techniques. This section gathers the conditions of experiments of each series of investigation.

A. Rheological properties.

From an industrial point of view, the stability of the slurry is critical for its potential application. The need of a tailored concentration of the slurries is essential to aim at process reproducibility. Therefore, adjustment of the Al load against the binder is required as it influences the rheological behaviour.

a. Stability measurements using the Turbiscan® technology.

For this purpose, the Formulation Turbiscan® LAB device has been used to characterize the suspension, with respect of multiple light scattering method [22]. The measurements of the stability are function of three parameters: the size of the particles, the concentration of the particles in solution and the refraction index of the samples. The slurries were analyzed into the small volume crucible (3 ml) provided by Formulation and the samples were analyzed twice a minute every 40 μm , for one hour long at 25°C.

b. Rheometer.

The evolution of the viscosity is also of a major interest to tailor the final application of the PARTICOAT slurries. This parameter can be calculated by the use of a rheometer [23]. To access to this measure, a TA Instrument AR 500 has been used with a 2° cone / plane geometry. The data acquisition has been done at 25°C over an applied shear rate from 0.1s^{-1} to 2500s^{-1} . As a result, the measured shear stress allowed to calculate the values of viscosity, using the TA software Rheology Advantage Data Analysis (v5.7.0).

B. Spectroscopic measurements.

a. Fourier Transform Infrared (FTIR).

The room temperature FTIR measurements were performed in a Thermo Nicolet FTIR Nexus spectrometer using a KBr beamsplitter, a DTGS detector and the ATR accessory. The OMNIC software was employed for the acquisition of the spectra with a 4 cm^{-1} resolution, 128 scans with the autogain mode. The range of wavenumbers analyzed varied from 4000 to 600 cm^{-1} .

b. Raman micro-spectroscopy.

High resolution Raman spectroscopy [24] has been carried out using a Jobin Yvon Horibat LabRam HR, with a monochromatic $\lambda_{\text{He-Ne}}$ ($\lambda=632.817\text{ nm}$) laser source. Settings of magnification were done using three lenses (x10; x50; x100), while filters allow to set up the intensity of the laser beam. The data acquisition was realized by a CCD sensor cooled by a Peltier element. The spectral resolution is of 0.5 cm^{-1} while the lateral resolution is close to $1\text{ }\mu\text{m}$. The measurement in depth is influenced by the sample morphology, the analyzed phases as well as the analyzing conditions [25-26]. Due to these considerations, the interactions depths will be considered effective on 1 to $5\text{ }\mu\text{m}$.

Measurements have been done with the x50 lens, running two ranges of frequency numbers on a $200\text{ cm}^{-1} < \nu < 1200\text{ cm}^{-1}$ interval. The LabSpec software (v5.58.25) was used for the treatment of the data and compared afterwards to the data from the literature or from the RRUFF database of spectra [27].

C. Calorimetric measurements.

Two calorimetric devices have been used, regarding their temperature ranges for the considered investigations. Both techniques utilize the same principles for the detection of thermal events happening to the samples. The variation of energy is measured between a sample and a reference by mean of acquiring the variation of energy consumption for activating the physico-chemical transformation of the samples (glass transition, melting, partial / full decomposition, oxidation, nitridation...).

a. Differential Scanning Calorimetry (DSC).

The DSC analyses [28] have been carried out using a TA Instruments DSC Q100. The measurements were performed in flowing N₂ gas (50 ml.min⁻¹) between 20°C to 550°C, using a 10°C.min⁻¹ heating ramp and analyzed with the software Universal Analysis 2000 (v4.5.0.5). Despite flowing N₂(g) can nitride Al, the pressure required to produce nitridation is about five times greater than that for oxidation [29-30] and therefore nitridation reactions were not expected. The dispersion size of the particles analyzed was centred at 6 µm.

b. Differential Thermal Analysis (DTA).

DTA investigations [31] have been done from 20°C up to 1100°C using a Netzsch STA 409 C/CD. Measurements were performed using a small (5-6 µm) and a coarser (20 µm) average particle size of Al, under flowing Ar gas (120 ml.min⁻¹), between 20°C and 1100°C with a 10°C.min⁻¹ heating ramp and a cooling ramp of 50°C.min⁻¹. The tiny amounts of O₂ (2 ppm) arising from the Ar gas and the oxidative species from the decomposition of the slurries allowed to oxidize the Al surfaces.

D. Microscopy analysis.

a. Optical observations.

The homogeneity of the surfaces of the sample was observed using an optical stereo microscope Leica M165C. Both surfaces of the PARTICOAT topcoat and cross-sections of the samples were observed before electron microscopy observations, which allow higher magnifications as well as other observation modes (back-scattering, elemental quantification...).

b. Scanning Electron Microscopy (SEM) coupled Energy-Dispersive Spectroscopy (EDS).

Two scanning electron microscopes, coupled to their respective energy dispersive spectrometers, were used to characterize the surfaces and cross-sections of the samples. Observations were done using both secondary electron (SE) and backscattering electron (BSE) modes, depending of the information needed [32].

The SE mode provides information on the topology of the samples. In contrast, the BSE mode gives information on the atomic weight of the elements, which allows to obtain information of the repartition of the chemical elements through the spatial dimensions (X; Y) of the samples.

The EDS measurements allow the semi-quantification of the chemical composition of the analyzed area (1 µm³), relying on the principles of the diffraction of the X-ray. It has to be noted that elements with a light atomic weight, i.e. hydrogen (H) cannot be quantified using this technique. The EDS measurements can be used as area, as spot analysis or to perform X-ray maps of the area of interest, the later being mainly used for the observations of the cross-sections.

To perform these analyses, a field emission gun electron microscope running under environmental mode (FEI QUANTA 200F coupled with an EDAX module) has been used for the surface analyses, while a tungsten filament electron microscope (JEOL 5410 LV coupled with an Oxford module) running under high-vacuum conditions, allowed to characterize the cross-sections of the samples. The use of the environmental mode allows to observe low conductive surfaces, i.e. ceramic oxides,

while high-vacuum conditions imply a gold sputtering (Cressington Sputter Coater 108 Auto) to conduct the electrons, and avoid the accumulation of load due to the use of the electrons. To characterize the cross-sections, the samples were embedded into a polymeric resin and then mechanically polished to the 1 μm grade using a paste containing diamond suspension.

The settings of both microscopes were 20 kV, a spot size of 3.6 with a working distance of 10 mm for the FEI QUANTA, while the measuring conditions of the JEOL were 20 kV, a spot size of 7-8 with a working distance of 20 mm.

E. X-Ray Diffraction (XRD).

In view to analyze the intermetallics and the ceramic compounds present in the samples, room temperature XRD measurements [33] have been done to characterize the phases contained into the substrates. The analyses of the compounds were realized using the softwares DIFFRAC^{plus} to allow a comparison with the JCPDS database of compounds (Joint Committee Powder Diffraction files System).

Post-mortem measurements have been carried out at the University of La Rochelle using a Bruker AXS D8 with a $\lambda_{\text{Cu}} \text{K}\alpha_1$ wavelength (0.15406 nm). For these purposes, 5° grazing incidence (asymmetrical mode) and a symmetric (Bragg-Brentano) mode were employed. The first one allows to collect information from the uppermost surface of the sample while the second allows to penetrate deeper into the bulk [34]. As a matter of fact, the penetration depth of the X-ray wavelength depends of the incidental angle, the phases of the samples and the atmosphere in which the measure is done, i.e. air, nitrogen, argon... . The XRD patterns were acquired for a 2 θ range between 10° and 90°, both with a step size of 0.02 acquired for 4s.

VI – Thermodynamic modelling.

In order to provide information on the stability of the systems, on the formation of intermetallic compounds as well as modelling the evolution of the phases for estimating the lifetime of the systems, softwares based on the use of the thermodynamic principles have been used.

A. Thermocalc[®] software.

Phase diagrams of binary and ternary systems have been assessed using the Thermocalc[®] software [35] coupled with the TCBIN [36] database for the binary phase diagrams, while TCNi5 [37] databases has been used for binary and ternary phase diagrams to allow a full calculation of the phases of interest.

From the latter ternary phase diagrams, isopleths systems were carried out plotting the effect of the temperature influence against the variation of the Al content. Hence, the use of this data allows to calculate phase stability domains regarding the complex composition of commercial superalloy material. Two systems have been considered by the modelling of the influence of the Al_xCr_y compounds on the PARTICOAT aluminizing process, while the TCP phases have also been integrated into the modelization.

The Thermocalc[®] module allows to perform calculation for predicting the thermodynamic equilibria of the systems, which means that the time is not included for those modelling purposes. Therefore, the DICTRA[®] software has been used to include the study of the diffusion mechanisms in these systems.

B. DICTRA® software.

The DICTRA® software shares its source code with the ThermoCalc® software, including the mechanism of diffusion [35]. It uses the same databases for the estimation of the phases of interest using the TCNi5 database coupled with a mobility database appended by the use of the MOBNI2 database [38]. Due to the different possibility of modelling, only the Al enrichment and the isothermal diffusion mechanisms will be investigated. In this view, the quantity of aluminium contained into the topcoat has been estimated to be assimilated as a bulk material as depicted by *Figure II-5(a)* and *Figure II-5(b)*, respectively. Basically, the system to model corresponds to an Al bulk material deposited on top of a Ni-based substrate (pure Ni or superalloy).

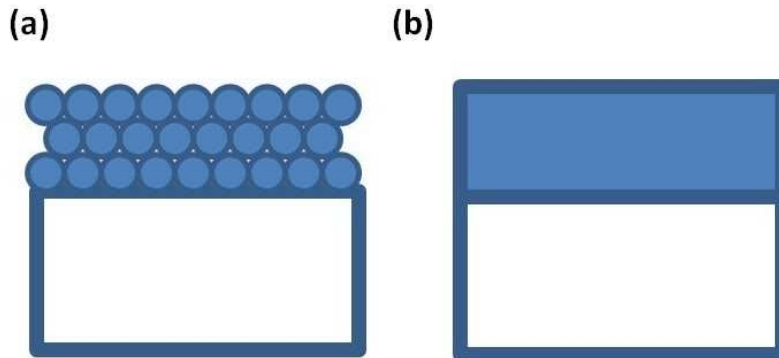


Figure II-5 - Estimation of (a) the topcoat of Al microparticles as (b) a bulk material with an equivalent amount of Al for the DICTRA modelling purposes.

Once the system is defined, the thermo-activated diffusion mechanisms induce the mobility of the atomic species into both bulks as represented by *Figure II-6*. From these assumptions, the PARTICOAT thermal treatment can be tailored and modelled as well as the short and long terms isothermal oxidation experiments for predicting the lifetime of the systems by means of the β -NiAl phase consumption.

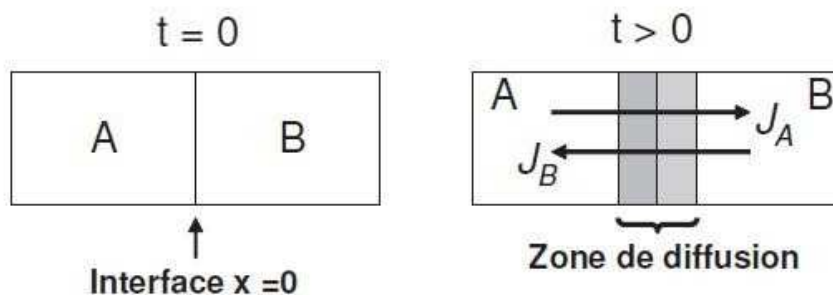


Figure II-6 - Diffusion coupled involved for a binary system (a) before thermal treatment and (b) during the thermal treatment.

References

- [1] National Aeronautics and Space Administration (NASA), NASA/TM – 2007 – 214479; Siemens, private communication (2010)
- [2] D.M. Shah, A. Cetel, *Superalloys 2000* (2000) 295
- [3] A. Pfennig, B. Fedelich, *Corrosion Science* 50 (2008) 2484
- [4] P.W. Schilke, GE Energy, *Advanced Gas Turbine Materials and Coatings*, (2004) GER-3569G
- [5] J. Favergeon, D. Brancherie, *Corrosion et protection des matériaux à haute température*, Ed. Presses des Mines ParisTech (2011) 205
- [6] C.C. Jia, K. Ishida, T. Nishizawa, *Metallurgical and Materials Transaction A* 25 (1994) 473
- [7] C.M.F. Rae, M.S. Hook, R.C. Reed, *Materials Science and Engineering A* 396 (2005) 231
- [8] A.A. Gromov, A. Ilyin, U. Förter-Barth, U. Teipel, *Propellants Explosives Pyrotechnics* 31 (2006) 401
- [9] R. Sarathi, T.K. Sindhu, S.R. Chakravarthy, *Materials Characterization* 58 (2007) 148
- [10] Y.F. Ivanov, M.N. Osmonoliev, V.S. Sedoi, V.A. Arkhipov, S.S. Bondarchuk, A.B. Vorozhstov, A.G. Korotkikh, V.T. Kuznetsov, *Propellants Explosives Pyrotechnics* 31 (2006) 401
- [11] G.A. Risha, S.F. Son, R.A. Yetter, V. Yang, B.C. Tappan, *Proceedings of the Combustion Institute* 31 (2007) 2029
- [12] E.L. Dreizin, *Progress in Energy and Combustion Science* 35 (2009) 141
- [13] PARTICOAT, internal communication (2008)
- [14] A.A. Gromov, Y.I. Strokova, U. Telpel, *Chemical Engineering & Technology* (2009) 1049
- [15] J. Sun, S.L. Simon, *Thermochimica Acta* 463 (2007) 32
- [16] J.M. LeBeau, Y. Boonyongmaneerat, *Materials Science and Engineering A* 458 (2007) 17
- [17] B. Bouchaud, *Electrosynthèse de nouveaux revêtements à base d'élément de terres rares destinés à accroître la durabilité à hautes températures des matériaux des turbines*, PhD Thesis, University of La Rochelle, France (2009)
- [18] F. Pedraza, B. Bouchaud, J. Balmain, G. Bonnet, J. Menuey, Patent WO 2011/012818 A1
- [19] F. Pedraza, B. Bouchaud, J. Balmain, G. Bonnet, J. Menuey, Patent WO 2011/012819 A1
- [20] L.P.H. Leurgens, W.G. Sloof, F.D. Tichelaar, E.J. Mitemejer, *Thin Solid Films* 418 (2002) 89
- [21] www.setaram.fr/SETSYS-Evolution-TGA-fr.htm
- [22] www.formulaction.com
- [23] D. Doraiswamy, *The Origins of Rheology: A Short Historical Excursion*, DuPont iTechnologies (note)
- [24] portal.acs.org: C.V. Raman: The Raman Effect, Indian Association for the Cultivation of Science (1998)

- [25] S. Guo, R.I. Todd, *Journal of European Ceramic Society* 30 (2010) 641
- [26] S. Guo, A. Limpichaipanit, R.I. Todd, *Journal of European Ceramic Society* 31 (2011) 97
- [27] rruff.info
- [28] P. Gabbott, *Principles and Applications of Thermal Analysis*, Blackwell Publishing, (2008)
- [29] T. Okada, M. Toriyama, S. Kanzaki, *Journal of Materials Science* 35 (2000) 3105
- [30] N. Renevier, T. Czerwec, A. Billard, J. von Stebut, H. Michel, *Surface and Coatings Technology* 116-119 (1999) 380
- [31] H.K.D.H. Bhadeshia, *Thermal Analysis Techniques*, University of Cambridge, Materials Science and Technology. www.msn.cam.ac.uk/phase-trans/2002/Thermal1.pdf
- [32] R.F. Egerton, *Physical Principles of Electron Microscopy*, Springer (2005) 125
- [33] K. Janssens, *Comprehensive Analytical Chemistry XLII* (2004) Chap 4: 129
- [34] B. Panicaud, J.M. Brossard, unpublished result
- [35] J.O. Andersson, T. Helander, L. Höglund, P. Shi, B. Sundman, *Calphad* 26 (2002) 273
- [36] www.thermocalc.com
- [37] http://www.thermocalc.se/res/pdfDBD/DBD_TCNI5-2.pdf
- [38] http://www.thermocalc.se/res/pdfDBD/DBD_MOBNi2-2.pdf

Chapter III

Elaboration and characterization of a water-based slurry containing PVA and Al microspheres for aluminizing purposes

In this chapter, the main goal is to characterize the slurry in its as-prepared state and their evolutions with time and temperature. In this sense, the rheological properties are studied first through sedimentation tests and steady shear flow measurements. The analysis of the transformations occurring into the slurry systems is monitored using FTIR, DSC and DTA-TGA measurements, at room temperature, up to 550°C and up to 1100°C, respectively. Each measurement has been done through an ageing process with time, up to nine days. Finally, wettability tests are performed to investigate the interaction between the substrate surface with the slurries. These tests allow to observe the viability of the application from an industrial point of view.

Table of contents

I. Rheological behaviour.....	59
A. Composition of the slurries and ageing phenomena.....	59
B. Rheological behaviour of the slurry.....	59
a. Sedimentation characterization of the slurries.....	59
b. Viscosity measurements.....	63
II. Physico-chemical properties of the slurry.....	65
A. Room temperature properties.....	66
B. Thermal annealing till the melting point of Al.....	67
C. Thermal annealing over the melting point of Al.....	72
III. Drying of the slurry.....	74
Summary and outlook.....	76
References.....	78

I. Rheological behaviour.

A. Composition of the slurries and ageing phenomena.

The solutions were prepared with Al microparticles produced by the wire-explosion technique [1] by Sibthermochim (Russia). The binder was composed of 90 wt.% of deionized water ($R=18.2 \text{ M}\Omega\cdot\text{cm}$) and the remaining 10 wt.% of polyvinyl alcohol (PVA) produced by MERCK. The compositions of three investigated slurries are gathered in the *Table III-1*. These quantities were chosen because of the viscosity purposes already tested during a previous study done by M. Mollard [2]. Each solution was analyzed under the same experimental conditions; the freshly prepared solution corresponding to the elaboration day (t_0) and the aged solutions for one day (t_1), two days (t_2), five days (t_5) and nine days (t_9) afterwards. The PVA raw material is analyzed at the same time as the slurries in order to compare the binder with and without the metallic load.

Table III-1 – Composition of investigated slurries.

Slurry	Mass (g)			Mass ratio		
	Al	H ₂ O	PVA	H ₂ O/PVA	PVA/Al	H ₂ O/Al
A (30 wt.% Al)	1	2.12	0.21	≈10	0.21	2.12
B (40 wt.% Al)	1	1.37	0.14	≈10	0.14	1.37
C (50 wt.% Al)	1	0.91	0.09	≈10	0.09	0.91

Since the solution is composed of three components, the rheological characterization is required to optimize the use of this slurry regarding the deposition technique. Stability measurements at room temperature have been carried out using multiple light scattering method (Turbiscan® LAB) [3] to monitor the destabilization phenomenon into the slurries while viscosity values have been acquired using a rheometer, both with 5-6 μm Al particle size dispersion.

B. Rheological behaviour of the slurry.

a. Sedimentation characterization of the slurries.

The stability of the slurries is of prime interest to allow the deposition process to be versatile. For this purpose, the destabilisation process has been monitored focussing on the sedimentation phenomenon of the metallic loads [4]. Several parameters allow to characterize such behaviour as described by the Stokes equations [5]. As a matter of fact, the size of the particles, the density of the binder, the load content and the shapes of the loads will contribute to modify the sedimentation phenomenon and rheological properties. As an example, *Figure III-1* depicts the evolution of the slurry A destabilization measurement realized on the as-prepared solution. The sample has been scanned on its whole area of interest, every two minutes as represented by the overlapping of each monochromatic line, up one hour. As a result, the evolution of the backscattering profile indicates the phenomena occurring in the crucible with respect of the reflecting element position.

At the top of the crucible, the decrease of the backscattered signal confirms the decrease of the concentration of the particles with time, while the same signal intensity increases at the bottom of the crucible. In essence, these phenomena are related to the displacements of the reflecting raw material (Al metallic load) into the crucible. This type of evolution is characteristic of the clarification and the sedimentation processes happening at the top and the bottom of the crucible, respectively. The evolution of the backscattered signal is characterized by its variation on the X-axis as well as on the Y-axis. The first axis gives information on the clarification / sedimentation front positions, while the second provides information on the load concentrations into the binder. Both values are acquired at a defined position into the crucible and a defined time for the experiment. In addition, one has to note that both phenomena have several points of inflexion as can be seen for the

sedimentation front at the bottom of the sample, which gathers three peaks highlighted by the red darts on *Figure III-1*. This variation is probably due to the heterogeneity of the particles dispersion range used for the measurements. As assumed from the derived Stokes law equation (*Equation III-1*), coarser particles sediment faster than the smallest ones. This equation describes the behaviour of a falling cloud of spheres in a Newtonian fluid [5], derived from the Stokes law. The evolution of the viscosity (η) is a function of the density of the solid load (ρ_s), the density of the liquid phase (ρ_l), the gravity acceleration term (g), the size of the particles (a) and the sedimentation speed (ω).

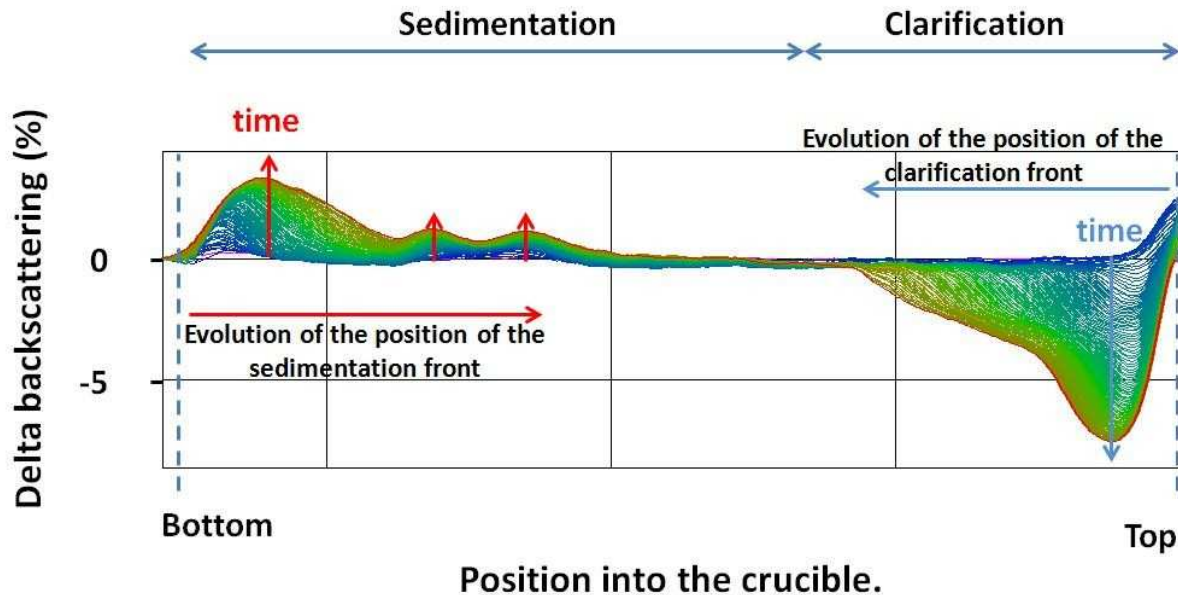


Figure III-1 - Backscattering variations as a function of the position into the sample, through time measurement (0 - 60 min) for the slurry A for its elaboration day.

$$\eta = \frac{2(\rho_s - \rho_l)ga^2}{9\omega} (1 - \phi)^{4 \pm 0.75} \quad \text{Equation <III-1>}$$

As a result of these considerations, the destabilization process is characterized by the evolution of its intensification rate (noted I_{xy} with x the ageing time and y the slurry) (*Figure III-2(a)*) as well as of its thickening rate (noted T_{xy} with x the ageing time and y the slurry) (*Figure III-2(b)*). In order to calculate these values, a full width at half maximum method is employed to quantify the densification of the sediment as well as its thickening. From *Figure III-2(b)*, the intensity and the thickness exhibit specific growth rates of $0.04 \text{ \%} \cdot \text{min}^{-1}$ and $0.05 \text{ mm} \cdot \text{min}^{-1}$, respectively. But as observed from *Figure III-2(b)*, such method is not successful since the slope of the sediment thickness front is nil in a first time while it has a value of $0.05 \text{ mm} \cdot \text{min}^{-1}$ for longer measuring times. From this observation, a two step characterization has been used to analyze the samples for short term ($t < 10 \text{ min}$) as well as for longer time intervals ($10 \text{ min} < t < 60 \text{ min}$), using the most important peak of the sediment. Even if this peak will not be well attributed to a centred particle size because of our particle dispersions, this signal is representative of the global slurry behaviour.

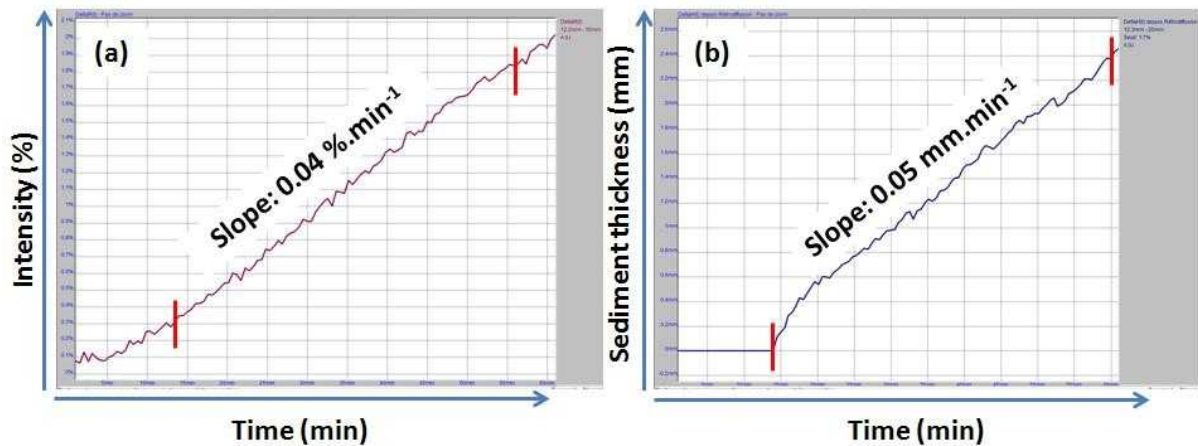


Figure III-2 - Characterization of the sedimentation behaviour of the slurry A from the backscattered signal with (a) the evolution of the intensity of the sedimentation peak and (b) the evolution of the thickness of the sediment. Both properties are plotted as a function of the measuring time.

The overlapping of the rates of intensification of the sediment is depicted in *Figure III-3(a)*, for the three slurries during short measuring times ($t < 10\text{min}$). It can be observed that the values of this parameter increase with ageing time up to nine days and irrespectively of the Al load content (*Table III-1*). The measurements of the slurries A and C show a quite different profile for the two and five days aged compared to the slurry B. In fact, the intensification rate of the sediment is lower for both ageing times ($(I_{2B}; I_{5B}) \approx 2 \cdot (I_{2A}; I_{5A}) \approx 2 \cdot (I_{2C}; I_{5C})$). Nevertheless, it has to be noted that the slurries have a densification growth of the same order of magnitude for the elaboration day and one day afterwards ($(I_{0A}; I_{1A}) \approx (I_{0B}; I_{1B}) \approx (I_{0C}; I_{1C})$) but this parameter is more important for the slurry B seven and nine days afterwards ($(I_{7B}; I_{9B}) \approx 1.5 \cdot (I_{7A}; I_{9A}) \approx 1.5 \cdot (I_{7C}; I_{9C})$) following the trend pronounced for the fifth and seventh day of ageing.

In a similar way, the growth kinetics of the thickening of the sediment is compared for the three slurries on the same time interval (*Figure III-3(b)*). As observed for the intensification process, the thickening rates of the three slurries are similar for the elaboration day and one day afterwards ($(T_{0A}; T_{1A}) \approx (T_{0B}; T_{1B}) \approx (T_{0C}; T_{1C})$). Some modification are visible for the values of the slurry B two and five days aged, which has a thickening rate twice faster than the ones for the slurries A and C ($(T_{2B}; T_{5B}) \gg 2 \cdot (T_{2A}; T_{5A}) \approx 2 \cdot (T_{2C}; T_{5C})$). The values changed again for the seventh measuring day with similar a rate for the slurry B and C compared to the slurry A ($T_{7B} \approx T_{7C} \approx 1.5 \cdot T_{7A}$) while the thickening rate is of the same order of magnitude nine days afterwards ($T_{9A} \approx T_{9B} \approx T_{9C}$).

The differences of the values can be correlated to the reliability of the procedure regarding the manufacturing step of the slurries. Indeed, the samples were shaken manually to homogenize the microparticles dispersion into the slurries. Therefore, the process can be random as it depends on the time of mixing and the homogenization strength given by the user. In addition, the reflecting elements (metallic loads) might not be well dispersed into the crucible or remain out of the measuring area lowering the intensification rate of the sediment due to a lower amount of migrating species. As a matter of fact, all evolutions of kinetics are very sensitive for short time measurements before reaching stationary variation, which also can explain the deviation of both intensification and thickening values.

The *Figures III-3(c)* and *Figure III-3(d)* depict the overlapping of the intensification velocity of the sediment and of the thickening of the sediment up to 60 minutes of measuring, respectively. For this time interval, the intensification kinetic attests of a decrease of the sedimentation process with reduction of its value. In addition, the three slurries exhibit the same phenomenon irrespectively of their compositions ($I_{0-9A} \approx I_{0-9B} \approx I_{0-9C}$), while a similar evolution is also observable for all thickening behaviours of the sediments ($T_{0-9A} \approx T_{0-9B} \approx T_{0-9C}$). The criteria values are equal after one day of ageing and stabilized up to the nine days ageing measurement. Both parameters confirm that the variations

occurring during the sedimentation process stabilize to reach a stationary state characterized by the overall positive velocity values after one hour of measurement.

As predicted by the derived Stokes law (*Equation III-1*), high values of both intensification and thickening observed during the first measuring time interval ($t < 10\text{min}$) can be attributed to the coarser particles contained into the dispersion justifying the higher kinetic values, while lower values measured up to 60 minutes are related to smaller particles present into the crucibles having a longer sedimentation time. In addition, a densification of the sediment might occur due to the migration of the small particles infiltrating the coarse particles network resulting in the lowering of the thickening process.

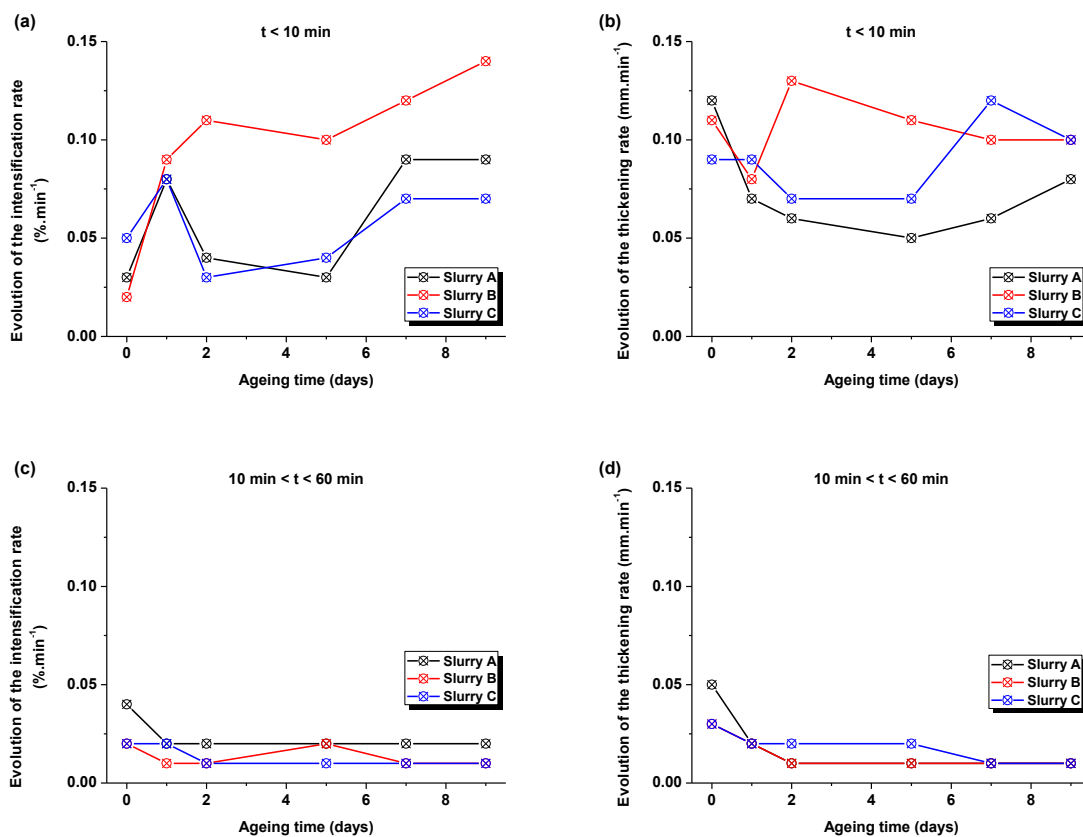


Figure III-3 - Characterization of the sedimentation process through the measurement of the intensification of the sediment and its thickening, respectively, after (a) and (b) 10 min of measurement and (c) and (d) up to 60 min.

Even if the approximation of the Stokes equation allows to predict the evolution of the behaviour of the slurries regarding several parameters, it did not allow to calculate a reliable viscosity value since the particles dispersion is random (homogeneity). It also has to be mentioned that the crucible size impaired with the particle size dispersion may have limited this calculation. As a consequence, viscosity measurements have been done using a rheometer to obtain a full characterization of this physical parameter.

b. Viscosity measurements.

The viscosity is a fluid property which indicates how resistant the fluid to flow. This characteristic is very important in process design and quality assessment for materials. Numerous factors influence the viscosity of solutions; primarily the concentration of particles, the temperature but also of the shear rate. Apparent viscosity has a precise definition. It is, as noted in *Equation III-2*, shear stress divided by shear rate:

$$\eta = f(\dot{\gamma}) = \frac{\tau}{\dot{\gamma}} \quad \text{Equation <III-2>}$$

With Newtonian fluids the shear stress is directly proportional to shear rate, the apparent viscosity and the Newtonian viscosity are identical. The rheological parameter of the PARTICOAT slurries has been characterized on a wide range of shear rates to monitor the response of the water based slurry containing Al microparticles, by means of shear flow measurements. In view of an air-spray deposition process, requires knowledge of the rheological behavior of the slurry [6]. For this, a cone / plate geometry has been used to carry out the measurements, using an applied shear rate from 0.1 s^{-1} to 2500 s^{-1} . *Figure III-4* represents an example of the shear stress measured with respect of the applied shear rate for the slurry A for its elaboration day. The rheogram exhibits a typical Newtonian behaviour. From this data, the viscosity (η) is calculated from the slope coefficient of the linear curve using the Newtonian fluid description [6].

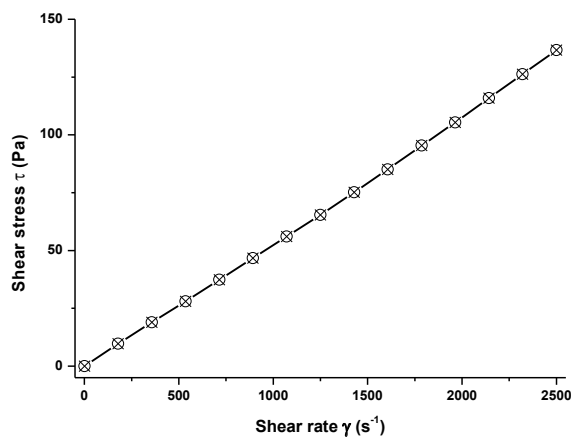


Figure III-4 – Flow curve of the slurry A for its elaboration day, at 25°C.

The three slurries have been analyzed along the ageing measurement process up to nine days. For comparative purposes, the relative viscosity (η_r) is used to monitor the different slurries evolution with respect of ageing measurements using the *Equation III-3*, which gives the expression of the relative viscosity (η_r) as a function of the viscosity of the solution (η_{solution}) divided by the viscosity of the solvent (η_{solvent}).

$$\eta_r = \frac{\eta_{\text{fluid}}}{\eta_{\text{solvent}}} \quad \text{Equation < III-3>}$$

It has to be mentioned that a “crusting” phenomenon was observed for all the slurries at low shear rates. The latter originates from the edge effects where evaporation of the water of the slurry led to the drying of a crust surrounding the sample. Considering this morphology for the slurry (crust + liquid phase), the rotation of the cone of the rheometer imply the measurement of higher viscosity values.

As represented in *Figure III-5*, the crusting phenomenon or edge effect was observed on analyzed slurries; the skin formation by dehydration on the outer surface of the sample. This effect can be minimized by applying a thin coating of oil on the surface or by using a solvent trap. Nevertheless, the slurry C containing the highest Al content exhibits a more pronounced “crusting” phenomenon nine days afterwards the elaboration as represented in *Figure III-6(b)* compared to the viscosity value of the slurries A and B (*Figure III-6(a)*). In order to extrapolate an appropriate value of this rheological parameter, these first high viscosity values resulting of this liquid / solid transformation were not taken into account for the calculation of the global viscosity in order to measure a representative value of the all the slurries, whose parameter is available for higher shear rates.

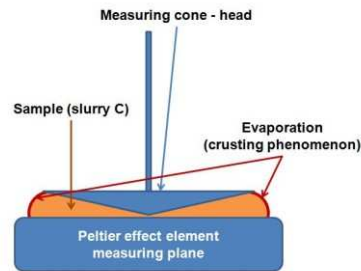


Figure III-5 - Geometry of the rheometer showing the "crusting" phenomenon.

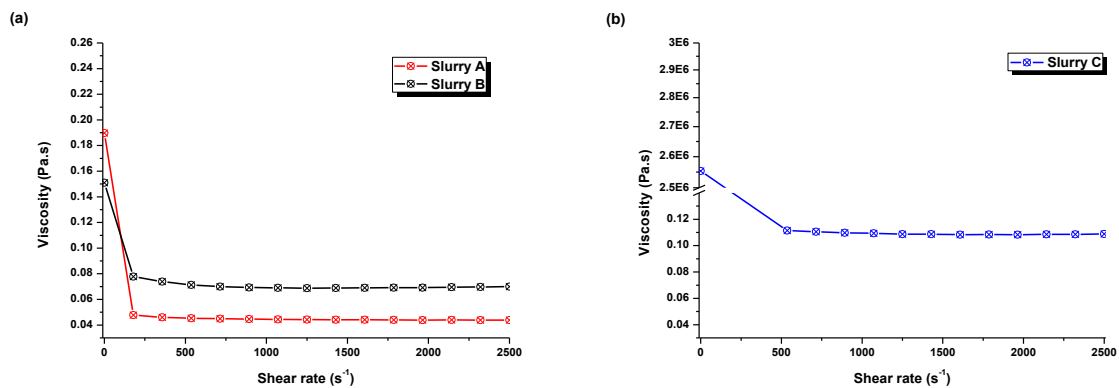


Figure III-6 – Evolution of the viscosity with shear rate for (a) the slurry A and B and (b) the slurry C, emphasizing the “crusting” phenomenon occurring on all the slurries but more pronounced for the slurry C composition, nine days afterwards the elaboration of the slurries.

Figure III-7(a) shows the overlapping of the evolution of the relative viscosity of the samples as a function of the ageing time. The relative viscosity of the slurry A, B and C are named η_{rA} , η_{rB} and η_{rC} , respectively. It can be observed that the higher the Al content, the higher the relative viscosity, i.e. $\eta_{rC} > \eta_{rB} > \eta_{rA}$ as reported by the groups of Mooney [7], Denn [8], and Toda *et al.* [9] who developed Stokes modified equations to predict the rheological behaviour of suspensions in respect of the loading agent (shape, density..). Nevertheless, it has to be noted that Toda *et al.* introduced the notion of compacity of the slurry based on the atomic organization, like for crystallographic domain. They fixed the maximal compacity to the value of 74%, corresponding to the maximum compacity of crystallographic structures. The later might not be adapted in case of rheological matter since fluid mechanics have also to be taken into account especially for air spray applications.

The variation of the parameter is slightly lowered between its day of elaboration and two days afterwards before stabilizing up to the end of the ageing process, irrespectively of the Al loads. In

fact, all the tested slurries became a bit more fluid through the measurements. As a comparison for the relative viscosity evolution, the viscosity value of the binder is plotted on *Figure III-7(b)*. Even if the addition of 10 wt.% of PVA induces an increase of the viscosity value higher than the one of the water ($\eta_{\text{water}}=0.001 \text{ Pa}\cdot\text{s}$), the same rheological trend is also observed upon the nine days of ageing.

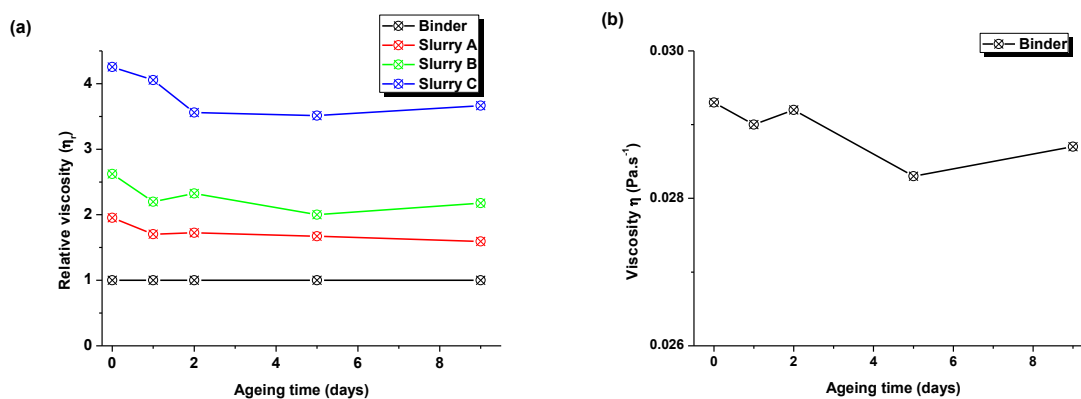


Figure III-7 – Rheological behaviour of the samples with (a) the overlapping of the relative viscosity evolutions of the slurries A, B and C and (b) inset of the viscosity evolution of the binder, both as a function of the ageing time.

A Newtonian behaviour was observed for all our solutions, which is a bit different than the study realized by the groups of Teiple *et al.* for nano sized particle suspensions [10] and Mitsumata *et al.* for micro sized particle dispersions (diameter $1.4 \mu\text{m}$) [11]. They respectively studied these behaviours using a paraffin oil binder and hydroxyl-terminated polybutadiene (HTPB) under steady flow [10] and dynamic tests [10-11]. They concluded that the structural organization of the solid phase dispersed into the binder rules the order of magnitude of the viscosity values, i.e. the higher viscosity values at low shear rates are explained by the need of energy to break the particle organization. Furthermore, the random particle dispersion that they observed for the low shear rates depends first on the particle size and second on the volume fraction, which might explain the deviation compared to our measurements.

Rheological measurements of all slurries showed that the solutions had a stability of the flow behaviour after almost two days of aging, characterized by a constant viscosity. Other investigations have been carried out to analyze the evolution of the physico-chemical properties of the mixtures. The room temperature FTIR measurements allowed us to observe the bonding phenomena through the same ageing with time procedure. In contrast, a complementary study at higher temperatures by DSC, DTA and TGA allowed us to identify the evolution of the slurry when a thermal treatment will be performed to elaborate the coating.

II. Physico-chemical properties of the slurry.

In order to increase the sensitivity on the different range of temperatures but also because of the characteristics of the devices, the analysis has been decomposed in two domains. The first one from room temperature up to $550 \text{ }^\circ\text{C}$ (DSC) using $5\text{-}6 \mu\text{m}$ Al dispersion in diameter, which allows to collect information on the transformations occurring under the melting temperature of the aluminium. The second one from room temperature to $1100 \text{ }^\circ\text{C}$ (TGA-DTA) using both the $5\text{-}6 \mu\text{m}$ and the $20 \mu\text{m}$ (average size) particles. This allows to correlate the evolution of the mass of the systems with oxidation processes as well as the oxidation reactivity with respect of the size of the particles.

A. Room temperature properties.

Before analyzing the slurries, pure PVA was studied as a raw material by the FTIR at room temperature (*Figure III-8(a)*), for which the blank of the atmosphere is subtracted. In agreement with other studies on organic compounds [12-15], the PVA (see chapter 1) powder displays absorption bands at 3296 cm^{-1} from hydrogen bonded stretching band ($\nu_{\text{O-H}}$), whereas the ones at 2938 and 2907 cm^{-1} are ascribed to C-H alkyl stretching groups. Signals at 2165 cm^{-1} have been ascribed to atmospheric CO_2 . Stretching bands from the carbonyl (C=O), C=C and carboxyl (COOH) stretching bonds showed respectively, absorption bands at 1713 , 1651 and 1570 cm^{-1} . Bending vibrations (δ) related to CH / CH_2 groups and hydroxyl (O-H) groups appeared at 1428 and 1323 cm^{-1} , respectively. The carboxyl stretching band signals correspond to C-O bond (1144 cm^{-1}) and PVA crystallinity (1094 cm^{-1}) [13], while the $\text{CH}=\text{CH}_2$ and $\text{CH}=\text{CH}$ groups give absorption bands at 915 and 847 cm^{-1} , respectively. However, quantification of this signal turned out to be particularly difficult because of overlapping with the carboxylic band.

Thereafter, ageing of the mixture (Al/ H_2O /PVA) was performed up to 9 days at room temperature and each spectrum is normalized in intensities to overlap them (*Figure III-8(b)*). Regardless of the composition of the slurry, no significant differences can be observed among the spectra even after 9 days of ageing. It was observed that mixing the binder and the metallic compounds resulted in small shifts in the absorption spectra for the $\text{CH}=\text{CH}$ (847 cm^{-1}) and the hydrogen bonds (1428 and 1323 cm^{-1}). Nevertheless, all FTIR spectra basically presented the same absorption bands from the elaboration day of the slurries up to 9 days later, thereby suggesting that the slurries are very stable. Nonetheless, it should be noted that few peaks could be masked because of the small amounts of PVA into the slurries and of its adsorption to Al microparticles [16-17].

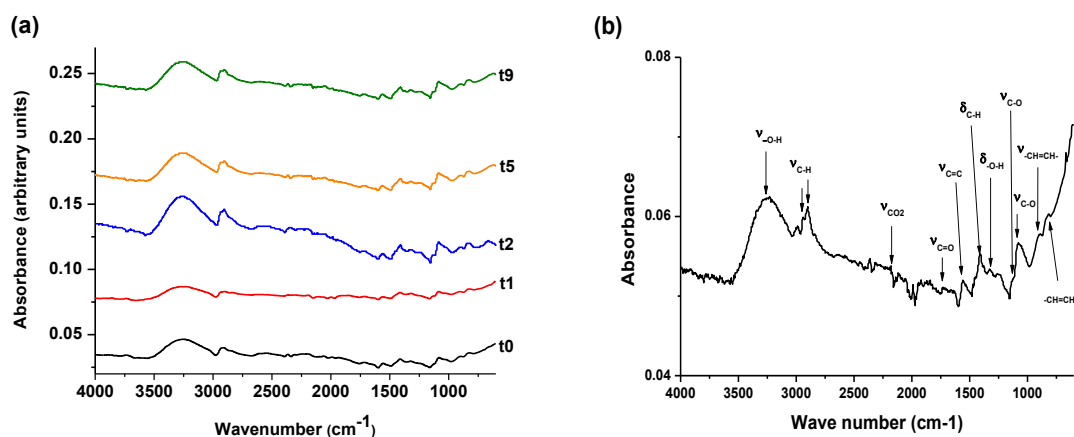


Figure III-8 - FTIR measurement spectrum at room temperature of (a) the aging measurements for the slurry A from the elaboration day up to 9 days and (b) inset of the slurry A spectra at t0.

Particular attention was also paid to the existence of Al-hydroxyl compounds, such as diaspore / boehmite type. Indeed, Yang *et al.* [12] reported the appearance of absorption bands (bending) related to the O-H group of the boehmite type at about $1,070$ and $1,400\text{ cm}^{-1}$ and claimed that the transformation temperature of this hydroxide into the oxide form could be more shifted towards higher temperatures due to the adsorption of PVA to boehmite. Other reports have also proposed the appearance of such signatures over a wide range of wavenumbers (between 800 and $1,100\text{ cm}^{-1}$) [18-20]. In spite of this, none of these bands can be clearly identified in the present spectra under these experimental conditions, which are room temperature FTIR under ambient air atmosphere. For this reason, the presence of hydroxide compounds within the slurries remains unclear. It has to be noted that the same physical state modification of the slurry C was observed during the

measurements like for the rheological ones. In regard of the analysis, the assumption that the oxyhydroxide, which surrounds the Al microspheres, may become thicker during the ageing time could be an explanation to the solidification process by means of more important agglomeration phenomenon of the particles to form bigger solid Al and Al oxides aggregates.

Because the purpose of the PARTICOAT slurry is the aluminizing of Ni-based substrates coupled to the formation of a thermal barrier coating, the solutions will have to undergo a thermal treatment during which the coating has to remain homogeneous. To perform this, information is required about the thermal behaviour of such a system.

B. Thermal annealing till the melting point of Al.

For the slurry to be applied onto a substrate, the mixture shall possess specific rheological properties [11;21-22] and be able to dry smoothly, while avoiding excessive cracking to elaborate homogeneous coating [23]. To satisfy this, the evolution of the transformation of the slurry was characterized by DSC at intermediate temperatures (up to 550°C), at which full decomposition of the binder is achieved [24]. As shown by the DSC curves depicted in *Figure III-9(a)*, the as-prepared solution was characterized by three main peaks. The first one at 60°C is related to free water present in the slurry. Secondly, an important endothermic peak at about 100°C corresponds to the boiling point of water. Thirdly, a broader one between 200°C and 300°C (which is highlighted in the inset) reveals the decomposition of the organic phase. This can be explained by the weak signals from the organic compound masked by the strong endotherm of water. Therefore, different drying steps were performed to discriminate better the signals associated with the PVA.

In this sense, a PVA film was prepared by drying the water/PVA mixture in room conditions. *Figure III-9(b)* shows a comparison between the DSC curves of a pure PVA film and of slurry B as an example (similar behaviour for the slurries A and C except for the energy values). Irrespectively of the drying time, the PVA film exhibited three endothermic peaks at about 40°C, 218°C and an more intense one at 275°C corresponding to free water, to the PVA melting point (T_m) and to the PVA decomposition point (T_{Decom}) [12], respectively. Once the organic compound signals identified, the differences with the profile of the slurry analyzed by DSC measurement can be highlighted. The slurry B curves show one endothermic peak at about 220°C (T_m) and a broad peak between 240°C and 360°C (T_{Decom}), which suggests bonding phenomena between the PVA organic compound and the Al metallic load. A tiny signal can also be observed at the temperature of 460°C and can be ascribed to the final deshydroxylation of the hydrated amorphous oxide layer, which surrounds the Al microparticles [17].

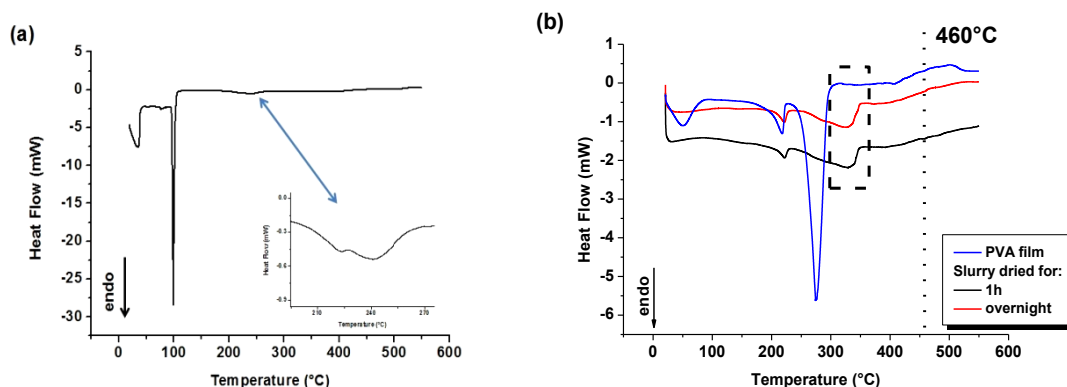


Figure III-9 - DSC curves of (a) the as-prepared solution with the inset emphasizing the existence of the broad decomposition peak and (b) comparison of the DSC signals of a pure PVA film (blue) with those of slurry B dried in room conditions for 1h (black) and overnight (red).

In order to observe any difference due to the variation of the metallic load contained into the slurries, *Figure III-10* gathers the overlapping of the DSC curves of the slurries A, B and C, all dried for 1h before doing the measurements. Slurry A exhibits two peaks related to free water and to the melting point of PVA, while slurries B and C exhibited a slight wavy shape for the free water and showed a well defined signal for the PVA melting point. This difference is attributed to the fact that slurry A contains 1.5 and 2.3 times greater amount of water than slurry B and C, respectively. Therefore, it derives that the drying time at room temperature was not long enough. A particular attention paid on the broad decomposition peak between 240°C and 360°C revealed the presence of two peaks in all three slurries, whose characteristic temperatures are summarized in *Table III-2*. When the content of Al microparticles increases, both peaks are slightly shifted towards higher temperatures. It seems also that the ratio of the intensities of those peaks ($I_{\text{peak 1}} / I_{\text{peak 2}}$) (*Figure III-11*) is higher than 1 for the slurry A, while the same value is smaller than 1 for the slurry C. From this observation, it can be inferred that a higher content of metallic load will require a higher temperature to decompose the bonding between the organic compound and the aluminium.

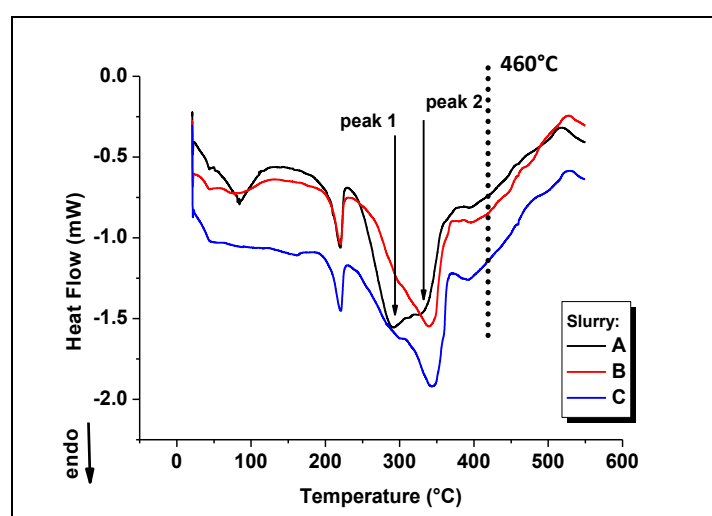


Figure III-11 - DSC curves of the slurry A (black), slurry B (red) and slurry C (blue) dried for 1h.

Table III-2 - Summary of the DCS peaks into the broad decomposition peak signal.

	Peak 1	Peak 2
Slurry A	290°C	328°C
Slurry B	301°C	339°C
Slurry C	303°C	344°C

The additional peak at 460°C (*Figure III-11*), attributed to the final deshydroxylation of the Al amorphous hydrated layer surrounding the particles, was observed for all tests even if its intensity was close to the detection limit of our device. The analysis and identifications of all the peaks are gathered in *Table III-3* and compared with the data extracted from the literature [12;25]. Small deviations can be observed for the melting temperature of the pure PVA, which can be attributed to differences in the raw chemical compounds themselves, i.e. crystallite size dispersion and impurities for a similar molecular weight. Considering the temperature of decomposition of the PVA bonded with the Al load, the temperature range is of the same order of magnitude than the one observed by Yang *et al.* [12] for a pure PVA / boehmite film. However, these authors measured a temperature of deshydroxylation lower by 50°C than in our case, which is related to the nature of the chemical bonds developed onto the particles. Another factor influencing this transition temperature is the processing route for manufacturing the microparticles, as mentioned by the group of Levin *et al.* [28]

who reported the metastable transformation sequences of the aluminas toward its stable α form. As a matter of fact, depending of the raw material or its manufacturing process, hydrated aluminas can be observed during the polymorphic transformation, having specific temperature range transformations for different temperature intervals.

Table III-3 - Summary of the characteristic temperatures obtained by DSC from our measurements ¹ compared to data extracted from ² [12] and ³ [25].

	T_m (°C)			T_{Decom} (°C)			$T_{amorphousAl_2O_3}$ (°C)			
	T_{peak}	T_{onset}	E (J.g ⁻¹)	T_{peak}	T_{onset}	T_{range}	E (J.g ⁻¹)	T_{peak}	T_{onset}	E (J.g ⁻¹)
Pure PVA ¹	218.4	196.9	48.9	275.7	256.9		404.2			
Pure PVA ²	223.0			312.0						
Pure PVA ³	230.1			331.2						
PVA boehmite film				280-485				415.0		
Slurry A ¹	220.1±0.1	204.3	5.7±0.4	340.0±1.5		260-370	49.4±3.2	459.8±0.1	458.0	
Slurry A ²	219.9±0.3	204.3	5.4±0.9	341.3±5.8		260-370	45.7±9.9	459.8±0.1	457.8	
Slurry A ³	220.1±0.2	204.6	3.6±0.2	344.5±2.2		260-370	27.8±3.7	459.8±0.1	457.8	

As reported by Umoren *et al.* [16] and Stoyanov *et al.* [26-27], PVA can be chemisorbed onto the Al microparticles surfaces, which could explain the existence of the broad peak related to the interactions between PVA and the Al microparticles and their further decomposition with temperature. Different layers and related bonding physico-chemical properties can be proposed (Figure III-12) [29]. As represented on the outer layer, low energy bonds (Van der Waals type) exist but as soon as the layers get closer to the metallic core, the nature of the physico-chemical bonds changes. Physisorbed or chemisorbed species constitute a second layer, while hydroxyl bonds appear towards the metal, increasing in energy. Finally, metal / oxide bonds appear close to the metal and are even more energetical. In view of a ramp of a thermal treatment, this structure implies that each layer reacts in a different manner depending of the temperature range. At low temperature, the low energy bonds will be readily decomposed, while the more energetic ones will remain. Therefore, the H bonding, the physisorbed / chemisorbed and finally the hydroxyl groups will be released by the effect of the temperature, to reveal the metallic oxide layers.

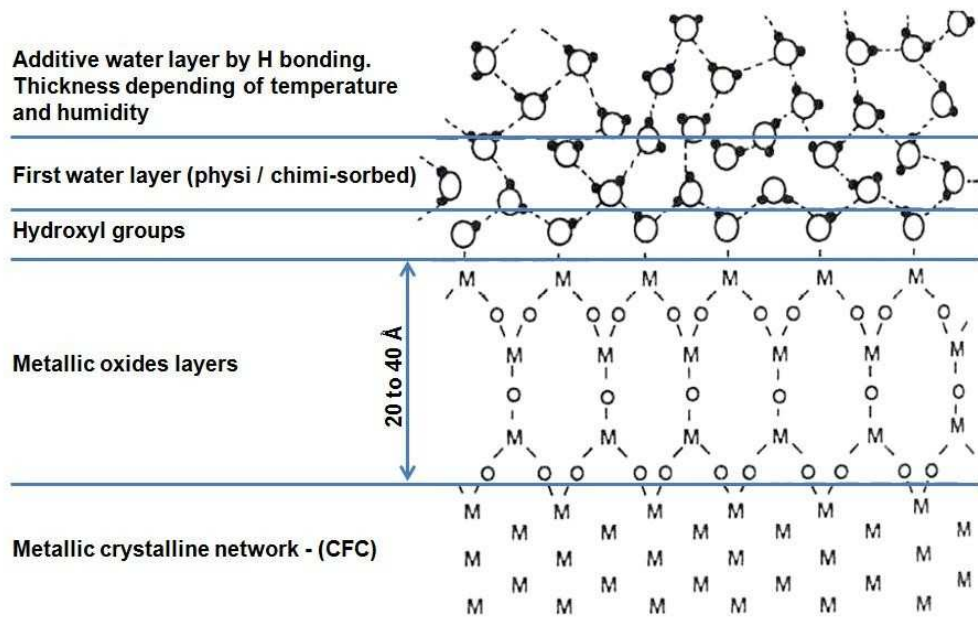


Figure III-12 – Simplified schematic of the physisorbed and chemisorbed species on the metallic aluminium surface [29].

In addition, Taxc *et al.* [30] reported that PVA could aggregate in water mixtures as undissolved PVA. From these assumptions, interactions between components can be proposed irrespectively of specific amount of the chemical elements of the slurries, as depicted in Figure III-13. When both parts of the PVA (dissolved and undissolved) remain in the water, one part of the organic compound adsorbs on the surfaces of the Al microparticles due to thermodynamic properties of these compounds [16] thus to enhance the corrosion resistance of the Al surfaces to protect. The other part agglomerates itself as pure undissolved PVA (Figure III-13(a)). By increasing the loading agent content, the total area on which the adsorption may occur is higher, allowing the undissolved PVA to be adsorbed onto the surface of the oxhydroxide layer surrounding the metallic core (Figure III-13(b)). Finally, when increasing even more the Al content, the organic amount into the binder is not high enough to cover completely the surface on which it can adsorb allowing the oxhydroxide to grow a bit further (Figure III-13(c)). These three schematics may be representative of the phenomena occurring into our slurries composition by means of bonding and energies (temperature) required to decompose (peaks 1 and 2, Table III-3) the binder from the systems.

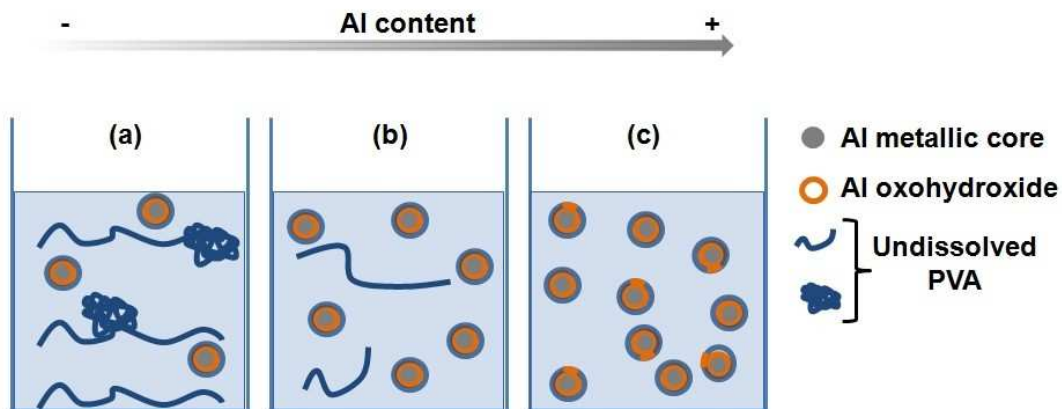


Figure III-13 - Diagrams of several representative contents for the slurry composition and phenomenon related to the binder / Al particle ratio based on the same PVA amount for all representations.

On the other hand, the peak observed in all the slurries at higher temperature (460°C) (Figure III-14 (b)) was not observed for the pure PVA and PVA/H₂O mixtures. In essence, this last peak is due to the Al powder itself. In fact, PVA could bond to the Al microparticles forming thin nanolayers (>4 nm) of oxyhydroxides (boehmite γ -Al(OH)₃, diaspore α -Al(OH)₃) or hydroxides (amorphous Al(OH)₃, gibbsite γ -Al(OH)₃, bayerite α -Al(OH)₃) [17;27;31]. Upon heat treatment, deshydroxylation could therefore occur to result in the formation of amorphous Al₂O₃ [12;32], which will further crystallize at temperatures between 460°C and 660°C [33]. It shall be noted that all these phenomena were observed in all the slurries regardless of ageing time (Figure III-14). This result suggests that ageing of the slurry did not affect the events once they had been previously dried for 1h.

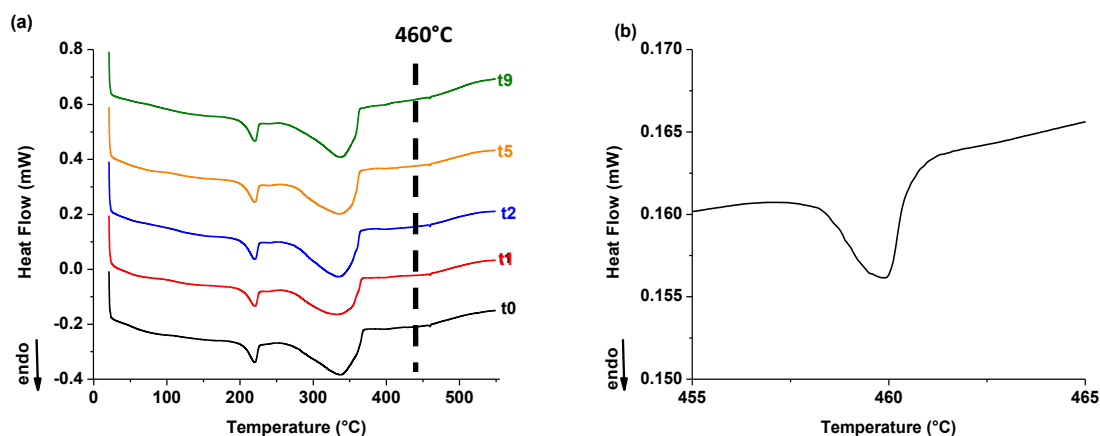


Figure III-14 - DSC curves of the slurry A (a) aged for 9 days and (b) zoom on the final decomposition peak (deshydroxylation) at 460°C.

The comparison of the DSC/TGA and DTA/TGA results is depicted in Figure III-15(a) and Figure III-15(b) respectively. In agreement with the previous findings (Figure III-11 and Figure III-14), the DSC curves exhibited three well defined signals corresponding to the melting point of PVA (220°C), to its decomposition (broad peak from 260°C to 360°C) and to the oxohydroxide formation (460°C). The change of the DTA slopes at 165 and 460°C suggested a likely exothermic reaction between boehmite and PVA, and structural changes in boehmite, respectively [12]. In addition, the TGA signal displayed a first weight loss from room temperature up to 130°C associated with the release of water and three additional inflection points at about 225°C, 275°C and 475°C. Rufino *et al.* [32] also observed similar weight losses that were related to the desorption of water from the surface of the particles followed by the subsequent deshydroxylation mechanisms of the aluminol groups contained in the amorphous layer surrounding the Al particles.

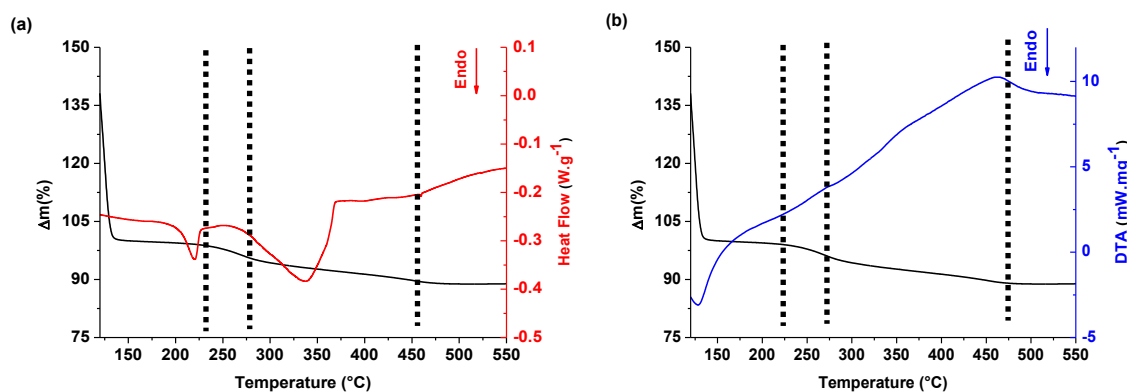


Figure III-15 - Thermal analysis of slurry A containing the 5-6 μ m particles dispersion showing (a) TGA (solid line) and DSC (dash line) curves and (b) TGA (solid line) and DTA (dash-dots straight) curves.

Regarding the thermal treatment required for the PARTICOAT concept, additional information is needed at even higher temperatures. To allow this, DSC and DTA/TGA measurements have been carried out to provide optimum detection sensibility of the thermal events over a higher temperature range (550°C to 1100°C).

C. Thermal annealing over the melting point of Al.

The slurry B has been selected for its average composition between the three slurries and its mass and energy variations are gathered in the *Figure III-16(a)* and *Figure III-16(b)*, and *Figure III-16(c)* and *Figure III-16(d)*, respectively. For the same ratio between the binder amount and the Al load, the effect of the particle size has been investigated with 5-6µm and 20µm particle dispersions. The measurements have been done under the same experimental conditions from 150°C up to 1100°C. Regardless of ageing time, the mass changes depicted on *Figure III-13(a)* and *Figure III-13(b)*, possess a similar trend for the 2 different sized dispersions. A continuous mass loss occurred, related to the evaporation of water and decomposition of the slurry (organic phase and Al deshydroxylation) till 550°C followed by a mass increase till 1100°C attributed to the oxidation of the Al particles. Such oxidation can result from the traces of oxidizing species in the gas (O_2 , H_2O , CO_2 , etc) or from the products of decomposition of the slurry (H_2O , CO_2 mainly). Indeed, Al metal requires extremely low partial pressures of oxygen to get oxidized ($2.7 \cdot 10^{-47}$ atm at 1000°C [34]). However, whereas the small particles underwent a mass gain of about 10 wt.% ($\Delta m_{5\mu m}$), the coarser ones were limited to 5 wt.% ($\Delta m_{20\mu m}$) represented in red areas on *Figure III-16*. This phenomenon was ascribed to a greater reactivity of smaller particles [35-36] (*Table III-4*), thus meaning that the smaller particles need less time than the bigger ones to transform into the same Al oxide, irrespectively of the temperature.

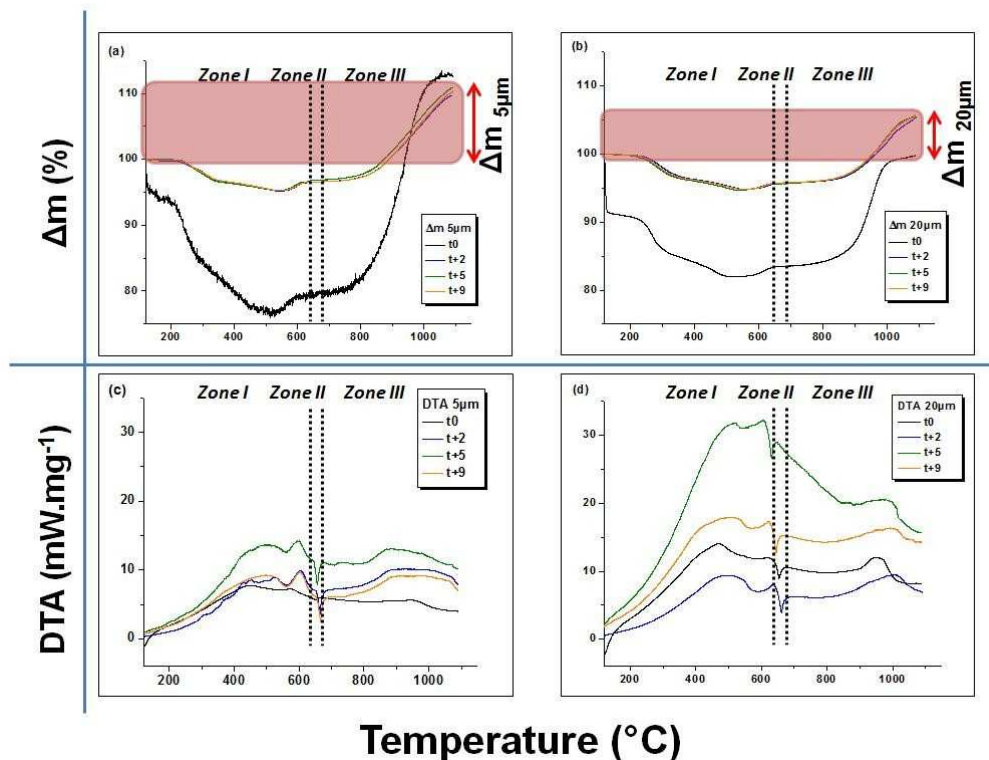


Figure III-16 - Thermal analysis of the slurry B showing the effect of the dispersion of the particle size during ageing for TGA curves of the slurry with (a) 5-6 µm particles dispersion and (b) 20 µm particles dispersion, DTA curves of the slurry with (c) the 5-6 µm particles dispersion and d) 20 µm particles dispersion.

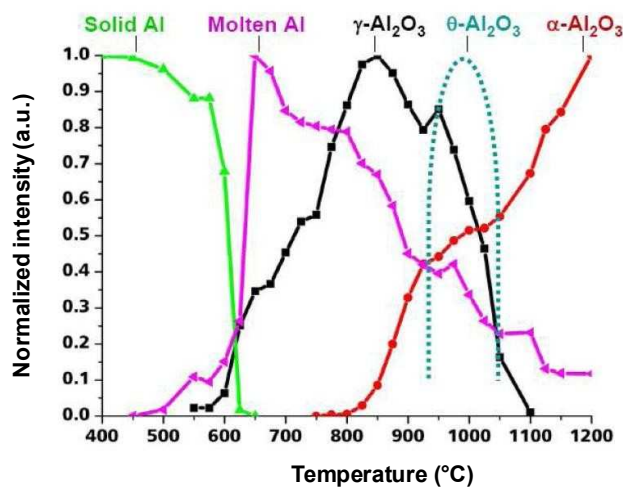
Table III-4 - Summary of mass gain (TGA) and energetic variations (DTA) of the slurry B (40wt.% Al).

Date	Δm (%)		ΔDTA (mW.mg ⁻¹)	
	5 μm	20 μm	5 μm	20 μm
t0	12.0	-0.2	5.1	10.3
t2	9.7	5.2	7.8	6.4
t5	11.0	5.4	9.2	13.5
t9	10.4	5.7	6.3	12.6

The DTA curves can be divided in three different domains highlighted on *Figure III-16*. The first one (till about 625°C), the second from 625°C to the melting point of Al and the last one from the Al melting point to 1100°C. In agreement with the DSC measurements, the first zone revealed an inflection point associated with the Al deshydroxylation accompanying the transformation of the boehmite type structure into the amorphous alumina [12]. The wavy shape of the curve is ascribed to some impurities remaining after cleaning the crucible before making the measurements.

The second zone presents an exothermic and an endothermic peak before and after the melting point of Al (close to 660°C), respectively. The exotherm could be related to the crystallization of the amorphous alumina phase [33;36], during which a slight mass increase was observed in the TGA measurements (*Figure III-16(a)* and *Figure III-16(b)*). This implies that the oxidation process of Al already begun at such low temperatures [33;36]. The endothermic peak corresponds to the melting of Al.

At higher temperatures (third zone), both dispersions displayed a slow mass gain followed by a strong increase of the slope before slowing down when the temperature was close to 1000°C, irrespectively of the particle size. Small exothermic variations are depicted in *Figure III-16(c)* and *Figure III-16(d)*, which also confirms the modification of the process regardless of the particle size. Nevertheless, from the present results, only the formation of $\alpha\text{-Al}_2\text{O}_3$ can be unambiguously proposed as this is associated with the sharp reduction of mass gains in *Figure III-16(a)* and *Figure III-16(b)* related to its higher stability at high temperature compared to the other alumina polymorphs. The variations of the TGA slopes (as well as of the DTA ones) correspond to different rates of oxidation, which can be attributed to the formation and crystallization of different transient aluminas before the formation of the stable $\alpha\text{-Al}_2\text{O}_3$, as observed by Kolarik *et al.* [37] who performed *in-situ* high-temperature X-ray diffraction (HT-XRD) of the Al-micropowders (*Figure III-17*).

Figure III-17 - Intensity curves of 2-5 μm Al on heating in air normalized to 1 taken from Kolarik *et al.* [37].

The range of temperatures at which these variations appeared and also their oxidation and transformation velocities are also in good agreement with a former study done on metastable aluminas [38], which strongly depend on the particle size [31;39]. Nevertheless, these authors reported the aluminas transformation sequence as follow, using microsized particles from the wire explosion technique: amorphous $\rightarrow \gamma\text{-Al}_2\text{O}_3 \rightarrow \theta\text{-Al}_2\text{O}_3 \rightarrow \alpha\text{-Al}_2\text{O}_3$.

For these experiments, the major differences in weight variations resulted from the different initial amounts of slurry put in the crucibles. Therefore, it can be concluded that ageing of the slurries did not modify their evolution with temperature up to 1100°C regardless of the particle size.

Overall, the slurries seemed to be stable enough except for slurry C that underwent physical change after 5 days at room temperature. The removal of the binder as well as the decomposition of the amorphous oxide, which will further on transform into transient aluminas to finally form the α -alumina, are the mechanisms observed as function of the temperature but regardless of the slurry compositions. As a complementary study, the drying process of the three slurries has been realized.

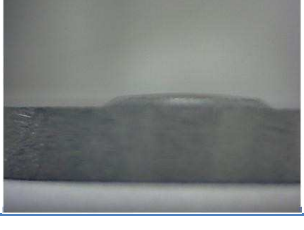
III. Drying of the slurry.

The tests have been done for comparing the drying time, at room condition (25°C / 1 atm / air) of the three slurries onto pure Ni coupons, as this material will be investigated in Chapter IV to study the aluminizing process. The samples were abraded to the #180 SiC paper grade before realizing the measurements. *Table III-5* gathers the picture of 5 microlitres droplets deposited on top on the metallic parts. The captions have been done 30 seconds, 5 minutes, 10 minutes and 20 minutes afterwards for comparing the influence of the aluminium concentration into the slurries.

As it is observed, the shapes of the three droplets are slightly different even after only 30 seconds of measurements. This can be explained by the orientation of the polishing lines at the surface of the Ni coupons which shall have been different. Nonetheless, these initial states are the baseline for the drying time of each sample. All the slurries will be compared one by one, irrespectively of the others, along the time increase.

Even after 20 minutes of exposure to air, the slurry A is not completely dry. Since the base of the drop does not extend (increased wettability) it is assumed that water evaporates with time. The behaviour of the slurries B and C are rather similar. Both of them are dried before reaching 20 minutes. As a matter of fact, both of them seem to be dry after 10 minutes. From these measurements, it seems that the increase of the relative Al content while reducing the water amount brings about a faster dry of the slurry. Therefore either slurry B or C should be more appropriate for industrial applications. Nevertheless, the different shape of the drop between slurry B and C can be attributed to the different orientation of the polishing lines and / or variations in the temperature of the substrate (room conditions).

Table III-5 – Comparison of the drying time of slurries onto pure Ni coupons, abraded with the #180 SiC paper grade, as function of the drying time.

Drying time	Slurry A	Slurry B	Slurry C
30 seconds			
5 minutes			
10 minutes			
20 minutes			

As a result of these considerations, it can be assumed that the drying time of the slurries is conditioned by the orientation of the droplet regarding the polishing lines. As a matter of fact, they are responsible of the surface dimension in contact with the air enhancing the evaporation of the free-water, thus leading to the solidification of the sample. Another important parameter is the temperature of the room where the measurements are carried out, the higher the temperature, the quicker the drying time. Furthermore, it shall be noted that surface is very rough (SiC # 180) to obtain convincing reproducible wettability results.

Summary and outlook

The characterization of a water based containing PVA and Al microspheres slurry for aluminizing purposes has been done through several complementary techniques.

Stability measurements have been performed to assess the information on the homogeneity of the load dispersion into the slurries, hence on the conservation of the slurry. For this purpose, the sedimentation phenomenon at room temperature has been studied for all the slurries investigated. The latter has been characterized by two parameters, their intensification rates (densification) and their thickening rates of the sediment phase. Both physical properties have been measured for two domains: a transitional one (short term measurements $t < 10$ min) and a stationary one ($10 \text{ min} < t < 60$ min), thus to provide information on the particles organization into the slurry. Intensification and thickening phenomena of the slurries are quite different for short term measurements, which are ruled by the dispersion of the particles, the particle size and the particle size dispersion into the systems evaluated. Both rates tend to stabilize to a similar value for the stationary domain, attesting of a comparable behaviour of the loads into the slurries, irrespectively of their contents. These observations provide information on the manufacturing process, which does not seem to be fully optimized in regard of the particles dispersion into the liquid phase but also due to the relatively fast migration processes of the particles into the slurries.

In addition to the measurements of destabilization phenomena, the rheological measurements allowed to confirm the increase of the viscosity value impaired with increasing the aluminium. For high concentration of the Al microparticles (50 wt.%), a fast “crusting” phenomenon has been observed nine days afterwards the elaboration, thus attesting of the liquid / solid transformation of the slurry by the fast evaporation of the free-water that dries the Al oxyhydroxide. In a similar manner, the increase of the mass fraction of the Al into the slurry rules also the drying time of the slurry because of the physico-chemical modifications. Overall, the higher the Al content, the faster the drying time, as observed with respect of the drying time of the slurry onto pure Ni coupons.

From these observations, FTIR measurements at room temperature have been done to monitor the evolution of the physico-chemical bonding due to the use of the different compounds (water / PVA / Al). The signatures of the components have been assessed for the elaboration day and measured up to nine days afterwards. No significant bonding evolutions have been found due to the small amount of PVA content regarding the metallic nature of the loads, but also regarding the shapes of the particles, which in general tend to reduce the infrared signals from the samples. Nonetheless, the solidification of the slurry C has been also observed, five days afterwards its elaboration, which is a little bit earlier compared to the sedimentation and rheological measurements. Such deviation may be likely explained because of the storage of the samples. Sedimentation and rheological studies have been carried out using sealed crucibles while FTIR ones were not sealed. From these considerations, interactions with the room atmosphere may have promoted this physical state modification, enhancing the solidification process.

In a same manner than the bonding evolution, it has to be noted that the behaviour of the hydrated aluminas has been difficult to monitor probably due to the experimental conditions since we performed measurements at room condition (25°C / 1 atm / air). It would have been more interesting to carry out the measurement using vacuum or high-temperature FTIR for such evolution in order to focus on the signatures of the $-\text{OH}$ groups.

Due to the aluminizing purposes of the PARTICOAT project, information have been collected regarding the thermal treatment, by means of DSC study up to 550°C and DTG-TGA measurements up to 1100°C . The use of the two techniques allowed to take advantage of the detection sensitivity of the devices considering the temperature ranges.

The DSC measurements allowed to obtain information on the water release ($T < 120^\circ\text{C}$), the PVA organic melting point (220°C) and also the degradation of the bonding between the PVA compound

and the Al microparticles ($250^{\circ}\text{C} < T < 360^{\circ}\text{C}$). In addition to this, we were able to confirm the temperature of deshydroxylation of our metallic particles ($T \approx 460^{\circ}\text{C}$), which allow to tailor the particles reactivity for the integrity of the final coating.

Finally, the DTA-TGA measurements provides the results on the crystallization of the amorphous aluminas ($550^{\circ}\text{C} < T < 660^{\circ}\text{C}$) but also the different oxidation regimes, which can be correlated to the polymorphic transformations of the alumina phases ($\gamma \rightarrow \delta \rightarrow \alpha$) already observed by high-temperature XRD measurements.

From the overall behaviour of the slurries with respect of physico-chemical properties evolutions and their drying properties, a suspension containing between 40 wt.% and 50 wt.% of Al microparticles seems to be appropriate for using for the aluminizing purposes. Based on this observation, the following study focuses on the use of a ≈ 45 wt.% of Al content into the slurry.

In addition, this full characterization allows to imagine other possibilities, taking into account the reactivity of the particles, by using different types of metallic loads to monitor their behaviour to obtain a synergy for improving the coating manufacturing. To study such purpose, a DSC-TGA device able to operate till 1600°C has been recently installed in the laboratory, and it could be convenient to evaluate the reactivity of the slurry with the substrate material as well as to investigate the reactivity of the slurry with additional loads (e.g. SiO_2 , MgO , CeO_2 particles).

References

- [1] Y.F. Ivanov, M.N. Osmonoliev, V.S. Sedoi, V.A. Arkhipov, S.S. Bondarchuk, A.B. Vorozhstov, A.G. Korotkikh, V.T. Kuznetsov, *Propellants Explosives Pyrotechnics* 31 (2006) 401
- [2] M. Mollard, Etude et développement de nouveaux revêtements à base de microparticules d'aluminium pour des applications à haute température, Master Thesis, Université de La Rochelle, France (2010)
- [3] www.formulaction.com
- [4] D. Lerche, T. Sobisch, *Journal of Dispersion Science and Technology* 32 – 12 (2011) 1799
- [5] H.A. Barnes, *ICHEME* (1992) 24 ISBN 0 85295 290 2
- [6] H.A. Barnes, *Handbook of Rheology*, University of Wales (2000)
- [7] M. Mooney, *Journal of Colloid Science* 6 (1951) 162
- [8] M.M. Denn, *Rheologica Acta* 24 (1985) 317
- [9] K. Toda, H. Furuse, *Journal of Bioscience and Bioengineering* 102 (2006) 524
- [10] U. Teipel, U. Förther-Barth, *Propellants Explosives Pyrotechnics* 26 (2001) 268
- [11] T. Mitsumata, T. Hachiya, K. Nitta, *European. Polymer Journal* 44 (2008) 2574
- [12] W.P. Yang, S.S. Shyu, E-S. Lee, A-C. Chao, *Materials Chemistry and Physics* 45 (1996) 108
- [13] H.S. Mansur, R.L. Oréfice, A.A.P. Mansur, *Polymer* 45 (2004) 7193
- [14] S.R. Sudhamani, M.S. Prasad, K. Udaya Sankar, *Food Hydrocolloids* 17 (2003) 245
- [15] R. Marupov, I.Ya. Kalontarov, G.I. Konovalova, *Zhurnal Prikladnoi Spektroskopii* 8 (1968) 657
- [16] S.A. Umoren, O. Ogbobe, P.C. Okafor, E.E. Ebenso, *Journal of Applied Polymer Science* 105 (2007) 3363
- [17] P. Karlsson, A.E.C. Palmqvist, K. Holmberg, *Advances in Colloid and Interface Science* 128-130 (2006) 121
- [18] J. Van den Brand, S. Van Gils, P.C.J. Beentjes, H. Terry, J.H.W. de Wit, *Applied Surface Science* 235 (2004) 465
- [19] J.T. Klopogge, H.D. Ruan, R.L. Frost, *Journal Materials Science* 37 (2002) 1121
- [20] L. Favaro, A. Boumaza, P. Roy, J. Lédion, G. Sattonnay, J.B. Brubach, A.M. Huntz, R. Tétot, *Journal of Solid State Chemistry* 183 (2010) 901
- [21] S. Ananthakumar, P. Manohar, K.G.K. Warriar, *Ceramics International* 30 (2004) 837
- [22] S. Ananthakumar, A.R.R. Menon, K. Prabhakaran, K.G.K. Warriar, *Ceramics International* 27 (2001) 231
- [23] J.M. LeBeau, Y. Boonyongmaneerat, *Materials Science and Engineering A* 458 (2007) 17
- [24] X. Montero, M. Galetz, M. Schütze, *Surface and Coatings Technology* 206 (2011) 1586

- [25] M. Moshin, A. Hossin, Y. Haik, *Materials Science and Engineering A* 528 (2011) 925
- [26] P. Stoyanov, S. Akhter, J.M. White, *Surface and Interface Analysis* 15 (1990) 509
- [27] A.A. Gromov, A. Ilyin, U. Förster-Barth, U. Teipel, *Propellants Explosives Pyrotechnics*. 31 (2006) 401
- [28] I. Levin, D. Brandon, *Journal of the American Ceramic Society* 81 (1998) 1995
- [29] J.C. Bolger, *Acid Base Interactions Between Oxide Surfaces and Polar Organic Compounds, Adhesion Aspects of Polymeric Coatings*, K.L. Mittal, Plenum Press, New York (1983) 3
- [30] J.C.J.F. Tacx, H.M. Schoffeleers, A.G.M. Brands, L. Teuwen, *Polymer* 41 (2000) 947
- [31] M.A. Trunov, M. Schoenitz, X. Zhu, E.L. Dreizin, *Combustion and Flame* 140 (2005) 310
- [32] B. Rufino, F. Boulc'h, M.V. Coulet, G. Lacroix, R. Denoyel, *Acta Materialia* 55 (2007) 2815
- [33] B. Rufino, M.-V. Coulet, R. Bouchet, O. Isnard, R. Denoyel, *Acta Materialia* 58 (2010) 4224
- [34] O. Kubaschewski, C.B. Alcock, *Metallurgical Thermochemistry*, 5th ed. Pergamon Press, Oxford (1979)
- [35] M.A. Trunov, S.M. Umbrajkar, M. Schoenitz, J.T. Mang, E.L. Dreizin, *Journal of Physical Chemistry B* 110 (2006) 13094
- [36] M.A. Trunov, M. Schoenitz, E.L. Dreizin, *Propellants Explosives Pyrotechnics* 30 (2005) 36
- [37] V. Kolarik, M. Juez-Lorenzo, H. Fietzek, *Materials Science Forum* 696 (2011) 290
- [38] N.N. Sirota, G.N. Shokhiva, *Kristall und Technick*, 9 (1974) 913
- [39] N. Eisenreich, H. Fietzek, M.M. Juez-Lorenzo, V. Kolarik, A. Koleczko, V. Weiser, *Propellants Explosives Pyrotechnics* 29 (2004) 137

Chapter IV

Formation of a Thermal Barrier Coating (TBC) system onto nickel-based substrates from a slurry containing aluminium microparticles

This part aims at explaining the use of the water-based slurry containing Al microparticles allowing to form the PARTICOAT coatings (thermal barrier layer / thermally grown oxide / bond coat). In this view, the considerations about the thermal treatment are shortly explained before studying the formation of both the top coat with the hollow spheres and the diffusion layer onto model substrates (pure Ni and Ni20Cr). Then, the PARTICOAT concept has been extrapolated to four commercial Ni-based superalloys, with various chemical compositions and crystal structure (SX: single crystal; DS: directionally solidified; EQ: equiaxed) according to their application field. The effect of alloying elements will be underlined regarding the major features of the coating (composition, microstructure and thickness).

Table of contents

I. Mechanisms of coating formation onto model substrates.	83
A. Considerations about the thermal treatment for the application of PARTICOAT.	83
B. The formation of the topcoat.....	85
C. The formation of the diffusion zone.	88
a. Polycrystalline nickel.	88
i. Formation of intermetallics at the intermediate step.	88
ii. Intermetallic formations after the complete thermal treatment.	93
b. Polycrystalline Ni ₂₀ Cr.....	95
II. Formation of the coatings on industrial Ni-based superalloys.	98
A. First stage thermal treatment.	98
B. Complete thermal treatment.	101
Summary and outlook	106
References.....	107

I. Mechanisms of coating formation onto model substrates.

The complete system is transformed by the influence of the temperature, but it has to be also considered that the mechanisms of formation are slightly different from the ones observed during Chapter III. In the latter, the global system was only composed of the aluminium microparticles and their surrounding oxides, whose natures are function of the temperature range [1]. In this chapter, the slurry is deposited onto Ni-based substrate and the evolution of the system is characterized.

A. Considerations about the thermal treatment for the application of PARTICOAT.

For aluminizing the Ni-based substrates, a thermal treatment is necessary to take advantage of the thermal events occurring in the slurry with temperature under Ar inert gas (see Chapter III). For this to happen, a three steps heat treatment has been used as illustrated by *Figure IV-1*. The latter is composed of one step at low temperature ($T < 500^{\circ}\text{C}$) to appropriately remove the binder with respect of its nature (water + small amount of polyvinyl alcohol), while the following ones correspond to a high activity / low temperature process and to a diffusion annealing, respectively. The overall treatment is carried out under flowing argon (g) atmosphere to ensure a limited oxidation of the particles and of the substrate, even if a reduced partial pressure of O_2 is sufficient to oxidize Al ($2.7 \cdot 10^{-47}$ atm at 1000°C [2]) into its $\alpha\text{-Al}_2\text{O}_3$ stable form at various temperatures and times [3]. Furthermore, the $5^{\circ}\text{C}\cdot\text{min}^{-1}$ heating ramp is appropriate to slowly degrade the binder, thus providing the green strength necessary to maintain the integrity of the coating (i.e. to avoid the weakening of the topcoat by an inappropriate removal kinetic), while the $50^{\circ}\text{C}\cdot\text{min}^{-1}$ cooling ramp allows to quench and freeze the microstructure of the entire system (*Figure IV-1*).

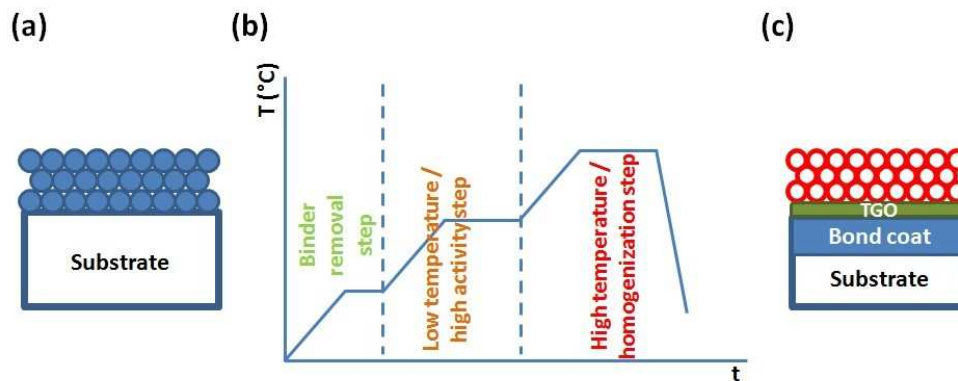


Figure IV-1 – (a) The as-deposited slurry design before realizing (b) the thermal treatment tailored for the formation of the PARTICOAT concept leading to (c) the targeted TBC system structure after heat treatment.

Before tailoring the thermal treatment of the PARTICOAT slurry, a first set of TGA measurements of the water-based binder only has been carried out using a $10^{\circ}\text{C}\cdot\text{min}^{-1}$ heating ramp, up to 700°C as presented by *Figure IV-2*. The use of this heating rate, which is twice more important than the one used for the thermal treatment, does not modify the reactivity of the component but might lightly shift the characteristic temperatures towards higher ones due to a delayed accumulation of the required energy for the thermal event to occur at the surface of the sample.

This experiment provided information on the decomposition behaviour of the slurry whether the decomposition rate first derivative of the mass variation (not shown) or its decomposition advancement (Δm (%)) are considered. Due to the use of a $10^{\circ}\text{C}\cdot\text{min}^{-1}$ ramp, a direct correlation of the time and the temperature is allowed since a factor 10 has to be used ($10 \cdot \text{time value} =$

temperature). As a result, it can be seen that almost 87.5% of the sample mass is lost before 100°C, due to the evaporation of free water. Then, a two steps decomposition behaviour is observed, as described in the previous chapter. A decrease of the mass by 95% appears up to 300°C at which an inflexion point separates the second decomposition step. The complete removal of the binder is considered as achieved slightly before the temperature of 500°C where less than 1% of the initial mass remains.

Considering the critical impact of the kinetics of binder removal for green bodies [4], the use of a lower temperature has been adopted to allow its appropriate decomposition. For this purpose, an isothermal step at 400°C for 1h has been chosen.

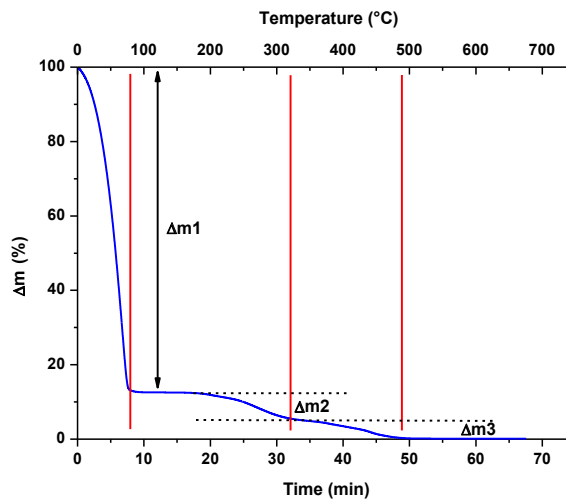


Figure IV-2 - TGA evolution of the water containing 10 wt. % of PVA for a $10^{\circ}\text{C}\cdot\text{min}^{-1}$ heating ramp up to 700°C .

To monitor the formation of the PARTICOAT system when applied onto a base material, different thermal treatments have been carried out using a thermobalance (TGA) to control the evolution of the mass related to decomposition phenomenon or to oxidation mechanisms. In addition, an argon gas atmosphere has been used with a constant gas flow ($16\text{ ml}\cdot\text{min}^{-1}$), which will take out the main part of the oxidizing species.

Figure IV-3(a) depicts the heat treatment realized on a pure nickel substrate. Three main domains can be observed. First, a mass gain can be observed up to about 60°C , which is related to the buoyancy phenomenon as well as the homogenization of the temperature into the chamber. Secondly, a mass loss corresponding to the removal of the binder is observed (see Chapter III). It has to be noted that a rough mass loss exists at the temperature of 350°C associated to the Curie temperature of pure nickel compound [5]. The phenomenon is due to the magnetic properties of the pure nickel and is emphasized by Figure IV-3(b).

Finally, the mass of the system increases from 400°C , thus suggesting the Archimedes phenomenon (heating ramp) and oxidation phenomena, which take place up to the final isothermal step at 1100°C . The effect of the temperatures used during this thermal treatment will be more developed in the section I.B of this chapter. This oxidation phenomenon is mainly ascribed to the Al microparticles transformation due to the low partial pressure of O_2 and is not expected to provide an oxidation of the substrates, i.e. pure Ni samples [6] even by considering the decomposition products of the water-based binder ($\text{H}_2\text{O} + \text{CO}_2$), the latter increasing slightly the amount of oxidizing species.

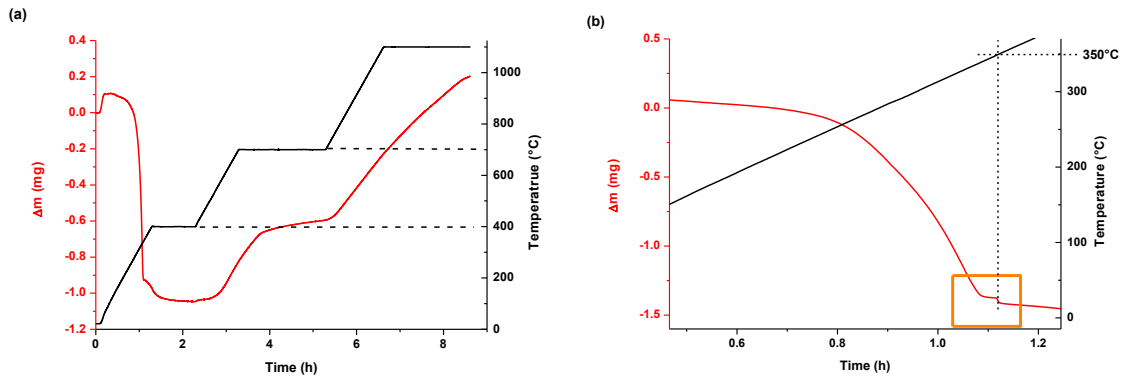


Figure IV-3 - TGA measurement of a pure nickel coupon aluminized using the PARTICOAT slurry process with (a) the full thermal treatment and (b) zoom emphasizing the Curie temperature signature.

In order to investigate the complete formation of the coating, the system has to be separated into two sub-systems: (i) the formation of the topcoat and (ii) the formation of the intermetallics in the diffusion coating. The following section will discuss the formation of the topcoat structure, basically by focussing on the Al microparticles zone, as pictured in (Figure IV-4).

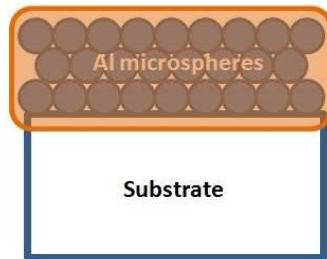


Figure IV-4 - Zone of interest in view of the formation of the top coat with hollow spheres.

B. The formation of the topcoat.

Apart from the binder removal stage, the formation of the topcoat occurring in two steps has been firstly characterized for the intermediate one, which ran at temperatures close to the melting point of Al ($T_m \approx 660^\circ\text{C}$). Thereafter, the evolution of the aluminium oxide structure has been studied after the second step at high temperature (1100°C).

The Al microparticles undergo several morphological and crystallographical transformations during the thermal treatment process. Figure IV-5(a) represents the morphology of the surface after the intermediate step. It is observed that the top coat seems homogeneous. In addition, the onset of the sintering of the particles is already evidenced and shown in Figure IV-5(b) between some particles (white arrows). At such low temperature, this sintering phenomenon can only be ascribed to solid state sintering of aluminium, which is a function of the particle sizes [7] as well as their agglomeration, but also their chemical composition and the temperature [7]. Indeed, one has to first keep in mind that a native thin oxide shell surrounds each microparticle. Secondly, a combined growth of each of the oxide layers surrounding each microspheres can contribute to this light sintering of the particles, as shown by Hart *et al.* [8] for temperatures between 350 and 540°C . The latter temperature is also relevant for the onset of the crystallization of the amorphous aluminium oxide into its $\gamma\text{-Al}_2\text{O}_3$ form.

Depending on the very nature of the oxide, the sintering process may require an even higher temperature. Indeed, Yeh *et al.* [9] and Wu *et al.* [10] reported successful sintering temperatures for Al oxides at about 1150°C and 1200°C, which is far higher compared to the melting temperature of bulk aluminium ($\approx 660^\circ\text{C}$). As a consequence, the step at 1100°C has been designed, on one hand, to completely transform the aluminium oxide into thermodynamically stable $\alpha\text{-Al}_2\text{O}_3$ and on the other hand to convert the intermetallic in the coating (see next section).

The surface morphology of the top coat after two hours at 1100°C is shown in *Figure IV-5(c)*. Firstly, it can be seen that the particles are empty. The white circles reveal a part of sintered oxide skeleton. The former metallic core seems to have been consumed due to the oxidation of the particles and to the diffusion of Al towards the substrate. In addition to these observations, *Figure IV-5(d)* seems to attest of the thickening of the oxide skin, as reported in the literature for microsized particles (4-5 nm for the amorphous initial skin [11-13]). XRD measurements have revealed the transformation into stable $\alpha\text{-Al}_2\text{O}_3$. Furthermore, a residual structure of the polymorphic transformations of the alumina can be seen by the presence of a whisker- / needle-like morphology, which has been already reported for the quick transformation of $\theta\text{-Al}_2\text{O}_3$ to $\alpha\text{-Al}_2\text{O}_3$ [14-15].

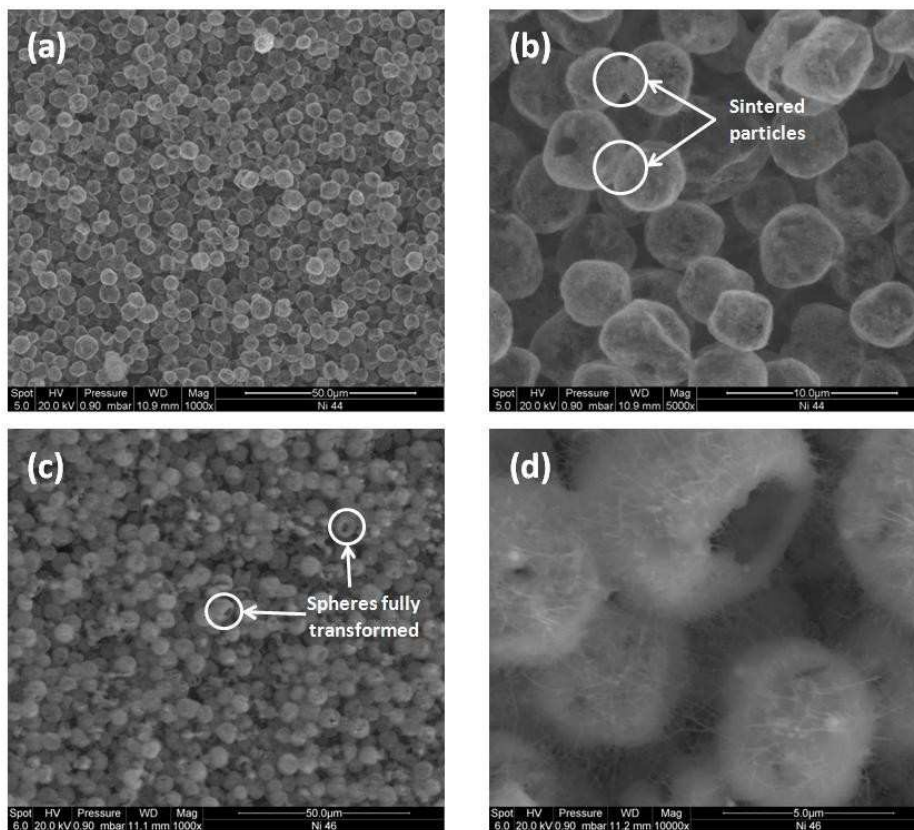


Figure IV-5 - Surface morphology of the top coat structure (a) at intermediate temperature (400°C – 1h + 700°C – 2h) and (b) zoom on the sintering of the particles at this step, while the surface morphology of the topcoat is depicted (c) after the complete thermal treatment (400°C – 1h + 700°C – 2h + 1100°C – 2h) with (d) a more advanced sintering process.

Depending on the thickness of the topcoat but also on the applied thermal treatment, the complete conversion into the $\alpha\text{-Al}_2\text{O}_3$ is observed for the PARTICOAT coating system. Nevertheless, some deviations have to be mentioned regarding the time to form this thermodynamically stable oxide compared to the observations from the literature. Indeed, the groups of Sirota *et al.* [3] and Garriga-Majo *et al.* [16] already studied the polymorphic transformation sequences of aluminas as a function

of time and temperature and they reported longer conversion times [3] compared to the present study (10 hours of thermal treatment). However it has to be mentioned that Sirota *et al.* realized their study considering the complete transformation of an anodic alumina thin film into α -alumina, while Garriga-Majo *et al.* investigated the transformation of the oxide layer grown on a Ni-based substrate aluminized using a different aluminizing slurry, i.e. Si-modified aluminide.

In addition to such crystallographic modification, the emptying of the Al metallic core has already been subjected to investigations. Depending on the temperature range, the Al physical state may evolve from solid to liquid, resulting in a modification of the density from 2.7 g.cm^{-3} to 2.4 g.cm^{-3} , thus leading to the expansion of the metallic core inside the microsphere [17], hence increasing the pressure. Secondly, the crystallization of the different alumina polymorphs is known to be accompanied by a volume contraction, i.e. by 13.8% from the θ to the α - Al_2O_3 [1]. Both phenomena are supposed to weaken the microsphere skeleton and lead to the appearance of cracks due to tensile stresses and shrinkage of the skin, as already proposed by Levitas *et al.* [18] and Rai *et al.* [19]. These authors reported the existence of a pressure gradient evolution up to 1.5-2 GPa between the Al core and the oxide shell, using nano-scale microspheres. Irrespectively of the order of magnitude of the pressure gradient, this phenomenon combined or not with the formation of cracks might promote enhanced diffusion of the aluminium content [20]

Based on the observations and existing models of Levitas *et al.* [21], Kolarik *et al.* [1] and Railsback *et al.* [22], the mechanisms involved in the transformation of the aluminium microparticles are proposed by *Figure IV-6*. First, the oxide skin grows and crystallizes into thermodynamically stable α phase following the amorphous $\rightarrow \gamma \rightarrow \theta \rightarrow \alpha$ sequence. In the meantime, the Al metallic core expands when Al liquid phase appears (solid to liquid transformation) promoting the formation of cracks into the alumina shell with respect of stress accumulations and the crystallization of the polymorphic aluminas. Depending of the Al content and the voids created by the Al consumed by oxidation, some cracks may be rehealed, while the liquid phase may flow out of the sphere by those same cracks promoted by the pressure gradient. Thus, α - Al_2O_3 with a needle-like morphology can be observed resulting of this liquid expulsion and fast oxidation processes and /or as a trace of the remaining θ oxide phase.

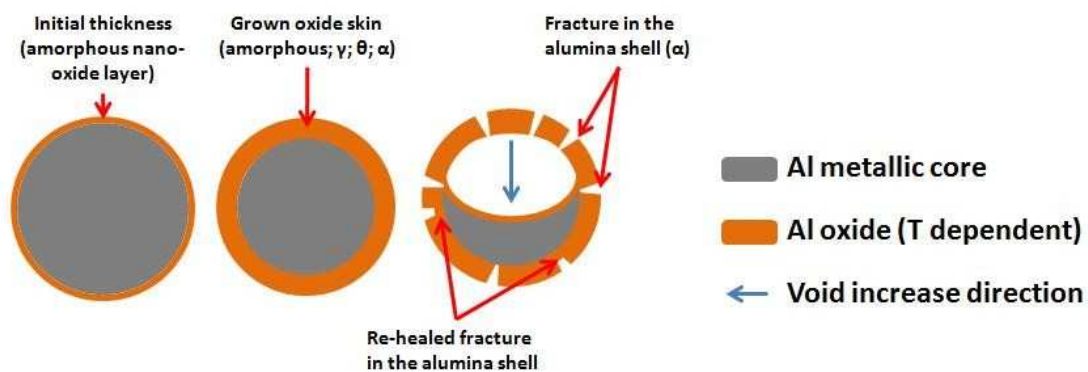


Figure IV-6 – Sketch of the proposed mechanisms involved during the heat treatment of the aluminium microspheres deposited on top of a substrate and their conversion in α - Al_2O_3 hollow sphere microstructure top coat. The fractures in the alumina shell also occur during the formation of the transient aluminas.

Once the ceramic topcoat has been investigated, the growth of the nickel-aluminide coating is discussed in the following section, focusing on the Al interdiffusion with the γ Ni or γ / γ' matrix of the substrate, as represented by *Figure IV-7*.

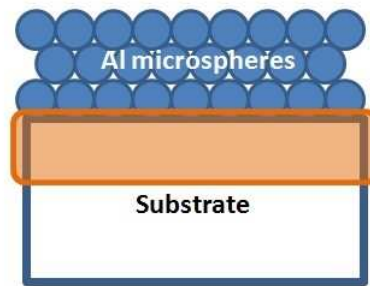


Figure IV-7 - Zone of interest in view of the Al enrichment process.

C. The formation of the diffusion zone.

Due to the novelty of this slurry based approach, the PARTICOAT concept had to be characterized first on model alloys to understand the mechanisms involved during its formation.

The main idea of the thermal treatment was to adapt it as a comparison to the pack cementation process with a low temperature / high activity step followed by a step at higher temperature to homogenize the Al content into the diffused layer. For this to happen, several thermal treatments have been studied to tailor the complete process. The system did not show significant event regarding the aluminizing process for temperatures below 600°C. Indeed, these temperatures did not provide enough energy to activate the Al interdiffusion with the substrate. Although, it is known that aluminium can self-diffuse and re-heal its surfaces for relatively low temperature range [23], Bonnet *et al.* [24] showed that no diffusion zone formed. Nevertheless, they showed the onset of the Al enrichment with small diffusion islands [24], mainly located at the grain boundaries of the pure Ni samples [25].

Therefore, this section will focus on the temperature range over 600°C, first considering model Ni and then Ni₂₀Cr. The latter is used as a model material for the Ni-based superalloys which usually contain less than this 20 wt.% Cr.

a. Polycrystalline nickel.

i. Formation of intermetallics at the intermediate step.

Figure IV-8 represents the binary phase diagram of Al-Ni in which it can be seen that for the temperature below 639°C, solid state diffusion processes will be exclusive. Above the eutectic point at the Al-rich side of the diagram at 639°C, liquid phases have to be considered regarding the interactions between the particles and the substrate. In addition, one has to note the specificity of using Al microspheres, which are surrounded by a thin oxide layer [26]. The driving force to transform the system, controlled by the temperature which determines the physical state of Al, has to be high enough to allow the aluminium to cross the Al thin oxide film physical barrier and then to flow towards the substrate. As a result, when increasing the temperature from 600°C to 650°C and then to 700°C, the metallic Al microparticles underwent modifications of their physical state (from solid to liquid) and also some structural modifications of the oxide shell of the spheres, i.e. crystallization of the amorphous Al oxide.

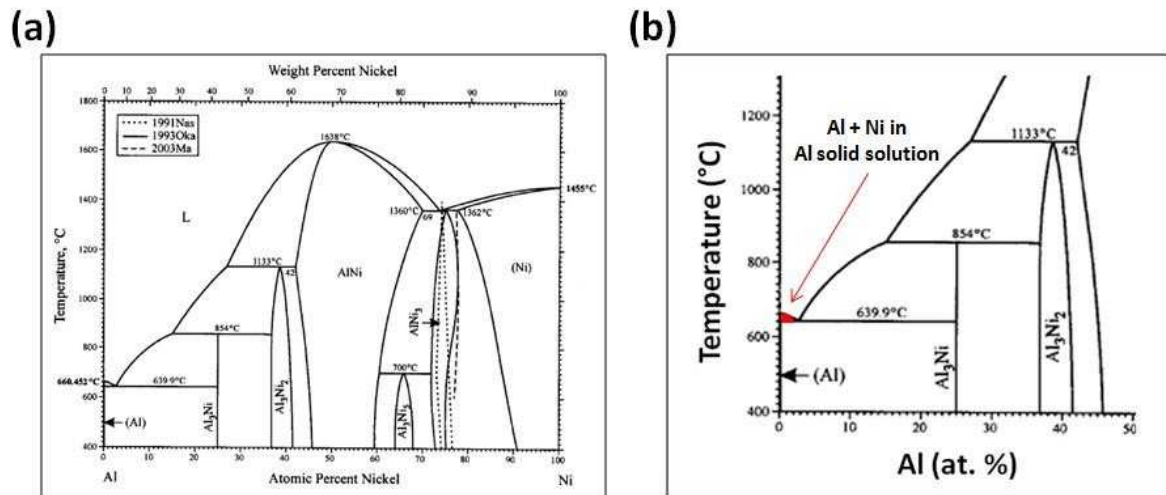


Figure IV-8 - Binary phase diagram of the Al-Ni system [48] and zoom on the Al rich zone formed during the first moments of the Al enrichment.

The effect of the annealing time (0h, 1h and 2h) on the Al diffusion profiles at 650°C and 700°C are given in Figure IV-9(a) and Figure IV-9(b), respectively. Figure IV-10 depicts the effect of the annealing temperature on the coating morphology and the diffusion depth after 2h treatment. In addition, the lines plotted onto the concentration profiles are extrapolated from the Al-Ni binary phase diagram to separate the phase domain of the system, and tend to provide theoretical information of the intermetallic phases likely formed.

As soon as the temperature of **650°C** is reached, an Al enriched zone of 10-15 μm is already formed just after quenching, while longer exposition time led to thicker diffusion zone up to approximately 35 μm (Figure IV-9(a)). After 2h of annealing (Figure IV-10(a)), XRD and EDS combined analyses showed the matrix of the coating is formed by the $\delta\text{-Al}_3\text{Ni}_2$ intermetallic compound. Two additional layers formed at the front of this Al enriched layer by means of a thin $\beta\text{-NiAl}$ layer on top of a thin $\gamma\text{-Ni}_3\text{Al}$ one. For summarizing, the global intermetallic sequence from the outer interface to the substrate is $\delta\text{-Al}_3\text{Ni}_2 \rightarrow \beta\text{-NiAl} \rightarrow \gamma\text{-Ni}_3\text{Al} \rightarrow \gamma\text{-Ni}$. At this temperature, the main difference is due to the annealing time, which rules the diffusion depth in the matrix as represented by Figure IV-9(a).

In contrast, when increasing the temperature to **700°C**, it is observed that the Al already diffused by 35 μm after 0h (Figure IV-9(b)). Increasing the annealing time at 700°C to 1h and to 2h resulted in rather similar thicknesses and relatively close to those observed for the longer times at 650°C. In this case, the Al_3Ni compound has not been found and the intermetallic formation follow the $\text{Al}_3\text{Ni}_2 \rightarrow \beta\text{-NiAl} \rightarrow \gamma\text{-Ni}_3\text{Al} \rightarrow \gamma\text{-Ni}$ sequence (Figure IV-10(b)). The main difference between those two annealing temperature is that all the aluminium is liquid at 700°C, while a part of it remains solid at 650°C, as shown by the Al-Ni binary phase diagram (Figures IV-8). In the case of the second temperature (650°C), a small domain of solid state diffusion has to be crossed before taking advantage of the full Al liquid phase. Therefore, even if the transformation kinetics of the phases at 650°C are slower, the heat released during the exothermic formation of the nickel aluminide component allow to form the Ni_2Al_3 compound [27].

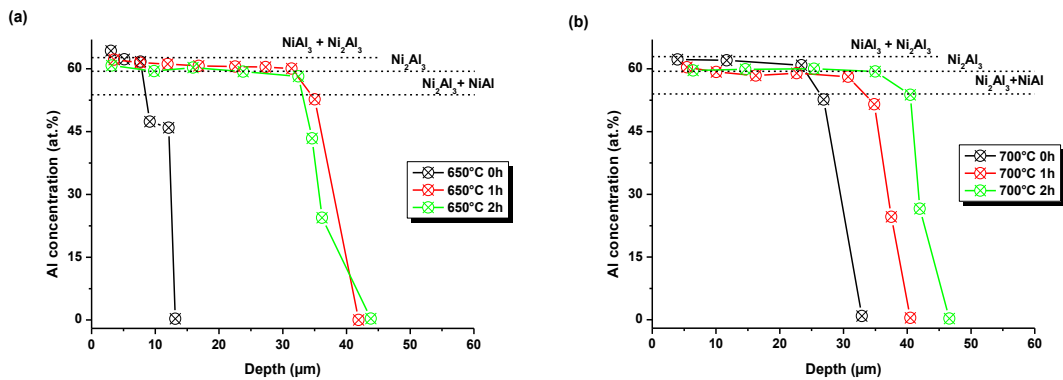


Figure IV-9 – Diffusion profiles of the Al concentration diffused into the pure Ni samples for several isothermal durations at (a) 650°C and (b) 700°C.

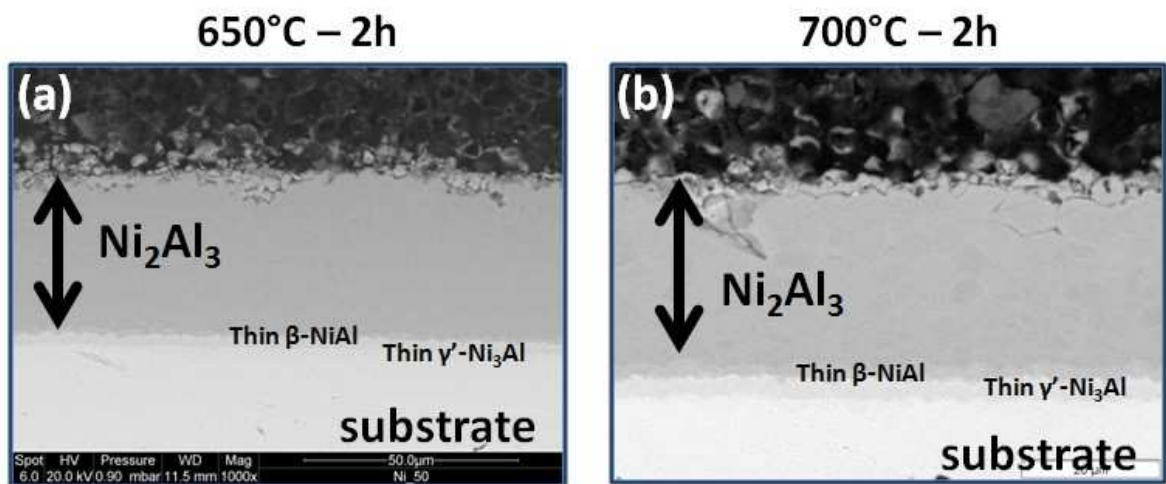


Figure IV-10 – Microstructure the PARTICOAT slurry applied on pure Ni (EQ) substrate after a thermal treatment in Ar(g) atmosphere with an isothermal step (a) at 650°C for 2h and (b) 700°C for 2h.

Figure IV-11 presents the XRD measurements, which have been done to characterize the intermetallic formations for both treatments at 650°C – 2h and 700°C – 2h. The two systems are composed of the same patterns supported by the formation of $\delta\text{-Ni}_2\text{Al}_3$ but also remaining metallic Al. Nevertheless, the higher temperature allows to consume more aluminium from the top coat reservoir, as suggested by the relative intensities of the peaks.

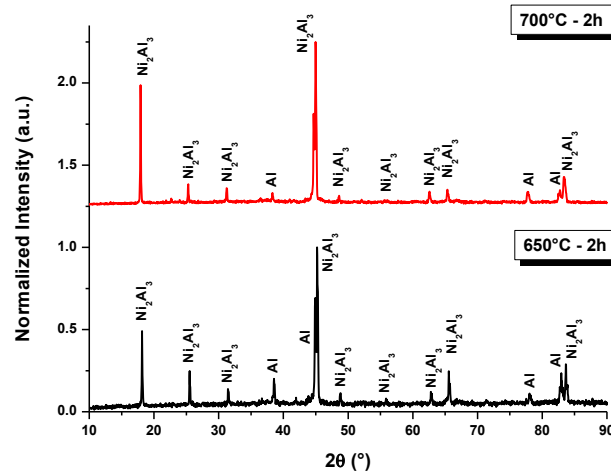


Figure IV-11 – Comparison of the XRD patterns of the PARTICOAT slurry applied onto pure Ni coupons acquired after thermal treatments at 650°C for 2h and 700°C for 2h.

Several groups already investigated nickel aluminide formations for this temperature range. While the group of Celko *et al.* [28] reported a transformation sequence of $\text{Al} \rightarrow \text{Al}_3\text{Ni} \rightarrow \text{Al}_3\text{Ni}_2 \rightarrow \text{Ni}$ when annealing at 630°C a Ni layer deposited by HVOF onto Al sheet, Janssen *et al.* [29] reported the $\text{Al} \rightarrow \text{Al}_3\text{Ni} \rightarrow \text{Al}_3\text{Ni}_2$ sequence for an isothermal annealing at 610°C of a pure Ni sample previously dipped into melted Al at 700°C. It has to be noted that they did not observe remaining pure Ni content due to the design of their experiments but also to the onset of diffusion that may initiate from the dipping process. Janssen *et al.* also mentioned the dissolution of 10 μm of pure Ni when dipping their sample into liquid Al at 700°C for only 6s [29] can explain the fast growing of the Ni-Al intermetallic compounds. In both studies [28-29], it was reported that the Al_3Ni_2 phase grows more rapidly than the Al_3Ni one. It has to be also mentioned that the Ni_5Al_3 phase did not form even at this temperature. Xiang *et al.* [30] mentioned the possibility to achieve the formation of the latter Ni_5Al_3 at 650°C after 1561h when studying the degradation kinetics of a Ni_2Al_3 / Ni coating deposited onto ferritic steels.

Several factors can explain this sequence of compound formations and their kinetics regarding this temperature range. The initial melting temperature of bulk aluminium (100 at. %) is at about 660°C. Even by considering the use of Al microparticles, it has been shown using a Thompson derived formula [31-32] that depending on their size, their melting temperature is slightly shifted to lower ones. This effect is more pronounced for nanoscaled materials than for microsized ones.

Looking also at the binary phase diagram, characteristic temperatures have to be considered, i.e. the $\text{Al} + \text{Al}_3\text{Ni}$ eutectic point at 639°C but also the solid solution till 660°C for Al rich compounds (*Figure IV-8(b)*), when taking into account a tiny addition of Ni diffused into the bulk Al [25]. Shifting of the melting temperature has been already reported whether if considering the influence of impurities [33] or more recently when studying the size effect on the thermal properties of Al powders using a melting temperature depressant (Si) added to a slurry containing Al microparticles [27]. In fact, as Galetz *et al.* [27] proposed, a liquid phase has to be considered during these intermetallic formations for which diffusion coefficient are much higher [25;34]. Furthermore, an incubation time seems to be necessary to take advantage of the complete liquid-like behaviour between zero and one hour of annealing.

As a matter of fact, one can note that a solid state diffusion domain exist between 639°C and 660°C, for the Al + Ni in solid solution into liquid aluminium domain, as represented by the red area in *Figure IV-8(b)*. At this point, liquid Al-rich phases move inwardly into the scale [35], while Ni dissolves into the latter [36]. The NiAl₃ phase has been reported to grow firstly [28] followed by the Ni₂Al₃ phases, which is known to have a faster kinetics of formation as reported by Janssen *et al.* [29] and Ren *et al.* [37], who investigated annealing of the Ni-Al intermetallics at 610°C and up to 540°C, respectively. Such faster growth rate of Ni₂Al₃ may be related to its lower activation energy (98.65 kJ.mol⁻¹) required for its formation compared to the one of the NiAl₃ compound (119.22 kJ.mol⁻¹) [37]. These assumptions on nickel aluminide formation on pure Ni support the observations during the establishment of the PARTICOAT coating, also supported by XRD measurements. Indeed, the NiAl₃ phase has not been detected for the two hours experiments at 650°C (*Figure IV-11*), which confirmed its quick vanishing with the annealing temperature, as also observed by Celko *et al.* [28]. The temperature promotes the Al flow towards the substrate while a sufficient annealing time leads to the homogenization of the coating thickness (*Figures IV-9*).

As an explanation, the amount of liquid phase involved into the reaction can explain the important kinetics of formation of the intermetallic phases. The *Figure IV-12* represents the evolution of the phase fraction as a function of the temperature for the Ni-Al intermetallic system. One has to note that these theoretical calculations have to be correlated with the experimental observation. As an example, the β-NiAl phase was not observed during the measurements after the annealing at 650°C nor at 700°C. Indeed, it can be observed that the appearance of the liquid phase begins at the eutectic temperature (639°C), from which the liquid amount increases. In addition, the amount of this phase at 700°C is twice more important than at 650°C, which allows to suggest that the dissolution phenomenon of the Ni into liquid Al is highly promoted in those conditions, hence leading to enhanced ingress of the Al into the substrate. Indeed, bright contrasts are visible in the top coat attesting that the dissolution of Ni in this liquid phase occurred. Recently, Galetz *et al.* [27] proposed a model of formation of the intermetallic from the application of microparticles based slurry for Ni-based substrate. They observed the same phenomena, which support the mechanisms observed during the present study.

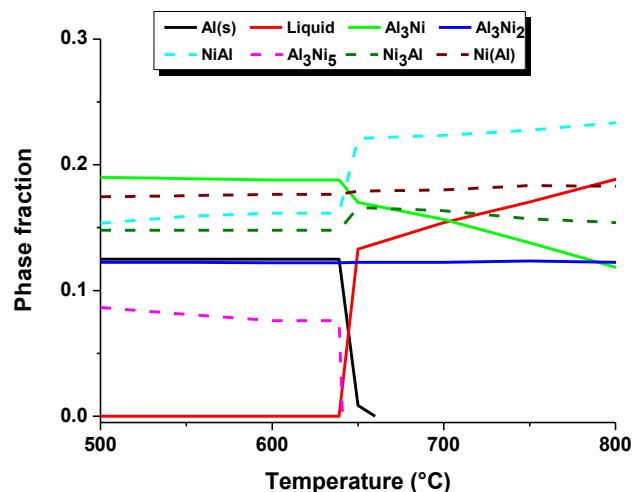


Figure IV-12 – Phase fraction evolution as a function of the temperature considering the Ni-Al binary system calculated using the lever rule. Note the evolution of the liquid phase fraction plotted in red [38].

In order to provide an appropriate oxidation resistance at high temperature the coating has to be stabilized. For this to happen, the Ni_2Al_3 phase has to be transformed into a more protective phase ($\beta\text{-NiAl}$) with respect of the Ni outward diffusion at higher temperature [39]. In addition, the $\gamma\text{-Al}_2\text{O}_3$ from the topcoat also has to be transformed into the more stable oxide ($\alpha\text{-Al}_2\text{O}_3$). For this to happen, a second step at 1100°C is realized to stabilize the coating system.

ii. Intermetallic formations after the complete thermal treatment.

In a similar way than for the intermediate step, several durations of annealing at 1100°C have been realized to follow the transformation of the Ni_2Al_3 phase into the targeted $\beta\text{-NiAl}$ one. *Figure IV-13(a)* gathers the EDS diffusion profiles of Al and Ni in pure Ni for 1h, 2h and 3h of isothermal dwell. It is observed that all the samples have a similar intermetallic sequence from the topcoat / coating interface towards the substrate with the subsequent formation of the $\beta\text{-NiAl}$, $\gamma\text{-Ni}_3\text{Al}$ and finally the $\gamma\text{-Ni}$ phase of the substrate. By maintaining such high temperature for 1h, a $10\mu\text{m}$ thick Al rich $\beta\text{-NiAl}$ (> 50 at.%) forms on top of a $\beta\text{-NiAl}$ ($55\mu\text{m}$). Below this layer, a thin $\gamma\text{-Ni}_3\text{Al}$ layer developed resulting of its narrow stability field, in which Al diffusion coefficients are rather similar or slightly smaller than in $\beta\text{-NiAl}$ [40]. The overall Al enriched zone, including the $\gamma\text{-Ni}(\text{Al})$, has a diffusion depth of $75\mu\text{m}$. One additional hour at 1100°C (2h) allows to form the stoichiometric $\beta\text{-NiAl}$, while the coating is $5\mu\text{m}$ thicker. XRD measurements (*Figure IV-13(b)*) confirmed the $\text{Ni}_2\text{Al}_3 \rightarrow \beta\text{-NiAl}$ transformation impaired with this step. Three hours of annealing at the same temperature did not lead to major modifications of the characteristic of the coating as shown by *Table IV-1*, even by considering the Ni outward diffusion at this temperature [39]. In any case, it has to be mentioned that the diffused zone obtained after 1h and 2h at 1100°C , respectively, are comparable to the one achieved using conventional pack cementation approaches [41]. In addition to the microstructure evolution of the coating, the signature of the $\alpha\text{-Al}_2\text{O}_3$ compound has also been revealed by the XRD measurements (*Figure IV-13(b)*), which is relevant of the transformation of the hollow microsphere topcoat in a thermodynamical stable oxide structure.

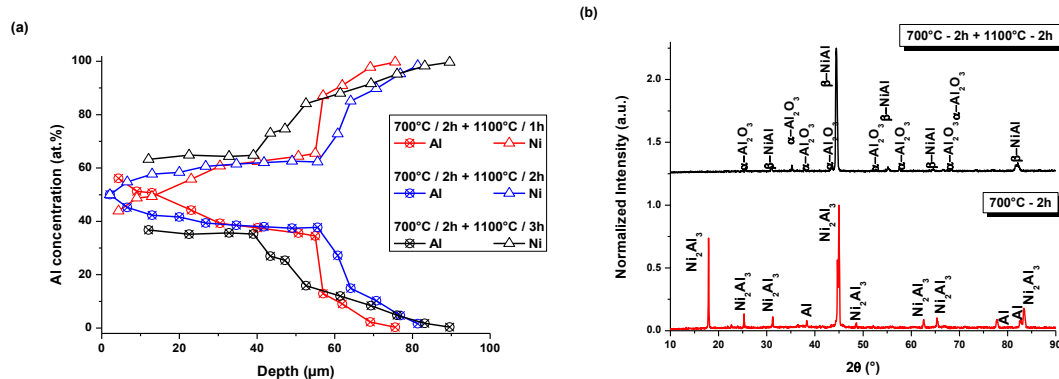


Figure IV-13 - (a) Diffusion profiles into pure Ni samples for several isothermal durations at 1100°C for 1h (in red), 2h (in blue) and 3h (in black). (b) XRD patterns after the complete thermal treatment ($700^\circ\text{C} - 2\text{h} + 1100^\circ\text{C} - 2\text{h}$).

Table IV-1 – Summary of the characteristics of the diffused zone formed onto pure Ni as a function of the thermal treatment and its duration.

Thermal treatment (temperature - annealing time)	Diffused zone				
	650°C - 2h	700°C - 2h	700°C - 2h + 1100°C - 1h	700 °C - 2h + 1100°C - 2h	700°C - 2h + 1100°C - 3h
Topcoat	adherent	adherent	sintered	sintered	sintered
Major phases	Ni ₂ Al ₃	Ni ₂ Al ₃	β-NiAl	β-NiAl	β-NiAl
Size of the major phase (μm)	≈35	≈40	≈55	≈55	≈40
Aluminized depth (μm)	45	45	75	80	90

Figure IV-14 shows the microstructure of the system after the complete thermal treatment in flowing Ar(g) atmosphere. It can be seen that the PARTICOAT concept is realized by the formation of an external hollow spheres topcoat, which formed on top of a diffused layer [25]. Investigation of the cross-sections (Figures V-14(a;b)) shows the growth of the Al enriched zone of 50 μm for the 700°C - 2h treatment (Figure V-14(a)) and of 70 μm thick for the complete thermal treatment (Figure V-14(b)).

The development of a thin thermally grown oxide layer formed at the topcoat / substrate interface (Figure IV-14) has been observed with the Al and O enrichment of the X-ray maps (not shown). This oxide formation might be promoted by the reduced partial pressure of O₂ into the treatment chamber, while the topcoat foam may also contribute to reduce the oxidizing species at this interface by modifying the gas outflow line and also because of remaining Al get oxidized. The foam tortuosity as well as its porosity might contribute to rule the permeation of the oxygen through it. Due to its thickness but also since the EDS technique imply a matrix effect of the surrounding compounds, local micro-Raman spectroscopy has been carried out to emphasize the nature of these alumina phases from the small amount of Cr³⁺ impurity contained into the model material (cf Chapter II). The signatures of two of them have been found using this technique. The α-alumina top coat has been confirmed at the centre of the sample while traces of θ-alumina were found close to the edges. The latter transient oxide signature came from areas where some random detachment of the ceramic top coat occurred subsequently to the thermal treatment, which one also includes the quenching step.

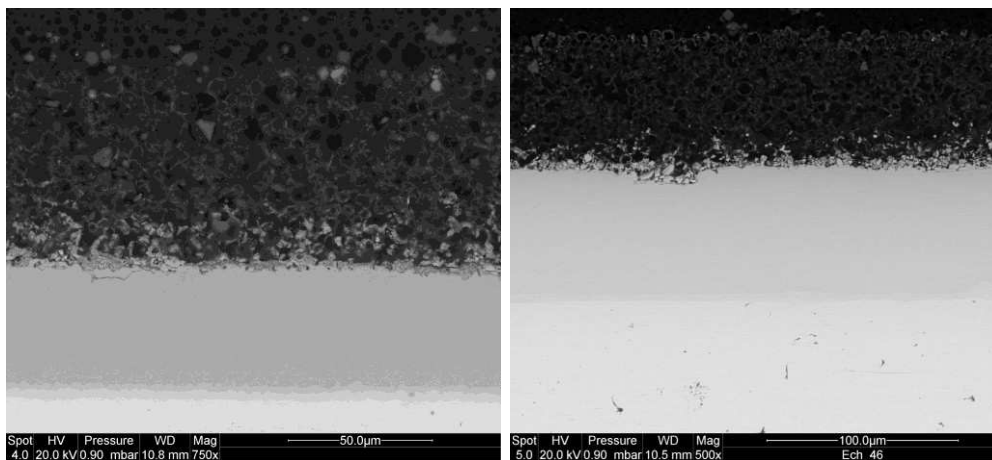


Figure IV-14 – Comparison of the microstructures of the PARTICOAT slurry applied onto pure Ni after (a) 400°C - 1h + 700°C - 2h and (b) the complete thermal treatment (400°C - 1h + 700°C - 2h + 1100°C - 2h).

Table IV-1 gathers the coating system feature (thermal treatment, topcoat behaviour, major phase...) for the steps investigated whether if considered at intermediate ($T \approx T_{m,Al}$) or at high temperature ($T = 1100^\circ\text{C}$) in case of the pure Ni substrate. Whereas at 650°C , a small incubation time is required due predominant solid state diffusion, the dissolution of Ni is spontaneously promoted into the liquid Al at 700°C , hence increasing kinetics. In both cases, the first thermal step is assimilated to a high activity / low temperature process. The topcoat remains adherent with onset of sintering, while the Ni_2Al_3 compound is the major phase developed into the substrate, in contrast with thermodynamic predictions. The step at 1100°C corresponds to a stabilization process, which allows the $\text{Ni}_2\text{Al}_3 \rightarrow \beta\text{-NiAl}$ transformation as well as the stabilization of the topcoat into the alpha alumina phase and greater sintering.

Since the aim of the PARTICOAT concept is to manufacture a protective coating for Ni-based superalloys, which usually contain chromium and other alloying elements (see Chapter I), the efficiency of the process had to be qualified onto an other model alloy to tailor its feasibility. In this view, the Ni20Cr material has been investigated as a first extrapolation of the process. Nevertheless, it has to be noted that the latter contained also 1.5 wt.% of silicon.

b. Polycrystalline Ni20Cr.

The use of the same heat treatment ($400^\circ\text{C} - 1\text{h} + 700^\circ\text{C} - 2\text{h} + 1100^\circ\text{C} - 2\text{h}$) in flowing Ar(g) has been applied for the second model alloy. It can be observed from the surface of the sample (*Figure IV-15(a)*) that it resulted in the partial detachment of the top coat. The diffusion and the growth of elongated areas occurred in several random zones formed from both dissolution of the substrate into the molten Al and diffusion phenomena of the Al. Between these zones, the surface of the raw substrate can be clearly identified without any piece of the top coat on top of it. The cross-section of the sample (*Figure IV-15(b)*) revealed island-like diffusion morphology on top of the appearance of Kirkendall porosity associated with segregation of chromium aluminide (Al_xCr_y) at the front of the diffused zone. These porosities are due to the difference of the diffusion coefficient of the Al and Cr elements in the Ni_xAl_y phases. Chromium is indeed well known to have a reduced solubility in Ni-Al intermetallic phases [42-46].

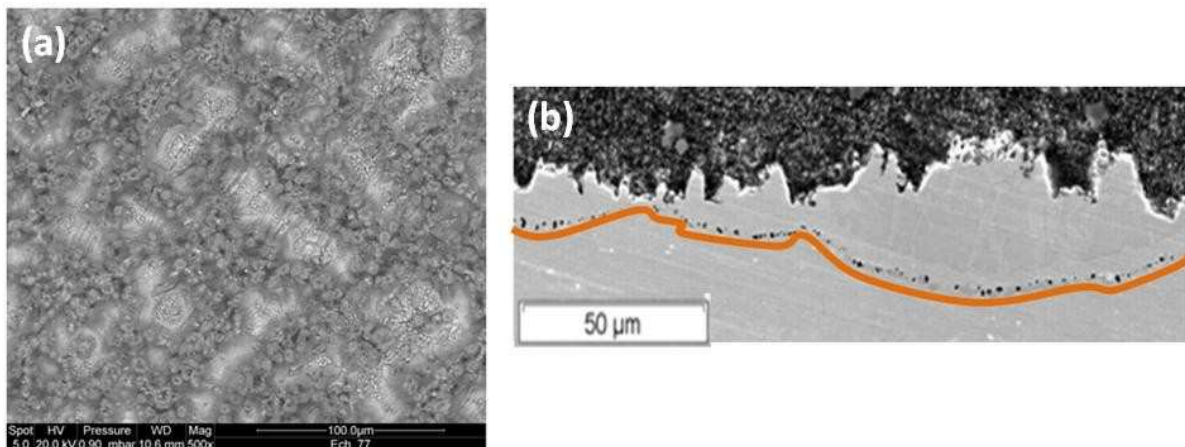


Figure IV-15 - Complete thermal treatment ($700^\circ\text{C} - 2\text{h} + 1100^\circ\text{C} - 2\text{h}$) in Ar(g) realized for the PARTICOAT slurry applied onto Ni20Cr substrate with (a) the surface of the sample showing the topcoat spallation and (b) the Al island diffused microstructure developed into the metallic substrate. Note the Kirkendall porosity interface underlined by the orange line.

From these experimental observations, thermodynamic outputs have been modelled to support the formation of these detrimental components regarding the aluminizing. *Figure IV-16(a)* represents the Ni-Al-Cr ternary phase diagram at 700°C , which shows the stability domain of these intermetallics

nearby the Al-rich domain. This provides useful information about the PARTICOAT process, confirming that an important Al flow occurs during the formation of the intermetallics to result in the aluminization of the substrates. From these theoretical approaches, the formation of Al_xCr_y compounds has been observed from *post-mortem* XRD measurements of the samples (Figure IV-16(b)). These compounds are known to act also as diffusion barrier for Al ingress, which has been often found in high activity / low temperature pack coatings [47]. The resulting Al-rich phases formed over this diffusion barrier imply the formation of brittle components at the top coat / coating interface. The coupled effect of these components (Al rich phases + Al_xCr_y) may be therefore responsible for the detachment of the top coat during the quenching.

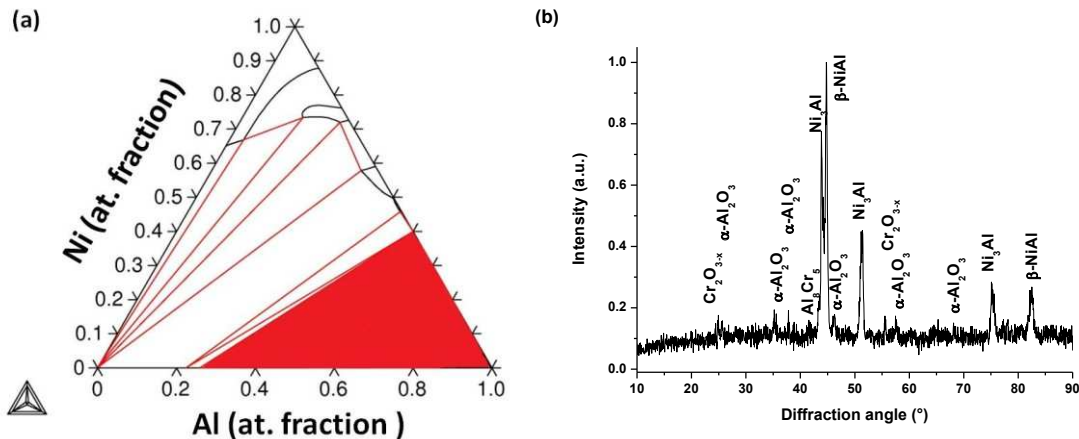


Figure IV-16 – (a) Ni-Al-Cr ternary phase diagram at 700°C modelled with Thermocalc (TCNi5). The red zone corresponds to the Al_xCr_y stability domain and (b) XRD patterns of Ni20Cr PARTICOATED and heat treated using the previous thermal treatment (400°C – 1h + 700°C – 2h + 1100°C – 2h).

In order to understand the mechanisms involved, one has to keep in mind that the chemical composition of the substrate contains 1.5 wt.% Si. Therefore, interactions with Cr and Si have also to be considered, in particular with regard to the appearance of eutectics. Indeed, from the Al-Ni binary phase diagram, the eutectic point is located at 639°C [48], while considering the effect of Cr addition and looking at the Al-Ni-Cr ternary phase diagram, the latter is slightly shifted to lower temperatures (635°C), as quoted by Rosell-Lacalau *et al.* [49]. Finally, another eutectic transformation exists for the Al-Si compounds at 577°C [50], which allows to further reduce the temperature of aluminizing using the Al microparticles slurry method as studied by Galetz *et al.* [27].

Taking into account these observations, a modification of the second step of the thermal treatment has been done by using an intermediate temperature of 625°C, i.e. between the two above-mentioned eutectic points of the Al-Ni-Cr ternary and Al-Si binary systems. Figures IV-17 gathers the cross-section evolutions of the coating morphology after 0h, 1h, 2h, 5h and 10h at 625°C. It can be seen that the topcoat spheres are not emptied (Figures IV-17) even after 10h at this intermediate temperature even if a light Al enrichment as been realized. Despite the detachment of the topcoat occurred during the quenching phase (mismatches of coefficient of thermal expansion), the microstructure of the samples still showed an island-like morphology diffusion type. X-ray mapping performed in the diffusion coating after the 5h treatment shows the Al enrichment (Figure IV-18(a)) associated with Ni (Figure IV-18(b)) while Cr (Figure IV-18(c)) segregates at the Ni_3Al / NiAl interface (EDS measurement) and also at the external interface as Al_8Cr_5 according to XRD (Figure IV-19). In the meantime, Si also segregates (Figure IV-18(d)) at the same location than Cr as presented by the X-ray map contrasts. Table IV-2 summarizes the characteristics of the Al-enriched zones on Ni20Cr alloy for the annealing treatment at 625°C up to 10h. Even by modifying the thermal treatment of the PARTICOAT concept on this substrate, 20 wt.% of Cr coupled to 1.5 wt.% of Si seem to constitute a limitation for such slurry aluminizing process, considering this chemical composition.

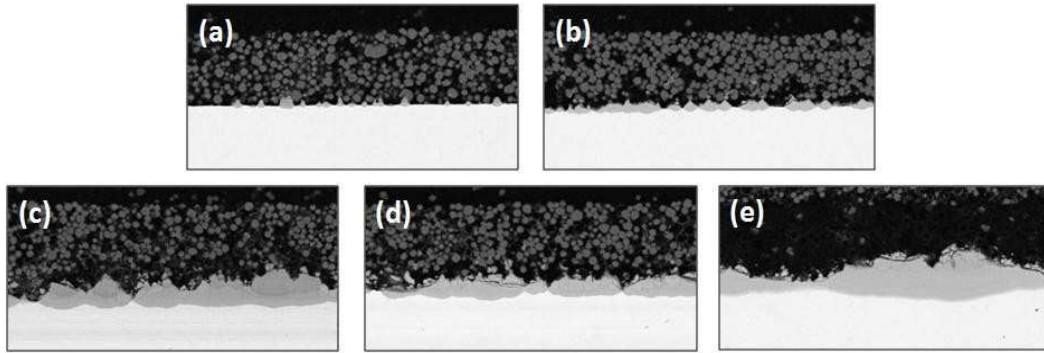


Figure 17 – Microstructure of the PARTICOAT slurry applied onto Ni20Cr(1.5Si) thermally treated at 625°C in Ar(g) for (a) 0h, (b) 1h, (c) 2h, (d) 5h and (e) 10h, showing the Al ingress with an island like morphology resulting in the topcoat detachment after 10h of annealing.

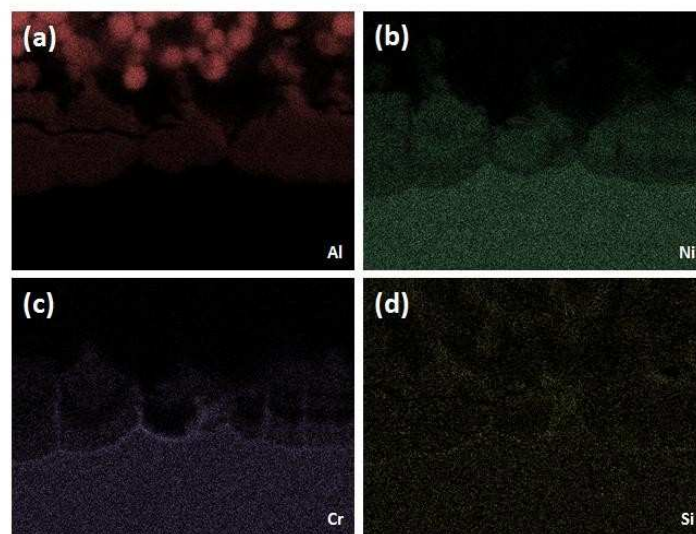


Figure IV-18 – X-ray mapping showing the elemental distribution of (a) aluminium, (b) nickel, (c) chromium and (d) silicon in the coatings obtained with a heat treatment at 625°C for 5h in Ar(g).

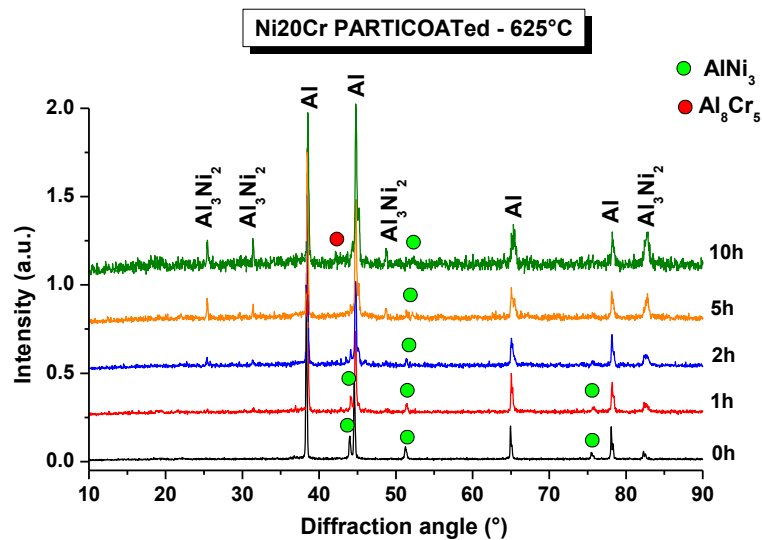


Figure IV-19 – XRD patterns of Ni20Cr samples PARTICOATed and thermally treated at 625°C for 0h, 1h, 2h, 5h and 10h. The growth of the Al_8Cr_5 compound develops with the longer annealing time.

Table IV-2 – Summary of the characteristics of the diffused zone formed onto Ni20Cr(1.5Si) as a function of the thermal treatment and its duration.

Thermal treatment (temperature - annealing time)	Diffused zone				
	625°C - 0h	625°C - 1h	625°C - 2h	625°C - 5h	625°C - 10h
Topcoat	adherent	adherent	adherent	adherent	detached
Major phases	Ni ₂ Al ₃	Ni ₂ Al ₃	NiAl ₃ +Ni ₂ Al ₃	NiAl ₃ +Ni ₂ Al ₃	NiAl ₃ +Ni ₂ Al ₃
Intensity of the Al _x Cr _y XRD signal	-	-	+	++	+++
Aluminized morphology	Island like				

Once the thermal treatment has provided information on its potential with respect of the model substrates, the temperatures have been selected to take advantage of the appearance of a liquid phase (700°C - 2h) for a quick aluminizing and then to stabilize the coating system at higher temperatures (1100°C - 2h). An extrapolation of this heat treatment has been carried out to real commercial Ni-based superalloys with lower and various Cr contents depending on their application fields (aero / land-base).

For this to happen, four substrates have been investigated: René N5 (SX: single crystal for aeroengine application), CM 247 LC (DS: directionally solidified similar compo to René N5), PWA 1483 (SX Land-based engine) and INCO 738 (EQ: equiaxed Land-based engine) (see Chapter II for the chemical compositions). The following sections are orientated with the increase of the chromium content. Explanations are focussed in a first time on René N5 and then compared to the three others substrates.

II. Formation of the coatings on industrial Ni-based superalloys.

A. First stage thermal treatment.

Figure IV-20 shows the cross-section morphology of René N5 after thermal treatment at 700°C for 0 and 2h. A duplex structure is observed *Figure IV-20(a)*. The SEM pictures and the EDS diffusion profiles (*Figure IV-20(b)*) suggested that a mixture of both phases exists for which a wavy microstructure is indicative of the evolution of a former eutectic phase after solidification [51]. XRD measurements confirmed the signatures of both NiAl₃ and Ni₂Al₃ compounds.

Figure IV-20(c) depicts the René N5 PARTICOAT annealed at 700°C for 2h. The same duplex zone still exists with the remaining wavy structure from the eutectic front. Nevertheless, its thickness ratio differs than the one formed for the treatment at 700°C for 0h. As a matter of fact, for the 700°C - 0h thermal treatment, the ratio e1/e2 rates 2/3 while the one for the 700°C - 2h treatment tends to 1/3. *Figure IV-20(d)* depicts the EDS profiles and suggests the formation of a Ni₂Al₃ matrix phase. *Table IV-3* and *Table IV-4* present the characteristics of the coating formed at 700°C - 2h regarding the nature of the coating matrix (measured from *Figure IV-22(a)*). Thicknesses of the coating formed on René N5 and the drop of the Al concentration are emphasized. At such intermediate temperature, the liquid Al dissolves Ni, as well as a part of the alloying elements. Their respective concentration profiles depend of their solubility limitation in the NiAl₃ and Ni₂Al₃ phases. The three other Ni-based superalloys investigated underwent the same phenomenon (*Table IV 3* and *Table IV-4*).

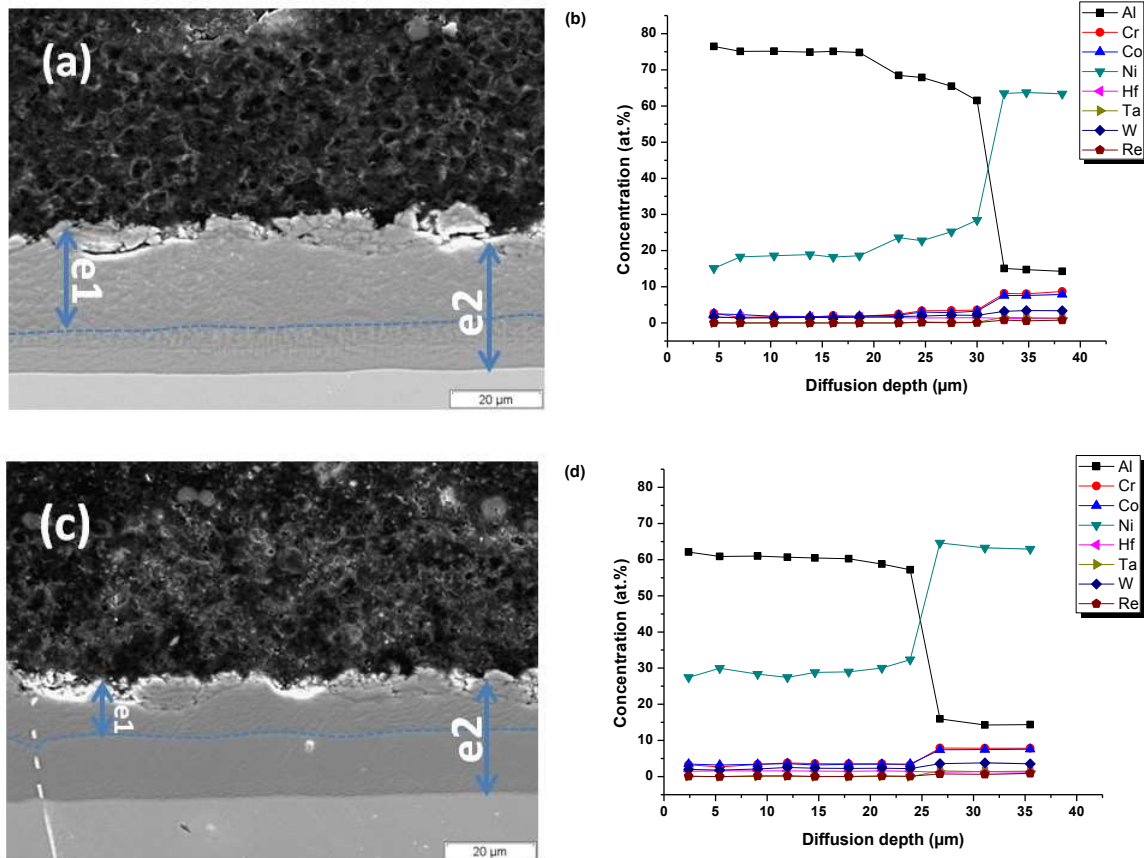


Figure IV-20 – Evolution of the microstructure formed for the René N5 material after the intermediate step at 700°C for (a) 0h and (b) its diffusion profile, while the caption (c) and (d) depict the thermal treatment at 700°C for 2h and its diffusion profile, respectively.

Figures IV-21 gathers the microstructures obtained for the four superalloys after the 700°C - 2h thermal treatment. Contrary to the Ni20Cr substrate, the topcoat has been found adhered for all the substrates investigated (René N5, CM 247, PWA 1483 and INCO 738), even after the 50°C.min⁻¹ quenching from the coating temperature. In all cases, a duplex zone is formed at this intermediate step. The evolution of the ratio e1/e2 evolves in the same way than for the René N5 substrate, which attests of the vanishing of the Al₃Ni eutectic matrix transforming into Ni₂Al₃ during two hours of annealing at 700°C. In addition, the four alloys have similar matrix compositions (Table IV-3 and Table IV-4), with the outer Ni₂Al₃ coating formed over the γ / γ' one. In this nickel aluminide coating, AlCr₂ compounds have been found dispersed, as shown by the contrast difference (Figures IV-21).

The dimensions of the Ni₂Al₃ matrix are in the same order of magnitude irrespectively of the alloy chemical composition (Table IV-3) while the two single crystals (SX) have the same extent of Al drop (≈ 2μm), the one of the directionally solidified (DS) is five times larger than the latter (Table IV-3). Assuming that the Al reservoirs deposited on top of all the substrates are the same before performing the thermal treatment, the thickness of the Al concentration drop from the Ni₂Al₃ matrix to the γ / γ' one is different depending of the structure of the materials and can be ascribed to the grain boundary effects [52]. Considering the distribution of Cr (Figure IV-22(b)), segregation close to the topcoat / Al enriched zone is visible for the superalloys containing around 12 wt.% or more, as it can be seen for the PWA 1483 and INCO 738. The René N5 and the CM 247 show an even distribution of this element in their respective Ni₂Al₃ matrix. Nonetheless, the XRD measurements confirmed the

presence of this alloying element precipitates (Al_xCr_y) in the coating for all systems, as summarized in Table IV-4.

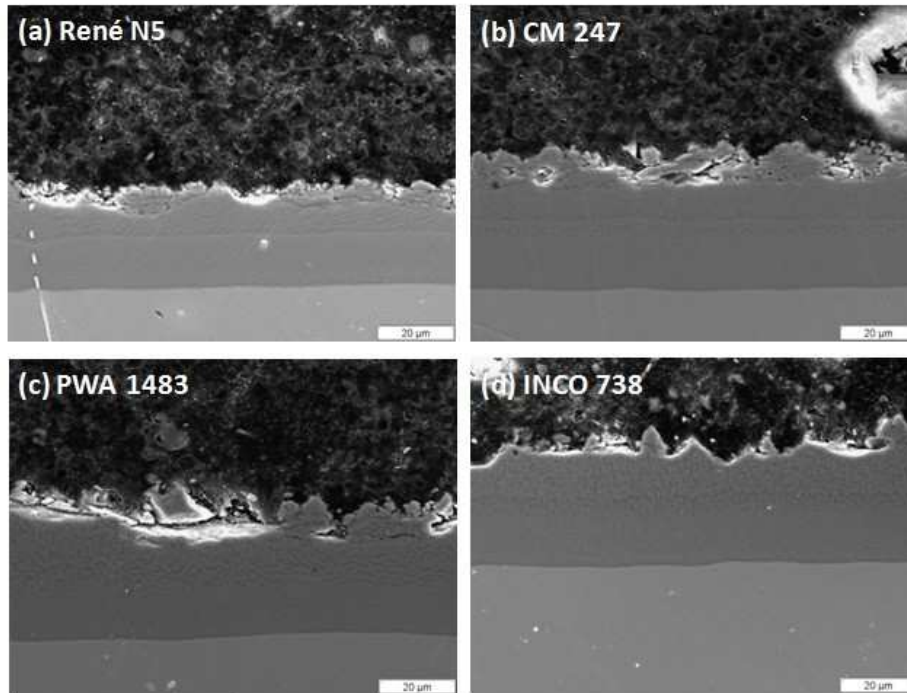


Figure IV-21 - Overview of the microstructure formed with the intermediate step at 700°C for 2h for (a) René N5, (b) CM 247, (c) PWA 1483 and (d) INCO 738 substrates.

Table IV-3 – Characteristics of the aluminized substrates after being thermally treated at 700°C for 2h in Ar(g) atmosphere.

	Substrate			
	René N5	CM 247	PWA 1483	INCO 738
Structure	SX	DS	SX	EQ
Cr content (wt.%)	7	8.1	12.2	16
Nature of the external matrix	Ni_2Al_3	Ni_2Al_3	Ni_2Al_3	Ni_2Al_3
Thickness of the external zone (μm)	≈ 25	≈ 28	≈ 25	≈ 32
Size of the Al concentration drop (μm)	≈ 2	≈ 10	≈ 2	≈ 5

Table IV-4 - XRD summary of the intermetallics formed during the intermediate step of the thermal treatment in Ar(g) for the four different superalloys.

Substrate	Thermal treatment	
	700°C 0h	700°C 2h
René N5	Al_3Ni ; Al_3Ni_2 ; Al	Al_3Ni_2 ; $AlCr_2$; Ni_3Al ; traces of oxides
CM 247	Al_3Ni ; Al_3Ni_2 ; Al	Al_3Ni_2 ; $AlCr_2$; Ni_3Al ; traces of oxides
PWA 1483	Al_3Ni ; Al_3Ni_2 ; Al	Al_3Ni_2 ; $AlCr_2$; Ni_3Al ; traces of oxides
INCO 738	Al_3Ni ; Al_3Ni_2 ; Al	Al_3Ni_2 ; $AlCr_2$; Ni_3Al ; traces of oxides

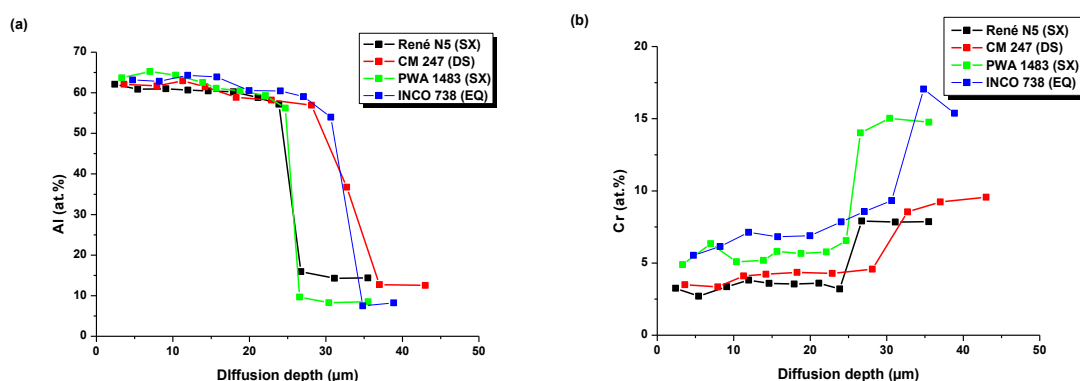


Figure IV-22 – (a) Al and (b) Cr composition profiles after PARTICOAT aluminizing and heat treatment at 400°C-1h + 700°C for 2h in Ar(g) atmosphere for the different Ni-based superalloys.

The $\text{Al}_3\text{Ni} \rightarrow \text{Al}_3\text{Ni}_2$ intermetallic formation sequence has already been reported in the literature by several authors, considering different types of systems. After studying the coating formation on superalloys, Thevand *et al.* [51] determined the conditions of growth of the Ni_2Al_3 coating on pure Ni using the pack cementation process. They concluded that the formation of a NiAl_3 phase can be promoted with respect of the solidification of a liquid phase formed at temperatures above $T_m(\text{NiAl}_3) \approx 854^\circ\text{C}$. Tamarin *et al.* [53] observed the same phenomenon using several Ni-based alloys.

In a similar manner than for the pure Ni substrate, a final step at higher temperature (1100°C) has been carried out to stabilize the coating.

B. Complete thermal treatment.

Figure IV-23(a) represents the cross-section of the coating formed after the complete thermal treatment for René N5. The topcoat transforms into the $\alpha\text{-Al}_2\text{O}_3$ foam structure (section I-B of this chapter), which is expected to confer thermal insulation to the substrate [54-55]. The bi-layered additive zone is composed by an outer part, which contains a great number of Cr-rich precipitates, as their occurrence and size are more significant at its top half than at its bottom. Under this Al enriched zone, the interdiffusion zone (IDZ) formed with a thickness of 25 μm. Such type of microstructure is typical of a high activity process followed by a homogenization step at higher temperature [56]. Considering this kind of design and depending of their chemical nature, the effect of the precipitates has to be considered carefully considering also the Al concentration of the phases of interest.

For example, Al_xCr_y compounds are supposed to exist at this temperature at the thermodynamic equilibrium for Al content between 30 and 40 wt.% (Annexe). The calculations indicate that their fractions are expected to be low, thus implying that they might dissolve into the phase formed or that they might transform into other Cr-rich phases. As depicted by the isopleth section* at 1100°C (Figure IV-24) for low Al contents (< 10 at.%), Cr is predicted to dissolve into a $\gamma\text{-Ni}$ phase but might also form TCP phases ($\mu\text{-WCrMo}$) [57]. The zone coloured in green gradient emphasizes the stability domain of the $\beta\text{-NiAl}$ phase. For Al amounts between 10 and 20 wt.%, Cr is expected to remain into TCP phases related to W, Mo and Co to form μ and λ or σ -phases, while a Cr BCC_B2 phase is predicted to form for higher Al concentration between 20 and 40 wt.%. This thermodynamic calculations supports the SEM observations of the additive layer (Figure IV-24), which seems to be divided into a rich zone of precipitates remaining on top of a zone with precipitates of smaller

dimensions due to the solubility limitation of Cr in the β -NiAl [42;45;58-59] and of the alloying and refractory elements [60-61]. One has also to note that the border at the e1/e2 ratio, formed during the intermediate step at 700°C for 2h, is still present in the rich precipitate area. The nature of this front has not been precisely identified, but has been ascribed to a legacy of the former eutectic NiAl₃ / Ni₂Al₃ matrix border. These phase evolutions implying different kind of intermetallics, the solubility of the different precipitates ruled the partitioning of the alloying elements inside the matrix.

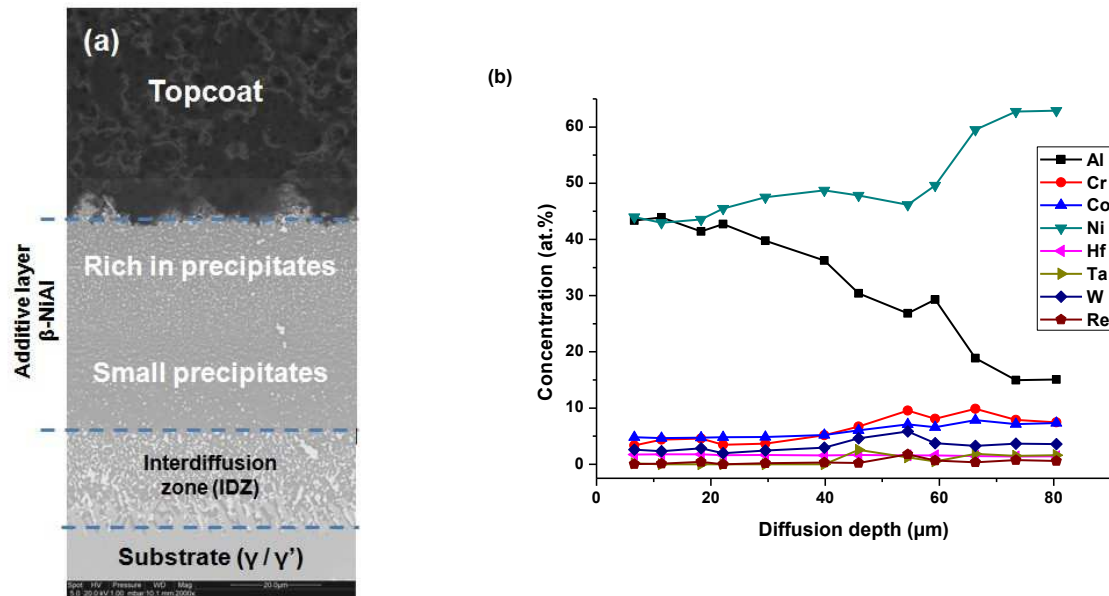


Figure IV-23 - Cross-section of a Ren  N5 substrate aluminized by the PARTICOAT slurry method. (a) Microstructure formed after the complete thermal treatment (400°C – 1h + 700°C – 2h + 1100°C – 2h) and (b) element concentration through the aluminide layer.

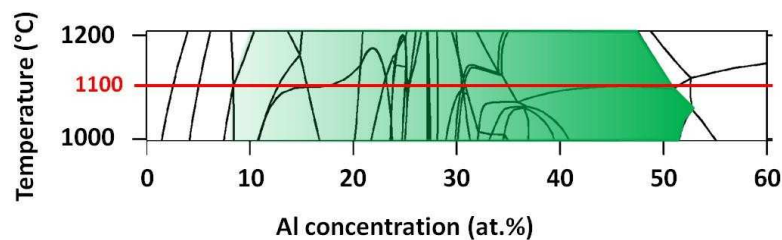


Figure IV-24 – Isoleth section of the Ren  N5 system between 1000°C and 1200°C, using the ThermoCalc® software (TCNi5), i.e. the area coloured in green gradation corresponds to the stability domain of the β -NiAl phase.

Once the versatility of the concept was confirmed with respect of its efficiency on Ren  N5 superalloys, a screening of the effect of alloying elements has been performed by investigating CM 247, PWA 1483 and INCO 738 superalloys (see Chapter II for the chemical compositions), mainly focussing on the Cr concentration effect but also on some refractory elements like Ta and W. Indeed, this type of segregations occur mainly by the grain boundaries to accumulate at the thermally grown oxide (TGO) interface, as shown by Mollard *et al.* by EPMA measurements [62].

* The full isopleths of the different systems are gathered in the Annexe section.

By increasing progressively the Cr content from 7 wt.% (René N5), to 8 wt.% (CM 247), to 12 wt.% (PWA 1483) and to 16 wt.% (INCO 738), the bond-coat successfully grew and the topcoat remained adherent, as shown in *Figures IV-25*. It is observed that all the substrates display a similar top coat foam structure and a three layered arrangement similar to the one described for René N5 substrate. A small deviation in the thicknesses of the diffused layers can be observed, probably due to the slurry amount deposited on the substrates, even if the latter has been systematically controlled before heat treating the samples. One has to keep in mind that the structure of the alloy (SX / DS / EQ) can also influence the diffusion processes with the grain boundaries influence to finally promote the formation of this three layered structure. *Figure IV-26* display EDS elemental profiles of Al and Cr in the different substrates.

Considering the Al content, all the substrates underwent the same $\text{Ni}_2\text{Al}_3 \rightarrow \beta\text{-NiAl}$ transformation. The overall enriched layer is about 75 μm thick while the aluminium concentration slowly decreases into the scale for finally revealing the γ/γ' matrix of the substrates (*Figure IV-26(a)*). For low Cr content alloys (René N5 / 7 wt.% Cr and CM 247 / 8.1 wt.% Cr), the Al diffusion profiles are rather similar, which is relevant of their quasi-similar chemical compositions (see Chapter II). In addition, it seems that their respective single crystal and directionally solidified structures do not play a major role in the formation of the coating. *Figure IV-26(b)* depicts the Cr diffusion profiles considering the same substrates. The initial low chromium content did not lead to the segregation of this element. Nevertheless, its content slightly increases with respect of the IDZ position, which is mainly composed of Cr and refractory element precipitates [63].

For higher chromium contents, i.e. PWA 1483 (12.2 wt.%) and INCO 738 (16 wt.%), the Al diffusion profiles (*Figure IV-26(a)*) present some irregularities at the top of the additive layer (first 10 μm depth zone). In addition, the Cr diffusion profiles (*Figure IV-26(b)*) revealed a chromium enrichment at the top of the additive layer, which can explain the irregularity on the Al diffusion profile, probably ascribed to the well known Cr restrained solubility into Ni_xAl_y compounds [42-46].

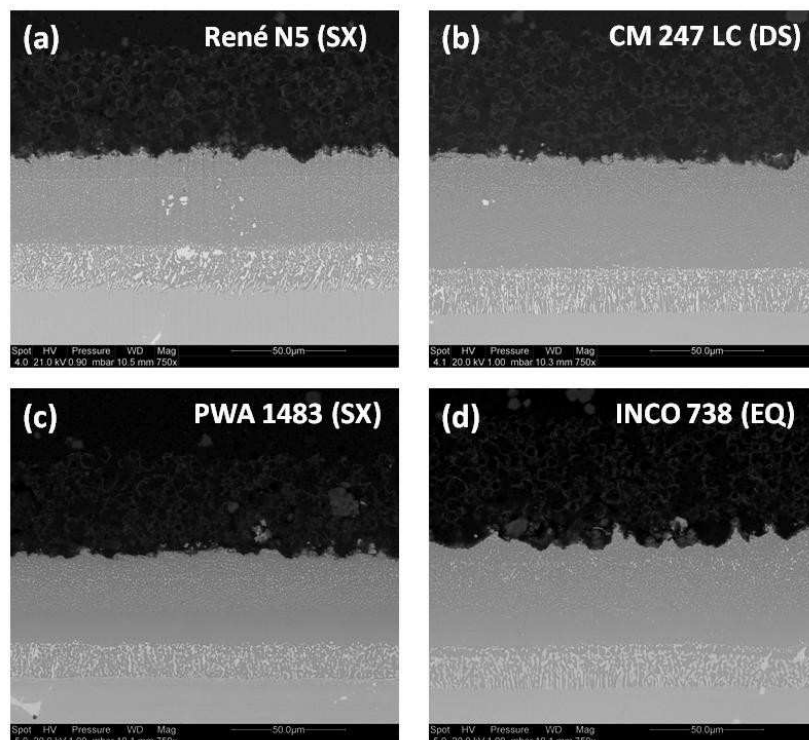


Figure IV-25 – Cross-sections of the substrates investigated for the PARTICOAT slurry aluminizing process on (a) René N5 (SX), (b) CM 247 (DS), (c) PWA 1483 (SX) and (d) INCO 738 (EQ). The samples have been heat treated using the 400°C - 1h + 700°C - 2h + 1100°C - 2h process, in Ar(g) atmosphere.

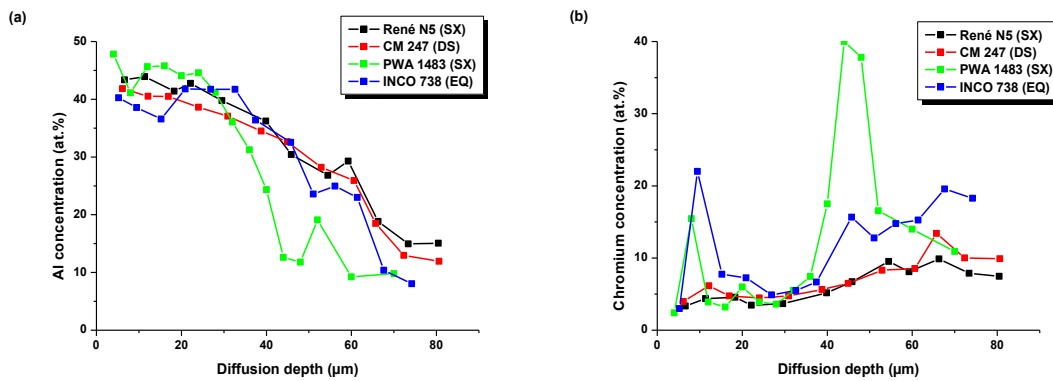


Figure IV-26 - EDS diffusion profiles analyzed on the four superalloys after the PARTICOAT slurry aluminizing, heat treated at 400°C - 1 + 700°C - 2h + 1100°C - 2h in Ar(g) atmosphere for (a) aluminium and (b) chromium.

Figure IV-27 depicts the XRD patterns for the systems that confirm the presence of the α -Al₂O₃ and the β -NiAl, ascribed to the top coat structure and the additive layer matrix, respectively. In addition, due to the same behaviour than for the high activity process followed by a homogenization step at higher temperature [56], precipitation of the alloying / refractory elements is observed for all the systems. Nonetheless, their dispersion and size allow to detect them on XRD measurements, through their distinctive signatures compared to those of the α -alumina and β -NiAl phases. Table IV-5 summarizes the presence of the phases observed into the scales by XRD measurement. One has to take care of the initial chemical composition of the respective systems, which might promote specific precipitate formations. As represented by Figure IV-28, the variation of the chemistry of the alloy (see Chapter II) will modify the stability domain of the intermetallic phases. In a similar manner, the appearance of the precipitates is ruled by their initial concentration and the phases formed through the thermal treatment. Similarly to the René N5 isopleth section (Figure IV-24), only the stability domain of the β -NiAl is coloured for the CM 247, PWA 1483 and INCO 738 systems to facilitate the reading. The lifetime of the systems can also be estimated using this representation (Chapter V-II.B).

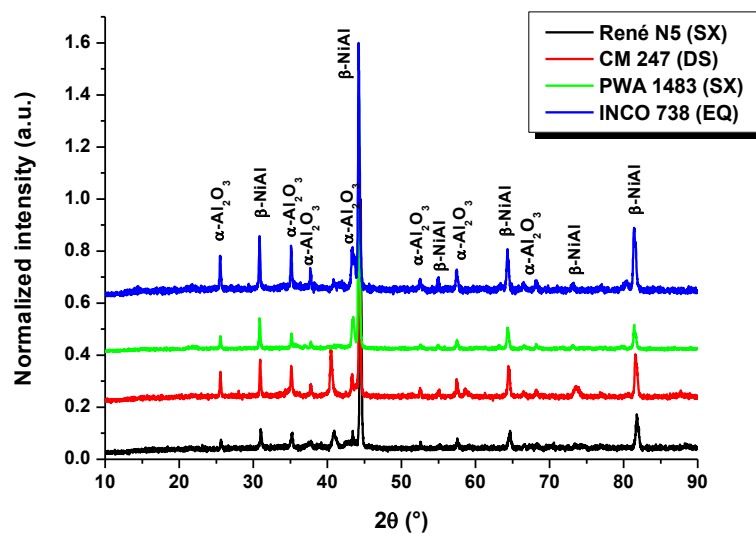


Figure IV-27 - XRD measurement of the Ni-superalloys after the PARTICOAT thermal treatment.

Table IV-5 - XRD summary of the intermetallics formed through the complete thermal treatment in Ar(g) (700°C 2h + 1100°C 2h) for the four superalloys.

Thermal treatment	Substrate			
	René N5	CM 247	PWA 1483	INCO 738
700°C 2h + 1100°C 2h	β -NiAl ; α -Al ₂ O ₃ , Al _x Cr _y , Ta _x O _y	β -NiAl ; α -Al ₂ O ₃ , Al _x Cr _y , HfO ₂	β -NiAl ; α -Al ₂ O ₃ , Al _x Cr _y , Ta _x O _y	β -NiAl ; α -Al ₂ O ₃ , Al _x Cr _y , Ta _x O _y

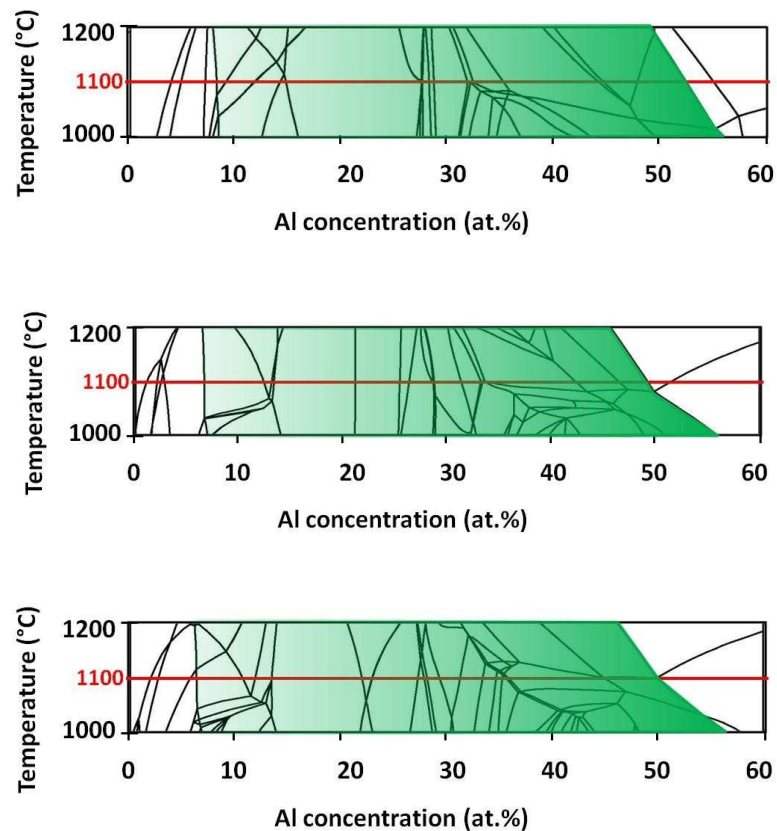


Figure IV-28 - Isopleth section of (a) CM 247, (b) PWA 1483 and (c) INCO 738 systems between 1000°C and 1200°C, using the Thermocalc® software (TCNi5), i.e. the area coloured in green gradation corresponds to the stability domain of the β -NiAl phase.

Summary and outlook

The aluminizing of several Ni-based substrates has been characterized from a slurry containing Al microparticles. Two model materials firstly allowed to provide information on the growth mechanisms of the coating while Ni20Cr allowed to gather information about chromium as alloying element.

Investigations on pure nickel material allowed to tailor a three steps thermal treatment (400°C – 1h + 700°C – 2h + 1100°C – 2h). These temperatures lead, respectively, to the decomposition of the binder, the aluminizing of the substrate as well as the onset of the formation of the PARTICOAT top coat and finally, the annealing of the intermetallics and the complete transformation of the top coat structure. As a result, the expected structure composed of an α -Al₂O₃ ceramic foam top coat, which formed over a β -NiAl coating has been successfully obtained.

Using a more complex substrate (Ni20Cr) did not give rise to the same results. This critical amount of Cr element promotes the formation of the Al_xCr_y detrimental compounds, which hinder the formation of the coating since the second step at 700°C. A modification of the thermal treatment did not allow to avoid these intermetallics. As a matter of fact, this high amount of Cr constitutes a limitation regarding this slurry method.

Nevertheless, René N5, CM 247, PWA 1483 and INCO 738 Ni based superalloys have been investigated and PARTICOATED. These materials have lower Cr content and their respective chemistries are composed by several other alloying elements, i.e. Co, Ta, Mo... Even with this modification of the chemical compositions, the process allowed to form the α -Al₂O₃ top coat and the β -NiAl coating after the thermal treatment designed for the pure Ni material. The Al enriched zone has a duplex structure with a rich precipitates zone on its outer area and with a lower concentration of this precipitates in the inner part. Such type of microstructure is rather similar to the one observed for pack cementation process at low temperature / high activity followed by an annealing treatment at high temperature.

Once the PARTICOAT structure was formed on the superalloys materials, one major question needs to be answered: how are the high temperature oxidation resistances of these coating systems? From this interest, all the materials cannot be compared for all the temperature due to their chemistry properties and their design regarding specific service conditions. The Chapter V focuses on characterizing this high temperature behaviour through long term isothermal oxidation experiments.

An optimization of the composition of the slurry might be possible to promote the formation of the PARTICOAT structure on several other types of materials with different chemistries, i.e. steels or other types of superalloys all by adopting the subsequent heat treatments. In addition, the development of so-called graded structures could also be an idea to enhance the top coat adhesion. Adding oxides particles should allow to match the thermal expansion coefficient of the substrates, while applying a layer between the top coat and the substrate may form a sandwich structure with a rather similar gradient of thermal properties.

References

- [1] V. Kolarik, M. Juez-Lorenzo, H. Fietzek, *Materials Science Forum* 696 (2011) 290
- [2] O. Kubaschewski, C.B. Alcock, *Metallurgical Thermochemistry*, 5th ed. Pergamon Press, Oxford (1979)
- [3] N.N. Sirota, G.N. Shokhiva, *Kristall und Technik*, 9 (1974) 913
- [4] Z. Lei, Z. Ke-Chao, L. Zhi-you, Z. Xiao-yong, *Metal Powder Report* 61 (2006) 28
- [5] X. He, H. Shi, *Particuology* (2012) doi: 10.1016/j.partic.2011.11.011
- [6] www.doitpoms.ac.uk/tlplib/Ellingham_diagrams/printall.php
- [7] S-J. L. Kang, *Sintering, densification, grain growth & microstructure*, Elsevier (2005) 8
- [8] R.K. Hart, J.K. Maurin, *Surface Science* 20 (1970) 285
- [9] T.S. Yeh, M.D. Sacks, *Journal of the American Ceramic Society* 71 (1988) 841
- [10] S.J. Wu, L.C. De Jonghe, *Journal of American Society* 79 (1996) 2207
- [11] A.A. Gromov, Y.I. Stokova, U. Teipel, *Chemistry and Engineering Technology* 32 (2009) 1049
- [12] M.A. Trunov, S.M. Umbrajkar, M. Schoenitz, J.T. Mang, E.L. Dreizin, *Journal of Physical Chemistry B* 110 (2006) 13094
- [13] L.P.H. Jeurgens, W.G. Sloof, F.D. Tichelaar, E.J. Mittemeijer, *Physical Review B* 62 (2000) 4707
- [14] T.F. An, H.R. Guan, X.F. Sun, Z.Q. Hu, *Oxidation of Metals* 54 (2000) 301
- [15] V.K. Tolpygo, D.R. Clarke, *Materials at High Temperature* 17 (2000) 59
- [16] D.P. Garriga-Majo, B.A. Shollock, D.S McPhail, R.J. Chater, J.F. Walker, *International Journal of Inorganic Materials* 1 (1999) 325
- [17] G.A. Storaska, J.M. Howe, *Materials Science and Engineering A* 368 (2004) 183
- [18] V.I. Levitas, *Combustion and Flame* 156 (2009) 543
- [19] A. Rai, K. Park, L. Zhou, M.R. Zachariah, *Combustion Theory and Modelling* 10 (2006) 843
- [20] V. Rosenband, *Combustion and Flame* 137 (2004) 366
- [21] B.S.M. Garima Chauman, *Influence of alumina shell on nano aluminium melting temperature depression*, Master of Science Thesis, Texas Tech University (United States of America), 2007
- [22] J.G. Railsback, A.C. Johnston-Peck, J. Wang, J.B. Tracy, *Journal of American Chemistry Society*, 4 (2010) 1913
- [23] J. Burke, T.R. Ramachandran, *Metallurgical Transactions* 3 (1972) 147

- [24] G. Bonnet, M. Mollard, B. Rannou, J. Balmain, F. Pedraza, X. Montero, M. Galetz, M. Schütze, *Defect and Diffusion Forum* 323-325 (2012) 381
- [25] F. Pedraza, M. Mollard, B. Rannou, J. Balmain, B. Bouchaud, G. Bonnet, *Materials Chemistry and Physics* 134 (2012) 700
- [26] P. Karlsson, A.E.C. Palmqvist, K. Holmberg, *Advances in Colloid and Interface Science* 128-130 (2006) 121
- [27] M.G. Galetz, X. Montero, M. Mollard, M. Günthner, F. Pedraza, M. Schütze, *Intermetallics*, "Dissolution and diffusion processes in the initial stages of slurry aluminization of nickel" (2012) submitted
- [28] L. Celko, L. Klakurkova, J. Svejcar, *Defect and Diffusion Forum* 297-301 (2010) 771
- [29] M.M.P. Janssen, G.D. Rieck, *Transaction of the Metallurgical Society of AIME* 239 (1966) 1372
- [30] Z.D. Xiang, D. Zeng, C.Y. Zhu, D.J. Wu, P.K. Datta, *Corrosion Science* 52 (2011) 3426
- [31] N.YU. Sdobnyakov, V.M. Samsonov, A.N. Bazulev, D.A. Kul'pin, *Bulletin of the Russian Academy of Sciences* 72 (2008) 1371
- [32] J. Sun, S.L. Simon, *Thermochimica Acta* 463 (2007) 32
- [33] B. Rufino, F. Boulc'h, M.V. Coulet, G. Lacroix, R. Denoyel, *Acta Materialia* 55 (2007) 2815
- [34] S.L. Lai, J.R.A. Carlsson, L.H. Allen, *Applied Physics Letters* 72 (1998) 1098
- [35] A. Kyriakopolous, M. Lynn, R. Ghomoshchi, *Journal of Materials Science Letters* 20 (2001) 1699
- [36] P. Visuttipitukul, N. Limvanutpong, P. Wangyao, *Materials Transactions* 51 (2010) 982
- [37] X. Ren, G. Chen, W. Zhou, C. Wu, J. Zhang, *Journal of Wuhan University of Technology-Mater. Sci. Ed.* (2009) 787
- [38] B. Rannou, M. Mollard, B. Bouchaud, J. Balmain, G. Bonnet, V. Kolarik, F. Pedraza, *Defect and Diffusion Forum* 323-325 (2012) 373
- [39] A. Chien, D. Gan, P. Shen, *Materials Science and Engineering A* 272 (1999) 207
- [40] J.M. Brossard, B. Panicaud, J. Balmain, G. Bonnet, *Acta Materialia* 55 (2007) 6586
- [41] F. Pedraza, C. Tuohy, L. Whelan, A.D. Kenedy, *Materials Science Forum* 461-464 (2004) 305
- [42] A. Chien, D. Gan, P. Shen, *Materials Science Engineering A* 206 (1996) 215
- [43] W. Huang, Y.A. Chang, *Intermetallics* 7 (1999) 863
- [44] H.L. Huang, Y.Z. Chen, D. Gan, *Materials Science and Engineering A* 328 (2002) 238
- [45] W.H. Tian, C.S. Han, M. Nemoto, *Intermetallics* 7 (1999) 59
- [46] M. Jain, S.P. Gupta, *Materials Characterization* 51 (2003) 243

- [47] P. Moretto, J. Bressers, D.J. Arrell, *Materials Science Engineering A* 272 (1999) 310
- [48] H. Okamoto, Al-Ni (aluminium-nickel), *Journal of Phase Equilibria and Diffusion* 25 (2004) 394
- [49] E. Rosell-Laclau, M. Durand-Charre, M. Audier, *Journal of Alloys and Compounds* 233 (1996) 246
- [50] K.W. Richter, H. Ipser, *Intermetallics* 11 (2003) 101
- [51] A. Thevand, S. Poizet, J.P. Crousier, R. Streiff, *Journal of Materials Science* 16 (1981) 2467
- [52] H. Mehrer, *Diffusion in Solids*, Springer (2007)
- [53] Y.A. Tamarin, *Protective Coatings for Turbine Blades* (2002) ASM International
- [54] X. Montero, M. Galetz, M. Schütze, V. Kolarik, M. Mollard, B. Rannou, B. Bouchaud, G. Bonnet, F. Pedraza, *Oxidation of Metals, Multipurpose TBC system based in alumina foam top coat and aluminium rich diffusion layer produced by micro-scaled aluminium slurries*, submitted
- [55] R. Roussel, V. Kolarik, M. Juez-Lorenzo, V. Kuchenreuther, F. Velasco, *Oxidation of Metals, High temperature coatings with multi-function on the basis of spherical micro aluminium particles*, submitted
- [56] D.K. Das, V. Singh, S.V. Joshi, *Metallurgical and Materials Transactions A* 29 (1998) 2175
- [57] C.M.F. Rae, M.S. Hook, R.C. Reed, *Materials Science and Engineering A* 396 (2005) 231
- [58] B. Bouchaud, J. Balmain, F. Pedraza, *Defect and Diffusion Forum* 289-292 (2009) 227
- [59] F. Pedraza, A.D. Kennedy, J. Kopecek, P. Moretto, *Surface and Coating Technology* 220 (2006) 4032
- [60] M.S.A. Karunaratne, C.M.F. Rae, R.C. Reed, *Metallurgical and Materials Transactions A* 32 (2001) 2409
- [61] C.C. Jia, K. Ishida, T. Nishizawa, *Metallurgical and Materials Transactions A* 25 (1994) 473
- [62] M. Mollard, *Elaboration de système barrière thermique par barbotine. Comportement du nickel et de ses superalliages revêtus en oxydation cyclique à hautes températures*, PhD Thesis, University of La Rochelle, France (2012)
- [63] C.M.F. Rae, R.C. Reed, *Metallurgical and Materials Transactions A* 32 (2001) 2409

Chapter V

High temperature isothermal oxidation behaviour of PARTICOATED Ni-based superalloys: the effect of the chemical composition of the substrate

Various nickel based superalloys with significant differences in their chemical compositions and structures (René N5, CM 247, PWA 1483 and INCO 738) have been PARTICOATED. This allowed to get a TBC system. Isothermal oxidation tests were carried out at high temperatures (900 and / or 1000 and / or 1100°C) up to 1000h, under flowing synthetic air. For this to happen, a screening of the conditions has been applied for each system with CM 247 LC as reference for all the temperatures (cf Chapter II). The effect of the chemical compositions and structures of the alloys on the oxidation and degradation mechanisms are discussed, focusing on chromium, titanium but also tantalum. In order to support the experimental data, thermodynamic calculations (isopleth modelling) allowed to assess the latter, giving information on the evolution of the chemistry of the different systems investigated.

Table of contents

I. Considerations about the behaviour of materials at high temperatures.	113
A. On the thermodynamics of the oxide scale formation.	113
B. Growth kinetics of the oxide scale: the case of the alumina scales.	114
II. Investigation of the oxidation resistance of the PARTICOATED superalloys.	115
A. The limitation of the materials with respect of the service conditions.	115
B. The isopleth as a tool to understand and predict the behaviour of the coating and the substrate.	118
C. Characterization of the PARTICOAT system during isothermal oxidation tests.	121
a. Oxidation kinetics.	121
b. Evolution of the top coat as a function of the chemistry of the systems.	125
c. Evolution of the thermally grown oxide (TGO).	126
d. Microstructural evolution of the bond coat.	127
e. Comparison between the PARTICOATED samples and the SVPA ones.	140
Summary and outlook	142
References.....	143

I. Considerations about the behaviour of materials at high temperatures.

High temperature oxidation results from the reaction between a solid (metal) and an oxidizing compound, which is usually oxygen or related oxidative compounds, and can lead to the ruin of the structural material. In addition to the oxidizing environment, such oxidation reactions are strongly dependant on the chemistry of the substrates. Therefore, thermodynamics can help in predicting the oxidation driving force of the system, while its progress is revealed by the evolution of the reactions kinetics involved during the high temperature oxidation.

A. On the thermodynamics of the oxide scale formation.

For a system at the equilibrium, thermodynamics allows to predict the conditions (temperature and oxygen partial pressure: p_{O_2}) for which the pure metal (M) will react with the oxidizing species to form the corresponding oxide, following *Equation V-1*:



The variation of the Gibbs free energy is given by the following equation:

$$\Delta_r G^0 = RT \times \ln(p_{O_2}) \quad \text{Equation V-2}$$

with p_{O_2} in pascals (Pa), T in Kelvin and R the gas constant. As a matter of fact, the oxidation reactions occur spontaneously when $\Delta_r G^0 < 0$. The oxidation reactions are thermally activated ($\Delta_r G^0 = f(T)$), i.e. the higher the temperature, the more spontaneous the reaction. These thermo-chemical properties have been gathered in Ellingham diagrams for the oxidation of pure elements. For one given temperature, the transition of a metal to its corresponding oxide is given by a specific value of the p_{O_2} . If this partial pressure is lower than the dissociation pressure of the metal / oxide transition, the metal is protected. On the contrary, if p_{O_2} is higher, the metal transforms into its oxide.

Depending on the properties of this layer, which is a matter of its thermodynamical properties and growth kinetics, the oxidation reaction will continue as long as the oxidizing species can react with the metal by the migration of the gas phase to the metallic component, or by the displacement of the metallic cations towards the gas phase. The O_2 adsorption at the metallic surface initiates and germination of the native oxide scale on a nanometre scale occurs. Further on, an oxide layer will form with a thickness of several microns. Such behaviour is ruled by several steps, as depicted by the *Figure V-1*. Once a homogeneous film is formed, the growth of the oxide layer is ruled by anionic and / or cationic diffusion through itself to continue the reaction with the metal core. Then, failure of the surrounding layer can appear by cracking, loss of cohesion and / or spallation. These processes will lead to two possibilities: the rehealing of the oxide scale or the propagation of the failure for finally bringing about the ruin of the material.

As discussed in the Chapter I, metallic structures have to be protected against the high temperature oxidation phenomena to avoid the degradation of the materials and to promote longer lifetime regarding the service conditions. Two types of oxide layer allow to withstand such criteria at moderate to high temperatures (500 – 1300°C), i.e. chromia and α -alumina. Nevertheless, the thermodynamic does not allow to predict the kinetics of these oxides formation, neither their likely allotropic transitions, i.e. $\gamma / \theta / \alpha$ in the specific case of alumina.

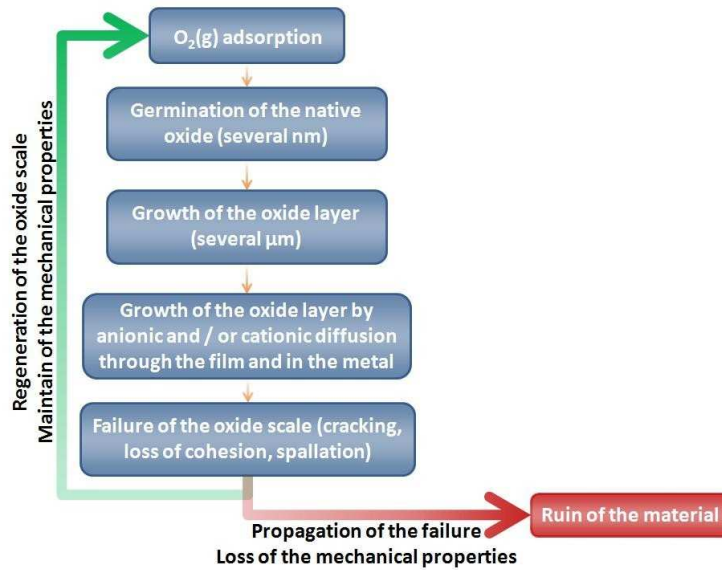


Figure 1 – Cyclic mechanism of the behaviour of the oxide scale at high temperature.

Depending on the service conditions, the growth of the oxide scales can be characterized by different oxidation laws corresponding to specific phenomena. The discussion in the next section summarizes some common knowledge on the kinetic laws adapted to the description of the oxidation processes and will focus on alumina scale.

B. Growth kinetics of the oxide scale: the case of the alumina scales.

The kinetic approach complements the thermodynamic one by allowing to estimate the oxidation rate of the metal or alloys. In most cases, the oxidation reaction can be summarized by the combination of two cases:

- The growth of an oxide scale developed at the gas / oxide and / or oxide / metal interface(s).
- The formation of a dense oxide formed by solid diffusion processes.

Based on the Wagner theory [1], analytical models exist to extract information of the experimental processes. The first case is often ascribed to the limiting transient phenomena taking into account the chemical reactions occurring at the interfaces. *Equation V-3* gives the so-called linear oxidation kinetic law, which describes a direct and constant oxidation of the metal. Therefore, this relation is described by the evolution of the mass (ΔM) per surface area (S) as a function of the time. Finally, the parameter extracted from such specific behaviour is k_l : the linear oxidation constant.

$$\frac{\Delta M}{S} = k_l \times t \quad \text{Equation V-3}$$

The second case is described by the so-called parabolic oxidation kinetic law, given by *Equation V-4*. This one is attributed to the phenomena where solid diffusion processes rule the growth of the oxide scale.

$$\left(\frac{\Delta M}{S} \right)^2 = k_p \times t \quad \text{Equation V-4}$$

Often, in most industrial systems the linear law appears at the beginning of the oxidation process and is followed by the parabolic one once a protective oxide scale has been formed, acting as a physical barrier to the oxidizing atmosphere. Such transition between the two behaviour depends on several parameters, i.e. the experimental conditions (roughness of the substrate, pO_2), as well as on the investigated temperature and on the chemical nature of the sample.

Therefore, a complete law can be formulated to take into account all phenomena involved during isothermal oxidations at high temperatures. Equation V-5 represents this formula:

$$t = cstt + \left(\frac{1}{k_l}\right)\left(\frac{\Delta M}{S}\right) + \left(\frac{1}{k_p}\right)\left(\frac{\Delta M}{S}\right)^2 \quad \text{Equation V-5}$$

Several groups of scientists have already investigated the complex growth mechanisms of the alumina scales, which are reported to have a parabolic behaviour [2]. The most conventional transient aluminas, i.e. γ / θ , seem to develop mainly by outward diffusion of the metallic cations, while the $\alpha\text{-Al}_2\text{O}_3$ has been reported to grow mainly by mixed diffusion processes [3]. Both phenomena of the oxygen anionic inward diffusion and cationic outward diffusion of the metallic element by volume and / or grain boundaries diffusion contribute to form several morphologies such as equiaxed or acicular ones [4-6]. Considering the alumina evolution at high temperatures, the transient $\theta\text{-Al}_2\text{O}_3$ has been reported to transform rapidly into the thermodynamically stable $\alpha\text{-Al}_2\text{O}_3$, between 900 and 1050°C [7-8]. For this reason, the contribution of each phase to the parabolic portion of the $\Delta M / S$ curves is hardly possible, especially when considering the significant number of factors associated with the experimental conditions.

Based on both thermodynamic and kinetic points of view, the evolutions of the PARTICOATED Ni-based superalloys have been investigated to study the effect of the temperature as a function of the chemistry of the alloys.

II. Investigation of the oxidation resistance of the PARTICOATED superalloys.

A. The limitation of the materials with respect of the service conditions.

As mentioned in Chapter I and based on a literature survey, the Ni-based superalloys used in this study (René N5, CM-247LC, PWA-1483 and IN-738LC) have different chemical compositions due to their respective designs regarding their respective application fields, at temperature range of service conditions. High amounts of Cr (PWA 1483 and INCO 738) are used to confer high temperature corrosion resistance by forming Cr_2O_3 scale (for $T < 950^\circ\text{C}$, cf Chapter I), while lower chromium content coupled with a sufficient quantity of Al allows to promote the formation of an alumina scale to resist to the high temperature oxidation processes (cf Chapter I). A tailoring of the aluminium content is necessary to keep the initial high mechanical properties of the Ni-based material, which is given by the γ / γ' matrix (cf Chapter I). Finally, alloying elements led to the reinforcement of the matrix to increase the mechanical resistance but contribute to lower the oxidation resistance of the base material. To introduce the following high temperature oxidation experiments, Table V-1 presents the respective chemical compositions of the four alloys.

Table V-1 – Chemical composition (at.%) of the substrates investigated for this study.

Substrate	Ni	Cr	Co	Mo	W	Ta	Nb	Al	Ti	Fe	Mn	Si	Others
René N5 (SX)	63.5	8.1	8.2	1.3	1.6	2.3	-	14	-	-	-	-	0.07 Hf 1 Re
CM 247 (DS)	63	9.3	9.3	0.3	3.1	1.1	-	12	0.9	-	-	-	0.5 Hf
PWA 1483 (DS)	61	13.8	9	0.6	1.2	1.6	-	7.8	5	-	-	-	-
INCO 738 (EQ)	59.5	17.6	8.3	1	0.8	0.5	0.5	7.2	4	traces	traces	traces	0.45 Hf

As underlined in *Table V-1*, the effect of the alloying elements on the oxidation and degradation mechanisms has been investigated during this study, and has been mainly focused on three elements (Cr, Ti, Ta). Cr is known to fulfil the requirement to build up an oxide layer, which improves the corrosion resistance of the alloys [9]. It can be observed that the four alloys have different amount of this element from low content [René N5 (8.1 at.% Cr), CM 247 (9.3 at.% Cr)] to a high content one, i.e. 17.6 at.% Cr (INCO 738). The PWA 1483 has been selected to ameliorate the screening as it contains 13.8 at.% of Cr.

Three of the four materials contain Ti and Ta. The first can develop a TiO₂ layer grown over a Cr₂O₃ oxide scale, in case of chromia-forming alloys [10], while the second is known to segregate as tantalum oxides (Ta_xO_y) at the grain boundaries but also underneath the α -alumina scale [11]. Both are also gamma-prime formers, which increase the mechanical properties of the alloys [12]. Nevertheless, their oxide forms are known not to protect against oxidation, by leading the spallation as well as increasing the oxidation kinetics [12].

In view of studying the degradation mechanisms of the PARTICOAT aluminized systems at high temperature, an adaptation of the temperatures has been done to avoid over-heating of the substrates. *Table V-2* gathers the experimental temperature conditions used for each alloy of interest, while oxidation tests were 100h, 500h and 1000h long. Regarding the chemical compositions of these superalloys, several studies were carried out to determine their optimum service temperatures. For instance, the INCO 738 (chromia-forming alloy) has a working temperature close to 825°C [13] and can be used in waste incineration plant or second / third stage of land based turbines. This alloy is known as a reference one considering the corrosion resistant materials [13]. The René N5 material (alumina-forming alloy) has been designed for aero-engine applications and can withstand working temperature as high as 1120°C [14], without additional protection system. These two alloys allowed to perform an optimization of the temperature and time conditions for the oxidation tests at high temperatures. The René N5 has been chosen to evaluate the PARTICOAT efficiency only for the highest temperature (1100°C), while the INCO 738 only ran for tests at 900°C. For PWA 1483, whose Cr content is lower than in INCO 738, but rather similar considering the amount of Ti, only the temperatures of 900°C and 1000°C have been investigated. Several groups also investigated this alloy in this temperature range [10;15]. CM-247LC, whose composition is close to that of René N5, has a small amount of Ti in its chemical composition but is often employed in land-based turbines [16]. Nevertheless, this material has been chosen as a reference in this study and has been investigated for the three temperatures of interest (900, 1000 and 1100°C).

Table V-2 – Summary of the targeted oxidizing temperatures for the oxidation experiments using the PARTICOAT coating systems.

Substrate (structure)	Oxidation test temperature								
	900°C			1000°C			1100°C		
	100h	500h	1000h	100h	500h	1000h	100h	500h	1000h
René N5 (SX)	X	X	X	X	X	X	✓	✓	✓
CM 247 (DS)	✓	✓	✓	✓	✓	✓	✓	✓	✓
PWA 1483 (SX)	✓	✓	✓	✓	✓	✓	X	X	X
INCO 738 (EQ)	X	✓	✓	X	X	X	X	X	X

X: condition not studied.

✓: tests performed.

These four superalloys are part of different generations of Ni-based superalloys. They are therefore representative of the three crystal structures: Equiaxed (EQ) INCO 738, directionally solidified (DS) CM 247 and single crystals PWA 1483 and René N5 materials. As explained in the Chapter I, the number (n) of the grain boundaries decreases from the EQ to the SX one as follows: $n_{EQ} > n_{DS} \gg n_{SX} \approx 0$. Thus, this manufacturing modification allows to change the diffusion properties of the alloying elements, i.e. especially the one known to diffuse at the grain boundaries [17]. Note however that the PARTICOATED materials exhibit different grain sizes depending on the mechanisms involved upon aluminization (Chapter IV, section I.C, p8).

To investigate the evolution of the systems with the high temperature oxidation tests, three main mechanisms have been identified, as described in Chapter I:

- The thermo-mechanical service conditions.
- The interdiffusion processes between the substrate and the aluminide bond coat.
- The formation of a protective, adherent, homogeneous, dense and stable oxide scale.

This study focuses on isothermal oxidation tests, which does not imply the strong effects of thermo-mechanical conditions (except for the oxide scale) but allows to study the mechanisms impaired with the interdiffusion processes that affect the composition and the microstructure of both the oxide scale, the coating and the secondary reaction zone (SRZ). The behaviour of the oxide scales, whose nature depends on the materials and the service conditions (see Chapter I), has been characterized by SEM investigations and room temperature XRD measurements, using *post-mortem* samples. In a similar manner, the interdiffusion processes between the additive layer and the oxide and between the additive layer/interdiffusion layer and the γ/γ' matrix of the substrate can be also rather relevant, in particular between the additive layer and the oxide scale in what the oxidation kinetics respect. These processes have been assessed using the same techniques.

In parallel, thermodynamic tools can help to predict the evolution of elemental partitioning with respect of the phase consumptions and transformations ruled by the thermo-activated interdiffusion phenomena. In this view, modelling of the chemical compositions has been done by means of isopleth simulation using the Thermocalc[®] software. Such inputs gave information about the coating and the substrate chemical composition.

B. The isopleth as a tool to understand and predict the behaviour of the coating and the substrate.

Several representations of the chemical components exist from a thermodynamical point of view, to predict their evolutions with time. As a matter of fact, when considering two chemical species, binary phase diagrams allow to predict stability domains but also the likely phase transformation of the system for a defined temperature and composition, usually in at.% or wt.%. By adding a third element, ternary phase diagrams provide information on the equilibrium between those three elements. More recently, with the development of softwares for thermodynamics, the calculations of more complex systems have been made possible to predict the behaviour of multi-components ones, i.e. alloys which can contain up to ten chemical species or even more.

From the database employed for this purpose, complex isopleths systems (Chapter II) have been modelled to understand the evolution of the coatings and superalloys matrixes. The latter allow to calculate phase stability domains regarding the complex composition of commercial superalloy material. Conventionally, these outputs are extracted from the combination of experimental and theoretical calculations. As introduced in the Chapter IV, several kinds of information can be extracted from such simulations. In this view, the Thermocalc[®] software has been used [18], using the specific TCNi5 database [19].

In the present case, we will focus on the stability domains of the nickel aluminide intermetallics as well as on the appearance/disappearance of additional phases (e.g. TCPs...) with respect of the Al concentration and as function of the temperature range (see *Table V-2*). In this section, only the approach undertaken the René N5 will be developed step by step for the sake of clarity. Then, the slightly different ones of the CM 247 LC, PWA 1483 and INCO 738 will be considered with the Thermocalc[®] tool, since their chemistries are different.

In order to introduce this type of modelling, *Figure V-2* depicts the influence of the temperature as a function of the Al concentration using the René N5 chemical composition (*Table V-1*).

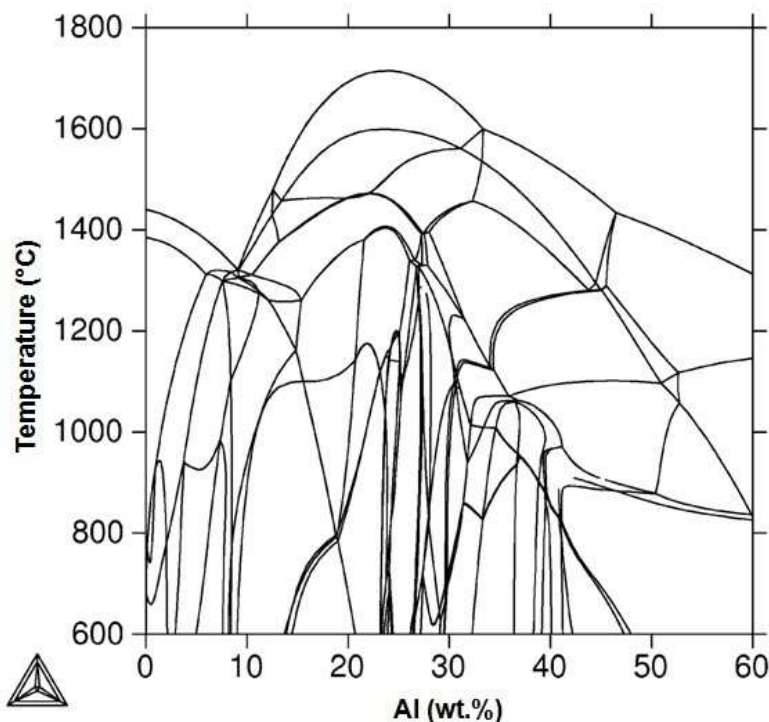


Figure V-2 – Isopleth of René N5 depicting the effect of the temperature as a function of the Al concentration (wt.%) on the stability of the phases.

Each domain delimited by the different curves are calculated by the ThermoCalc[®] algorithm. All of these areas represent an equilibrium of phases. One can note the complexity of such representation. Considering the specific chemical composition of the Ni-based superalloys, the variation of the Al content, i.e. during aluminizing process or service condition, imply the transformation of the phase by shifting the equilibrium towards the Al lower content (Al consumption) or towards the richer ones (aluminizing).

This variation is crucial as it rules the behaviour of the complete material. As explained in Chapter I, the lifetime of the Ni-based structures depends of the existence of the γ/γ' matrix, which provides the mechanical resistance of the material. In addition, adding Al can lead to the formation of the β -NiAl, which is responsible of the high temperature oxidation resistance of such systems. During the service conditions, the Al interdiffusion with the alloying elements promotes the formation of the TCP phases, which will reduce the lifetime of the system. One has to note that other intermetallics phases might develop with time. Nevertheless the following explanations focus on these three types of phases.

All those considerations cannot be avoided at high temperature since they are function of the evolution of the Al content. *Figure V-3* gathers the domain of existences of these γ/γ' matrix (*Figure V-3(a)*), β -NiAl (*Figure V-3(b)*) and TCP phases (*Figure V-3(c)*). These overall representations show the complexity of the isopleth since several phases may co-exist for the same Al content. The complete isopleth of the René N5 is displayed in *Annexe*, including the detail of the phase for a content higher than 10 wt.% Al.

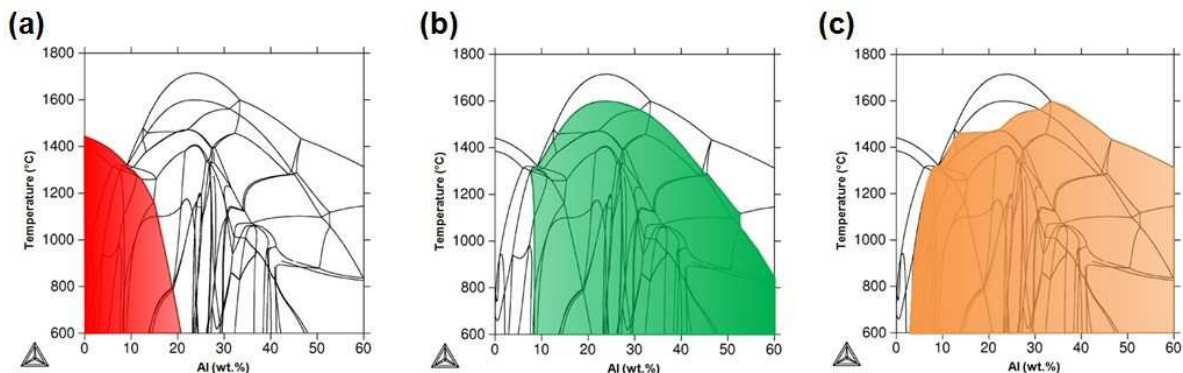


Figure V-3 – Isopleth of René N5 depicting the domains of stability of (a) γ/γ' , (b) β -NiAl and (c) the TCPs phases.

In order to make the reading of the isopleth easier, only a section of the temperature of interest is presented here, i.e. 1100°C for the René N5. *Figure V-4* shows the effect of the phase transformation affecting two main characteristics required to enhance the lifetime at high temperature. One has to keep in mind that such representation results from the calculations obtained at the equilibrium of the system. A sweeping of the Al concentration has been done to correspond to the aluminizing process, which is similar to an Al enrichment of the substrate. It implies that the all the phases present in the René N5 or which may develop in service condition (Ni_xAl_y , oxides, TCP, ...) can be found in such representation. The red star presents the initial content of Al of René N5 (14 at.%). If a direct degradation of the raw system is considered, a shift of the Al content towards the lower concentration in Al will lead to promote the disappearance of the β phase while the γ/γ' matrix will enhance the mechanical resistance of the substrate. In contrast, an increase of the Al fraction will promote the formation of the β phase in the coating, i.e. during the aluminizing process. The latter will have lower mechanical properties but higher ones with regard the oxidation resistance properties.

In order to explain how to extract information from this graph, the following explanation is divided in two sub-sections to present the stability domain of the β -NiAl in a first time. Then, the conditions leading to the formation of the TCP phases will be described. These components are known to reduce the life time of the Ni-based superalloys by consuming strengthening elements and forming brittle interfaces from a thermo-mechanical fatigue point of view [20]. In a similar manner, information of all the desired phases can be extracted by applying the same process.

The area coloured in green on *Figure V-4* corresponds to the β -NiAl phase stability. The darker green represents an Al rich β -NiAl while the light green is ascribed to a Ni rich β -NiAl. The Al gradient can be therefore linked to the potential evolution of the oxidation resistance properties. Indeed, it is often reported that the higher the Al concentration in the additive layer, the greater and longer the oxidation resistance [21]. In the meantime, the degradation of the coating by the Al consumption by oxidation and by interdiffusion into the γ / γ' matrix modifies the mechanical properties [22-23]. This diffusion of the aluminium into the matrix of the substrates is also known to promote the formation of the SRZ, which contains the TCP phases [20]. These phases contribute to highly influence the high temperature behaviour of the Ni based superalloys during service conditions.

The observation of the isopleth shows that the material will undergo several phase transformations during service conditions, and that the final behaviour of the substrate is ruled by the formation /disappearance of such phases. Either their combination may lead to a positive synergy or may provide a loss of the overall resistance of the material, both due to the thermo-activated interdiffusion processes and the initial chemistry of the Ni-based alloy.

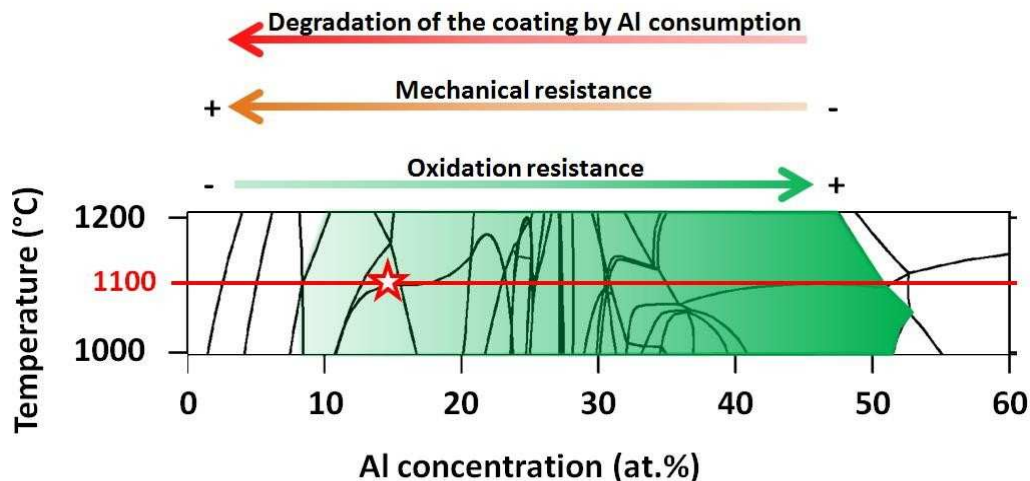


Figure V-4 - Isoleth section of the René N5 system between 1000°C and 1200°C, using the Thermocalc® software (TCNi5), i.e. the area coloured in green gradation corresponds to the stability domain of the β -NiAl phase. The red star represents the initial concentration in Al of the René N5 superalloy.

Considering the mechanical resistance properties, the positive synergy is improved by the size and the dispersion of the precipitates, which have to remain small and homogeneously dispersed [24]. As a second example using the René N5 system, *Figure V-5* represents the domain of existence of the TCP phases, which will grow during the service conditions. In a similar manner than for the β -NiAl on *Figure V-4*, the coloured domain represents the conditions to form such TCP phases, indicative of the Al consumption towards the matrix of the substrate. It can be observed that such phases exist over a wide aluminium content but their appearance is only significant with long term oxidation tests [20].

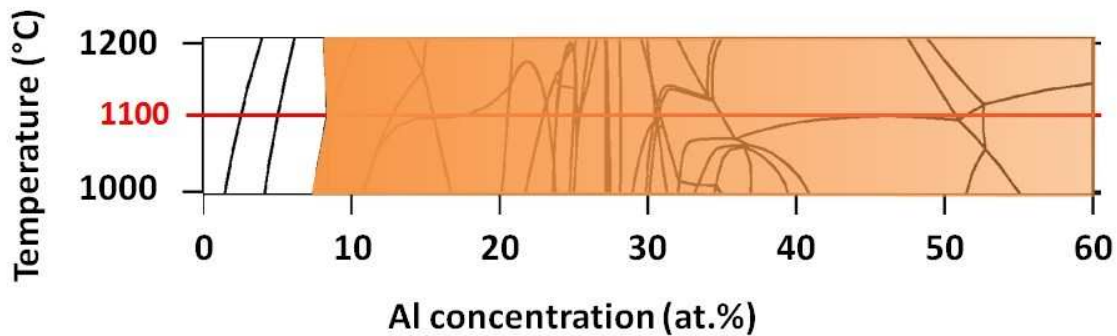


Figure V-5 - Isoleth section of the René N5 system between 1000°C and 1200°C, using the Thermocalc® software (TCNi5), i.e. the area coloured in orange gradation corresponds to the stability domain of the TCP phases.

As discussed above for the isopleths of René N5, all the chemical species can be involved in the formation of different phases. Therefore, depending on their initial chemical composition (and microstructure / crystal orientation), each material will undergo several phase transitions during their lifetimes upon exposure to oxidizing conditions at high temperature that can contribute to the degradation mechanisms of the substrates.

In a first approach to investigate the behaviour of the different PARTICOATED substrates, the oxidation kinetics have been studied to monitor the effect of several time / temperature conditions, as previously gathered in Table V-1, from 900°C for 100h up to 1100°C for 1000h depending of the chemistry of the substrate.

C. Characterization of the PARTICOAT system during isothermal oxidation tests.

a. Oxidation kinetics.

The thermogravimetric measurements of the **CM 247**, **René N5** and **PWA 1483** substrates are presented by Figures V-6(a-c), for their respective service temperatures. All of the samples have been coated by applying 10 mg.cm⁻² of the PARTICOAT slurry. This discussion is orientated as a function of the temperature, with the explanation of the PARTICOAT behaviour for the three temperatures investigated with the **CM 247**. Then, the effect of the modification of the chemistry of the alloys is investigated for **René N5** and **PWA 1483**, for their respective temperature conditions. From these measurements, the resulting k_p values are gathered in Table V-3, using both parabolic and complete laws.

Figure V-6(a) gathers the evolution of the mass per surface area of **CM 247** substrate, during oxidation at 900, 1000 and 1100°C up to 100h. All the curves display a fast mass gain for the first hours followed by a transition period and then a modification of the kinetic that looks like parabolic. At **900°C**, this rapid mass gain and the transient step are done within the first hours. After this, the mass gain variation slows down for the overall duration of the experiment, attesting of the growth of a more protective oxide scale. At **1000°C**, the transitional step is a bit longer (5h), and then the mass gain increases more rapidly than at 900°C. Finally, measurements at **1100°C** resulted in a longer transitional duration with a greater mass gain. This time, such phenomenon is estimated at 10h for the CM 247 material. The kinetics of oxidation is a function of the temperature as it can be seen from the slope of these three different experimentations at those three high temperatures. In addition, one can note that after 100h of test, the higher the temperature, the higher the $\Delta M / S$ ratio: $(\Delta M / S)_{900^\circ\text{C}} < (\Delta M / S)_{1000^\circ\text{C}} < (\Delta M / S)_{1100^\circ\text{C}}$. Similarly, Figure V-6(b) and Figure V-6(c) gather the mass evolution as a function of the isothermal duration of **René N5** and **PWA 1483**, respectively.

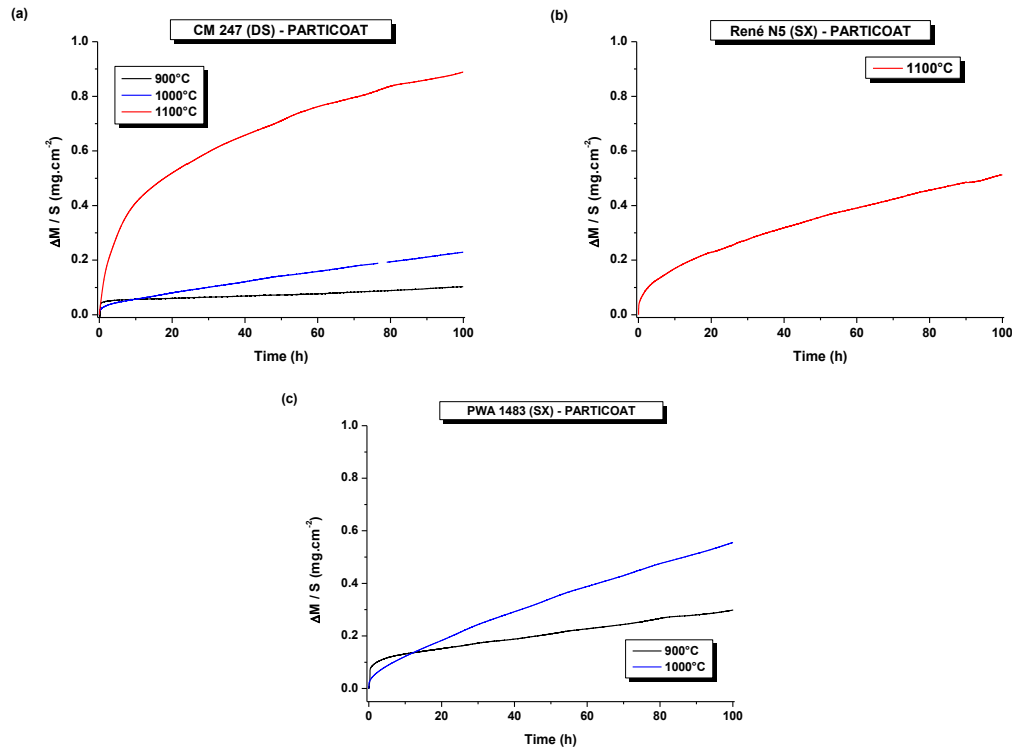


Figure V-6 – Evolution of the mass gain per surface area ($\Delta m / S$) with respect to the oxidation time in synthetic air for PARTICOATED (a) CM 247, (b) René N5 and (c) PWA 1483 nickel based superalloys.

By comparing the parabolic coefficient of the oxidation kinetics, it can be seen that the one of PARTICOATED **CM 247** increases from one order of magnitude every 100°C, from 900°C ($k_p_{900^\circ\text{C}}=2.5 \cdot 10^{-14} \text{ g}^2 \cdot \text{cm}^{-4} \cdot \text{s}^{-1}$) to 1100°C ($k_p_{1100^\circ\text{C}}=1.91 \cdot 10^{-12} \text{ g}^2 \cdot \text{cm}^{-4} \cdot \text{s}^{-1}$), with an intermediate value at 1000°C ($k_p_{1000^\circ\text{C}}=1.5 \cdot 10^{-13} \text{ g}^2 \cdot \text{cm}^{-4} \cdot \text{s}^{-1}$).

Similarly, the **PWA 1483** PARTICOATED followed the same trend at 900°C ($k_p_{900^\circ\text{C}}=2.2 \cdot 10^{-13} \text{ g}^2 \cdot \text{cm}^{-4} \cdot \text{s}^{-1}$) and 1000°C ($k_p_{1000^\circ\text{C}}=9.2 \cdot 10^{-13} \text{ g}^2 \cdot \text{cm}^{-4} \cdot \text{s}^{-1}$), but the k_p values are one order of magnitude greater than for PARTICOATED **CM 247** at the same temperatures. Finally, **René N5** PARTICOATED oxidized at 1100°C has a k_p value of $7.15 \cdot 10^{-13} \text{ g}^2 \cdot \text{cm}^{-4} \cdot \text{s}^{-1}$, which is rather similar to the one observed for **CM 247** PARTICOATED at the same temperature.

The determination of the oxidation kinetics by the use of a parabolic law (Equation V-4) supposes that the growth of the oxide scale is ruled by the diffusion processes (cationic and / or anionic) into the growing scale. This kinetic parameter is function of the temperature and the O_2 partial pressure ($p\text{O}_2$), which will also lead to the oxidation of the material in presence of a $p\text{O}_2$ high enough. Finally, the behaviour of the material depends of its nature per se, i.e. whether if it is a pure metal or an alloy. However, it has to be noted that such parabolic law has a higher accuracy when the growth of a single oxide is considered [1]. In addition, several factors can influence the discrepancies between the experimental measurements and the numerical analysis when using the parabolic law. These factors are mostly significant for short oxidation times and include [25-26]:

- The surface finishing.
- The heating ramp.
- The diffusion at the grain boundaries.
- The allotropic transformation of the oxide scale (i.e. $\theta\text{-Al}_2\text{O}_3 \rightarrow \gamma\text{-Al}_2\text{O}_3 \rightarrow \alpha\text{-Al}_2\text{O}_3$), which imply a modification of the diffusion properties.
- The growth of several oxides in the oxide scales, which is function of the chemistry of the alloy.

Such phenomena were already investigated by Pieraggi [25-26] suggested the use of a complete law (*Equation V-5*) to describe more precisely the oxidation behaviour. This model introduces the role of a linear constant (k_l) to take into account the chemical interactions at the gas-oxide and / or oxide-metal interfaces, which can be considered as limited once a continuous and protective oxide scale is developed.

From these considerations, calculations have been done using the complete law model and the corresponding k_p values are gathered in *Table V-3*, in order to be compared with the ones obtained using the parabolic law model. In most cases, both laws seem to provide similar values with less than half an order of magnitude. The overall calculations indicate that the oxide layer grows mainly by diffusion processes since the k_p values allow to fit the $\Delta M / S$ with a good accuracy. The additional k_l value (not presented here) allows to estimate the major growth of the oxide, that is followed by the allotropic transformation from the metastable $\text{Al}_2\text{O}_3 \rightarrow \alpha\text{-Al}_2\text{O}_3$, which is the most thermodynamically stable form [27].

Table V-3 – Oxidation constant rate of the nickel based materials aluminized using the PARTICOAT slurry approach.

Substrate	Time range (h) for the parabolic law	Parabolic law k_p ($\text{g}^2.\text{cm}^{-4}.\text{s}^{-1}$)	Complete law k_p ($\text{g}^2.\text{cm}^{-4}.\text{s}^{-1}$)
Oxidation at 900°C			
CM 247	0 – 10	-----	$1.64.10^{-14}$
	10 – 100	$2.5.10^{-14}$	
PWA 1483	0 – 10	-----	$5.43.10^{-13}$
	10 – 100	$2.20.10^{-13}$	
Oxidation at 1000°C			
CM 247	0 – 100	$1.5.10^{-13}$	$4.40.10^{-13}$
PWA 1483	0 – 10	-----	$2.01.10^{-12}$
	10 – 100	$9.19.10^{-13}$	
Oxidation at 1100°C			
René N5	0 – 100	$7.15.10^{-13}$	$8.12.10^{-13}$
CM 247	0 – 15	-----	$1.11.10^{-12}$
	15 – 100	$1.91.10^{-12}$	

Figure V-7 reports the k_p values of the four systems compared to the representation of Grabke *et al.* for a pure $\beta\text{-NiAl}$ [2]. The three superalloys investigated for the 100h of oxidation are gathered with the comparison of the PARTICOAT concept applied on pure Ni from one of our former study [28]. Discrepancies are observed compared to the value of the parabolic constant of the different types of Al oxides. For example, one can note that the $\alpha\text{-Al}_2\text{O}_3$ seems not to be completely stabilized since a deviation appears for all the four systems presented. As a matter of fact, we can say that several types of oxides grow at the surfaces of the samples, whether it is a duplex composition of Al oxides or that other less protective oxides contribute to increase the k_p values, i.e. such as Cr_2O_3 , NiAl_2O_4 , tantalum oxides, titanium oxides... The nature of these oxides depends of the chemistry of the Ni superalloys considered.

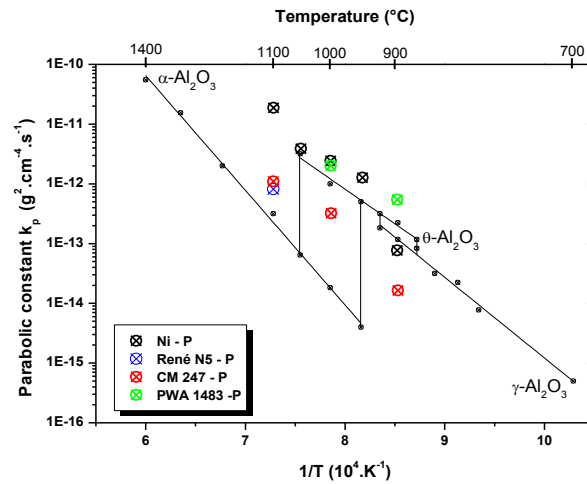


Figure V-7 – Arrhenius representation of the k_p value determined from the kinetics of oxidation of several PARTICOATED systems compared to the k_p values from a pure β -NiAl [2].

In a previous study at the LaSIE laboratory [28], the behaviour of PARTICOATED pure Ni has been studied during 100h isothermal oxidation tests at 900, 1000 and 1100°C. When comparing such system with a conventional pack cementation coating one, several mechanisms were observed. It was found that the thermal treatment of the PARTICOAT slurry contributed to stabilize the α - Al_2O_3 . This heat treatment occurs up to 1100°C and allows to form a ceramic top coat of this thermodynamically stable Al oxide. From this assessment, the oxidation rates determined for the tests at 900°C were lower than the ones calculated for the pack cemented samples. Nevertheless, the same parameter has been found higher for the PARTICOATED samples for higher temperatures (1000°C and 1100°C). In the case of the PARTICOATED samples, the top coat foam structure has been shown to contribute to this modification of the kinetics of oxidation. Depending of the initial amount of applied slurry, a part of the Al can remain in the top coat and oxidizes as following the polymorphic transformation of the Al oxides ($\gamma \rightarrow \theta \rightarrow \alpha$ - Al_2O_3), which are known to have higher oxidation kinetics (Figure V-7). In addition, traces of Ni were detected in the top coat structure after the elaboration of the coating (see Chapter IV) that may lead to the formation of NiO compound at first, for then reacting with the α - Al_2O_3 and forming the NiAl_2O_4 spinel [29]. The overall process led to the enhancement of the kinetics of oxidation. Because of this contribution of the top coat, tests have been carried out by removing the top coat structure. As a result, similar kinetics of oxidation have been observed for both pack cemented samples and the samples aluminized using the PARTICOAT slurry, without the top coat [28].

In order to ascertain whether these phenomena appearing on pure Ni could be extrapolated to the different PARTICOATED superalloys, a direct comparison has been established between CM-247 and René N5 aluminized by the SVPA (Snecca Vapour Aluminizing Process) and oxidized at 1100°C for 100h as shown in Figure V-8 (a,b). In both cases, the PARTICOATED samples presented higher $\Delta M/S$ ratio compared to the SVPA ones and therefore seem to confirm the above mentioned phenomena [28] in spite of the TGO already grown upon the formation of the PARTICOAT coating [30]. Looking at the CM 247, more significant variations of the mass gain can be observed between the PARTICOAT and SVPA systems than for the René N5. The k_p values of all the systems are gathered in Table V-4. As a matter of fact, there is a difference of half or one order of magnitude between the PARTICOATED samples and the ones protected using the conventional SVPA method.

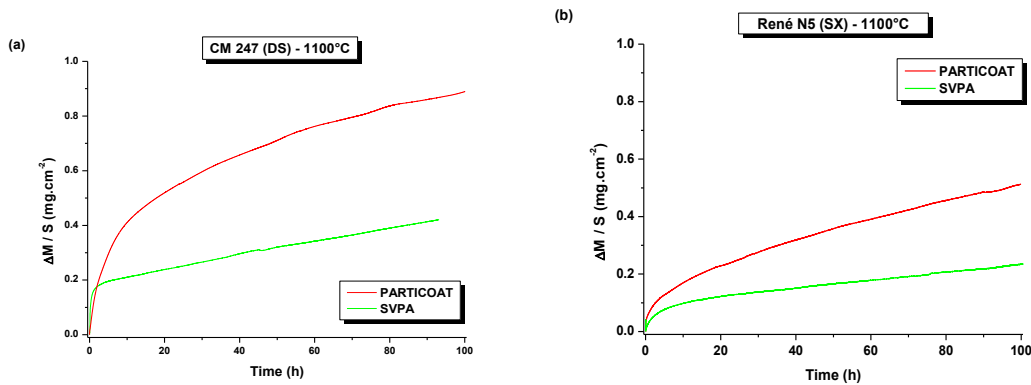


Figure V-8 – Comparison of the mass gain per surface area ($\Delta m / S$) with respect of the oxidation time in synthetic air at 1100°C, showing (a) CM 247 and (b) René N5 systems protected using the PARTICOAT slurry approach and the SVPA method.

Table V-4 – Comparison of the oxidation constant rate of the René N5 and CM 247 aluminized using the PARTICOAT slurry approach and the SVPA method.

Substrate	Protective system	Time range (h) for the parabolic law	Parabolic law k_p ($\text{g}^2 \cdot \text{cm}^{-4} \cdot \text{s}^{-1}$)	Complete law k_p ($\text{g}^2 \cdot \text{cm}^{-4} \cdot \text{s}^{-1}$)
CM 247	PARTICOAT	0 – 15 15 - 100	----- $1.91 \cdot 10^{-12}$	$1.11 \cdot 10^{-12}$
	SVPA	0 - 100	$4.35 \cdot 10^{-13}$	$6.96 \cdot 10^{-13}$
René N5	PARTICOAT	0 – 15 15 - 100	----- $7.15 \cdot 10^{-13}$	$8.12 \cdot 10^{-13}$
	SVPA	0 - 100	$1.13 \cdot 10^{-13}$	$1.68 \cdot 10^{-13}$

Therefore, regardless of the conventional method of aluminizing (pack [28] or SVPA [this study]) it seems that the overall oxidation constants are lower than for PARTICOAT. In addition to the contribution of the top coat (incorporation of Ni and by remnants of Al still trapped in the spheres), another key factor can be also related to the actual active surface for oxidation. Indeed, because of the very nature of the top coat (microsized hollow spheres), the surface is much higher and the ratio $\Delta M/S$ should be therefore lower. Further studies by using for instance the Brunauer Emmett Teller technique (BET) [31] could allow to establish a more reliable estimation of the “real” surface for the oxidation, leading to lower k_p values than the ones calculated in the present study.

From the first 100h of oxidation, the microstructural evolutions of the systems were investigated up to 1000h of experimentations. The latter allowed to observe the degradation mechanisms of the systems first by considering the top coat structure, and secondly, the transformation of the phases ruled by the interdiffusion phenomena.

b. Evolution of the top coat as a function of the chemistry of the systems.

The results on the adherence of the top coat (from visual observations) are gathered in Table V-5. Keeping in mind the screening of conditions applied as a function of the substrates, the top coats of hollow $\alpha\text{-Al}_2\text{O}_3$ spheres produced during the PARTICOAT process have been found to be adherent for all the investigations. The only discrepancies observed during the study are related to the edge effects. The latter depends of the geometry of the samples (see Chapter II) and may lead to light spallation of the outer part of the top coat. These edge effects have been observed for all the samples.

As a matter of fact, the thermal stresses generated during the cooling of the sample at the end of the isothermal tests ($50^{\circ}\text{C}\cdot\text{min}^{-1}$) may produce this random top coat detachment. However, it had been already observed that the coatings showed some inhomogeneities at the edge of the samples after annealing. To avoid this very local phenomenon, the top coat adherence has been estimated for the central area with the cross section of the sample and found to be successful, irrespectively of the chemistry of the coatings (alloy).

Table V-5 – Summary of the adherence (visual observations in the centre of samples) of the PARTICOAT top coat as a function of the oxidation temperature and time for the different substrates investigated.

Oxidation time (h)	Substrate			
	René N5	CM 247	PWA 1483	INCO 738
Oxidation at 900°C				
100h	X	Adherent	Adherent	X
500h	X	Adherent	Adherent	Adherent
1000h	X	Adherent	Adherent	Adherent
Oxidation at 1000°C				
100h	X	Adherent	Adherent	X
500h	X	Adherent	Adherent	X
1000h	X	Adherent	Adherent	X
Oxidation at 1100°C				
100h	Adherent	Partially detached	X	X
500h	Adherent	Partially detached	X	X
1000h	Adherent	Partially detached	X	X

X: condition not studied.

From this characterization of the ceramic top coat during the isothermal long terms measurements, a deeper investigation has been carried out focusing on the evolution of the thermally grown oxide zone, which is often related to the adherence or spallation of the thermal barrier top coats [32].

c. Evolution of the thermally grown oxide (TGO).

Note that upon the elaboration of the coating in the annealed condition a very thin thermally grown oxide of alumina grew onto all the substrates at the interface between the hollow microsphere top coat and the bond coat. However, when exposed to high temperature oxidizing conditions, these systems evolve due to the oxidation processes (top coat + TGO) but also from the interdiffusion processes (TGO + bond coat + substrate).

Table V-6 shows the summary of the phases detected by *post mortem* XRD measurements on the PARTICOATED samples after the oxidation runs. It has to be underlined that all the diffractograms presented a great number of peaks and their interpretation was extremely complex. Therefore, the major trends are discussed in the following. The signature of the thermodynamically stable $\alpha\text{-Al}_2\text{O}_3$ phase has been found for all the systems due to the hollow spheres top coat structure but also to its growth at the TGO position. In addition, depending on the chemistry of the substrates and as a result of the interdiffusion processes, different alloying elements can segregate at the TGO position, as it has been already suggested by EPMA tests after PARTICOAT aluminizing [17]. The titanium containing materials (**CM 247**, **PWA 1483** and **INCO 738**) all form titanium dioxides, while they might also form tantalum oxides depending of their initial contents of the latter (**CM 247**). In a similar manner, hafnium oxides have been found for the CM 247 alloy. The advancement of degradation of the

coated systems is often followed through the appearance of the NiAl_2O_4 spinel phase [16]. Indeed, this phase has been found on several alloys but its occurrence strongly depends on the substrate/temperature. Only **PWA 1483** formed the NiAl_2O_4 spinel at 900°C , between 500h and 1000h but appeared already after 100h of oxidation at 1000°C . In contrast, 1100°C were required to observe this phase in **CM 247** but was not observed after 1000h of oxidation at 1000°C . This suggests that it is required to activate thermally its formation in the presence of additional oxides such as Ta_xO_y . This hypothesis is confirmed with **René N5** that did not form the NiAl_2O_4 but formed CrTaO_4 in addition to several types of tantalum oxides (noted Ta_xO_y in the *Table V-6*) and traces of WO_2 oxides.

Table V-6 – Summary of the thermally grown oxide characteristics as a function of the temperature and time through the oxidation of several chemical compositions of the coatings.

Oxidation time (h)	Substrate			
	René N5	CM 247	PWA 1483	INCO 738
Oxidation at 900°C				
100h	X	$\alpha\text{-Al}_2\text{O}_3 / \text{Ta}_x\text{O}_y / \text{TiO}_2 / \text{HfO}_2$	$\alpha\text{-Al}_2\text{O}_3 / \text{TiO}_2$	
500h	X	$\alpha\text{-Al}_2\text{O}_3 / \text{Ta}_x\text{O}_y / \text{TiO}_2$	$\alpha\text{-Al}_2\text{O}_3 / \text{TiO}_2$	$\alpha\text{-Al}_2\text{O}_3 / \text{TiO}_2$
1000h	X	$\alpha\text{-Al}_2\text{O}_3 / \text{Ta}_x\text{O}_y / \text{TiO}_2 / \text{HfO}_2$	$\alpha\text{-Al}_2\text{O}_3 / \text{NiAl}_2\text{O}_4 / \text{TiO}_2$	$\alpha\text{-Al}_2\text{O}_3 / \text{TiO}_2$
Oxidation at 1000°C				
100h	X	$\alpha\text{-Al}_2\text{O}_3 / \text{Ta}_x\text{O}_y / \text{TiO}_2 / \text{HfO}_2$	$\alpha\text{-Al}_2\text{O}_3 / \text{NiAl}_2\text{O}_4 / \text{TiO}_2$	X
500h	X	$\alpha\text{-Al}_2\text{O}_3 / \text{Ta}_x\text{O}_y / \text{TiO}_2 / \text{HfO}_2$	$\alpha\text{-Al}_2\text{O}_3 / \text{NiAl}_2\text{O}_4 / \text{TiO}_2$	X
1000h	X	$\alpha\text{-Al}_2\text{O}_3 / \text{Ta}_x\text{O}_y / \text{TiO}_2 / \text{HfO}_2$	$\alpha\text{-Al}_2\text{O}_3 / \text{NiAl}_2\text{O}_4 / \text{TiO}_2 / \text{Ta}_4\text{O}$	X
Oxidation at 1100°C				
100h	$\alpha\text{-Al}_2\text{O}_3 / \text{Ta}_x\text{O}_y / \text{WO}_2$	$\alpha\text{-Al}_2\text{O}_3 / \text{NiAl}_2\text{O}_4 / \text{Ta}_x\text{O}_y / \text{TiO}_2 / \text{HfO}_2$	X	X
500h	$\alpha\text{-Al}_2\text{O}_3 / \text{Ta}_x\text{O}_y / \text{AlTaO}_4 / \text{WO}_2$	$\alpha\text{-Al}_2\text{O}_3 / \text{NiAl}_2\text{O}_4 / \text{Ta}_x\text{O}_y / \text{TiO}_2 / \text{HfO}_2$	X	X
1000h	$\alpha\text{-Al}_2\text{O}_3 / \text{Ta}_x\text{O}_y / \text{AlTaO}_4 / \text{WO}_2$	$\alpha\text{-Al}_2\text{O}_3 / \text{NiAl}_2\text{O}_4 / \text{Mo}_x\text{O}_y / \text{TiO}_2 / \text{HfO}_2$	X	X

X: condition not studied.

The overall modifications of the thermally grown oxide, where a part of the alloying elements segregate, suppose that the bond coat also underwent transformations of phases. Similarly to the investigation of the top coat and the development of the TGO, the evolution of the bond coat has been observed using X ray map analysis.

d. Microstructural evolution of the bond coat.

Figure V-9 to Figure V-17 gather the SEM cross sections in the backscattered electron (BSE) mode and the X-ray maps of the systems after 100, 500 or 1000h at 900, 1000 or 1100°C depending on the experimental conditions chosen for the substrates. The X-ray mappings have been focused on three major distinct elements in the substrates/coatings: Cr, Ta and Ti. Based on their initial partitioning after the thermal treatment, the evolution of their segregations has been studied regarding their affinities (solubility limitation, diffusion coefficient...) with the Ni_xAl_y phases.

In the SEM / BSE mode, the lighter the element, the darker the chemical contrast. Therefore, the β -NiAl phase appears darker than the γ' -Ni₃Al. From this standpoint, it was observed that the transformation of the β -NiAl phase into the γ' -Ni₃Al phase by Ni outward diffusion [33-34] occurred with pockets of bright contrast throughout the coating, in particular when increasing the temperature and time (Table V-7). One has to note that the γ' -Ni₃Al, which is found for the CM 247 at 900°C and 1000°C has to be considered cautiously as it seems that a thinner coating was initially deposited.

Table V-7- Summary of the matrixes evolution into the bond coat of the PARTICOATED systems as a function of the temperature and time through the oxidation of several chemical compositions of the substrates.

Oxidation time (h)	Substrate			
	René N5	CM 247	PWA 1483	INCO 738
Oxidation at 900°C				
100h	X	β -NiAl / γ' -Ni ₃ Al	β -NiAl	X
500h	X	β -NiAl / γ' -Ni ₃ Al	β -NiAl	β -NiAl / γ' -Ni ₃ Al
1000h	X	β -NiAl / γ' -Ni ₃ Al	β -NiAl	β -NiAl / γ' -Ni ₃ Al
Oxidation at 1000°C				
100h	X	β -NiAl / γ' -Ni ₃ Al	β -NiAl	X
500h	X	β -NiAl / γ' -Ni ₃ Al	β -NiAl	X
1000h	X	β -NiAl / γ' -Ni ₃ Al	β -NiAl	X
Oxidation at 1100°C				
100h	β -NiAl / γ' -Ni ₃ Al	β -NiAl / γ' -Ni ₃ Al	X	X
500h	β -NiAl / γ' -Ni ₃ Al	β -NiAl / γ' -Ni ₃ Al	X	X
1000h	β -NiAl / γ' -Ni ₃ Al	β -NiAl / γ' -Ni ₃ Al	X	X

X: condition not studied.

Refractory elements precipitate and segregate underneath the thermally grown oxide (TGO) layer, which depends of the chemistry of the alloys. In the additive layer, the $\beta \rightarrow \gamma'$ transformation mainly occurred at the coatings grain boundaries. In addition, this transformation also occurred at the interdiffusion zone (IDZ), where the refractory precipitates coarsen and extend further into the substrate (Secondary Reaction Zone: SRZ) due to Al inward, Ni outward diffusion and their solubility limitation in the Ni_xAl_y phases. The kinetic of this phase modification depends on the global synergy between the elements.

The associated EDS mappings confirmed the previous XRD observations about the TGO development with the segregation of the three alloying elements of interest at several "random" positions. Cr is mainly present at the IDZ [20] and therefore does not contribute to form the Cr₂O₃ oxide. In contrast Ta and Ti are found both at the bond coat/TGO interface and within the IDZ. Therefore, they are available to form the oxides observed by XRD and therefore may promote spallation (Table V-5). This behaviour has already been observed for the Ta element [35] and for Ti [10] and can be related to the relatively high diffusion coefficient of both refractory elements in these systems [11]. One has to note that the precipitates of refractory elements that formed upon the coating process dissolve with temperature and time in the coating, as clearly exemplified in CM 247 at 1100°C (Figure V-16 and Figure V-17). This phenomenon is relevant of a pronounced $\beta \rightarrow \gamma'$ phase transformation as the solubility limitations of the refractory elements differ considering the γ' phase [36] or the β phase [37-39]. One of the best examples is Cr, whose solubility has been reported to be very low (about 4

wt%) in β -NiAl [35;40-41] but increases in γ' phase [42]. Therefore, Cr segregates at the vicinity of the grain boundaries where the β to γ' transformation occurs.

In addition, the displacement of the equilibrium to lower Al contents towards the substrate involves the formations of (W, Re, Cr)-rich TCP phases with different morphologies depending on the phase formed [20]. The extension of the SRZ composed of the brittle TCP phases may therefore lead to a degradation of the mechanical properties of the coated systems upon mechanical loading (e.g. fatigue and creep) [20]. *Table V-8* gathers the averaged thickness of the SRZ of the systems investigated under different experimental conditions. It can be seen that the higher the temperature and/or the longer the experiments, the thicker the SRZ.

At 900°C, CM 247 has the smallest SRZ after 500h of experimentation, while PWA 1483 has a thicker one than INCO 738 for both durations (500h and 1000h). The value of the SRZ of CM 247 after 1000h has not been calculated because the precipitates were re-solubilized in the γ/γ' matrix. This sample seems to have been coated with a lower amount of the slurry leading to faster degradation mechanism. At 1000°C, the extension of the SRZ of PWA 1483 is more pronounced than the one of CM 247 for the two durations. Finally, at 1100°C, the dimension of the SRZ of René N5 is much thicker than the one observed for the other substrates at lower temperature, while TCP phases present in CM 247 were re-solubilized even before the 500h of oxidation at this temperature.

The behaviour of the TCP phases has been already investigated by several authors [11;20]. As a matter of fact, the alloying elements, which contribute to its extension, are responsible of different types of morphologies, i.e. needle like or round ones. In addition, one has to keep in mind that this needle like morphology can also be ascribed to the formation of Al nitrides, which form with long term of oxidation [43-46].

Oxidation tests at 900°C for 100h

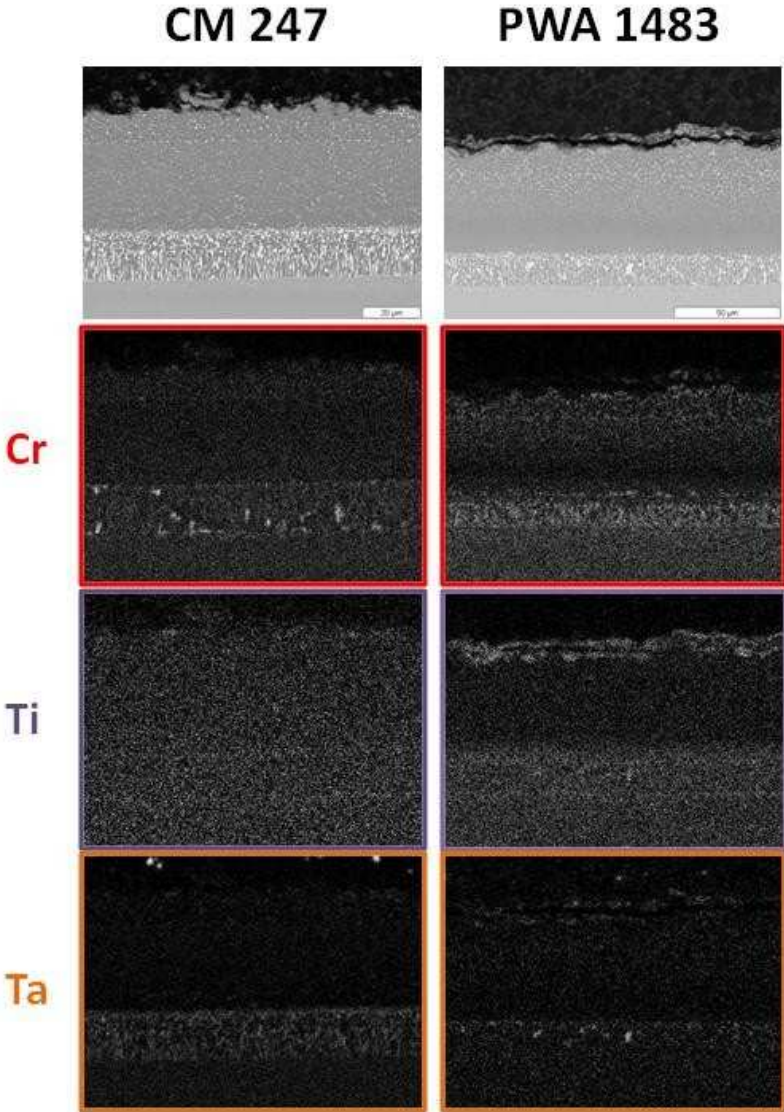


Figure V-9 – Cross-sections of (a) CM 247 and (b) PWA 1483 using the PARTICOAT slurry, and their respective partitioning of (c-d) chromium, (e-f) titanium and (g-h) tantalum, after 100h of oxidation tests at 900°C under synthetic air conditions.

Oxidation tests at 900°C for 500h

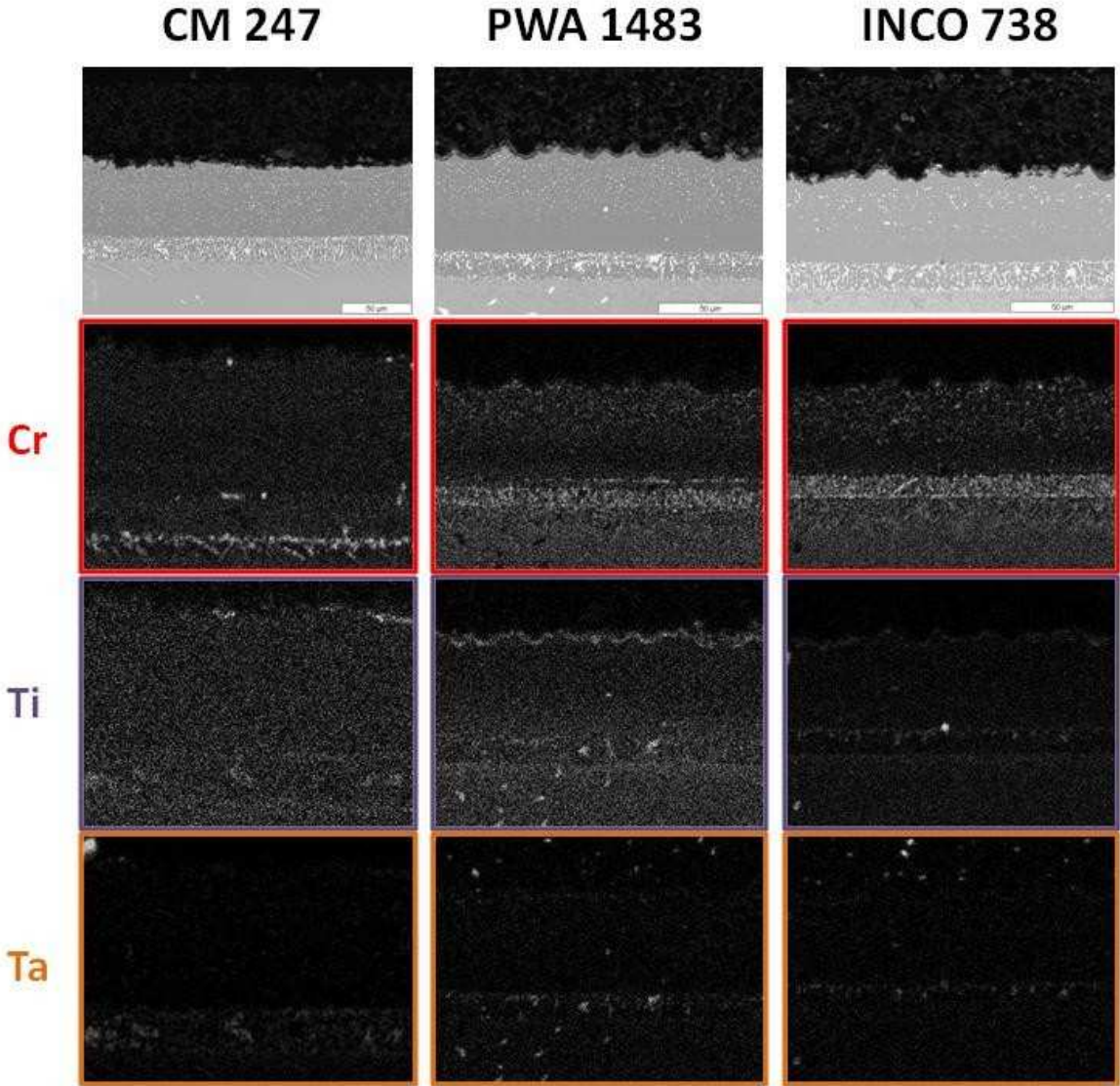


Figure V-10 - Cross-sections of (a) CM 247, (b) PWA 1483 and (c) INCO 738 using the PARTICOAT slurry, and their respective partitioning of (c-d-e) chromium, (f-g-h) titanium and (i-j-k) tantalum, after 500h of oxidation tests at 900°C under synthetic air conditions.

Oxidation tests at 900°C for 1000h

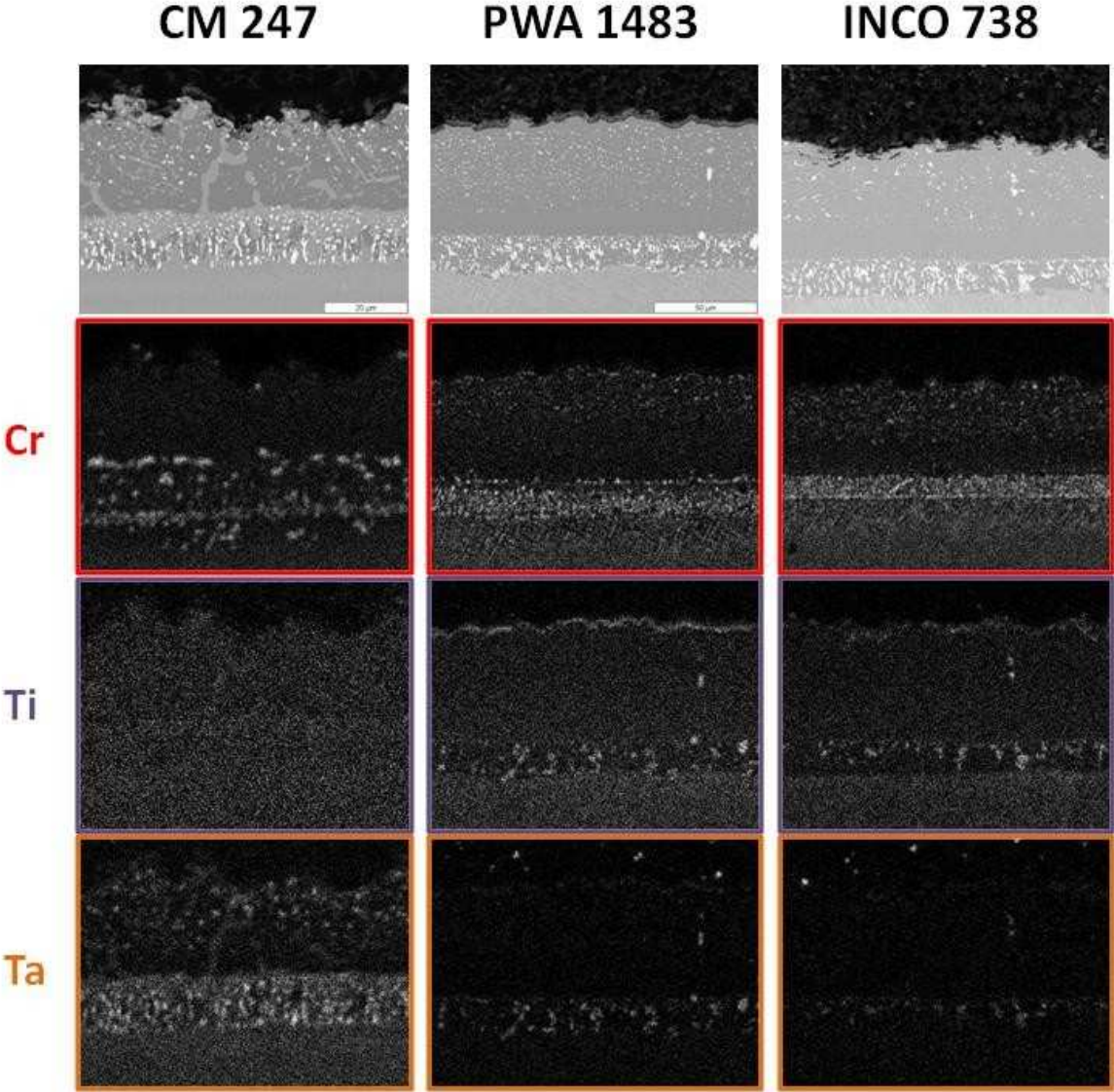


Figure V-11 – Cross-sections of (a) CM 247, (b) PWA 1483 and (c) INCO 738 using the PARTICOAT slurry, and their respective partitioning of (c-d-e) chromium, (f-g-h) titanium and (i-j-k) tantalum, after 1000h of oxidation tests at 900°C under synthetic air conditions.

Oxidation tests at 1000°C for 100h

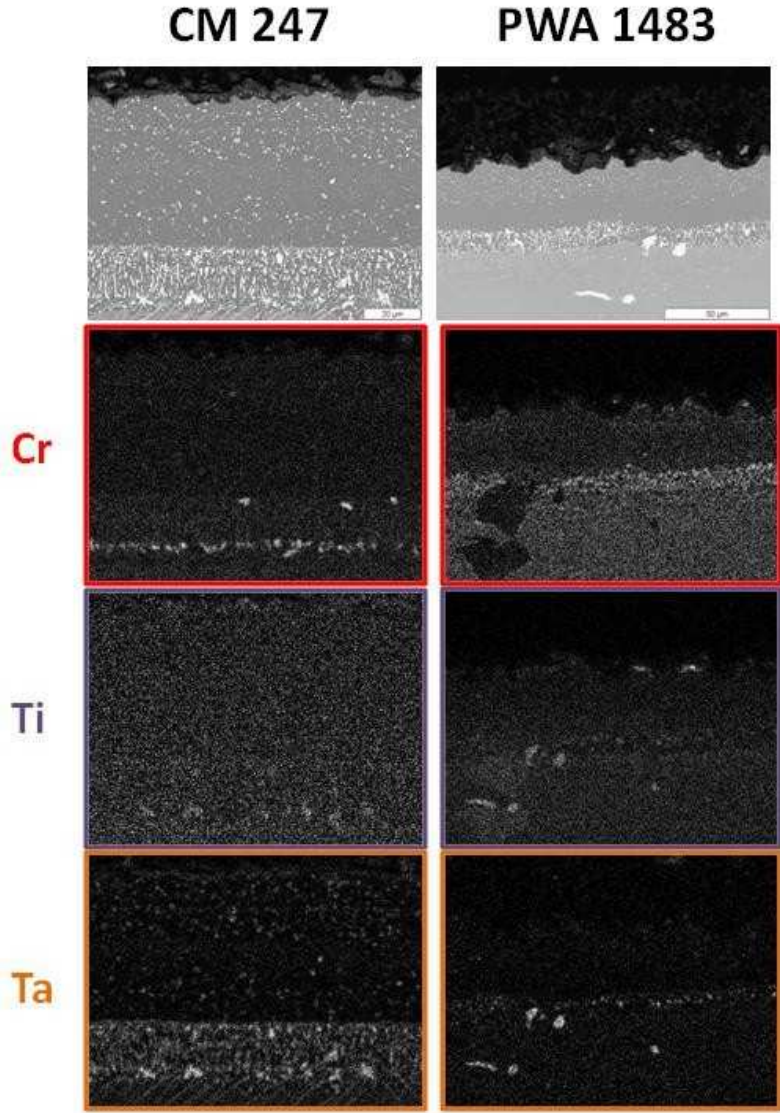


Figure V-12 - Cross-sections of (a) CM 247 and (b) PWA 1483 using the PARTICOAT slurry, and their respective partitioning of (c-d) chromium, (e-f) titanium and (g-h) tantalum, after 100h of oxidation tests at 1000°C under synthetic air conditions.

Oxidation tests at 1000°C for 500h

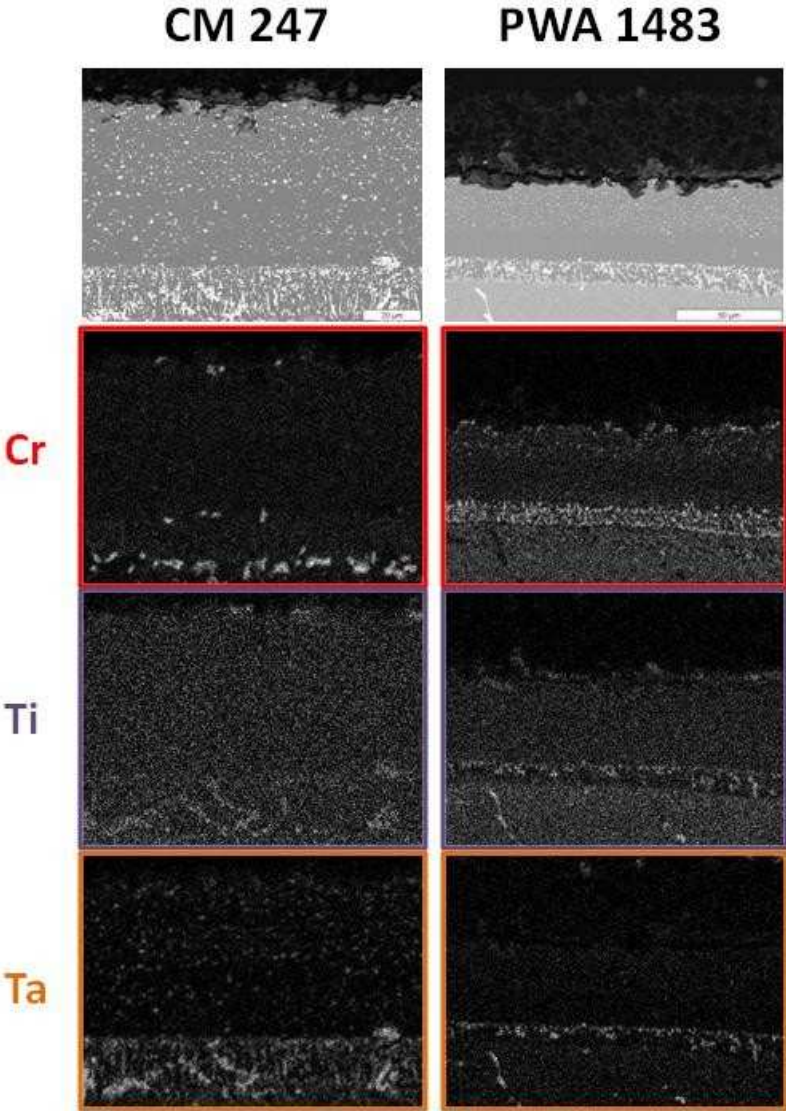


Figure V-13 - Cross-sections of (a) CM 247 and (b) PWA 1483 using the PARTICOAT slurry, and their respective partitioning of (c-d) chromium, (e-f) titanium and (g-h) tantalum, after 500h of oxidation tests at 1000°C under synthetic air conditions.

Oxidation tests at 1000°C for 1000h

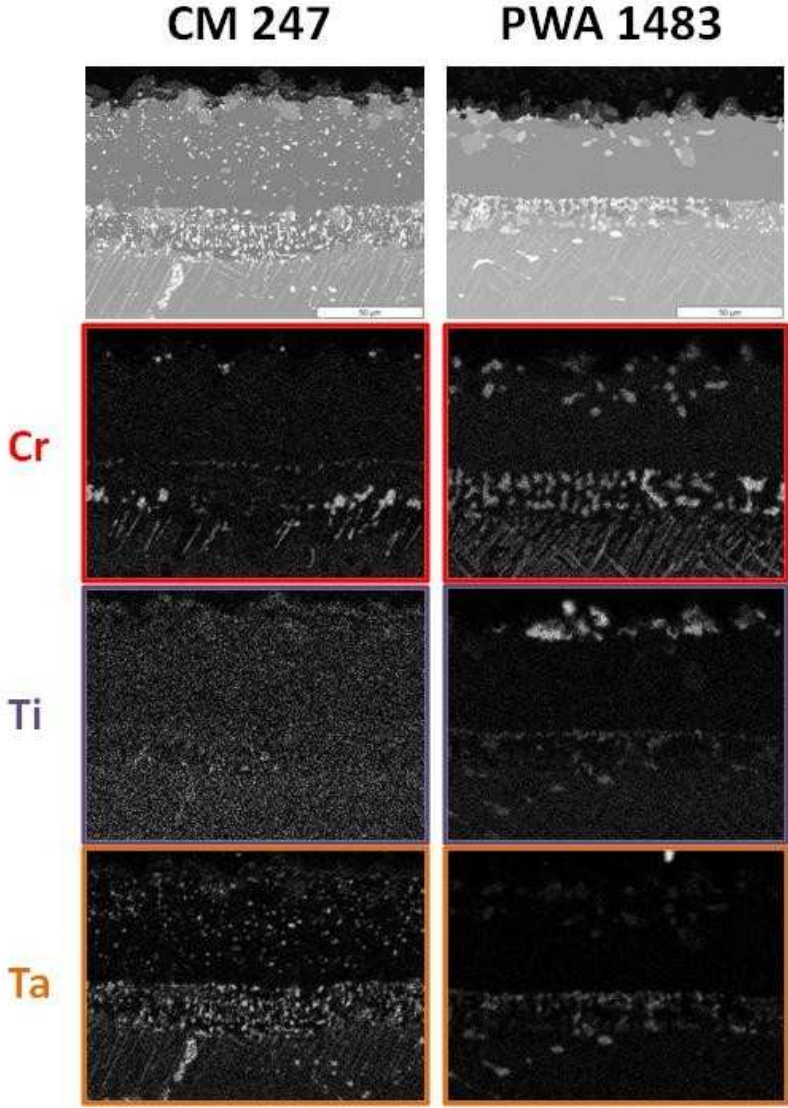


Figure V-14 – Cross-sections of (a) CM 247 and (b) PWA 1483 using the PARTICOAT slurry, and their respective partitioning of (c-d) chromium, (e-f) titanium and (g-h) tantalum, after 1000h of oxidation tests at 1000°C under synthetic air conditions.

Oxidation tests at 1100°C for 100h

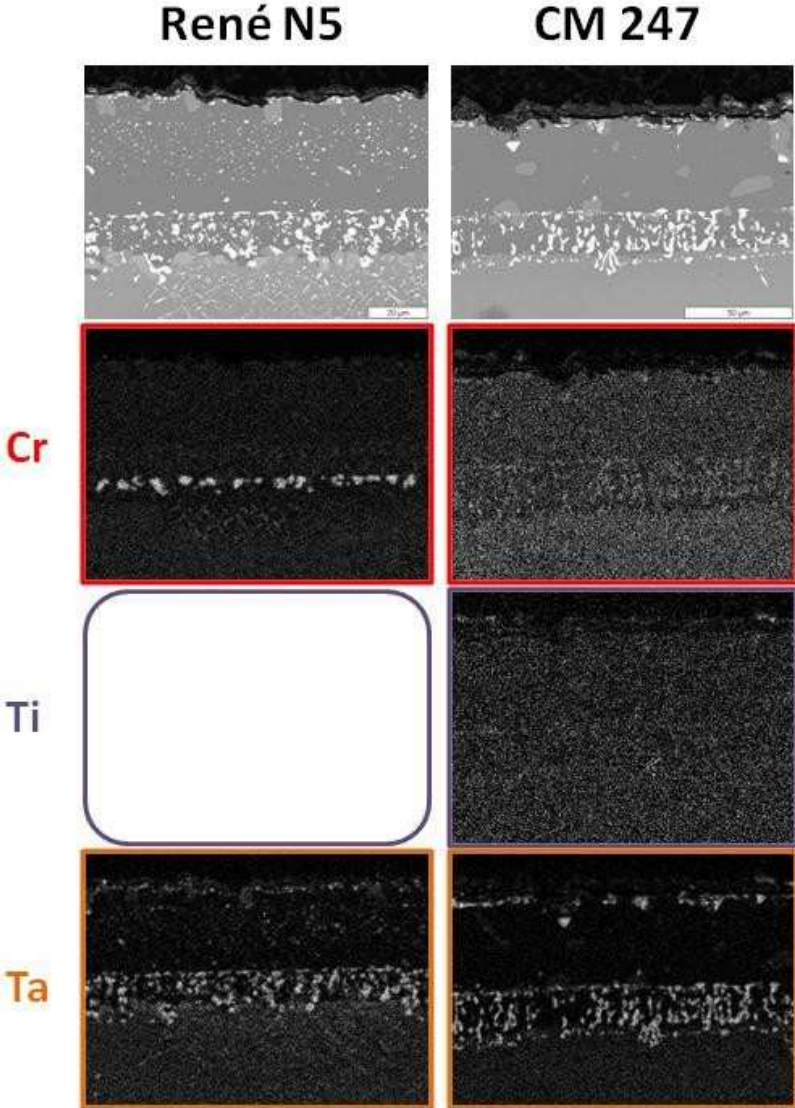


Figure V-15 - Cross-sections of (a) René N5 and (b) CM 247 using the PARTICOAT slurry, and their respective partitioning of (c-d) chromium, (e-f) titanium and (g-h) tantalum, after 100h of oxidation tests at 1100°C under synthetic air conditions.

Oxidation tests at 1100°C for 500h

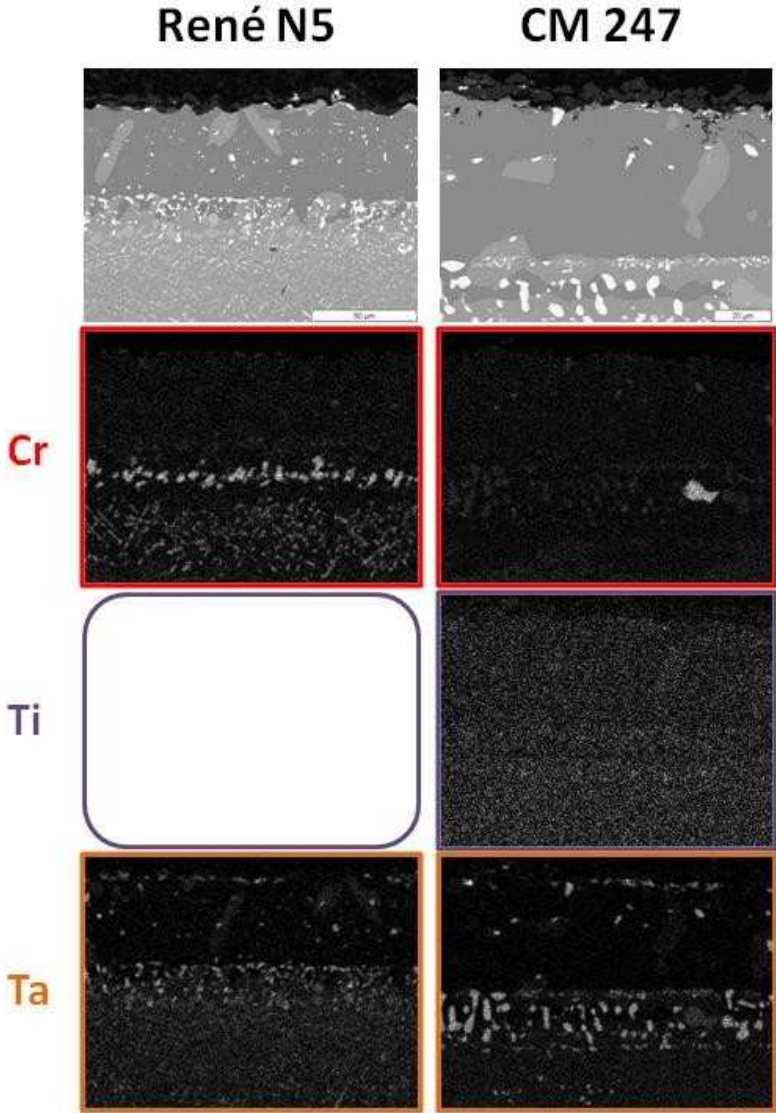


Figure V-16 - Cross-sections of (a) René N5 and (b) CM 247 using the PARTICOAT slurry, and their respective partitioning of (c-d) chromium, (e-f) titanium and (g-h) tantalum, after 500h of oxidation tests at 1100°C under synthetic air conditions.

Oxidation tests at 1100°C for 1000h

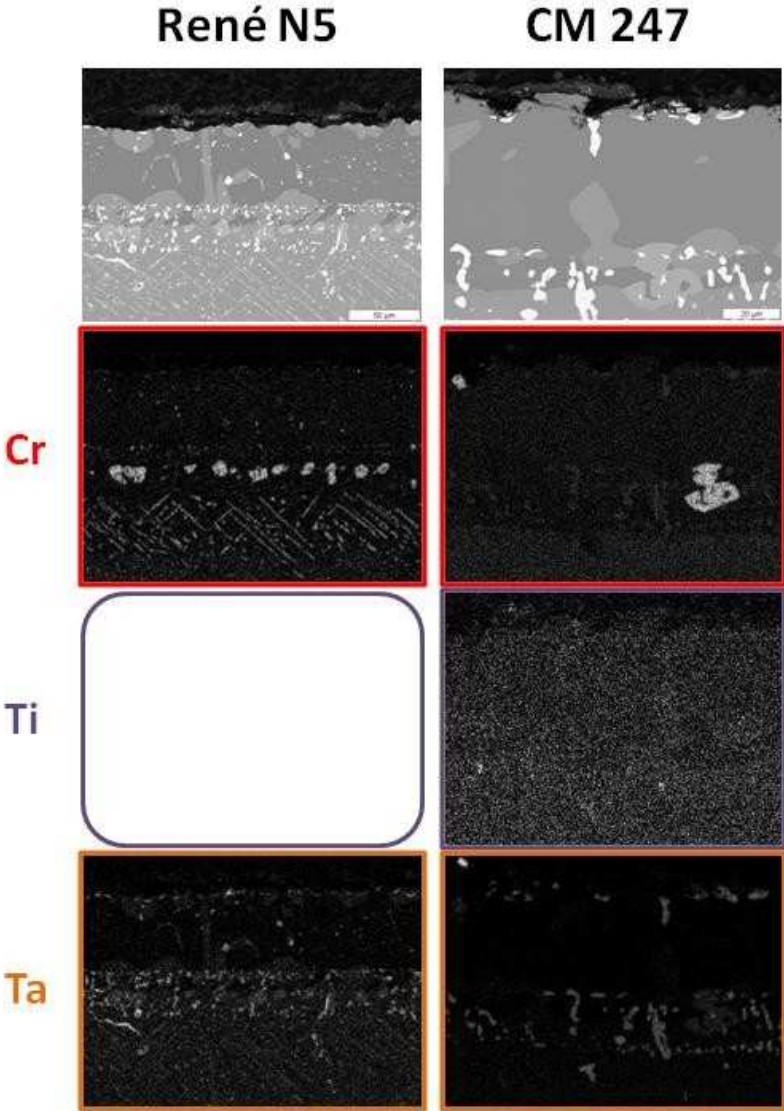


Figure V-17 - Cross-sections of (a) René N5 and (b) CM 247 using the PARTICOAT slurry, and their respective partitioning of (c-d) chromium, (e-f) titanium and (g-h) tantalum, after 1000h of oxidation tests at 1100°C under synthetic air conditions.

Table V-8 – Characterization of the Secondary Reaction Zone behaviour of the as a function of the oxidizing time at high temperatures.

Substrate	Average thickness of the SRZ (μm)	
	Oxidation at 900°C	
Time (h)	500	1000
INCO 738	18	23
PWA 1483	19	28
CM 247	12	-----
Oxidation at 1000°C		
Time (h)	500	1000
PWA 1483	21	36
CM 247	12	28
Oxidation at 1100°C		
Time (h)	500	1000
CM 247		
René N5	45	62

Once the behaviour of the PARTICOATED systems have been investigated up to 1000h of experimentations at several temperatures, a comparison of this protective system has been done with a conventional SVPA often employed in the industry and focusing on the highest temperatures for the René N5 material.

e. Comparison between the PARTICOATED samples and the SVPA ones.

Figure V-18 gathers the cross section of the two systems with the SVPA depicted by Figures V-18(a.c) and the PARTICOATED one by Figures V-18(b.d), for 500h and 1000h at 1100°C of isothermal oxidation. Generally speaking, similar oxidation and interdiffusion phenomena resulted in the degradation of both coatings. They developed an α -Al₂O₃ layer on top of their respective coating while a NiAl₂O₄ spinel grew in turn over this aluminium oxide. This spinel formed once the Ni diffusion became preponderant with respect that of Al [47]. One has to note that this oxide scale is thicker in case of the PARTICOATED samples than the SVPA one even after only 500h at such high temperature. The major difference between the two protective systems is that the SVPA one has a wavy surface, ascribed to the rumpling phenomenon. The latter has been reported to be due to the dimension of the grain, bigger in case of the SVPA than in the PARTICOATED samples, while the segregation of the refractory elements lead to reduce the rumpling phenomenon [37-38;48]. In addition, the areas in which the β phase transformed into γ' , coarsening of the precipitates also occurred because of the volume contraction [38;48] associated with this transformation, which expels the coarse refractory elements [37;39]. It shall be noted that the γ' pockets displayed twinning plans thereby suggesting a reversible martensitic transformation that was not clearly observed for the SVPA coatings

As a matter of fact, the $\beta \rightarrow \gamma'$ phase transformation has been reported to contribute to rumpling [49] because of the substantial volumetric changes that bring about the appearance of stresses and strains [38;48]. Recently, Bouchaud *et al.* [48] mentioned that this phase transformation may be related to the formation of the L1₀ structure, which is the martensitic transformation of the β -NiAl into γ -Ni₃Al. This transformation is more advanced in case of the PARTICOAT system due to the higher number of grain boundaries, which allow a more important outward diffusion of this element towards the coating. This transformation also led to the rejection of the refractory elements from the matrix for precipitating in the coating. The dimension of these ones is of prime interest as they hinder the displacement of the dislocations in the system and allow to enhance the mechanical resistance of the coating. This synergistic effect is promoted as long as the precipitates remains small in dimension, i.e. nano and or micro-precipitation, and homogeneously dispersed in the coating [50-51].

As a comparison to the rumpling phenomenon observed for conventional system [52], the oxide scales formed with the PARTICOAT coated systems does not relax by creep as it is pinned by the hollow spheres top coat, which should in turn easily accommodate the cooling stresses [53]. In addition, the Ta-rich precipitates grown at the coating / top coat interface may reinforce the hardness of this interface providing a limitation to the influence of the rumpling effect.

The IDZs underwent the $\beta \rightarrow \gamma'$ transformation due to the Al consumption by interdiffusion, while Ni diffuses outwardly and the heavy elements segregate at the same positions. This transformation is once again more advanced in the PARTICOAT samples, which has to be correlated with the initial state of the coating. As a matter of fact, the SVPA coatings are richer in Al and have coarser grains than the PARTICOAT ones, which is relevant of a delayed phase transformation during service condition. Similar to the transformation observed for the SRZ of the PARTICOAT systems, the TCP phases transformed into round shapes at the IDZ/SRZ interface while they remained with a needle like structure at the SRZ/substrate matrix interface.

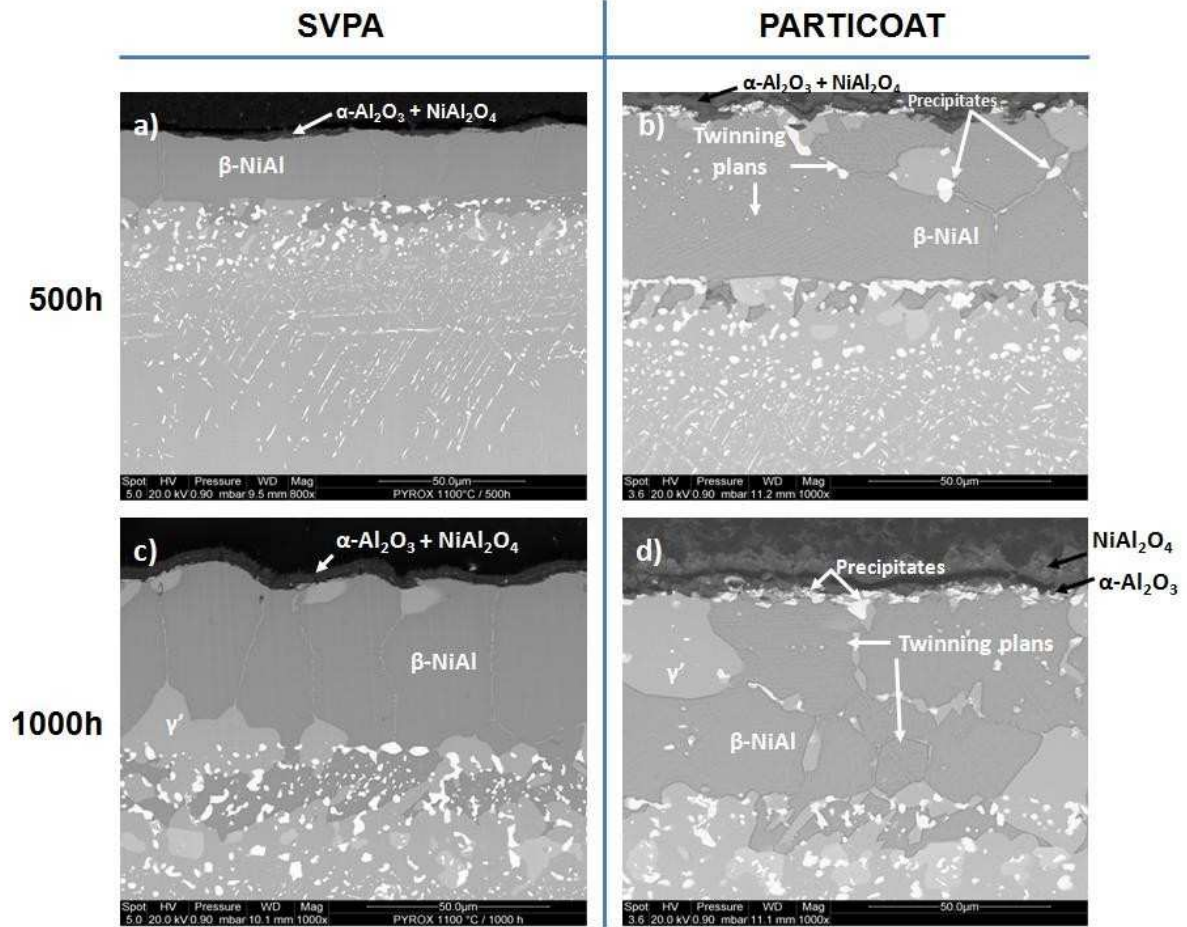


Figure V-18 – Comparison of the cross-sections of René N5 aluminized coupons oxidized at 1100°C for 500h for (a) the SVPA technique and (b) the PARTICOAT slurry related technique and the evolution of the microstructures of the samples after 1000h of oxidation for (c) the SVPA and for (d) the slurry process, respectively.

Summary and outlook

The high temperature oxidation behaviour of the different PARTICOATED superalloys has been estimated on four Ni-based superalloys and compared to one conventional system nowadays in use (SVPA technique) onto René N5. The specificity of the slurry related technique has been characterized by the evolutions of its top coat, TGO and bond coat.

The structure composed by the thermodynamically stable α -Al₂O₃ hollow microspheres has been found to be adherent over the 1000h of experiment of all the conditions chosen, except at the edge of the samples and in case of CM 247 LC at 1100°C. Nevertheless, this specific top coat structure seems to contribute to increase the oxidation kinetics of the PARTICOATED systems compared to the conventional ones as was demonstrated onto pure nickel. As the hollow character of the spheres has been neglected, one has to note that the actual reactive surface will need to be more precisely defined in order to better calculate the $\Delta M/S$ ratio. Any increase of the surface shall indeed result in a decrease of the oxidation kinetics and may provide closer results to the conventional ones.

The coating has been found to be equiaxed irrespectively of the initial structure of the base material (SX, DS, EQ), which imply the formation of numerous grain boundaries. From this assessment, the behaviour of the coating is ruled by the influence of the temperature and the duration of the oxidation experiments. The longer the experiment, the more Ni diffuses outwardly, leading to the β -NiAl \rightarrow γ' -Ni₃Al transformation. This transformation is significant of a loss of the high temperature oxidation resistance. In addition, this transformation also involves solubility matter for the different alloying elements of the initial γ/γ' matrix. In this view, the segregations of Cr, Ta, and Ti have been monitored to investigate the behaviour of their precipitates. The latter is ruled by the thermo-activated interdiffusion mechanisms and contributes to the growth of the TGO when accumulating at the bond coat / top coat interface but also at the extension of the SRZ at the coating / substrate interface.

When segregating at the first interface (top coat / coating) the refractory element precipitates allow to improve the resistance to the rumpling phenomena but the Al consumption towards the γ/γ' matrix promote the growth of the SRZ. As a matter of fact, the extension of the secondary reaction zone has been shown to strongly depend on the chemistry of the substrate, i.e. the higher the Cr, the Ti and the Ta contents, the thicker the SRZ.

A potential technical solution might be used in order to control such Al consumption and to maintain the oxidation resistance properties of the bond coat. Also, the extension of this detrimental SRZ can be restrained with respect of the temperature and time influence. Recently, an electrodeposited layer has been developed based on the use of the rare earth oxides. It has been found that such layer has interesting properties for the limitation of the interdiffusion mechanisms, and can be extrapolated to the control of the development of such SRZ. The following Chapter focuses on such likely technical solution.

References

- [1] C. Wagner, *Journal of the Electrochemical Society* 99 (1952) 379
- [2] M.W. Brumm, H.J. Grabke, *Corrosion Science* 33 (1992) 1677
- [3] R. Prescott, M.J. Graham, *Oxidation of Metals* 38 (1992) 233
- [4] J. Jedlinski, S. Mrowec, *Material Science Engineering* 87 (1987) 281
- [5] K. Messaoudi, A.M. Kuntz, B. Lesage, *Material Science Engineering A247* (1998) 248
- [6] V.K. Tolpygo, *Oxidation of Metals* 51 (1999) 449
- [7] N. Eisenreich, H. Fietzek, M.M. Juez-Lorenzo, V. Kolarik, A. Koleczko, V. Weiser, *Propellants Explosives Pyrotechnics* 29 (2004) 137
- [8] V. Kolarik, M. Juez-Lorenzo, H. Fietzek, *Materials Science Forum* 696 (2011) 290
- [9] J.R. Nicholls, N.J. Simms, W.Y. Chan, H.E. Evans, *Surface and Coatings Technology* 149 (2002) 236
- [10] A. Pfennig, B. Fedelich, *Corrosion Science* 50 (2008) 2484
- [11] B. Bouchaud, J. Balmain, F. Pedraza, *Defect and Diffusion Forum* 289-292 (2009) 277
- [12] R.C. Reed, *The Superalloys, Fundamentals and Applications*, Cambridge (2006)
- [13] P.W. Schilke, GE Energy, *Advanced Gas Turbine Materials and Coatings*, (2004) GER-3569G
- [14] National Aeronautics and Space Administration (NASA), *NASA/TM – 2007 – 214479*
- [15] D.M. Shah, A. Cetel, *Superalloys 2000* (2000) 295
- [16] Siemens, private communication (2010)
- [17] M. Mollard, *Elaboration de système barrière thermique par barbotine. Comportement du nickel et de ses superalliages revêtus en oxydation cyclique à hautes températures*, PhD Thesis, University of La Rochelle, France (2012)
- [18] www.thermocalc.com
- [19] www.thermocalc.se/TCDATA.htm
- [20] C.M.F. Rae, M.S. Hook, R.C. Reed, *Materials Science and Engineering A* 396 (2005) 231
- [21] M. Schütze, M. Malessa, V. Rohr, T. Weber, *Surface and Coatings Technology* 201 (2006) 3872
- [22] Y.A. Tamarin, *Protective Coatings for Turbine Blades* (2002) ASM International
- [23] G.K. Dey, *Sadhana* 28 (2003) 247; T. Czeppe, S. Wierzbinski, *International Journal of Mechanical Sciences* 42 (2000) 1499
- [24] M.V. Acharya, G.E. Fuchs, *Materials Science and Engineering A381* (2004) 143
- [25] B. Pieraggi, *Oxidation of Metals* 27 (1987) 177
- [26] D. Monceau, B. Pieraggi, *Oxidation of Metals* 50 (1998) 477

- [27] I. Levin, D. Brandon, *Journal of the American Ceramic Society* 81 (1998) 1995
- [28] M. Mollard, B. Rannou, B. Bouchaud, J. Balmain, G. Bonnet, F. Pedraza, *Comparative degradation of nickel aluminized by slurry and by pack cementation under isothermal conditions*, *Corrosion Science* (2012) in press
- [29] I. Beszeda, D.L. Beke, Y. Kaganovskii, *Surface Science* 569 (2004) 5
- [30] F. Pedraza, M. Mollard, B. Rannou, J. Balmain, B. Bouchaud, G. Bonnet, *Materials Chemistry and Physics* 134 (2012) 700
- [31] G. Leofanti, M. Padovan, G. Tozzola, B. Venturelli, *Catalysis Today* 41 (1998) 207
- [32] A. Portinha, V. Teixeira, J. Carneiro, J. Martins, M.F. Costa, R. Vassen, D. Stoeber, *Surface and Coatings Technology* 195 (2005) 245
- [33] B.A. Pint, S.A. Speakman, C.J. Rawn, Y. Zhang, *Journal of Metals* 58 (2006) 47
- [34] J. Haynes, B.A. Pint, W.D. Porter, I.G. Wright, *Materials at High Temperature* 21 (2004) 87
- [35] B. Bouchaud, J. Balmain, F. Pedraza, *Oxidation of Metals* 69 (2008) 193
- [36] T.S. Chester, N.S. Stoloff, W.C. Hagel Wiley, *Superalloys II* (1987)
- [37] R.C. Pennefather, D.H. Boone, *Surface and Coatings Technology* 76-77 (1995) 47
- [38] V.K. Tolpygo, D.R. Clarke, *Acta Materialia* 52 (2004) 5115
- [39] P.Y. Hou, A.P. Paulikas, B. W. Veal, *Materials at High Temperatures* 22 (2005) 535
- [40] A. Chien, D. Gan, P. Shen, *Material Science and Engineering A* 206 (1996) 512
- [41] J. Angenete, K. Stiller, *Surface and Coatings Technology* 150 (2002) 107
- [42] M.S.A. Karunaratne, C.M.F. Rae, R.C. Reed, *Metallurgical and Materials Transactions A* 32 (2001) 2409
- [43] F.J. Perez, F. Pedraza, M.P. Hierro, J. Balmain, G. Bonnet, *Oxidation of Metals* 58 (2002) 563
- [44] F.J. Perez, F. Pedraza, M.P. Hierro, J. Balmain, G. Bonnet, *Surface and Coatings Technology* 153 (2002) 49
- [45] A. Aguëro, M. Gutiérrez, V. Gonzalez, *Materials at High Temperature* 25 (2008) 257
- [46] A. Aguëro, *Energy Materials* 1 (2008) 35
- [47] F. Pedraza, B. Bouchaud, J. Balmain, G. Bonnet, V. Kolarik, J. Menuey, *Materials Science Forum* 696 (2011) 284
- [48] B. Bouchaud, J. Balmain, F. Pedraza, *Materials Science Forum* 595-598 (2008) 11
- [49] M.W. Chen, M.L. Glynn, R.T. Ott, T.C. Hufnagel, K.J. Hemker, *Acta Materialia* 51 (2003) 4279
- [50] R. Bianco, R.A. Rapp, *Journal of Electrochemical Society* 140 (1993) 1181
- [51] B.A. Pint, M. Treska, L.W. Hobbs, *Oxidation of Metals* 47 (1997) 1

[52] B. Rannou, B. Bouchaud, J. Balmain, G. Bonnet, F. Pedraza, *Comparative isothermal oxidation behaviour of new aluminide coatings from Al particles containing slurries and conventional out-of-pack aluminide coatings*, Oxidation of Metals (2012) submitted

[53] J. Favergeon, D. Brancherie, Corrosion et protection des matériaux à haute température, Ed. Presses des Mines ParisTech (2011) 205

Chapter VI

Investigation of a special design: Influence of a rare-earth oxide-based diffusion barrier in combination with the PARTICOAT concept

The PARTICOAT concept has been used to increase the high temperature oxidation resistance of four Ni-based superalloys. Nevertheless, as with conventional coatings, the previous results showed that the coatings degraded by interdiffusion both at the thermally grown oxide/coating and at the coating/substrate interfaces, this happening irrespectively of the chemistry of the substrates.

This chapter therefore focuses on the likely effect of a proprietary interlayer to reduce the outward diffusion of the alloying elements (Cr, Ti, Ta...), as well as their segregation, and to limit the development of the secondary reaction zone (SRZ) between the coating and the substrate due to Al inward diffusion. The use of ceria film combined with the PARTICOAT concept is proposed to prevent those degradation processes. Characterizations have been done after realizing the thermal treatment of this special design, but also after high temperature oxidation tests at 900 and 1100°C.

Table of contents

I. Characterization of the special design using a proprietary interlayer and the PARTICOAT concept.	149
A. Deposition process of the “diffusion barrier”.	151
B. Evolution with temperature of the microstructure of the special design onto pure Ni.	154
II. Extrapolation to Ni-based superalloy: example of CM 247 LC.	156
A. Reactivity towards the PARTICOAT and high temperature oxidation behaviour.	156
1. Formation mechanisms influenced by the temperature and the chemical composition.	156
2. High temperature behaviour.	159
B. Considerations for the formation of the special design.	161
Summary and outlook.	164
References.	166

I. Characterization of the special design using a proprietary interlayer and the PARTICOAT concept.

The idea to use a special design came from the elaboration problems observed when trying to deposit PARTICOAT onto the Ni₂₀Cr(1.5Si) model substrate but also onto INCO 738 in a less extended way. The segregation of Cr, impeding the Al inward diffusion, and formation of brittle phases, i.e. Al_xCr_y, contributed to the difficulties experienced for aluminizing and to the topcoat detachment during the quenching step (cf Chapter IV), respectively.

From these experimental observations, the use of a special design has been proposed on the one hand to aim at restraining the upward flow of Cr, while allowing the Al inward flow to form the diffused layer / bondcoat. On the other hand, this shall also allow to reduce the same aluminium consumption by the substrate during the exposure, thus limiting the development of the secondary reaction (SRZ), and would constitute a major advantage for lengthening the oxidation resistance property with service conditions (time + temperature).

Apart from the expensive γ / γ' coatings [1], which have been designed for reducing the interdiffusion mechanisms and despite their good results, the concept of limiting the interdiffusion processes to extend lifetime has been investigated by several groups for past years, using different approaches. Müller *et al.* [2] used an alumina film placed between a Ni-based superalloy (CMSX-4) and an overlay coating (MCrAlY) to reduce the interdiffusion of the coating towards the substrate. In addition, they needed to use TiN to match the coefficient of thermal expansion between the three components (substrate / alumina film / overlay coating). They observed the stability of the alumina diffusion barrier (DB) after 100h of oxidation at 1100°C but did not mention the behaviour of such system for longer time exposure. Haynes *et al.* [3] investigated the sputtering of Hf-Ni and Hf-Pt as potential high temperature diffusion barrier. The first option resulted in a limited stability at high temperature during tests at 1150°C, while the second formed a HfPt₃-type compound dissolving during the aluminizing process. In the meantime, Narita *et al.* [4] developed a duplex Re(W)-Cr-Ni/Ni(Cr)-Al coating systems. For this to happen, they realized quite complex and long manufacturing processes (three electroplating steps and two pack cementation stages). They finally succeed to reduce the modification of the microstructure of their substrate and their diffusion barrier remained stable. In addition, such system allowed to reduce the Al interdiffusion from its reservoir, whereas a small SRZ still formed. More recently, Cavaletti *et al.* [5] studied the effect of a Ni-W based diffusion barrier. Unfortunately, this solution has shown worst results than without the use of a DB during comparative high temperature oxidation tests. They suggested that the interdiffusion of S and W in the coating systems contributed to degrade the global system. In the meantime, one has to note that they observed the delayed formation of the SRZ. Wang *et al.* [6] formed a (Ru,Ni)Al/NiAl diffusion barrier coating using two manufacturing steps (electroplating + EBPVD). They observed a significant reduction of the dimension of the SRZ during the determination of the interdiffusion value for high temperature experiments (1050°C) under vacuum conditions.

Recently, the use of a rare-earth oxide film has been studied at the LaSIE laboratory [7-9] to improve the high temperature oxidation behaviour of a René N5 single-crystal Ni-based superalloy substrate through a friendly approach satisfying new environmental directives [10]. For this to happen, a cathodic electrodeposition (CELD) process has been set up to deposit a ceria oxide from a water-based electrolyte. This resulted in enhanced the oxidation resistance of the superalloy for both isothermal and cyclic oxidation conditions at 1100°C [11-13]. For this to happen, they showed that this ceria deposit could restrain the Cr upward diffusion, but also could mostly limit the Al inward diffusion during high temperature oxidation exposure. The use of such multi-cracked overlay oxide-based coatings is therefore expected to allow the aluminizing of the substrate by tailoring its

morphology, thickness and microstructural and compositional properties in view of a special design coating system.

In addition, one has to note that the ceria has compatible thermal properties compared to the ones of Ni-based superalloys and the ones of Al_2O_3 , mainly the thermal expansion as well as the thermal conductivity coefficients as presented in *Table VI-1*.

Table 1 - Density (ρ), coefficient of thermal expansion (α) and thermal conductivity (λ) of several bulk compounds taken from [14].

Compounds	IN-738	SiO_2	Cr_2O_3	Al_2O_3	CeO_2	MgO	Y_2O_3	ZrO_2	HfO_2	La_2O_3
ρ ($\text{g}\cdot\text{cm}^{-3}$)	-	2.2-2.6	5.22	3.86	7.20	3.58	5.03	5.80 - 6.04	9.68	6.51
α ($10^{-6}\cdot\text{K}^{-1}$)	17.6	a: 0.5 c: 9.6	9.6	8.9	13.0	13.9	9.3	m: 7.0 t: 12.0	5.86	11.9
λ ($\text{W}\cdot\text{m}^{-1}\cdot\text{K}^{-1}$)	-	- a: 1.38	-	35.6-39	2.77 ^[15]	50-72	-	-	1.14	-

a: amorphous, c: crystallized, m: monoclinic, t: tetragonal.

From these properties, a special design has been investigated, with the combined effects of this ceria CELD overlay coating and the PARTICOAT aluminizing slurry, to compare to the baseline results of the PARTICOAT protective system. *Figure VI-1* shows the initial microstructures of the two systems before the use of any thermal treatment. The CeO_2 layer is deposited during a first manufacturing step while the Al microspheres are deposited on top of it, using a second step.

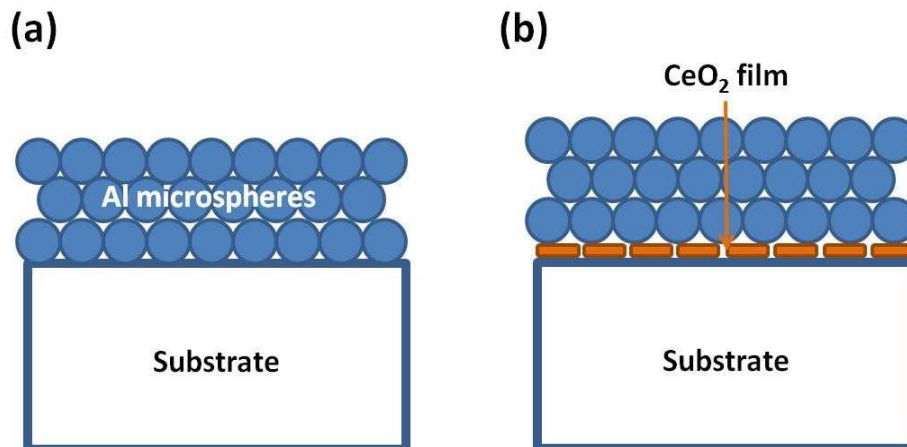


Figure VI-1 - Designs of (a) the initial PARTICOAT concept applied by air-spraying of the slurry and (b) the duplex system achieved in two step: first, an interlayer applied by the cathodic electrodeposition process, then the PARTICOAT concept is deposited on top of it.

The thermal treatment defined for the PARTICOAT concept ($400^\circ\text{C} - 1\text{h} + 700^\circ\text{C} - 2\text{h} + 1100^\circ\text{C} - 2\text{h}$) has been used without further optimization. The expected microstructure is shown in *Figures VI-2*. The ceria film should be distributed during the two steps at 700°C and 1100°C . In a first time, the interlayer is expected to stay at the topcoat / substrate interface during the Al inward diffusion step at $700^\circ\text{C} - 2\text{h}$, while the step at $1100^\circ\text{C} - 2\text{h}$ upon which Ni outward diffusion occurs should allow to distribute CeO_2 in the β -NiAl additive layer. From this expected design, the ceria film may be localised at the two following interfaces (thermally grown oxide / bond coat and bond coat / substrate), while a part of it may be partitioned in the bond coat, as represented by the orange dots (*Figure VI-2(b)*).

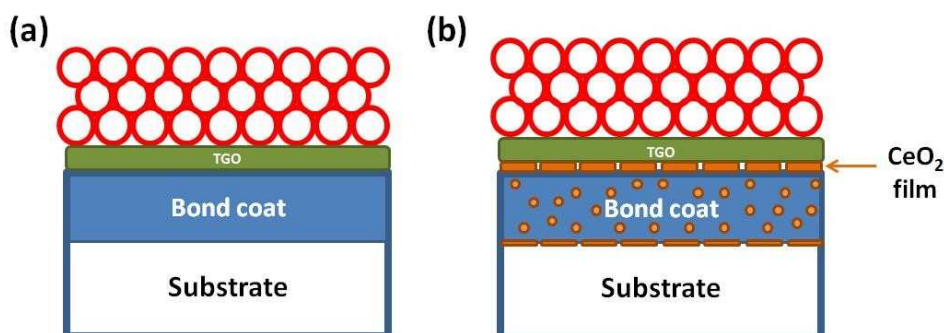


Figure VI-2 – Effect expected of the thermal treatment on both designs: (a) the initial PARTICOAT concept applied by air-spraying of the slurry and (b) the duplex system achieved in two step: first, an interlayer is applied by the cathodic electrodeposition process [8-9], then the PARTICOAT concept is deposited on top of it.

In this view, the behaviour of this special design has been first investigated onto pure Ni to observe the mechanisms involved during the formation of this coating system. Then, an extrapolation to the CM 247 LC Ni-based superalloy has been carried out to study the behaviour of this design during oxidation experiments at high temperature.

A. Deposition process of the “diffusion barrier”.

The use of the cathodic electrodeposition has been chosen to apply the ceria film on top of the substrates [7-9], using a conventional three-electrode cell, represented by Figure VI-3.

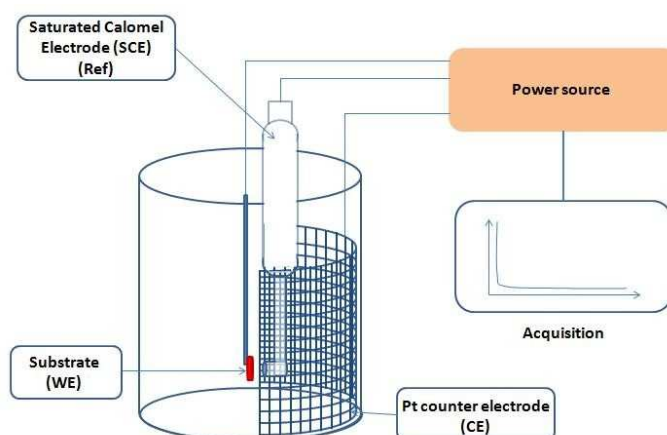


Figure VI-3 – Design of the electrolytic cell using a three-electrodes cell.

From the previous work of B. Bouchaud, using a concentrated cerium nitrate water-based solution (0.1 mol.l^{-1}) at room temperature, one current density has been chosen (-1 mA.cm^{-2}) [8-9]. Three durations of deposition (5, 10 and 20 min) were applied to investigate the resulting features of the films such as its morphology and microstructure, its composition, thickness and homogeneity. Figure VI-4 gathers the SEM surfaces of the Ni20Cr SiC #180 polished samples fully covered, with adherent overlay coatings. Increasing the deposition time leads to the vanishing of the polishing lines along which the deposit grew mainly by a nucleation and growth process [7]. As depicted by Figure VI-5, a cracks network formed due to the high kinetics and accumulation of stresses, which relaxed during the deposition time and thickening of the deposits [7]. Such process presents a linear variation of its mass, as depicted by Figure VI-6.

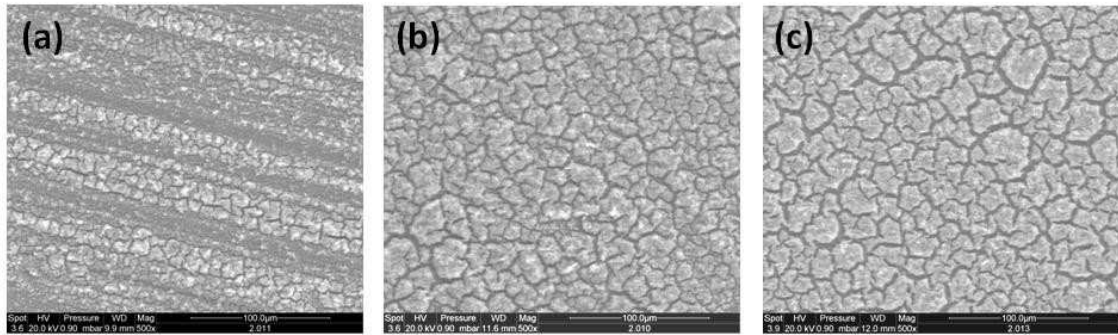


Figure VI-4 –Influence of the time of electrodeposition on the surface morphology after (a) 5 min, (b) 10 min and (c) 20 min for the same current density (-1 mA.cm^{-2}) on Ni20Cr.

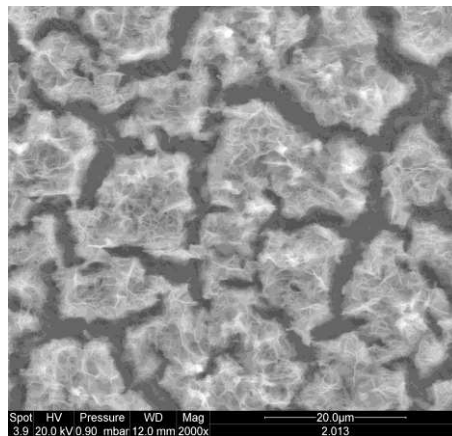


Figure VI-5 – Morphology of the surface of the rare-earth coating at higher magnification. The CeO_2 islands are delimited by a crack network through which the substrate can be observed.

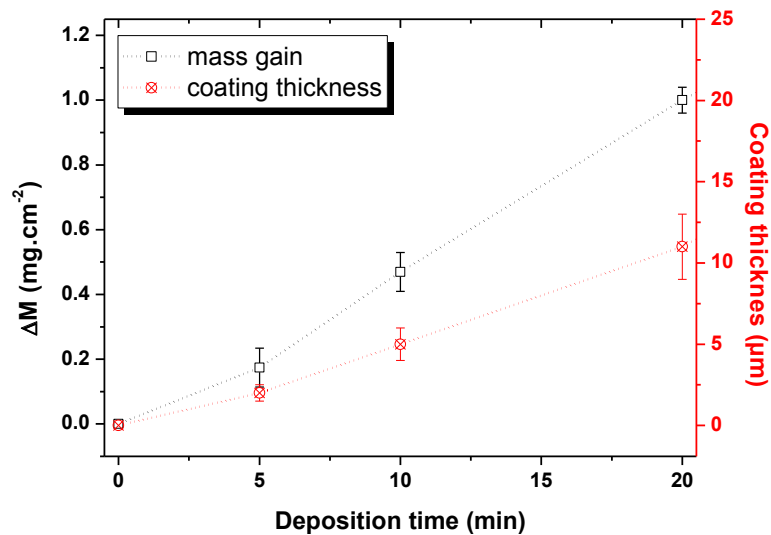


Figure VI-6 – Variation of the mass of the overlay coating as a function of the deposition time for René N5 single crystal substrate.

In order to characterize this deposit, Raman micro-spectroscopy analyses of the deposit in its “as-deposited” conditions have been performed. The signatures of the components formed after 5, 10

and 20 min of electrodeposition are gathered and overlapped in *Figure VI-7*. The corresponding peaks at 454 cm^{-1} and 606 cm^{-1} are both relevant of Ce-O vibration bonding. The first one is associated with the F_{2g} mode and is ascribed to the crystallized / amorphous characteristic of the ceria oxide but also significant of the amount of oxygen lattices contained in the rare-earth oxide film [16-18]. In its “as deposited” form, the film can contain both Ce^{4+} and Ce^{3+} species. From these observations, the film is supposed to be composed of $\text{Ce}(\text{OH})_3$ and CeO_2 or by a non-stoichiometric oxide like the CeO_{2-x} [7]. The three peaks at 714 , 741 and 1048 cm^{-1} might be attributed to carbonate [19] for the first one, while the two others are relevant of nitrate ions from the electrochemical solution trapped due to high kinetics and incomplete reactions [7;20-21], in agreement with several studies [22-24]. Bouchaud [7] showed that nitrates and carbonates are decomposed before 550°C , while the film is partially crystallized. At higher temperature, they mentioned the formation of a non-stoichiometric component formed (CeO_{2-x}), which can thereafter act as an oxygen trap to reduce the $p\text{O}_2$ during high temperature oxidation experiments [7;13].

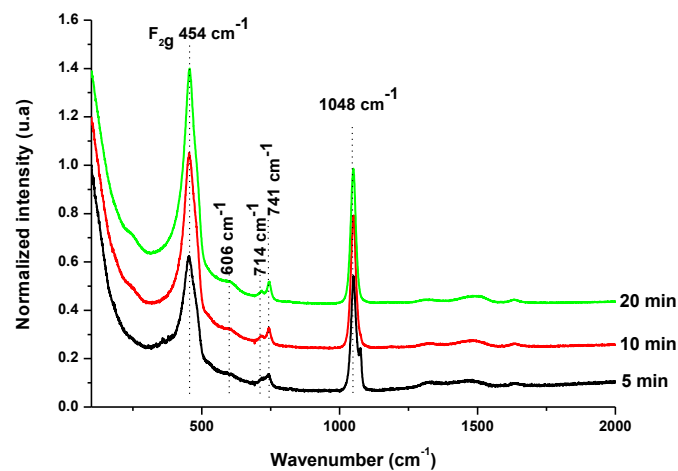


Figure 7 – Raman micro-spectroscopy analyses of ceria overlay on pure Ni as deposited.

From the properties of the CELD overlay coating, a compromise allowed to provide the optimum design to aluminize using the PARTICOAT slurry. For this to happen, a 10 minutes deposition time led to the formation of a fully covering, homogeneous and relatively thin coating, as shown in *Figure VI-8(a)* and *Figure VI-8(b)*, respectively. The chemical contrasts present on the surface analyse confirm the needle-like morphology of the rare-earth oxide layer as well as its cracks network [13], while the cross section provides information on the thickness of the overlay, which is *ca.* $5\text{ }\mu\text{m}$.

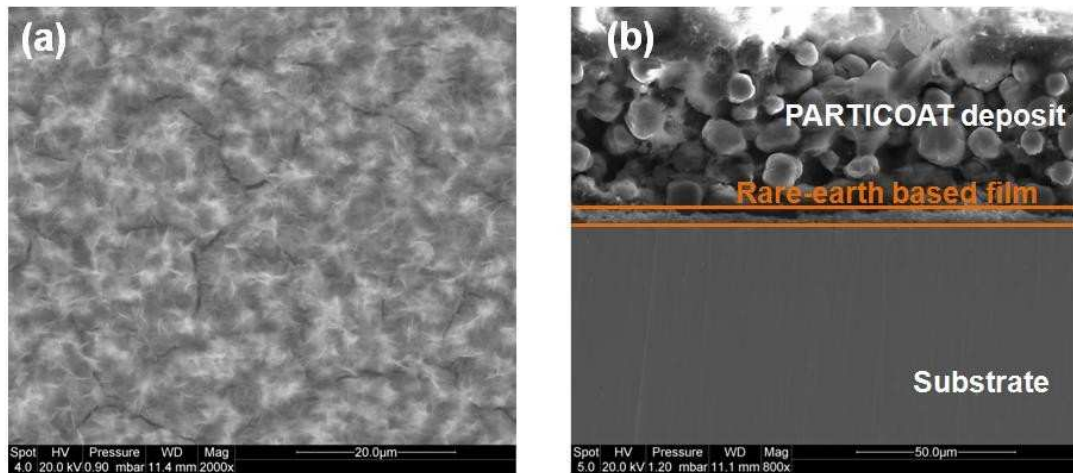


Figure VI-8 – (a) Morphology of the as-deposited rare-earth oxide proprietary interlayer after 10 min of electrodeposition using $-1 \text{ mA}\cdot\text{cm}^{-2}$ and (b) cross section of the special design including both interlayer and PARTICOAT deposit before any thermal treatment.

B. Evolution with temperature of the microstructure of the special design onto pure Ni.

Figure VI-9 gathers the comparison between the PARTICOAT concept (reference) formed onto pure Ni and the special design using the ceria interlayer. Both samples underwent the same thermal treatment ($400^\circ\text{C} - 1\text{h} + 700^\circ\text{C} - 2\text{h} + 1100^\circ\text{C} - 2\text{h}$) in inert Ar(g) atmosphere and resulted in the similar microstructure than the PARTICOAT concept (hollow spheres topcoat + thermally grown oxide + additive layer) for the complete thermal treatment. Nevertheless, the mechanisms implied in this formation of intermetallics differ.

Indeed, after the step at 700°C for two hours of annealing (Figure VI-9(a) and Figure VI-9(b)), the chemistries of the systems are completely different. While the “simple” PARTICOAT system allows the formation of an Al enriched zone, with a Ni_2Al_3 matrix (cf Chapter IV), the special design did not lead to the formation of an aluminium modified zone, as shown by the chemical contrasts in Figure VI-9(b)). The Al microspheres remained full of their initial content, while the cerium-based deposit is still clearly visible at the PARTICOAT deposit / substrate interface. As a matter of fact, the Al liquid phase formed at 700°C did not lead to the dissolution / diffusion mechanisms, as the one observed during the “simple” PARTICOAT aluminizing process [25-26].

On the contrary, the step at 1100°C for two hours (Figure VI-9(c) and Figure VI-9(d)) allowed the aluminizing of both systems, irrespectively of their initial chemistries. Considering the special design, XRD measurements, presented by Figure VI-10, confirmed the formation of the same $\alpha\text{-Al}_2\text{O}_3$ component and $\beta\text{-NiAl}$ additive layer observed for the “simple” PARTICOAT coating (cf Chapter IV). In the meantime, traces of perovskite oxide have also been found by XRD measurements, with the signature of the CeAlO_3 compound. Such component can form from the solid state reaction between the CeO_2 and $\alpha\text{-Al}_2\text{O}_3$ [7;11].

In the case of the special design, the duplex structure develops with additional bright contrasts in the topcoat, which can be ascribed to the migration of Ni by outward diffusion during the thermal treatment. One can also note that the coating with the interlayer seems to be as thick (top coat and diffusion layer) as the PARTICOAT reference design even if the amounts of initial slurry deposited on top of the substrate seems different (Figure VI-9(c) and Figure VI-9(d)) due to discrepancies during

the experimental deposition conditions. The “simple” PARTICOAT initial deposit is bigger than the special design, as shown by the remaining skeletons of the Al microparticles.

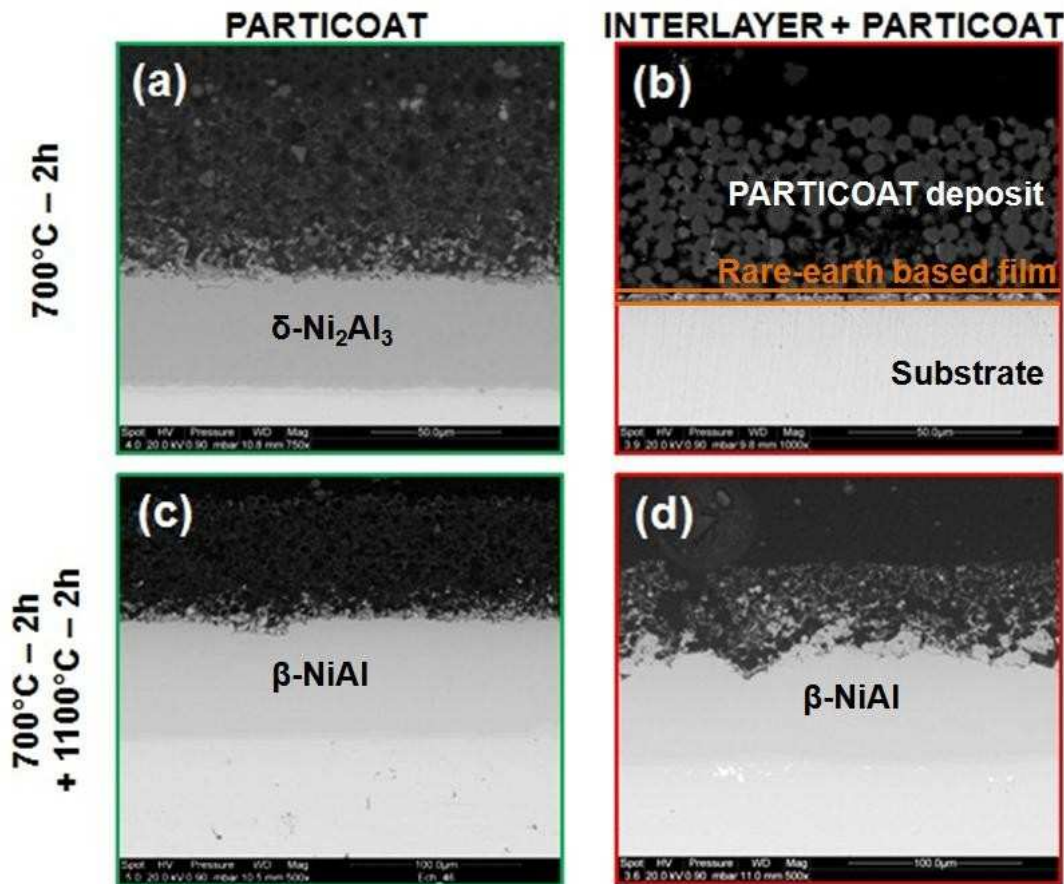


Figure VI-9 - Microstructures formed for the PARTICOAT concept and the special design (Interlayer + PARTICOAT) on pure Ni, with (a) and (b) the respective microstructure obtained after the 700°C – 2h thermal treatment and (c) and (d) after the homogenization step at 1100°C for 2h.

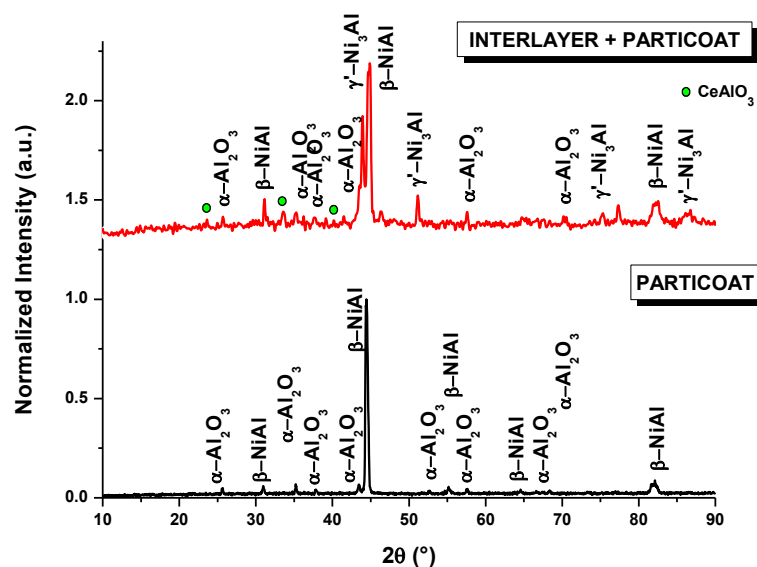


Figure VI-10 – XRD measurement comparing the « simple » PARTICOAT system and special design (ceria interlayer + PARTICOAT), formed on pure Ni after the following thermal treatment: 400°C – 1h + 700°C – 2h + 1100°C – 2h in flowing Ar(g) atmosphere.

Once the special design has been formed onto pure Ni, the mechanisms of formation have been investigated onto CM 247 LC to observe the evolution of the microstructure impaired with the PARTICOAT thermal treatment. This Ni-based superalloy has been chosen to investigate the potential of the special design, first, because of the availability of raw materials we had for this study, and secondly, to study the applicability of this concept for a “low” Cr-containing superalloy. Then, the high temperature oxidation tests have been studied at 900 and 1100°C. A comparison with the results obtained for the “simple” PARTICOATED CM 247 LC allows to emphasize the behaviour of the PARTICOAT modified design.

II. Extrapolation to Ni-based superalloy: example of CM 247 LC.

A. Reactivity towards the PARTICOAT and high temperature oxidation behaviour.

1. Formation mechanisms influenced by the temperature and the chemical composition.

Figure VI-11 gathers the cross sections of CM 247, for the two designs: the PARTICOAT reference one and the special design including the rare-earth oxide interlayer. After 2h at 700°C (*Figure VI-11(a)* and *Figure VI-11(b)*), one can note that the microstructure is completely different with respect of the addition of the ceria film. For the simple PARTICOAT system, the hollow sphere topcoat is already formed as well as an Al enriched layer, which is composed by a Al_3Ni_2 matrix (*Chapter IV*). Similarly to pure Ni after the step at 700°C, the use of the cerium oxide film led to the non-enrichment in aluminium of the Ni-based substrate, as presented by the back scattered image. *Figure VI-12* depicts the X-ray maps of the chemical elements composing the CM 247 substrate with the addition of the Ce element. The γ / γ' matrix of the Ni-based superalloys remained unchanged. Cr did not segregate at the substrate / ceria film interface, while small Ni, Ta and W enrichments seemed to occur close to the ceria film position and / or in the Al topcoat. The aluminium stayed in the microsphere particles and all microspheres remained full of their initial Al content. One has to mention that the overall thicknesses of the topcoat are rather similar for those samples. The temperature of 700°C for 2h did not allow the Ce element to react from its initial position at the Al microsphere deposit / substrate interface.

The step at 1100°C for 2h, which is depicted by the *Figure VI-11(c)* and *Figure VI-11(d)*, provided the formation of similar microstructures compared to the one observed for pure Ni. The $\alpha\text{-Al}_2\text{O}_3$ hollow topcoat structure is formed over the $\beta\text{-NiAl}$ additive layer. The deposition of similar amounts of the slurry (reflected by similar thicknesses of the topcoat at 700°C) led to a 1.5-fold thicker additive layer in case of the special design system. In addition, the shells of the oxidized Al microparticles seem thinner than the ones formed for the reference design.

During the “simple” PARTICOAT aluminizing process, all the O_2 available in the gas phase reacted with the liquid / solid Al to form alumina component, with respect of the temperature and the dissociation pressure of this metallic element. From this reaction, part of the aluminium content is consumed by the oxidation process, while the other part contributes to the Al enrichment of the substrate by dissolution / diffusion processes (cf *Chapter IV*).

Compared to the mechanisms described for the reference design, the use of the ceria film modified the aluminizing process. One has to keep in mind that the rare-earth oxide interlayer is non-stoichiometric (CeO_{2-x}) and can absorb oxygen anions to compensate the high amount of oxygen

lattices to satisfy the stoichiometric deviance [7;13]. Then, when such a film is used with the PARTICOAT design, the oxygen will be consumed by the oxidation of aluminium into alumina while a part of the oxidizing agent will be trapped by the CeO_{2-x} compound. This may contribute to reduce the oxidation kinetics of the aluminium into alumina, then increasing the available fraction of Al to provide the aluminizing and increasing the size of the additive layer.

X-ray maps have been realized to observe the evolution of the elemental partitioning and are presented in *Figure VI-13*. Ce exists at the topcoat / additive layer interface but also deeper in the additive layer, where Cr and Co partitioning seem to be slackened. This effect is much more pronounced for chromium. Ce seems to hinder the formation of Cr segregation at this position, then controlling the outward flux of this alloying element. During longer time exposure, this may reduce the possibility to form a secondary reaction zone for which Cr is known to agglomerate [27]. The tiny Ta and W enrichment of the top coat observed after 700°C/2h become brighter after the full heat treatment and Ni also clearly incorporates to this zone. In contrast, Ti seems to segregate at the top coat/diffusion layer interface but its precise location is difficult to assess. Complementary EPMA investigation should be useful to increase the accuracy of the partitioning. Similar to pure Ni system with the special design, traces of CeAlO_3 compound have been detected.

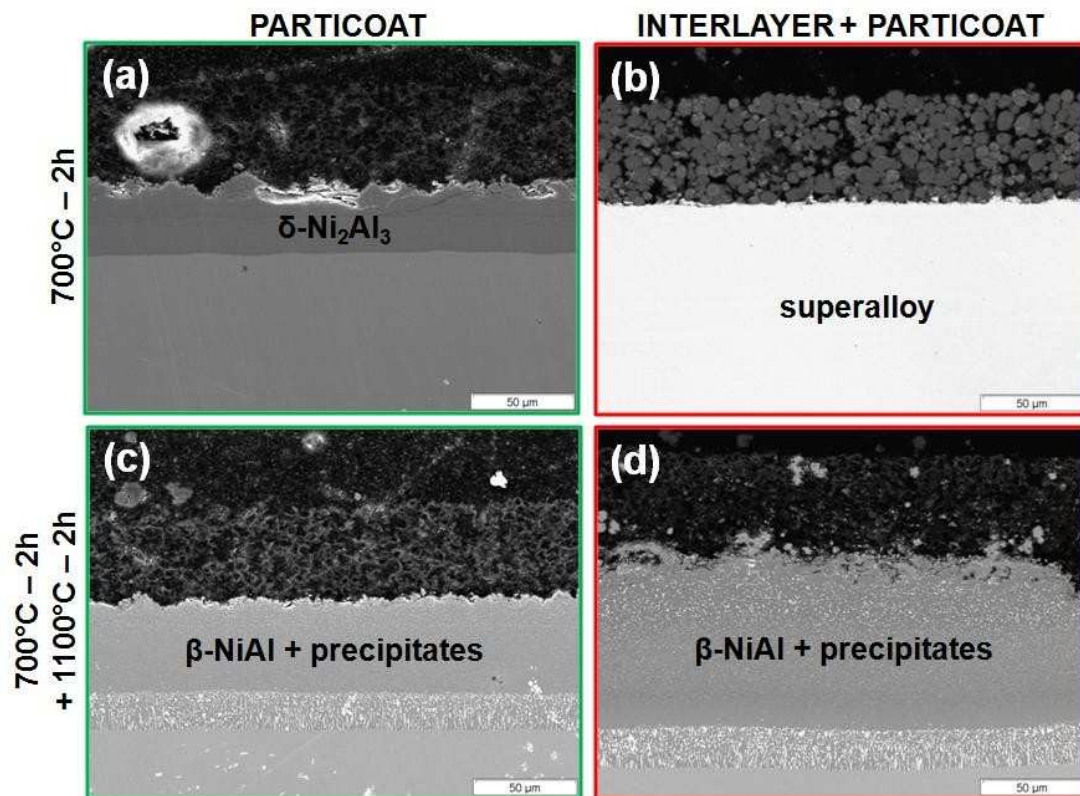


Figure VI-11 – Microstructures formed for the PARTICOAT concept and the special design (Interlayer + PARTICOAT) on CM 247 Ni-based superalloy, with (a) and (b) the microstructure obtained after the 700°C – 2h thermal treatment and (c) and (d) after the homogenization step at 1100°C for 2h.

Once the formation of the special design of PARTICOAT has been proven, the oxidation resistance tests have been investigated for high temperature conditions at 900 and 1100°C.

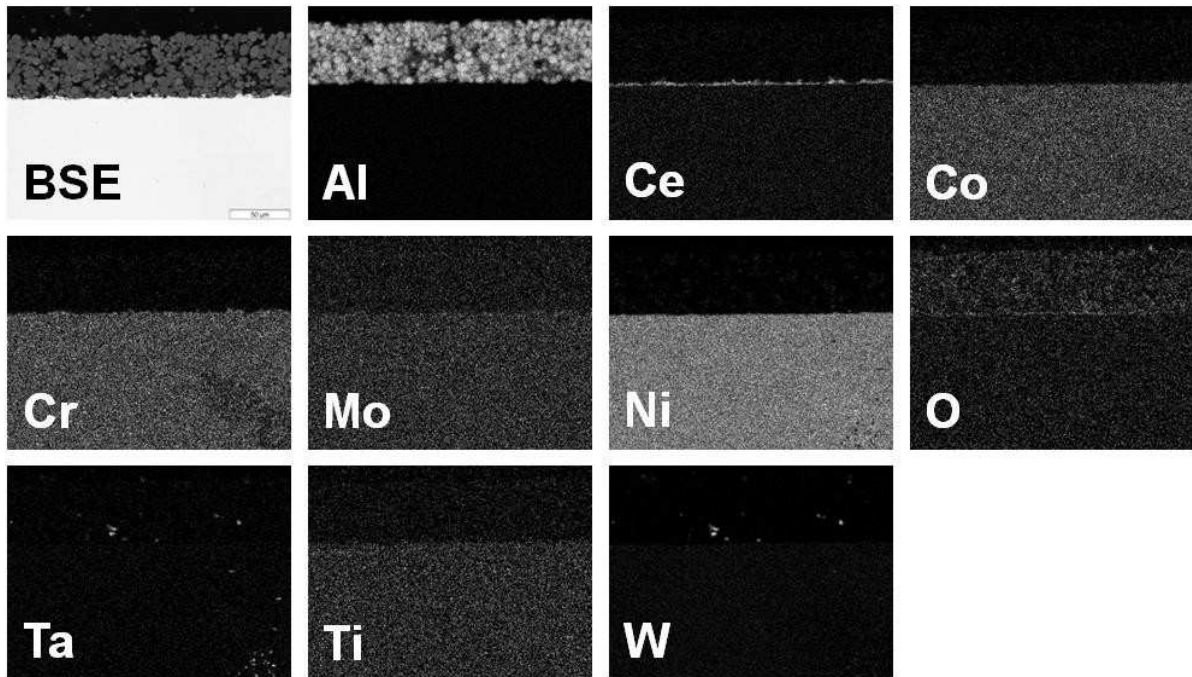


Figure VI-12 – X-ray maps of the elemental partitioning for the special design after the step at 700°C for 2h under inert Ar(g) atmosphere, showing the different chemical elements constituting the CM 247 Ni-based substrate and the cerium oxide/Particoat coating.

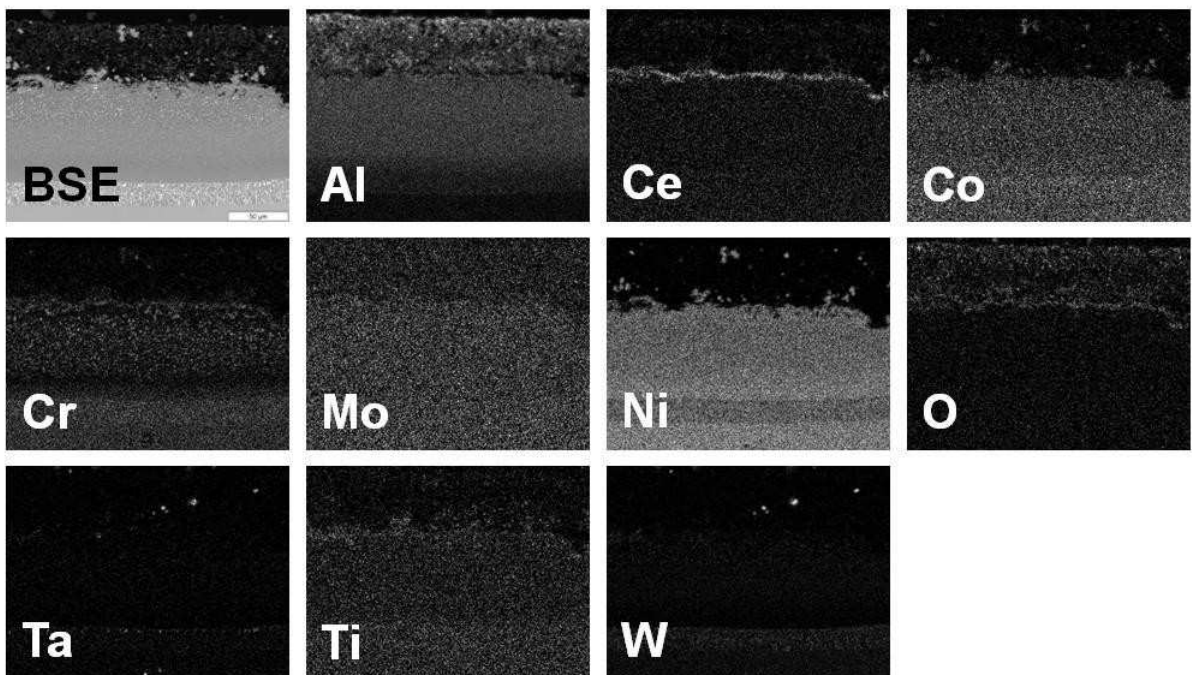


Figure VI-13 - X-ray maps of the elemental partitioning for the special design after the step at 1100°C for 2h under inert Ar(g) atmosphere, showing the different chemical elements constituting the CM 247 Ni-based substrate and the cerium oxide/Particoat coatings.

2. High temperature behaviour.

Figure VI-14 gathers the surface and cross section analyses of CM 247, for the special design at 900°C, for 500 and 1000h of tests. The topcoat seems to be brittle, as suggested by the cracks network after 500h of oxidation (*Figure VI-14(a)*), while the foam structure partially detached from the system for the same duration, or completely for longer oxidation tests up to 1000h (*Figure VI-14(c)*). In both cases, cross-section analyses revealed that the additive layers did not formed homogeneously, having Al island diffusion morphologies (*Figure VI-14(b)*). This may affect the adhesion property of the topcoat during thermo-mechanical solicitation (quench). In addition, the thermally grown oxide (TGO) grew thicker (*Figure VI-14(d)*) compared to the reference design. X-ray mapping analyses confirmed the Al, Ce and O enrichment at the topcoat / coating interface. XRD measurements allowed to detect the signature of the CeAlO₃ compound. At this temperature, the $\beta \rightarrow \gamma'$ transformation did not develop significantly, as for the “simple” PARTICOAT design (cf Chapter V). It has to be mentioned that the development of a secondary reaction zone (SRZ) did not occur at 900°C after 500h nor after 1000h of oxidation.

Figure VI-15 presents the results of the oxidation experiments at 1100°C up to 1000h. As observed at 900°C, samples with the special design underwent the same phenomenological degradation mechanisms, which are more pronounced due to the higher temperature. The reaction between ceria and alumina led also to the detachment of the topcoat even if some part of it remained pegged, whether for 500h of test (*Figure VI-15(a)*), or for 1000h (*Figure VI-15(c)*). The influence of the temperature provide the onset of the $\beta \rightarrow \gamma'$ transformation (*Figure VI-15(b)*), but as previously observed for the experiments at 900°C, the SRZ did not form either. Nevertheless, the additive layer did not behave uniformly, as shown by the chemical contrast, which is probably a legacy of the formation of the special design during the thermal treatment or during the ceria deposition step itself, which is critical for the morphological, microstructural and compositional features of the deposited layers onto which the slurry will be applied. A further optimization of the cracks network may allow to optimize the Al enrichment of the substrate, and also to reinforce the TGO as well as the topcoat. One can also note that the growth of several oxides, which compose a thick TGO, provides thermal mismatch due to different coefficients of thermal expansion. This also contributes to weaken the adhesion of the topcoat in case of the special design.

Table VI-2 gathers the characteristics of the special design compared to the reference one for the understanding of the formation of the intermetallics, including the growth of a SRZ. One can note that the mechanisms of formation are rather different from the two systems even if the PARTICOAT concept is realized in both cases. As a matter of fact, the introduction of this electrodeposited layer at the surface of the Ni-based substrates imposes to take several others conditions to understand the overall interactions. The latter will be described in the next section.

Oxidation tests at 900°C in flowing synthetic air

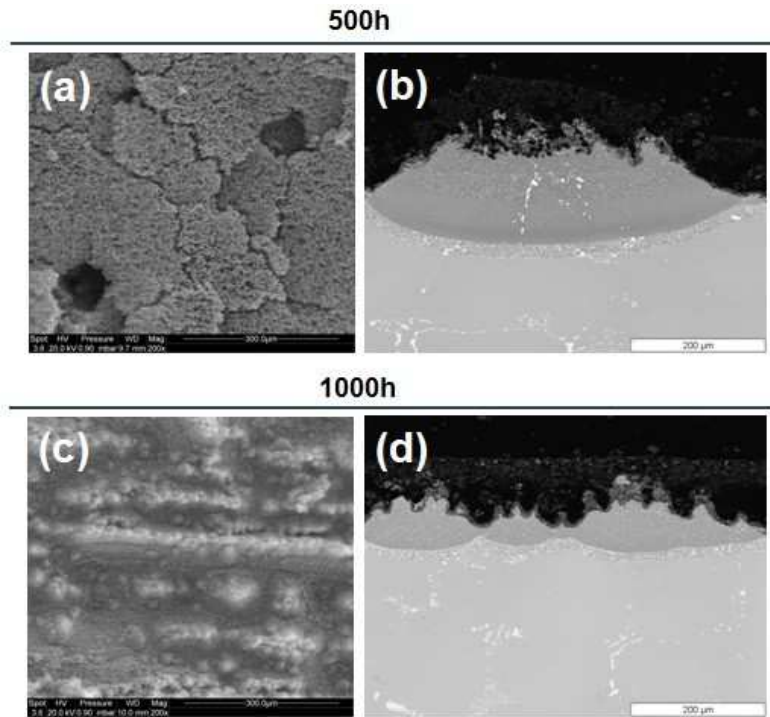


Figure VI-14 – Surface analyses and cross-sections investigation of CM 247LC, after 500h (a) and (b), and (c), respectively, and after 1000h (d) and (e), respectively.

Oxidation tests at 1000°C in flowing synthetic air

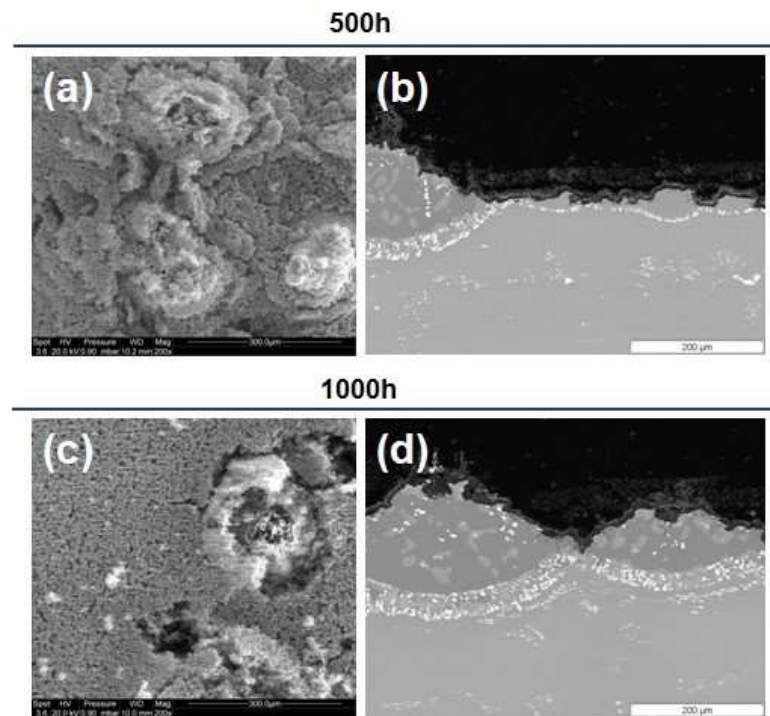


Figure VI-15 – Surface analyses and cross-sections investigation of CM 247LC oxidized at 1100°C in flowing synthetic air, after 500h (a) and (b), and (c), respectively, and after 1000h (d) and (e), respectively.

Table VI-2 – Characteristics of the two systems (reference and special design) and comparison of the properties regarding the thermal treatment defined for the PARTICOAT concept formation CM 247 LC.

	Coating system	
	PARTICOAT (reference)	CeO ₂ film + PARTICOAT (special design)
Matrix of the Al enriched layer at 700°C – 2h	Ni ₂ Al ₃	None
Matrix of the Al enriched layer at 1100°C – 2h	β-NiAl + precipitates	β-NiAl + precipitates
Topcoat behaviour	Adherent	Partially detached
Formation of the SRZ for high temperatures oxidation tests (900°C and 1100°C)	Yes, strongly dependent of the temperature (cf Chapter V)	None
Nature of the TGO	α-Al ₂ O ₃ + NiAl ₂ O ₄ + alloying element segregations	α-Al ₂ O ₃ + CeAlO ₃ + alloying element segregations

B. Considerations for the formation of the special design.

Two major differences can be underlined concerning the special design and the PARTICOAT reference one. The mechanisms of formation of the intermetallics are changed since the beginning of the thermal treatment while the behaviour regarding the high temperature oxidation tests is also conditioned by the proprietary interlayer and its partitioning in the system.

During the thermal treatment at 700°C, the aluminium contained in the microspheres dissolved a part of the substrate for the reference design, thus leading to the hollow microspheres structure. The introduction of the rare-earth overlay blocked this Al enrichment process, while higher temperatures led to the aluminizing of the substrate and the formation of the PARTICOAT concept. To explain this deviation, one has to re-consider the characteristics of the system.

Figure VI-16 presents the different interfaces to take into account for the reactivity of the two systems. The interface for the oxidation reaction between the gas phase and the Al microspheres has been simplified and positioned only as the “1st interface”. One has to note that the “real” interface should surround all the spheres over all the topcoat (i.e. we do not have a flat surface like in conventional bulk materials). *Table VI-3* presents the nature of these different interfaces, characterized before any thermal treatment application.

The PARTICOAT concept has two main interfaces at the beginning of the thermal treatment. The first is placed at the oxidizing gas phase / topcoat outer surface, while the second is defined by the inner surface of the topcoat / surface of the substrate. Comparatively, the special design has only the first interface (oxidizing gas phase / topcoat outer surface) in common with the PARTICOAT reference design. The second interface is defined by the surface of the Al microspheres / surface of the cerium oxide overlay coating, while the third one is composed by the overlay coating / surface of the substrate, as presented in *Table VI-3*.

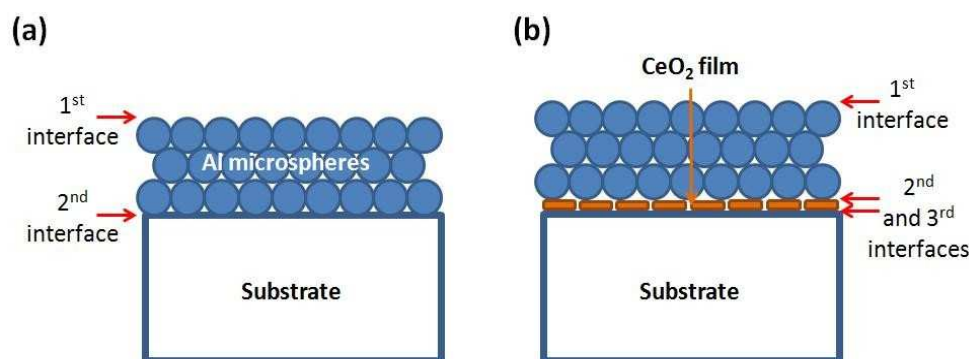


Figure VI-16- Summary of the positions of the interfaces for (a) the PARTICOAT systems and (b) the special design.

Table VI-3- Nature of the interfaces composing the PARTICOAT design compared to the special design.

	Coating system	
	PARTICOAT (reference)	CeO ₂ film + PARTICOAT (special design)
1 st interface	Gas phase / surface of the Al microspheres	Gas phase / surface of the Al microspheres
2 nd interface	Surface of the Al microspheres / surface of the substrate	Surface of the Al microspheres / surface of the rare-earth overlay coating
3 rd interface	None	Surface of the rare-earth overlay coating / surface of the substrate

From these interfaces, the formation of the PARTICOAT coatings is ruled by the driving force from the chemical potential between the amorphous / crystallized Al₂O₃ and / or Al with the Ni substrate (pure or alloyed). This parameter allows the chemical species to enhance the dissolution / diffusion processes regarding their respective interactions.

In case of the special design, the second interface is the place of reactions between the Al microspheres (metallic core + surrounding Al oxide) and with the cerium oxide based overlay coating. Several groups already investigated the possible reactions between the cerium oxides (CeO₂ and Ce₂O₃) with alumina, i.e. γ -Al₂O₃ and α -Al₂O₃, to form cerium aluminium oxides [28-29]. Prakash *et al.* [30] already shown the possibility to take advantage of the oxygen storage capacity (OSC) of the cerium oxides [31], when oxidizing CeO₂ and γ' -Al₂O₃, to form CeAlO₃ [30]. Due to this OSC, such cerium based component allows to enhance the high temperature oxidation resistance behaviour of the Ni-based alloys [11-13]. They concluded that the formation of the CeAlO₃ compound at the alumina / ceria interface by solid state reaction which might be responsible of an enhanced adherence of the scales. Nevertheless, additional reaction between Ce and Al, i.e. CeAl₂, might contribute to weaken the integrity of the oxide scales due to coefficient of thermal expansion.

Similarly to the reaction with aluminium, the ceria film can also react with the Ni γ / γ' matrix of the substrate but also with the alloying elements, i.e. Cr, Ti, *etc.* Czerwinski *et al.* [32] studied a sol-gel deposit of ceria (CeO₂) incorporated into growing native oxide when deposited on pure Ni, pure Cr, and INCO 600 (Ni-based alloy, 14-16 wt.% Cr, 6-10 wt.% Fe) and oxidized these samples up to 900°C. They only mentioned the reduced oxidation kinetics as also observed by several groups when depositing a RE_xO_y coating on the substrate [11-12;33-34]. Nevertheless, a reaction between the Ni and / or Cr elements with the rare-earth oxide compound has not been mentioned in their studies. Maosheng *et al.* [35] mentioned the possibility to form the CeTi₂O₆ phases when synthesizing titanium doped ceria powders. As a matter of fact, the TGO developed during the present high temperature study may involve more than the CeO₂ and α -Al₂O₃ reaction and the overall alloying elements present in the initial chemistry of the base alloy should be therefore considered.

After the complete thermal treatment ($400^{\circ}\text{C} - 1\text{h} + 700^{\circ}\text{C} - 2\text{h} + 1100^{\circ}\text{C} - 2\text{h}$), the cerium based film is localized at two positions: the TGO / bond coat interface and the bond coat / $\gamma - \gamma'$ matrix of the substrate one, as shown by *Figure VI-17*. Those two positions greatly affect the behaviour at high temperature.

The first interface allow the Ce to react with Al and / or alloying elements to form several type of perovskite compound [28-29;35], while some eventually un-reacted CeO_{2-x} component may trap oxygen [30-31] unconsumed by the selective oxidation at the topcoat and / or TGO layers.

The second position of the cerium based film constitutes a selective diffusion barrier, as shown by *Figure VI-13*. As an example, Cr did not segregate at this position, but partially diffused in the additive layer as suggested by the chemical contrast of its X-ray mapping (*Figure VI-13*). This allowed to avoid the formation of a SRZ during long term high temperature experiments, the latter being promoted by the behaviour of this element [36].

Between these two positions, ceria seems to be homogeneously dispersed in the $\beta\text{-NiAl}$ additive layer (*Figure VI-13*) and may therefore provide an oxide dispersion effect (ODS) [37-38]. Nevertheless, more precise investigations should be planned to fully investigate this partitioning.

From these observations, the ceria-based interlayer can be considered as a potential technical solution to avoid the growth of the secondary reaction zone once the homogeneity of the coating is constant, thereby enhancing the high temperature resistance (mechanical and oxidation) of the Ni-based superalloys. Nevertheless, complementary tests should be done whether considering more accurate investigations (EPMA and micro-XRD spot analyses) or mechanical tests (4 point bend testing, creep and thermal cyclic oxidation tests).

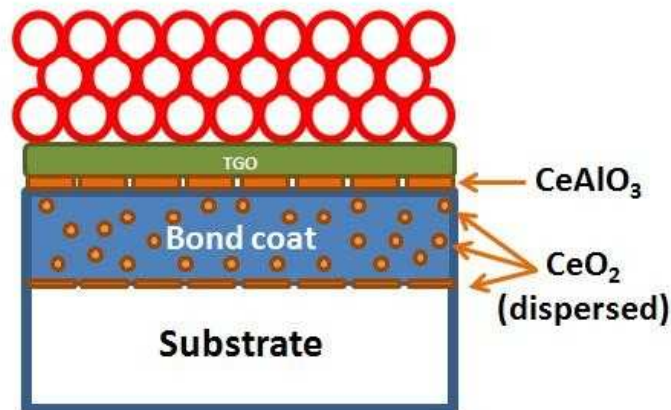


Figure VI-17 – Summary of the positions of the interfaces for high temperature oxidation experiments.

Summary and outlook

The electrodeposition of a ceria film has been used to perform a special design based on the PARTICOAT concept. As a result, a similar microstructure was formed with an α - Al_2O_3 hollow spheres topcoat developed over a thermally grown oxide (TGO) and a β -NiAl additive layer. Nevertheless, the nature of the TGO differs for both systems, as well as their behaviours regarding high temperature oxidation experiments.

The mechanisms of formation of the intermetallics have been changed by the addition of this rare-earth overlay coating. The number of interfaces being increased, the chemical reactions between the Al microspheres and the ceria based coating and of this ceria coating with the substrate, induce a modification of the initiation of the Al enrichment temperature. Compared to the reference design, the Al enrichment has not been observed at 700°C after 2h of isothermal duration, while the increase of the temperature to 1100°C finally activates the dissolution / diffusion processes to complete the special design. In addition, the formation of a mixed oxide compound has been detected from the solid state reaction between Al_2O_3 and CeO_2 to form CeAlO_3 perovskite component. One of the major observations is the non-homogeneous additive layer, probably because the blocking of CeAlO_3 . As a matter of fact, the design of the ceria based interlayer can be modified whether by considering its thickness or its cracking to promote optimum aluminizing conditions as well as an enhance portioning of this element in the additive layer for improving the behaviour of the system regarding the service conditions.

High temperature oxidation experiments have been realized at 900 and 1100°C to investigate the potential of such system for the two extreme temperatures investigated during the characterization of the “simple” PARTICOAT design.

The α - Al_2O_3 topcoat detached from the TGO, while the growth of a secondary reaction zone has not been observed up to 1000h of experiments. The two observations occurred for both experiments at the two temperatures. The development of a thick thermally grown oxide, containing CeAlO_3 , may contribute to fragilize the adhesion of the topcoat, probably due to coefficient of thermal expansion mismatch. The reactivity of the rare-earth oxide film with the alloying elements, but also its positioning during the thermal treatment and high temperature oxidation experiments should also be investigated more accurately by the use of EPMA measurements added to micro-XRD spot analyses to obtain information on the phases formed with time and temperature, while four point bending tests should be planned to observe the influence of such film on the mechanical properties of the TGO impaired with the design of the interlayer (thickness, cracking). Thermal and creep cyclic oxidation tests should be also planned to investigate the influence of the proprietary interlayer on the mechanical resistance of the system, which should be reinforce with the non-formation of the TCP at the SRZ.

Further modifications of the electrodeposition process can be therefore planed to reduce / prevent the reaction between CeO_2 and Al_2O_3 at high temperature. Recently, lanthanum oxide has been found to combine with both compounds, but also by preserving them from their mutual interactions, which should allow to provide a synergistic effect regarding the high temperature behaviour of such type of coating.

Based only on the initial special design (ceria based layer + PARTICOAT), a further study should lead to the tailoring of the latter, in agreement with appropriate thermodynamic calculations using reliable databases. The Al-O-Ce, Al-O- CeO_2 and Al-O- Ce_2O_3 ternary phase diagrams should support the onset of this future tailoring of this special design and give information on the PARTICOAT deposit added to the rare-earth oxide overlay. In the same feature, the Al-Ni- CeO_2 and Al- Al_2O_3 - CeO_2

ternary phase diagrams will give information for the formation of the CeAlO_3 perovskite compound and lead to possible solutions to reinforce the adhesion of the topcoat.

References

- [1] T. Izumi, N. Mu, L. Zhang, B. Gleeson, *Surface and Coatings Technology* 202 (2007) 628
- [2] J. Müller, M. Shierling, E. Zimmermann, D. Neuschütz, *Surface and Coatings Technology* 120-12 (1999) 1
- [3] J.A. Haynes, Y. Zhang, K.M. Cooley, L. Walker, K.S. Reeves, B.A. Pint, *Surface and Coatings Technology* 188-189 (2004) 153
- [4] T. Narita, F. Lang, K.Z. Thosin, T. Yoshioka, T. Izumi, H. Yakuwa, S. Hayashi, *Oxidation of Metals* 68 (2007) 343
- [5] E. Cavaletti, S. Naveos, S. Mercier, P. Josso, M.P. Bacos, D. Monceau, *Surface and Coatings Technology* 204 (2009) 761
- [6] Y. Wang, H. Guo, H. Peng, L. Peng, S. Gong, *Intermetallics* 19 (2011) 191
- [7] B. Bouchaud, *Electrosynthèse de nouveaux revêtements à base d'élément de terres rares destinés à accroître la durabilité à hautes températures des matériaux des turbines*, PhD Thesis
- [8] F. Pedraza, B. Bouchaud, J. Balmain, G. Bonnet, J. Menuet, Patent WO 2011/012818 A1
- [9] F. Pedraza, B. Bouchaud, J. Balmain, G. Bonnet, J. Menuet, Patent WO 2011/012819 A1
- [10] REACH report, Official Journal of the European Union (2006) EC. No 1907/2006
- [11] F. Pedraza, B. Bouchaud, J. Balmain, G. Bonnet, J. Menuet, *Materials Science Forum* 696 (2011) 278
- [12] F. Pedraza, B. Bouchaud, J. Balmain, G. Bonnet, V. Kolarik, J. Menuet, *Materials Science Forum* 696 (2011) 284
- [13] F. Pedraza, B. Bouchaud, J. Balmain, G. Bonnet, J. Menuet, *Materials Science Forum* 696 (2011) 336
- [14] W. Martienssen, H. Warlimont, *Handbook of Condensed Matter and Materials Data* (2005) Springer]
- [15] X.Q. Cao, R. Vassen, D. Stoeber, *Journal of the European Ceramic Society* 24 (2004) 1
- [16] B.M. Reddy, A. Khan, Y. Yamada, T. Kobayashi, S. Loidant, J.C. Volta, *Journal and Physics and Chemistry B107* (2003) 475
- [17] I. Kosacki, T. Suzuki, H.U. Anderson, P. Colomban, *Solid State Ionics* 149 (2002) 99
- [18] J.E. Spanier, R.D. Robinson, F. Zhang, S.W. Chan, I.P. Herman, *Physical Review B64* (2001) 245
- [19] Y. Hamlaoui, F. Pedraza, L. Tifouti, *Corrosion Science* 50 (2008) 2182
- [20] Y. Hamlaoui, F. Pedraza, C. Remazeilles, S. Cohendoz, C. Rébéré, L. Tifouti, J. Creus, *Materials Chemistry and Physics* 113 (2009) 650
- [21] L. Martinez, E. Roman, J.L. de Segovia, S. Poupard, J. Creus, F. Pedraza, *Applied Surface Science* 257 (2011) 6202

- [22] M.I. Canac, M.I. de Barros Marques, M.A. Marques, A.M. Gaspar, M.L. de Almeida, *Journal of Molecular Liquids* 117 (2005) 69
- [23] M.K. Marchewka, A. Pietraszko, *Journal of Physics Chemistry of Solids* 66 (2005) 1039
- [24] M.C. Hales, R.L. Frost, *Polyhedron* 26 (2007) 4955
- [25] B. Rannou, M. Mollard, B. Bouchaud, J. Balmain, G. Bonnet, V. Kolarik, F. Pedraza, *Defect and Diffusion Forum* 323-325 (2012) 373
- [26] F. Pedraza, M. Mollard, B. Rannou, J. Balmain, B. Bouchaud, G. Bonnet, *Materials Chemistry and Physics* 134 (2012) 700
- [27] C.M.F. Rae, M.S. Hook, R.C. Reed, *Materials Science and Engineering A* 396 (2005) 231
- [28] R.L. Putnam, A. Navrotsky, E.H.P. Cordfunke, M.E. Huntelaar, *Journal of Chemical Thermodynamics* 32 (2000)911
- [29] A.I. Leonov, E.K. Keler, *Inorganic and Analytical Chemistry* (1962) 1819
- [30] A.S. Prakash, C. Shivakumara, M.S. Hegde, *Materials Science and Engineering B* 139 (2007) 55
- [31] O.A. Bereketidou, M.A. Goula, *Catalyst Toda* (2012)
<http://dx.doi.org/10.1016/j.cattod.2012.07.006>
- [32] F. Czerwinski, J.A. Szpunar, *Journal of Sol-Gel Science and Technology* 9 (1997) 103
- [33] H. Lui, W. Chen, *Corrosion Science* 49 (2007) 3453
- [34] Y. Zhou, X. Peng, F. Wang, *Scripta Materialia* 55 (2006) 1039
- [35] F. Maosheng; W. Lianghua, L. Yanhua, Z. Xuezhen, H. Shiyu, L. Yongxiu, *Solid State Sciences* 11 (2009) 2133
- [36] M.S.A. Karunaratne, C.M.F. Rae, R.C. Reed, *Metallurgical and Materials Transactions A* 32 (2011) 2409
- [37] R. Bianco, R.A. Rapp, *Journal of Electrochemical Society* 140 (1993) 1181
- [38] B.A. Pint, M. Treska, L.W. Hobbs, *Oxidation of Metals* 47 (1997) 1

Conclusions & Outlook

This following manuscript aimed at introducing a part of the investigation realized within the framework of the PARTICOAT European project (FP7-NMP-2007-LARGE-1-CP-IP-211329-2). In this view, the Al microspheres containing slurry has been characterized as well as its feasibility for the aluminizing purpose and finally, its efficiency for high temperature oxidation phenomenon has been compared to conventional systems (SVPA). For this to happen two types of model alloys have been used (pure Ni and Ni20Cr), while four Ni-based superalloys (René N5 (SX), CM 247 LC (DS), PWA 1483 (SX), INCO 738 (EQ)) allowed to perform a screening regarding the specification of the chemistries of the materials, as well as their structure (single crystal: SX, directionally solidified: DS, equiaxed: EQ). In addition, a special design of diffusion barrier has been investigated, through the electrolytic deposition of a proprietary reactive element oxides diffusion barrier previously patented in the LaSIE laboratory.

A first approach has been done focusing on the characterization of the slurry, to qualify its physico-chemical properties. Various compositions of this water based binder have been investigated. For each composition, a set of experiments have been done to investigate the physico-chemical properties of the PARTICOAT slurry. Those characterization processes have been done over nine days of ageing to observe the evolution of the slurry with time, except for the drying process, which has been investigated only for as-prepared solutions. The slurries were found to be stable except for the higher content aluminium one, which solidified after seven days of ageing.

This global set of experiments allowed to choose the chemical composition of the slurry (45 wt.% of Al) to investigate the PARTICOAT concept. Nevertheless, further optimizations of this set of characterization as well as of the slurry can be planned. FTIR measurement experimentations have to be modified to investigate the evolution of the Al oxyhydroxydes compounds, which investigations should be possible by the use of vacuum or high temperature FTIR module. The addition of a dispersant will have to be considered in order to control the partitioning of the particles in the slurry, especially by considering their size and the viscosity of the binder. The use of additives such as the temperature depressants, i.e. silicon, or more complex Si based compounds, which can form alumino-silicates, will have to be investigated to observe their effect on the PARTICOAT concept. In a similar view, the interactions of the Al microspheres with oxide particles (MgO, CeO₂) may be tailored and characterized by a comparable set of experiments. High temperature DSC measurements have also to be planned to compare the effect of different atmospheres, i.e. in argon, argon-hydrogen (5%), nitrogen, air, on the behaviour of the aluminium particles, whether simple PARTICOAT slurry or modified one with additional loads.

Once the slurry has been characterized, a second part of the present study has been focused on the investigation of the PARTICOAT concept (α -Al₂O₃ quasi foam topcoat structure formed over a β -NiAl coating) and its reactivity with a thermal treatment. For this to happen, two model alloys (pure Ni and Ni20Cr) have been used, in a first time, to study the mechanisms and limitations of the manufacturing process for the formation of the PARTICOAT design.

Pure Ni coupons allowed to tailor the following thermal treatment to realize this concept: 400°C – 1h + 700°C – 2h + 1100°C – 2h under Ar(g) flowing atmosphere, with a 5°C.min⁻¹ and 50°C.min⁻¹ for the heating and cooling ramps, respectively. As opposed to this successful process, Ni20Cr(1.5Si) model alloy showed a limitation for this aluminizing slurry composition. The formation of Al_xCr_y compounds have been observed, which hindered the Al enrichment of the substrates with this chemical composition, while brittle phases led to the detachment of the topcoat during the quenching from

high temperature. From this issue, a modification of the chemistry of the binder has to be investigated to optimize its versatility with high Cr containing alloys, i.e. by tailoring the activity of the particles.

The extrapolation of the PARTICOAT concept to four Ni-based superalloys (René N5, CM 247 LC, PWA 1483, INCO 738) has been successfully realized. Their respective complex chemistries but also their respective crystal structures (SX, DS, EQ), led to a coating comparable to the one observed for conventional Al pack cemented one formed with low temperature / high activity process followed by an annealing treatment at high temperature.

From these PARTICOATED materials, the oxidation resistances at high temperature have been studied, in a third part, using appropriate temperatures (900 and / or 1000 and / or 1100°C) regarding the specifications of each Ni-based material. The effect of the PARTICOAT aluminizing slurry has been characterized by the evolutions of the topcoats, thermally grown oxide zones (TGO) and bond coats of the substrates.

The topcoat has been found adherent for all the samples, except at their edge and in case of CM 247 LC at 1100°C. In order to characterize this specific ceramic structure and its adhesion with the substrate, Mollard investigated the behaviour of such system through high temperature cyclic oxidation experiments at the LaSIE laboratory.

Despite this, it has been shown that advanced investigations have to be done to estimate the “active” surface for the calculation of the oxidation kinetics of the samples, which are extrapolated from the $(\Delta M/S)^2$ values. The real surface, which rules the oxidation mechanisms, is complex to determine due to the tortuosity of the quasi foam structure. BET analyses may be useful to determine this surface. Nevertheless, a statistical approach should be used to determine also the standard deviation of the surface of this hollow microspheres topcoat. In addition, the behaviour of the ceramic hollow structure has also to be characterized in view of investigating any lotus or sacrificial effect considering the α -Al₂O₃ topcoat and its protective properties against such corrosive agent. For this purpose, several type of components have to be tested at room temperature, i.e. water, diodomethane, while the influence of the temperature has also to be investigated by using molten salt, i.e. a mixture of Na₂SO₄ and V₂O₅.

The adhesion of the topcoat has been shown impaired with the chemistry of the alloys and the behaviour of the alloying elements at the TGO position. The formation of the coating gave an equiaxed additive layer with numerous grain boundaries through which the alloying elements can diffuse and segregate. In addition, the longer the oxidation, the more Ni diffuses outwardly leading to the β -NiAl \rightarrow γ' -Ni₃Al transformation, which is significant of the loss of the oxidation resistance property. This phase modification is also responsible of the heavy element outward diffusion due to the modification of their respective solubilities in the Ni_xAl_y phases. The overall interdiffusion of the chemical elements of the superalloys, as well as of the coating, led to the formation of TCPs at the SRZ position. These phases are known to be responsible of the embrittlement of the system during high temperature exposure. Therefore, the investigation of an interdiffusion barrier has been designed.

From these two parts dedicated to the experimental observations of the PARTICOAT coating system, whether for the thermal treatment or the high temperature oxidation experiments, modelization outlooks can be planned. As a first approach, the global system has to be simplified and separated in different sub-systems. The thermal treatment and the high temperature modelling will have to be realized separately.

Considering the complete system (slurry deposit onto raw material), several points of view can be investigated. The transformation of the aluminium microspheres into $\alpha\text{-Al}_2\text{O}_3$ one can be modelled, while the formation of the coating ($\beta\text{-NiAl}$ additive layer) will have to be considered separately.

For the latter, the Al quantity initially present in the topcoat has to be converted in an equivalent Al content to provide the aluminium reservoir for the enrichment of the substrate, as represented by *Figure 1*. For this to happen, the notion of compacity of the topcoat will have to be introduced, and extrapolated from the crystallographic approach in a first time. This value should be estimated between 46% and 74% from the atomic organisation of the cubic structured and the diamond one, but also presuming that the partitioning of the topcoat is “ordered” and homogeneous (shape of the load, particle size, size dispersion...).

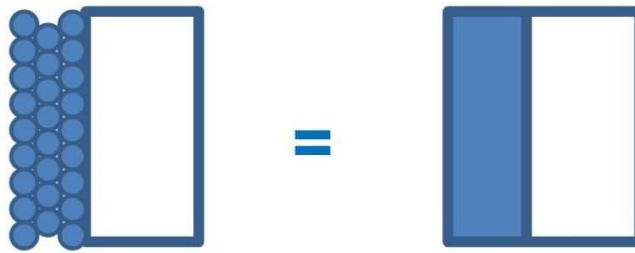


Figure 1 – Conversion of the initial Al content contained in the microsphere as a bulk equivalent.

In addition, this first approach should be focused only on simple material in a first time, basically pure Ni, while the alloying elements will have to be carefully introduced one by one to optimize the modelling parameters to fit the experimentally obtained EDS profiles. For this modelling purpose, the DICTRA® software has been recently acquired by the LaSIE laboratory and should be used carefully to carry out this theoretical approach. Nevertheless, one has to keep in mind that all the results obtained by this approach are strongly dependent of the reliability of the databases used with this type of software. As a first result of these modelling explanations, *Figure 2* gives experimental and theoretical fit for the high temperature oxidation of pure Ni PARTICOATED at 1100°C for 100, 250 and 500h.

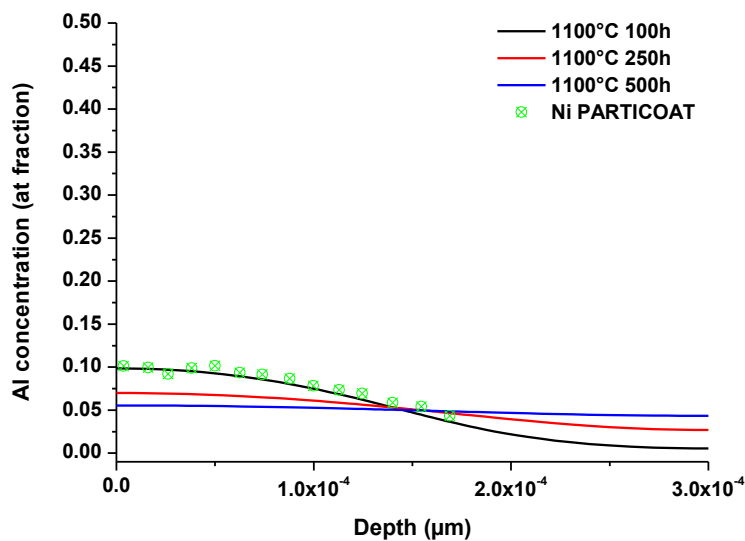


Figure 2 – EDS profile of pure Ni PARTICOATED oxidized at 1100°C for 100h and DICTRA® modeling for 100, 250 and 500h using the TTNi8 database.

From this first diffusion approach, more complex ones will have to be planned, i.e. to allow the modelling of oxide scale growth, precipitation behaviour and influence of the grain boundaries. In this view, several possibilities exist, which can be based on the use of the already acquired at the LaSIE laboratory Thermocalc and DICTRA databases. An other option is to create the databases by realizing thermodynamic calculations and kinetic measurements aimed at the systems of interests for the future investigations of the laboratory.

The commercial TC Prisma software may allow to model the precipitation behaviour of the alloying elements in the coating during the thermal treatment but also during the long term isothermal oxidation, while more complex programming interfaces can also be investigated comparatively to the one developed by the CEA with the EKINOX code. Commercial softwares such Matlab, Systus or Comsol can allow these type of designing of the alloy structure by programming single crystal, directionally solidified or equiaxed structure, as shown by *Figure 3*, i.e. to investigate the influence of grain boundaries (size, geometry, type, low / high angle, triple junction...).

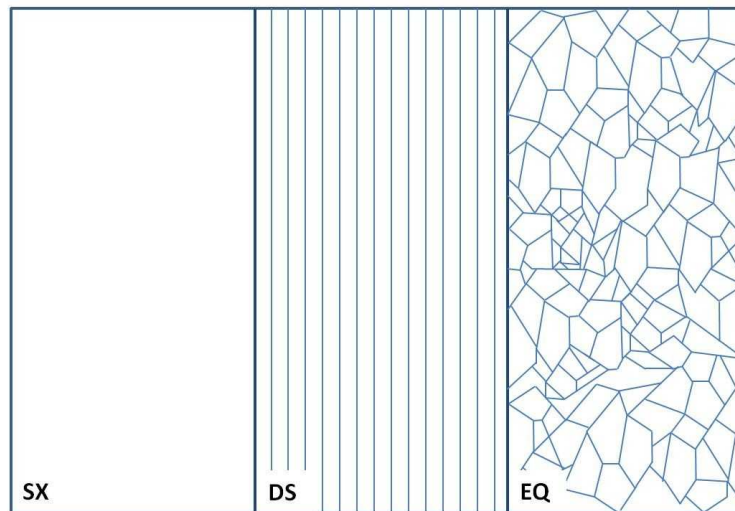


Figure 3 – Alloy structures to take in consideration for modeling purposes to monitor the grain boundaries effect.

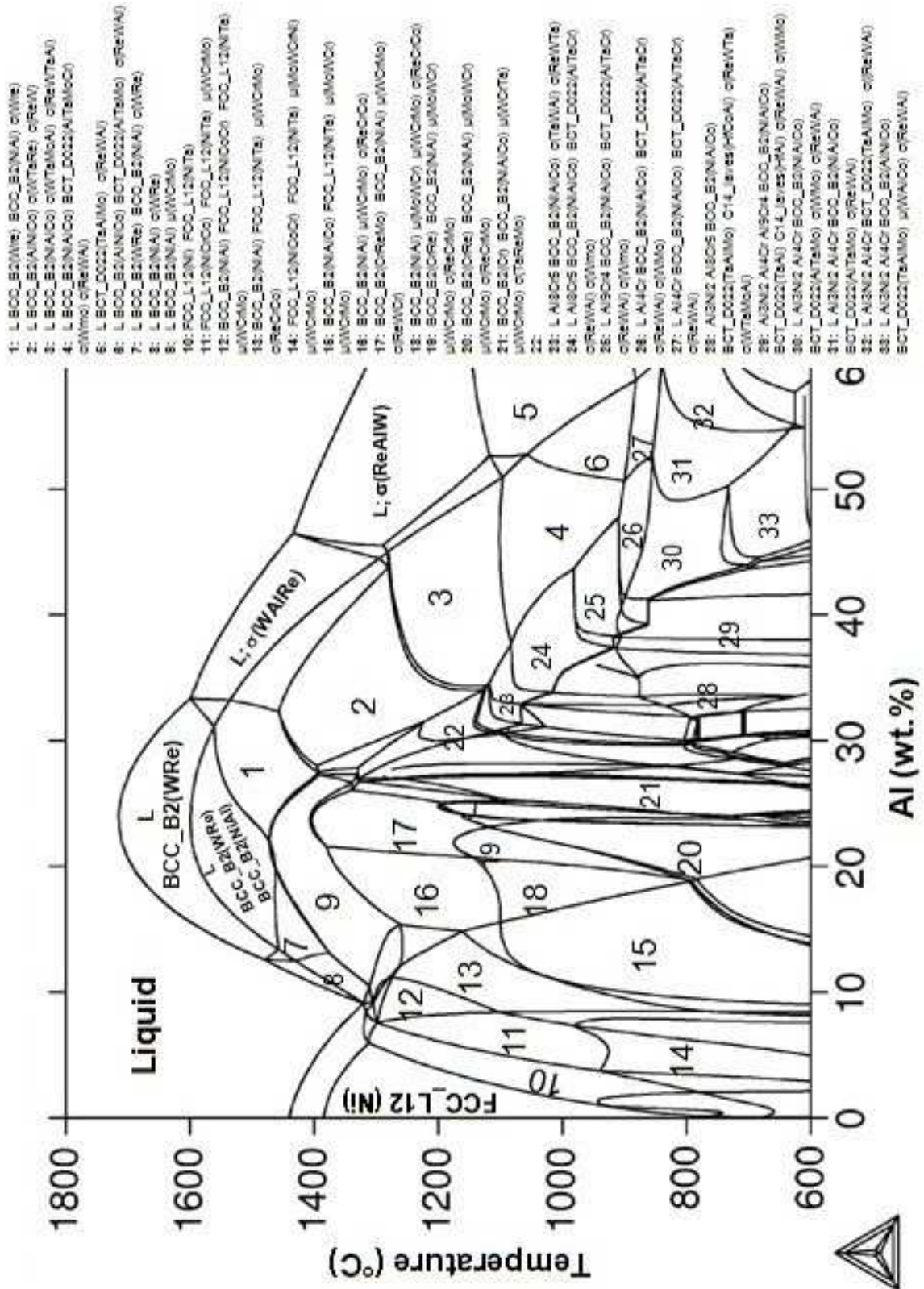
Finally, one part of the present study has been dedicated to the investigation of a special design using a rare-earth oxide-based diffusion barrier to limit the degradation mechanisms by interdiffusion processes. The use of a ceria-based interlayer applied onto substrate before the PARTICOAT deposition has been realized and thermally treated with the thermal treatment define for the “simple” PARTICOAT design. As a result, the initial concept (α -Al₂O₃ hollow spheres topcoat TGO and β -NiAl additive layer) has been formed. The formation of the TCPs at the secondary reaction has been avoided during the high temperature oxidation experiments up to 1000h at 1100°C. In addition, this technical solution to limit the interdiffusion processes has been found to segregate as a film at the additive layer / interdiffusion zone interface and at the TGO position, which has been found to grow excessively by the reaction of ceria and other chemical components, i.e. α -alumina. The Ce partitioning in the β -NiAl additive layer has also been observed by X-ray mapping.

From these observations, a lot of outlooks emerged. First, a screening has to be done in order to find the optimal design of such interlayer, whether dealing of its thickness or its cracked network. Second, an investigation of the partitioning of the ceria-based film has to be investigated in a more accurate way. Model substrates will have to be used to understand all the mechanisms impaired with the presence of certain alloying elements in restrain inward and / or outward diffusion processes. The cerium element state will also have to be more defined whether as an oxide or as a metallic element.

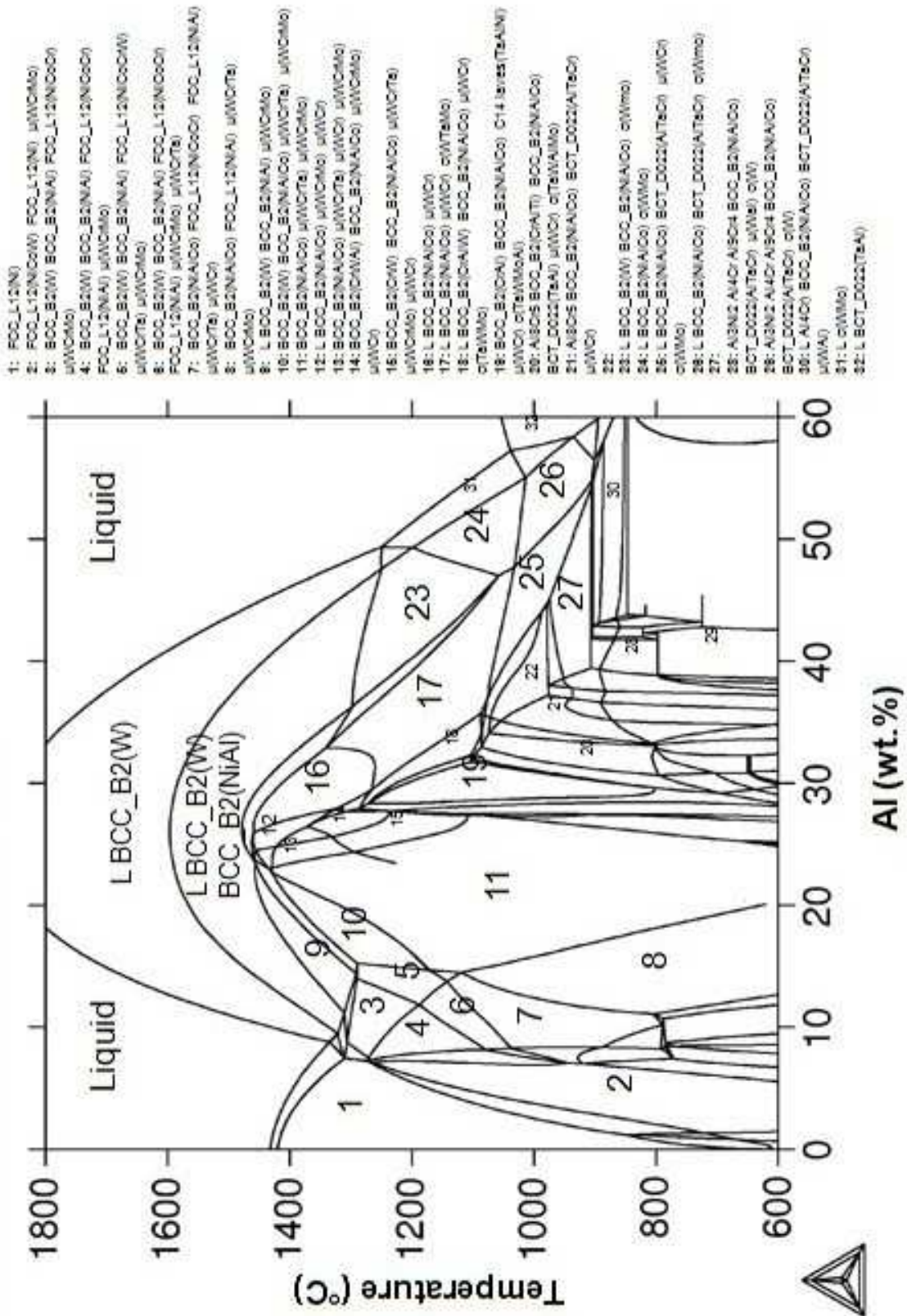
This will allow to provide useful information for the reactive element theory and their effect depending of the manufacturing process.

In addition of these experimental outlooks, appropriate techniques of characterization can be therefore considered. High temperature DSC measurements can provide information on the reactivity of these compounds, while TEM and or SIMS analyses should give some clues of the partitioning of the cerium compounds. Mechanical tests should also be planned to confirm or infirm the effect of non-formation of the SRZ, and its influence on the mechanical properties of such a special design.

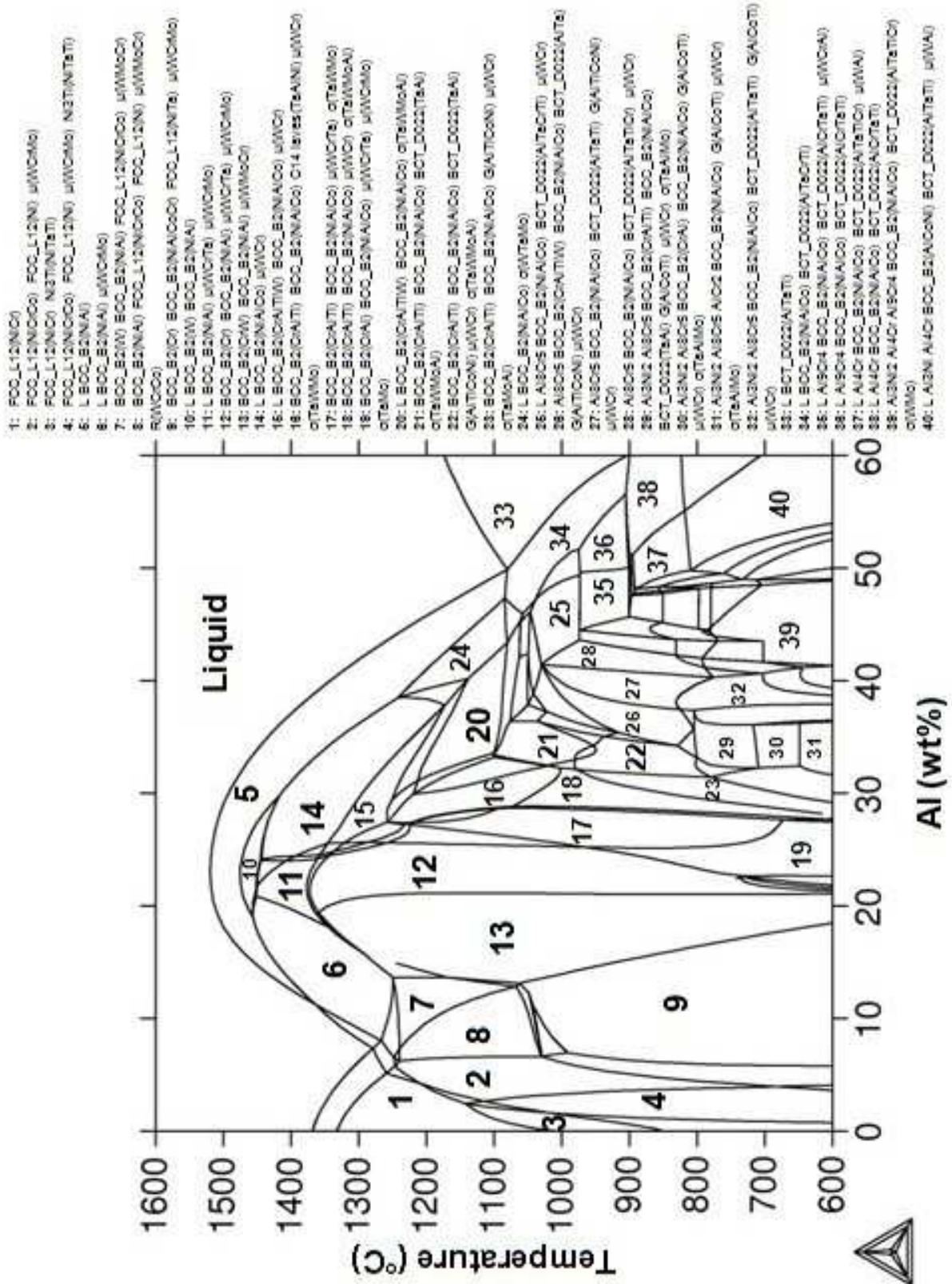
Annexes



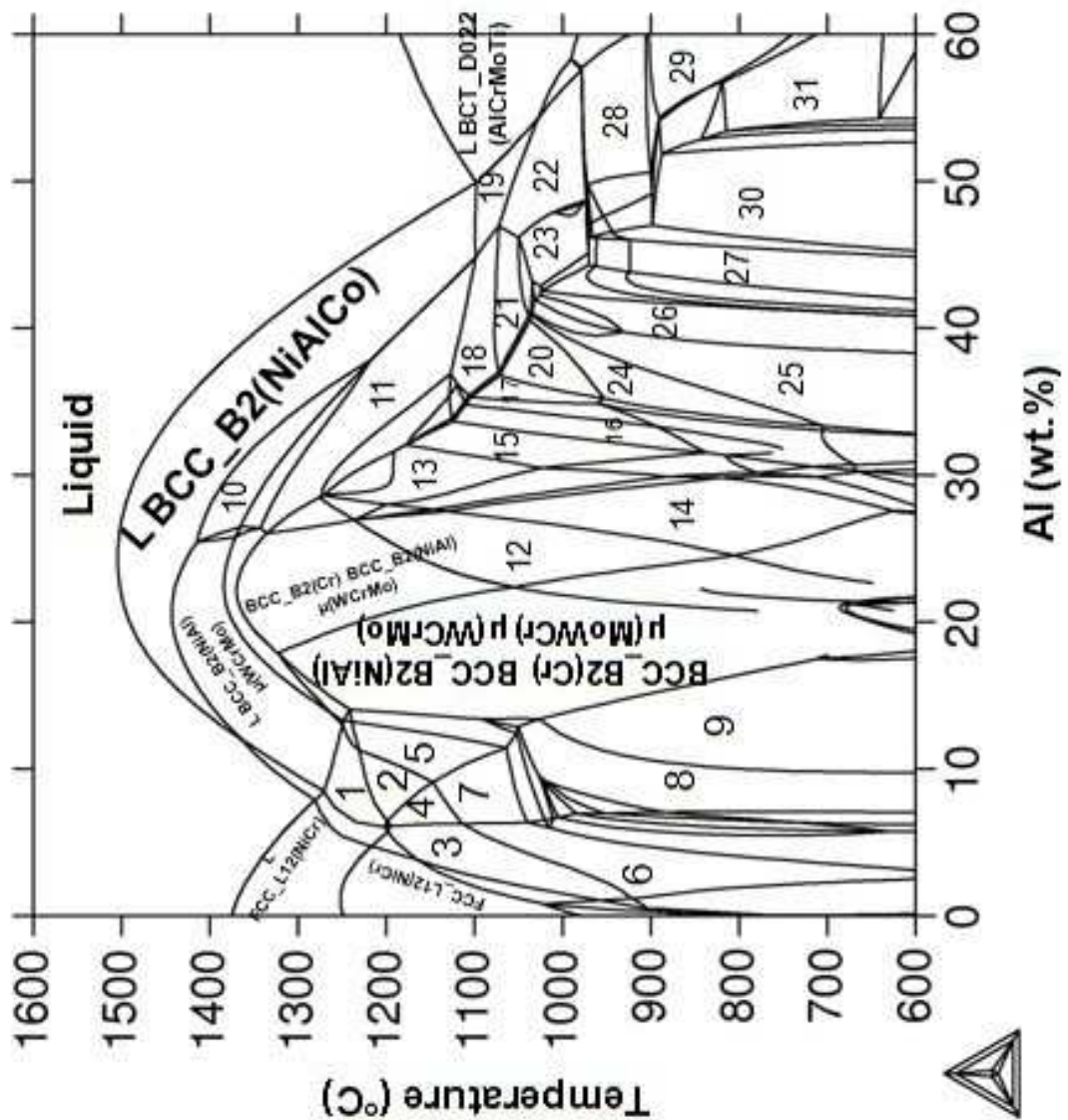
Isopleth of René N5 modelled with TCNI5 database, taking into account the Al_xCr_y compounds.



Isopleth of CM 247 modelled with TCNi5 database, taking into account the Al_xCr_y compounds.



Isopleth of PWA 1483 modelled with TCNi5 database, taking into account the Al₃Cr^y compounds.



- 1: L BCC_B2(NiAl) FCC_L12(NiCrCo)
- 2: BCC_B2(NiAl) FCC_L12(NiCrCo) μ(WCrCo)
- 3: FCC_L12(NiCrCo) FCC_L12(Ni) μ(WCrMo)
- 4: BCC_B2(NiAl) FCC_L12(NiCrCo) FCC_L12(Ni) μ(WCrMo)
- 5: BCC_B2(NiAl) FCC_L12(NiCrCo) μ(WCrMo) μ(WCrCo)
- 6: FCC_L12(NiCrCo) FCC_L12(Ni) μ(WCrMo) μ(WCrCo)
- 7: BCC_B2(NiAl) FCC_L12(NiCrCo) FCC_L12(Ni) μ(WCrMo) μ(WCrCo)
- 8: BCC_B2(Cr) BCC_B2(NiAlCo) FCC_L12(Ni) μ(WCrMo) μ(WCrCo) μ(WCrCo)
- 9: BCC_B2(Cr) BCC_B2(NiAlCo) μ(WCrMo) μ(WCrCo)
- 10: L BCC_B2(NiAlCo) μ(WCrCo)
- 11: L BCC_B2(Cr) BCC_B2(NiAlCo) μ(WCrCo) μ(WCrCo) C14
- 12: BCC_B2(Cr) BCC_B2(NiAlCo) μ(WCrCo) μ(WCrCo) C14
- 13: BCC_B2(Cr) BCC_B2(NiAlCo) C14
- 14: BCC_B2(Cr) BCC_B2(NiAlCo) μ(WCrCo) μ(WCrCo) C14
- 15: BCC_B2(Cr) BCC_B2(NiAlCo) μ(WCrCo) μ(WCrCo) C14
- 16: BCC_B2(Cr) BCC_B2(NiAlCo) μ(WCrCo) μ(WCrCo) C14
- 17: BCC_B2(Cr) BCC_B2(NiAlCo) μ(WCrCo) μ(WCrCo) C14
- 18: BCC_B2(Cr) BCC_B2(NiAlCo) μ(WCrCo) μ(WCrCo) C14
- 19: BCC_B2(Cr) BCC_B2(NiAlCo) μ(WCrCo) μ(WCrCo) C14
- 20: BCC_B2(Cr) BCC_B2(NiAlCo) μ(WCrCo) μ(WCrCo) C14
- 21: L BCC_B2(NiAlCo) BCC_B2(NiAlCo) μ(WCrCo) μ(WCrCo) C14
- 22: L BCC_B2(NiAlCo) BCC_B2(NiAlCo) μ(WCrCo) μ(WCrCo) C14
- 23: L BCC_B2(NiAlCo) BCC_B2(NiAlCo) μ(WCrCo) μ(WCrCo) C14
- 24: L BCC_B2(NiAlCo) BCC_B2(NiAlCo) μ(WCrCo) μ(WCrCo) C14
- 25: L BCC_B2(NiAlCo) BCC_B2(NiAlCo) μ(WCrCo) μ(WCrCo) C14
- 26: L BCC_B2(NiAlCo) BCC_B2(NiAlCo) μ(WCrCo) μ(WCrCo) C14
- 27: L BCC_B2(NiAlCo) BCC_B2(NiAlCo) μ(WCrCo) μ(WCrCo) C14
- 28: L BCC_B2(NiAlCo) BCC_B2(NiAlCo) μ(WCrCo) μ(WCrCo) C14
- 29: L BCC_B2(NiAlCo) BCC_B2(NiAlCo) μ(WCrCo) μ(WCrCo) C14
- 30: L BCC_B2(NiAlCo) BCC_B2(NiAlCo) μ(WCrCo) μ(WCrCo) C14
- 31: L BCC_B2(NiAlCo) BCC_B2(NiAlCo) μ(WCrCo) μ(WCrCo) C14

Isopleth of INCO 738 modelled with TCNi5 database, taking into account the Al_xCr_y compounds.

Résumé français

L'utilisation de matériaux métalliques intervient dans de très nombreux domaines. En fonction des conditions de mise en œuvre, ceux-ci peuvent subir de nombreux phénomènes de dégradation. Une des préoccupations de l'industrie est donc de limiter les coûts associés aux processus d'entretien et de remplacement des assemblages défectueux.

Dans le cas des machines thermiques ou des installations travaillant à température élevée, les conditions de services imposées - températures jusqu'à 1500°C, présence d'espèces chimiques agressives (O_2 , SO_2 , H_2O ...) - conduisent à une forte augmentation des vitesses des réactions d'oxydation et des processus de dégradation. Dans de telles conditions, la résistance des matériaux repose en général sur la formation et la croissance à leur surface d'une couche d'oxyde protectrice. Cette dernière agit comme barrière à la diffusion à l'état solide des espèces réactives. Pour être efficace, cette couche d'oxyde doit être thermodynamiquement stable, homogène, adhérente et sa vitesse de croissance doit être faible. Les oxydes les plus fréquemment rencontrés sont alors la chromine (Cr_2O_3) et l'alumine (Al_2O_3).

Les alliages employés sont à base de fer, cobalt ou nickel, auxquels on ajoute les éléments plus oxydables chrome et l'aluminium, à des teneurs suffisantes pour promouvoir, lors de l'oxydation, la croissance externe d'une couche protectrice de Cr_2O_3 ou Al_2O_3 . Dans le cas de la chromine, la température d'utilisation est cependant limitée aux alentours de 950°C en raison de la volatilisation d'espèces chromées.

Dans le cas particulier des turbines aéronautiques et terrestres, les pièces des sections les plus chaudes sont constituées de superalliages à base nickel, en raison de leurs excellentes propriétés mécaniques à haute température. Afin d'optimiser ces dernières, il s'est avéré nécessaire de réduire la teneur en aluminium, au détriment des capacités de résistance à l'oxydation. Différentes solutions techniques ont donc été recherchées pour pallier à ce problème. La première consiste à élaborer, par des techniques de type CVD, un revêtement de diffusion destiné à enrichir la proche surface des substrats en Al (formation d'aluminure de nickel). Une autre solution repose sur l'utilisation de dépôts de type « overlay », notamment de composition MCrAlY (M = Fe, Co, Ni), souvent appliqués par pulvérisation. Ces deux types de revêtements peuvent a priori être employés pour les turbines hautes pressions ou basses pressions, les revêtements MCrAlY étant toutefois plutôt utilisés dans les turbines terrestres.

La protection contre l'oxydation liée à la formation d'une couche d'alumine peut parfois s'avérer insuffisante lorsque la température dépasse 1100°C. Dans un tel cas, il convient de limiter la température atteinte par la surface à l'aide d'une couche d'un isolant (barrière thermique), en général en zircone yttrée, associé à une sous-couche d'aluminure modifié au platine (Ni,Pt)Al. Cependant, cette solution est très coûteuse, en raison du prix du platine (environ 40 € le gramme), et de celle de l'EB-PVD pour la barrière thermique (procédé fortement directionnel à faible rendement, de 15 à 20 %). Par ailleurs, l'élaboration du revêtement de diffusion met en jeu des composés toxiques (utilisation d'activateurs de type halogénure comme NH₄F).

Cependant, les systèmes finissent toujours par évoluer et se dégrader. En particulier, la couche d'aluminure s'appauvrit en aluminium, d'une part par oxydation pour former l'alumine, d'autre part par inter-diffusion avec les éléments constitutifs du superalliage. Celle-ci conduit à la formation d'une zone de réaction secondaire (SRZ) qui induit une fragilisation. De plus, les sollicitations liées à l'imposition de cycles thermiques chauffage/refroidissement sont susceptibles de provoquer l'écaillage et/ou la délamination, totale ou partielle, de la barrière thermique.

De nouvelles solutions techniques ont dû être développées pour retarder les phénomènes de dégradation. L'introduction d'éléments réactifs permet de renforcer l'adhérence des couches et de ralentir les réactions d'oxydation, ces effets dépendant fortement de la méthode d'introduction. Des revêtements dits γ/γ' ont été récemment développés. Leur composition chimique, relativement proche de celle des superalliages base nickel, ralentit l'inter-diffusion ce qui retarde la dégradation du système. Pour aller encore plus loin, certains auteurs ont proposé d'introduire un revêtement supplémentaire de type barrière de diffusion (Cr, Re, SiAlON ...).

Toutefois, les exigences actuelles, tant au niveau économique (réduction des coûts d'exploitation) qu'environnemental (moins de rejets), demandent d'améliorer encore les rendements des turbines aéronautiques, ce qui nécessite d'augmenter à nouveau les températures de service. Il faudra pour cela modifier les compositions des substrats et/ ou des revêtements.

La présente étude s'inscrit dans le cadre du projet européen « PARTICOAT », qui vise à proposer un concept novateur d'élaboration de systèmes barrière thermique, à coût réduit et plus respectueux de l'environnement. Le procédé envisagé consiste à projeter une barbotine, obtenue à partir d'une dispersion de microparticules d'aluminium dans un liant à base aqueuse, sur la surface du matériau à revêtir. Un traitement thermique approprié doit ensuite permettre d'obtenir en une seule étape un système barrière thermique complet (couche additive + couche de liaison + barrière thermique).

Par ailleurs, l'utilisation de l'électrodéposition cathodique a permis d'élaborer des couches d'oxyde d'élément réactif (procédé breveté) destinées à jouer le rôle de barrière de diffusion.

Plusieurs aspects ont donc été considérés. En premier lieu, la barbotine à base aqueuse, additionnée d'alcool polyvinylique (PVA), et contenant des microsphères d'aluminium, a été caractérisée à l'aide de techniques complémentaires, en vue d'optimiser les conditions de dépôt.

La stabilité de la solution et l'homogénéité de répartition des particules d'aluminium dans la barbotine ont été évaluées par étude du phénomène de sédimentation à température ambiante, en fonction de la composition chimique. Ce dernier dépend de deux caractéristiques : le taux d'intensification (densification) et le taux d'épaississement de la phase sédimentaire. Les mesures effectuées montrent deux domaines distincts : un domaine de transition (temps d'analyse inférieurs à 10 minutes) et un domaine stationnaire (temps d'analyse de 10 à 60 minutes). Aux temps courts, les phénomènes d'intensification et d'épaississement sont régis par la dispersion des particules, leur

dimension et la dispersion de tailles. Les valeurs obtenues tendent à se stabiliser dans le domaine stationnaire, indiquant que les charges présentent un comportement comparable, indépendamment des fractions massiques utilisées.

Des mesures rhéologiques ont permis de confirmer que la viscosité augmente avec la charge en particules d'aluminium. Aux fortes teneurs (50 % massique), un phénomène de croustage a été observé neuf jours après élaboration des barbotines, révélateur de l'évaporation de l'eau libre. De même, le temps de séchage de la barbotine diminue lorsque la fraction massique en aluminium augmente. Ces observations ont conduit à réaliser des mesures par infrarouge (FTIR) à température ambiante afin de suivre, pendant neuf jours, l'évolution des liaisons physico-chimiques des différents composants de la barbotine (eau/PVA/Al). Aucune évolution significative des liaisons n'a été mise en évidence, en raison, d'une part, de la faible quantité de PVA relativement à la charge en aluminium et, d'autre part, de la forme sphérique des particules, qui réduit l'intensité des signaux réfléchis. L'évolution des alumines hydratées (suivi des signaux des groupes -OH) s'est également révélée difficile à suivre, probablement en relation avec la nature du liant (H₂O + PVA) ainsi que de part les conditions expérimentales (25°C sous air ambiant). Des résultats plus probants pourraient peut-être être obtenus en réalisant les mesures infrarouges sous vide ou à température plus élevée.

L'influence sur la barbotine d'un traitement thermique a ensuite été étudiée à l'aide d'expériences de DSC réalisées jusqu'à 550°C, complétées par des mesures d'ATD-ATG jusqu'à 1100°C, ce qui a permis de couvrir une large gamme de températures. Les mesures par DSC fournissent des informations relatives à l'évaporation de l'eau ($T < 120^{\circ}\text{C}$), à la température de fusion de l'alcool polyvinylique (PVA) employé (220°C) et à la dégradation des liaisons entre le PVA et les microsphères d'Al ($250^{\circ}\text{C} < T < 360^{\circ}\text{C}$). La température de déshydroxylation des microparticules d'aluminium a également été confirmée ($T \approx 460^{\circ}\text{C}$). Toutes ces données sont destinées à pouvoir adapter le traitement thermique à la réactivité des particules. Enfin, les mesures ATD-ATG ont permis d'obtenir des informations sur la cristallisation des alumines amorphes ($550^{\circ}\text{C} < T < 660^{\circ}\text{C}$) et d'observer les différents régimes d'oxydation corrélés aux transformations polymorphiques des différentes phases d'alumine ($\gamma \rightarrow \delta \rightarrow \alpha$), déjà observées par diffraction des rayons X à haute température (HT-XRD).

Sur la base de ces études complémentaires, et en tenant compte des évolutions des propriétés physico-chimiques ainsi que des propriétés de séchage, la charge en microparticules d'aluminium retenue pour la barbotine est comprise entre 40 et 50 m.%.

Ces études permettent d'envisager de futures optimisations de la chimie de la barbotine, par exemple en jouant sur la composition, pour moduler son comportement et, éventuellement, améliorer les propriétés des revêtements élaborés selon le concept PARTICOAT. Dans cette optique, un appareil de type ATG-DSC, pouvant atteindre 1600°C, a été récemment acquis par le laboratoire. Il doit permettre d'évaluer la réactivité de différentes barbotines en fonction du type de charges ajoutées (SiO₂, MgO, CeO₂ ...).

Dans un second temps, différents substrats à base nickel (deux matériaux modèles, Ni pur et Ni₂₀Cr, ou superalliages commerciaux) ont été aluminisés à partir d'une barbotine du type précédemment décrit. Les caractérisations effectuées sur les deux matériaux modèles ont permis de préciser les mécanismes de formation du revêtement. Le substrat Ni₂₀Cr a plus particulièrement permis de recueillir des informations sur l'effet de l'élément d'alliage chrome.

Les études menées avec le nickel pur ont conduit à définir un traitement thermique comprenant trois paliers de température (400°C-1h + 700°C-2h + 1100°C-2h). Ces trois températures correspondent respectivement à la décomposition du liant, à l'aluminisation du substrat simultanément au début de

la formation d'un topcoat et, finalement, à l'évolution des phases intermétalliques formées vers celle attendue et à la consolidation du topcoat. La structure finale, de type barrière thermique, est bien celle escomptée : couche additive d'aluminure de nickel (β -NiAl), couche de liaison en alumine, barrière thermique. Dans le cas du substrat Ni20Cr, les résultats obtenus diffèrent. La forte teneur en chrome provoque la formation d'aluminure de chrome (Al_xCr_y), avec pour effet d'empêcher, dès la seconde étape à 700°C, la formation du revêtement. La modification du traitement thermique ne permet pas d'éviter cette formation d'aluminures de chrome. Il apparaît donc qu'une forte teneur en chrome constitue une limitation au procédé d'aluminisation utilisant une barbotine, du moins pour la composition retenue. Des essais de revêtement selon le procédé PARTICOAT ont ensuite été réalisés en appliquant le traitement thermique défini pour le nickel aux différents superalliages à base nickel René N5, CM 247, PWA 1483 et INCO 738. Ceux-ci présentent différentes structures (polycristalline (EQ), à solidification dirigée (DS), monocristalline(SX)) et compositions chimiques. En plus du chrome (à une teneur toujours inférieure à 20 %), ils contiennent d'autres éléments d'alliage tels que Co, Ta, Mo ... Ces variations de la composition semblent n'avoir que peu d'influence sur la capacité du procédé PARTICOAT à aluminiser ce type de substrat. La zone enrichie en aluminium comporte dans sa partie supérieure de nombreux précipités riches en Cr (très peu de précipités dans la partie inférieure). Cette microstructure est semblable à celle obtenue avec des matériaux aluminisés par un procédé conventionnel, par exemple par cémentation en caisse (procédé basse température/haute activité) suivie d'un traitement d'homogénéisation à température plus élevée.

L'optimisation de la composition chimique de la barbotine devrait permettre de réaliser l'aluminisation d'autres types de matériaux comme par exemple les aciers, en adaptant également le traitement thermique appliqué. De plus, le développement de structures « gradées » pourrait conduire à une amélioration de l'adhérence au substrat du topcoat. L'ajout à la barbotine de particules d'oxyde pourrait constituer un moyen de rapprocher les valeurs des coefficients de dilatation thermique du topcoat et du substrat. On pourrait aussi envisager d'introduire une interphase entre le topcoat et le substrat en vue d'obtenir une structure de type sandwich et un gradient des propriétés thermiques.

La caractérisation du comportement en conditions d'oxydation à haute température des différents systèmes revêtus selon le procédé PARTICOAT a ensuite constitué une étape clé de ce travail. Dans le cas du René N5, les résultats ont été comparés à ceux obtenus avec des échantillons revêtus à l'aide du procédé industriel APVS, Aluminisation en Phase Vapeur Snecma.

Les tests d'oxydation réalisés pendant 1000 h à 1100°C ont montré que l'adhérence du topcoat au substrat est conservée, sauf à proximité des arêtes des échantillons (effet de bord) et sauf dans le cas du CM 247. Les prises de masse des échantillons revêtus selon Particoat sont plus élevées que celles obtenues avec la protection conventionnelle. Ce résultat a été attribué à la présence d'aluminium résiduel dans le topcoat à la fin du traitement thermique, celui-ci ayant une structure quasi mousse (constituée de sphères creuses d'alumine résultant de l'oxydation des microparticules d'Al).

Quelle que soit la structure initiale des superalliages (SX, DS ou EQ), la couche additive est polycristalline et comporte donc de nombreux joints de grains, qui constituent des chemins préférentiels pour la diffusion. L'existence de ces joints de grains et la température élevée favorisent la diffusion externe des éléments lourds ainsi que du nickel, ce qui conduit à la transformation de phase β -NiAl \rightarrow γ' -Ni₃Al. Cette transformation est indicatrice de la perte des capacités de protection contre l'oxydation du revêtement. La diffusion des espèces provoque également une modification de la solubilité des différents éléments d'alliage au sein de la matrice γ/γ' initiale. La ségrégation des éléments Cr, Ta et Ti sous formes de précipités a donc été étudiée. La précipitation des éléments réfractaires conduit par exemple à une augmentation de la résistance au phénomène de

« rumpling », i.e. d'ondulation de l'interface topcoat/substrat. La diffusion d'Al en direction de la matrice γ/γ' favorise la formation et la croissance de la zone de réaction secondaire (SRZ). Celle-ci dépend aussi fortement de la chimie du substrat : plus les teneurs en Cr, Ti et Ta sont élevées, plus large sera la SRZ.

Finalement, avec pour objectif de diminuer la vitesse de dégradation des revêtements, l'électrodéposition cathodique a été mise en œuvre afin de déposer, préalablement à l'aluminisation PARTICOAT, une couche de cérine à la surface des substrats. Celle-ci est destinée à agir en tant que barrière à la diffusion des espèces. L'introduction de cette couche a entraîné une modification des mécanismes de formation des composés intermétalliques. La création de nouvelles interfaces induit en effet un changement de la température de début de l'aluminisation. Aucun enrichissement en Al du substrat n'est alors observé lors de l'étape à 700°C. Cet enrichissement se produit toutefois à température plus élevée puisque de l'aluminium a effectivement diffusé après le palier à 1100°C. Un oxyde mixte de type pérovskite (CeAlO_3) a également été détecté, résultant d'une réaction à l'état solide entre l'alumine α et la cérine (CeO_2). La diffusion d'Al ne s'effectue cependant pas de manière homogène en raison même de la présence d'oxydes. Il conviendra d'optimiser les caractéristiques de la couche de cérine, en particulier son épaisseur et son taux de fissuration, afin de faciliter le transport de l'aluminium vers le substrat et d'améliorer la répartition du cérium dans le revêtement final.

Le comportement d'échantillons ainsi revêtus a été étudié en conditions d'oxydation à 900°C et 1100°C, pour évaluer le potentiel de ce système particulier. A l'issue de 1000h de test, on observe, quelle que soit la température, que le topcoat s'est détaché de l'oxyde thermique. En revanche, aucune SRZ n'est apparue au sein du substrat. Le développement d'une épaisse couche oxyde thermique, contenant CeAlO_3 , contribue très certainement à la diminution de l'adhérence du topcoat, via les différences de coefficient d'expansion thermique entre les différents composés.

La réactivité de l'oxyde de cérium vis-à-vis des éléments d'alliage, comme la localisation de cet élément de terres rares suite au traitement thermique et aux expériences d'oxydation à haute température, devront être déterminées de façon plus précise, par exemple par EPMA. Des tests de flexion quatre points devraient permettre de déterminer l'influence de la couche de cérine sur les propriétés mécaniques de l'oxyde thermique formé. Des tests d'oxydation cyclique et de fluage permettraient par ailleurs d'obtenir des informations sur l'influence de l'électrodépôt sur la résistance mécanique du système global ainsi que sur la formation, au niveau de la SRZ, des phases TCP (Topologically Close Packed).

Revêtements élaborés à partir d'une barbotine à base de microparticules d'aluminium destinés à la protection des superalliages base Ni contre l'oxydation à haute température

En raison de leur bonne résistance mécanique à haute température, les superalliages base nickel sont employés dans les turbines aéronautiques et de production d'énergie. Ils doivent alors être capables de résister aux phénomènes d'oxydation « sèche » intervenant entre 900 et 1500°C. Ces matériaux sont donc protégés par des revêtements à base d'aluminure de nickel (β -NiAl). De plus, dans les sections les plus chaudes des turbines ($T > 1050^\circ\text{C}$), une barrière thermique (BT) est ajoutée afin de diminuer l'impact de la température sur le substrat. Dans le cadre du projet de recherche Européen « PARTICOAT », le travail décrit dans cette thèse a porté sur l'élaboration d'un système complet de revêtements protecteurs (BC+BT) à l'aide d'un procédé en une seule étape, à partir d'une barbotine obtenue par dispersion de microparticules d'Al dans une base aqueuse, milieu susceptible de satisfaire aux directives environnementales européennes.

Des caractérisations rhéologique et physico-chimique ont montré la stabilité de la barbotine jusqu'à sept jours. Après dépôt de cette dernière par pulvérisation, un traitement thermique adapté a conduit, via la formation intermédiaire d'Al liquide, à l'obtention d'un revêtement d'aluminure de nickel (β -NiAl) comparable à ceux obtenus par les procédés industriels actuels. L'oxydation des particules d'Al permet la formation simultanée d'une « mousse » d'alumine (concept PARTICOAT) superficielle. Après validation des mécanismes réactionnels mis en jeu sur un substrat modèle de nickel pur, l'extrapolation du procédé à différents superalliages base nickel (René N5 (SX), CM-247 (DS), PWA-1483 (SX) et IN-738LC (EQ)) a donné des revêtements présentant différentes compositions et microstructures. Un intérêt particulier a alors été porté sur l'étude de l'influence des éléments d'alliage (Cr, Ta, Ti) et de leur ségrégation au sein du revêtement. Le comportement à haute température des échantillons revêtus a pu être évalué à l'aide de tests d'oxydation isotherme (1000h sous air entre 900 et 1100°C). Il a ainsi été montré que les phénomènes d'oxydation et d'interdiffusion régissent les mécanismes de dégradation. Par ailleurs, l'électrodéposition de cériine préalablement à l'application du procédé de revêtement PARTICOAT a permis de limiter fortement les phénomènes d'interdiffusion et de stabiliser la couche d'aluminure de nickel.

Mots-clés : Barbotine, microparticules d'aluminium, aluminure de nickel, barrière thermique, oxydation à haute température, barrière de diffusion.

Slurry coatings from aluminium microparticles on Ni-based superalloys for high temperature oxidation protection

Because of their good mechanical resistance at high temperature, Ni-based superalloys are used for aero-engine and land-based turbines but undergo "dry" oxidation between 900 and 1500°C. These materials are thus coated with nickel-aluminide coatings (BC). An additional thermal barrier coating (TBC) is generally applied in the hottest sections of the turbines ($T > 1050^\circ\text{C}$) to lower the impact of the temperature on the substrate. In the framework of the European research programme "PARTICOAT", this PhD work was focused on the growth mechanisms of a full protective coating system (BC+TBC) in a single step process, using a water-based slurry containing a dispersion of Al micro-particles to satisfy the European environmental directives. The rheological and physico-chemical characterizations showed the slurry stability up to seven days. After depositing the latter by air spraying, a tailored thermal treatment resulted in a nickel-aluminide coating (β -NiAl) similar to the conventional industrial ones but through an intermediate Al liquid phase stage. Simultaneously, the oxidation of the Al micro-particles brought about the formation of a top alumina "foam" (PARTICOAT concept). After a validation step of the mechanisms involved in pure Ni substrate, the extrapolation of the process to several Ni-based superalloys (René N5 (SX), CM-247 (DS), PWA-1483 (SX) and IN-738LC (EQ)) revealed different coating compositions and microstructures. A particular attention was therefore paid onto the effect of alloying elements (Cr, Ta, Ti) as well as their segregation in the coating. The high temperature behaviour of the coated samples has been studied through isothermal oxidation (1000h in air between 900 and 1100°C) and showed that the oxidation and interdiffusion phenomena ruled the degradation mechanisms. Besides, the electrodeposition of ceria before the application of the PARTICOAT coating allowed to strongly limit interdiffusion phenomena and stabilized the nickel aluminide coating.

Keywords: Slurry, aluminium micro-particles, nickel aluminide, thermal barrier coating, high temperature oxidation, diffusion barrier.

Laboratoire des Sciences de l'Ingénieur pour l'Environnement

Bâtiment Marie-Curie, Avenue Michel Crépeau

17042 La Rochelle Cedex

